Titre: Title:	Ni on FeCrAlloy Partially Oxides Methane at Short Contact Time and High Pressure
Auteur: Author:	Gianluca Pauletto
Date:	2020
Type:	Mémoire ou thèse / Dissertation or Thesis
Référence: Citation:	Pauletto, G. (2020). Ni on FeCrAlloy Partially Oxides Methane at Short Contact Time and High Pressure [Thèse de doctorat, Polytechnique Montréal]. PolyPublie. https://publications.polymtl.ca/5341/

URL de PolyPublie: PolyPublie URL:	https://publications.polymtl.ca/5341/
Directeurs de recherche: Advisors:	Johannes Lercher, & Gregory Scott Patience
Programme: Program:	Génie chimique

POLYTECHNIQUE MONTRÉAL
affiliée à l'Université de Montréal

Ni on FeCrAlloy partially oxides methane at short contact time and high pressure

GIANLUCA PAULETTO
Département de génie chimique

Thèse présentée en vue de l'obtention du diplôme de *Philosophiæ Doctor*
Génie chimique

Août 2020

POLYTECHNIQUE MONTRÉAL
affiliée à l'Université de Montréal

Cette thèse intitulée :

Ni on FeCrAlloy partially oxides methane at short contact time and high pressure

présentée par **Gianluca PAULETTO**
en vue de l'obtention du diplôme de *Philosophiæ Doctor*
a été dûment acceptée par le jury d'examen constitué de :

Michel PERRIER, président
Gregory PATIENCE, membre et directeur de recherche
Johannes LERCHER, membre et codirecteur de recherche
Miroslav GRMELA, membre
Anne GAFFNEY, membre externe

DEDICATION

Alla mia Famiglia e a Seda :
la miglior parte della mia vita.

ACKNOWLEDGMENTS

I would first like to express my gratitude to Prof Gregory S. Patience for giving me the chance and the economic support to complete my PhD under his supervision while also being co-supervised by Prof Johannes A. Lercher in Munich. I am sure we will be able to collaborate in the future.

Thanks to Prof Johannes A. Lercher for welcoming me at his research group and for his and Prof Andreas Jentys' precious and always available guide during my Lab work at the Catalysis Research Center (TUM).

A special thanks to my special French engineers Lauriane, Alice and Mathilde : without their help I would have not been able to achieve the same results.

Thanks to Prof Jeffrey Miller and Nicole (Purdue University) for being always ready to help me with the characterization of the catalytic materials, I could not find any better, more reliable and faster help.

Thanks to Prof Daria Boffito for her daily support, conversations, smiles, happiness and coffee time.

Thanks to Federico, Marco, Davide, Dalma, Jacopo, Stefano, Minerva and Adrien : with some of you I have shared the office with others I have eaten and spoken Italian during cold Canadian days.

Thanks to Nicolas, Andrew and Seda for reading and correcting my poor English.

Thanks to Niklas and Verena for helping me during my activities at TUM.

I would also like to express my deep gratitude to Prof Angelo Vaccari, Prof Joachim Sauer and Chris, Prof Gianpiero Groppi and Matteo, Dr Luca Basini, Dr Annette Trunschke, Prof Andrew Tong and Frank, Prof Patricia Benito, Prof Stefano Trasatti, Prof Giuseppe Maschio and Paolo that, while I have managed to interact with, they have helped me during my PhD project.

RÉSUMÉ

Le méthane est en train de devenir le principal vecteur d'énergie et élément de construction chimique non seulement en raison de sa disponibilité mais aussi parce que sa transformation en énergie et en produits chimiques implique une production d'émissions de gaz à effet de serre plus faible que celle du charbon et du pétrole. Même si le méthane est une ressource naturelle dont la disponibilité est limitée, c'est aussi un produit chimique vert produit par des digestions anaérobies de la biomasse. Pour remplacer les procédés chimiques actuels, de nouveaux procédés chimiques plus efficaces doivent challenger les procédés actuels. L'introduction des nouvelles technologies dans les activités industrielles dépend davantage de l'économie des procédés que des effets antropogènes sur l'environnement. Des exemples clairs de l'importance de l'économie des procédés sont le torchage des gaz et la production d'hydrogène. Actuellement dans le monde, la même quantité de méthane utilisée en un an par l'Allemagne et la France correspond à la quantité de gaz échoué. Cela correspond également à 1 % de l'émission totale de CO_2. La disponibilité d'hydrocarbures de faible poids moléculaire, associés à l'extraction du pétrole, dans des endroits éloignés où le flux de gaz est inférieur à $1000 \mathrm{Nm}^3\,\mathrm{h}^{-1}$ est actuellement considérée comme un problème plus qu'une ressource. Le transport par gazoduc et la transformation en énergie électrique ou en liquides facilement transportables ne sont pas rentables économiquement et ce flux est donc brûlé à la torche. De cette façon, la combustion du gaz naturel non seulement diminue la qualité de l'air mais produit également de la chaleur et de la lumière qui modifient l'écosystème local traditionnel. L'évacuation du gaz naturel aurait cependant une influence plus forte sur les niveaux d'ozone troposphérique, car l'effet de serre du CH_4 est beaucoup plus important que celui du CO_2.

Le reformage du méthane à la vapeur (SMR) est la principale réaction pour la production de gaz de synthèse et d'hydrogène dans l'industrie chimique. Même si le reformage du méthane à la vapeur est actuellement l'un des procédés chimiques qui émettent le plus de CO2, avec une contribution de 3 %, les nouveaux procédés de production tels que l'oxydation partielle catalytique (CPOX) ne l'ont pas remplacé, car l'économie globale du procédé de reformage du méthane à la vapeur est inférieure à celle du CPOX, compte tenu de la technologie disponible.

Ces dernières années, le CPOX a fait l'objet d'une attention nouvelle. Contrairement au reformage automatique (ATR), il évite l'utilisation de fours de préchauffage volumineux, polluants et coûteux, car fonctionnant de manière adiabatique. Il est applicable pour la production d'H_2 et est flexible à la fois sur le flux et la composition des matières premières. Le CPOX peut également convertir un flux de gaz naturel contenant du CO_2 car le reformage à

sec (DR) à cette température ne dépose pas de carbone sur la surface du catalyseur.

Nous avons abordé la conception d'un micro reformeur CPOX, pour la production de gaz de synthèse, sous deux angles. Le premier consistait à mettre au point un nouveau catalyseur qui évite le dépôt de carbone et minimise les produits de combustion complète, en particulier le CO_2. La deuxième étape, qui consistait à tester les catalyseurs à une pression supérieure à 15 bar dans un réacteur de 15 mm, a été utilisée pour la conception d'un réformeur à l'échelle pilote après une analyse technico-économique. Le réformeur CPOX pilote a été couplé à un réacteur Fischer Tropsch à lit fluidisé pour convertir $6\,m^3\,h^{-1}$ de méthane.

Les concepts de la conception du catalyseur étaient l'homogénéisation de la température dans le lit catalytique, ce qui réduit les points froids et chauds qui affectent la sélectivité du produit. Nous avons identifié le FeCrAl comme support de catalyseur en raison de sa conductivité thermique supérieure à celle de la plupart des supports céramiques traditionnels. Nous voulions également développer un catalyseur qui stocke l'oxygène et évite la formation de carbone tout en diminuant la disponibilité d'O_2 en surface sur la phase active métal-oxyde métallique. En ce qui concerne la conception du procédé, nous avons choisi un CPOX à temps de contact court (SCT) qui réduit l'oxydation complète tout en diminuant le volume du réacteur, les problèmes de sécurité et les investissements en capital. Le dernier réacteur CPOX SCT de 15 mm a fonctionné à $8\,l\,min^{-1}$ de CH_4, 900 °C et 15 bar.

Nous avons synthétisé et caractérisé, en collaboration avec l'université de Purdue, 12 catalyseurs différents à base de Ni, qui ont favorisé le Pt et/ou le Ru sur le CeO_2, le tout supporté par une gaze de FeCrAl. La synthèse a été spécialement conçue pour améliorer l'adhésion du catalyseur à la surface du métal et pour augmenter facilement sa production, et éviter l'étude et l'identification de la forme finale du catalyseur. La mise en œuvre du processus dans le réacteur SCT de 15 mm a été pensée pour le criblage du catalyseur à la fois en termes d'activation des liaisons C-H et de résistance du catalyseur à la formation de coke, suivi d'une régénération dans un réacteur de 6 mm fonctionnant à 1 bar. 2.25 % de Ni a favorisé 0.1 % de Ru sur 9 % de CeO_2 /FeCrAl (Ni2510) a donné le meilleur résultat de réaction et la meilleure résistance du catalyseur. Ce catalyseur a été testé à 15 bar sous différents rapports CH_4/O_2, de températures et de temps de contact. Dans ces conditions, les performances étaient bien inférieures à celles attendues d'un test à basse pression, car la réaction en phase gazeuse commence à produire de la suie, ce qui diminue la sélectivité du gaz de synthèse et pose des problèmes de sécurité. L'inflammation possible du mélange réactif a également entraîné des dommages au catalyseur, notamment la fusion du support métallique à une température supérieure à 1200 °C.

Compte tenu de la tendance à la conversion du méthane et de la sélectivité du gaz de synthèse obtenue à partir de Ni2510 et d'une combinaison de Ni2510 et de Ni/Al_2O_3, il a été possible de conclure que la réaction utilisant uniquement le Ni2510 suit un mécanisme de réaction directe apparent qui n'implique pas une réaction de reformage mais une limitation du transfert de masse de l'O_2. Pour la mise à l'échelle du réacteur et l'intégration du reformeur CPOX avec le réacteur à lit fluidisé FT. Nous avons identifié une méthode pour intégrer l'unité GTL (micro gaz to liquid) dans une batterie de puits de pétrole en concevant le processus complet tout en considérant la possibilité de faire fonctionner le CPOX à différentes températures et pressions. Pour être économique, le procédé doit comprendre une seule étape de compression en amont du SCT-CPOX, fonctionner à 20 bar et à une température supérieure à 900 °C. Comme le CPOX utilise l'air comme flux de coréactifs, le réacteur FT est un réacteur à passage unique sans recyclage et doit donc fonctionner à une conversion élevée du CO. Le coût total de l'unité GTL a un coût d'investissement légèrement inférieur à 1 million CAD$ alors que, compte tenu de la durée de vie de 10 ans de la centrale, le bénéfice annuel n'est que de 20 000 dollars. L'augmentation du nombre et la pénétration sur le marché de cette conception affecteraient fortement l'économie du processus car les coûts d'investissement diminueraient fortement. Comme le procédé fonctionne sous pression et à des températures supérieures à la température d'auto-inflammation, nous avons réalisé une analyse préliminaire de la sécurité du réformeur en tenant compte des différentes conditions d'alimentation et des compositions de produits qui pourraient contenir un mélange de CH_4 et H_2 avec O_2.

ABSTRACT

Methane is becoming the main energy vector and chemical building block not only because of its availability but also because its transformation into energy and chemicals involve a lower production of greenhouse emissions compared to coal and petroleum. Even if methane is a natural resource with limited availability, it is also a green chemical produced via biomass anaerobic digestions. To replace the current chemical processes, new and more efficient chemical routs must challenge the current ones. The penetration in the industrial activities of new technologies depends on process economy more than antropogenic impacts on the environment. Clear examples of the importance of the process economy are stranded gas flaring and hydrogen production. Currently in the world the same amount of methane used in one year by Germany and French corresponds to the amount of stranded gas. This also corresponds to 1 % of the total CO_2 emission. The availability of low molecular weight hydrocarbons, associated with the oil extraction, in remote locations where gas stream are below $1000 \mathrm{Nm^3\,h^{-1}}$ is currently seen as a problem rather than a resource. Transportation via gas pipeline and transformation into electrical energy or easily transportable liquids are not economic and therefore this stream is flared. In this way, burning natural gas not only decreases air quality but also produces heat and light that modify the traditional local ecosystem. Natural gas venting would however have stronger influences on the ozone levels, as the greenhouse effect of CH_4 is much higher then CO_2.

Steam methane reforming (SMR) is main reaction for the production of synthesis gas and hydrogen in the chemical industry. Even if SMR is right now one of the most CO_2 emitting chemical process, contributing with 3 %, new production processes as catalytic partial oxidation (CPOX) have not replaced it yet as the overall process economy of SMR is lower than CPOX, considering the available commercial technology.

CPOX has in the last years attracted new attention. Differently than auto thermal reforming (ATR), it avoids big, polluting and expensive preheating oven as it can work adiabatically. It is applicable for the production of H_2 and it is flexible both on the feedstock flow and composition. CPOX can also convert stream of natural gas containing CO_2 because dry reforming (DR) at this temperature does not deposit carbon on the catalyst surface.

We approached the design of a micro CPOX reformer, for the production of synthesis gas, from two point of view. The first was developing an novel Ni catalyst that avoiding carbon deposition it also minimizes full combustion products, in particular CO_2.

The second step focused on test of the catalysts at pressure higher than 15 bar in a 15 mm reactor. We have used this as proof of concept for a micro Gas-to-Liquid unit after complet-

ing a techno-economic analysis. The pilot CPOX reformer could be coupled with a fluidized bed Fischer Tropsch reactor to convert 6 $m^3 h^{-1}$ of methane.

The concepts of the catalyst design were the homogenization of the temperature within the catalytic bed decreasing the cold and hot spots that affect the product selectivity. We identified FeCrAl as catalyst support because of its thermal conductivity higher than most of the traditional ceramic support. We also wanted to develop a catalyst that, being able to store oxygen, avoids carbon formation. At the same time we also had to decrease the O_2 availability on the active site surface to minimize the maximize the selectivity toward synthesis gas. Regarding the reformer design we selected a short contact time (SCT) CPOX that decreases complete oxidation while minimizing reactor volume, safety problems and capital investments. The final 15 mm SCT-CPOX reactor operated up to 8 l min^{-1} of CH_4, 900 °C and 15 bar.

We synthesized and characterized, in collaboration with Purdue University, 12 different Ni based catalysts promoted Pt and/or Ru on CeO_2 supported on FeCrAl gauze. The synthesis was specifically tailored to improve adhesion of the catalyst on the metal surface and to easily scale up its production avoiding study and identification of the final catalyst shape. Implementation of the process in our 15 mm SCT reactor went thought an initial screening of the catalysts comparing both C-H bond activation and resistance to coke formation. These tests were completed in a 6 mm reactor operating at 1 bar. 2.25 % of Ni promoted 0.1 % Ru on 9 % CeO_2/FeCrAl (Ni2510) gave the best performance. Afterward, this catalyst was tested at different CH_4/O_2 ratio, temperature and contact time at 15 bar. At this conditions the performance were much lower than expected from low pressure test, because the gas phase reaction started producing soot, decreasing synthesis gas selectivity and bringing up safety problems. Possible ignition of the reactive mixture also resulted on catalyst damage including melting of the metal support at temperature above 1200 °C.

Considering the trend of methane conversion and synthesis gas selectivities obtained from Ni2510 and a combination of Ni2510 and Ni/Al_2O_3 it was possible to conclude that the reaction using only Ni2510 follows an direct reaction mechanism that does not involve reforming reaction. In situ x-ray absorption spectroscopy also confirmed the absence of indirect reaction mechanism as the Ni was oxidized thus not activa in reforming.

For the scale up of the reactor and the integration of the CPOX reformer with a FT fluidized bed reactor, we have identified a method to integrate the micro gas to liquid (GTL) unit in a oil well battery designing the process considering operation of CPOX at different temperature and pressure. To be economic the process must include a single compression step upstream the SCT-CPOX, operate at 20 bar and temperature higher than 900 °C. As CPOX uses air as a co-reactant, FT reactor is a single pass without recycle and therefore must work at high

CO conversion. The final cost of the GTL unit has a capital cost slightly lower then 1 million CAD$ while, considering 10 years lifetime, the annual profit is approximatly 20 000. Penetration in the market and numbering-up would strongly affect the economy of the process as the capital costs decreases of at least 25%. As the process operates under pressure and at temperatures higher than the auto-ignition temperature we completed a preliminary safety analysis of the reformer considering different feeding conditions and product compositions that could contains mixture of CH_4 and H_2 with O_2.

TABLE OF CONTENTS

LIST OF TABLES

LIST OF FIGURES

LIST OF SYMBOLS AND ABBREVIATIONS

ψ	elemental stoichiometric coefficient
σ_{B}	Stefan-Boltzmann constant
τ	tortuosity
ε	void fraction
b	constant varies from 0.63 to 0.65
C_{r}	constant equal to 2.65
d_{c}	foam cell diameter
d_{f}	diameter fiber
$d_{\mathrm{s,av}}$	average strut diameter
d_{h}	hydraulic diameter
d_{sauter}	Sauter mean diameter
E_{r}	Rosseland extinction coefficient
h	heat transfer rate coefficient
K_{r}	constant equal to 16.67, 14.5 or 8
K_{r}	radial dispersion coefficient
$k_{\mathrm{eff,ax}}$	axial effective conductivity
$k_{\mathrm{eff,cond}}$	effective conduction
$k_{\mathrm{eff,conv}}$	effective convection
$k_{\mathrm{eff,rad}}$	effective radiation
k_{eff}	effective conductivity
k_{g}	intrinsic gas conductivity
k_{m}	mass transfer rate coefficient
k_{parallel}	in-series conductivity
k_{s}	intrinsic solid conductivity
k_{serial}	in-parallel conductivity
N_{Nu}	Nusselt number
N_{Pe}	Peclet number
N_{Pr}	Prandtl number
N_{Re}	Reynolds number
N_{Sc}	Schmidt number
N_{Sh}	Sherwood number
S_{V}	surface to volume ratio
s_{A}	specific surface area

T	temperature
x	characteristic length
z	axial coordinate
A	air
ATR	auto-thermal reforming
BET	Brunauer–Emmett–Teller surface area
C	carbon
CFD	computational fluid dynamics
CPOX	catalytic partial oxidation
DC	direct current
DMR	dry methane reforming
EDS	energy dispersive X-ray spectroscopy
F	flow
F	fuel
FT	Fisher Tropsch
GHSV	gas hourly space velocity
GTL	gas-to-liquid
HA	hexaaluminate
HT	hydrotalcite-type
KIER	Korea Institute of Energy Research
LDHs	layered double hydroxides
NSR	NOx storage-reduction
OCM	Oxidative coupling of methane
PI	process intensification
PVA	polyvinyl alcohol
RF	radio frequency
S	steam
SCE	saturated calomel electrode
SCR	selective catalytic reduction
SCS	solution combustion synthesis
SEM	scanning electron microscope
SMR	steam methane reforming
TEM	transmission electron microscope
TWC	three way catalysts
VOC	volatile organic compounds
W	weight

WGS	water gas shift
XPS	X-ray photoelectron spectroscopy
XRD	X-ray diffraction

LIST OF ANNEXES

CHAPTER 1 INTRODUCTION

1.1 Background and problem identification

Stranded natural gas (CH_4) from oil extraction represents a lucrative potential revenue stream that has been so far unexploited while it is still contributing to the carbon footprint. Often this stream is flared, only marginally vented, without exploiting the high energy density (higher than $50\,MJ\,kg^{-1}$). The total amount of CH_4 flared worldwide corresponds to the same amount that Germany and France require every year Elvidge et al. (2016); Ismail (2012).

The main issue concerning capture and utilization of CH_4 lies in the remote locations of the oil wells Ma et al. (2016a). Companies are forced to shut in extraction sites because the economic value of the associated gas is too low to justify a multi-million dollar pipeline or liquefaction project to transport the gas.

Several technologies exist to convert CH_4 into added value products through gas to liquids (GTL) processes at the commercial scale. They all have a first step where CH_4 reforms to syngas, and a second one where the final products include liquids. In industry the technologies used in the production of synthesis gas are steam methane reforming (SMR), partial oxidation (POX) and a combination of these two is used in auto-thermal reforming (ATR) Rostrup-Nielsen and Christiansen (2011). The most common second step used in GTL is the Fischer Tropsch (FT) reaction that converts syngas into hydrocarbons, because methanol production and dimethyl ether pose more challenges. These processes are however neither applicable nor profitable to recover CH_4 from wells, which mostly operate under $2100\,bbl\,d^{-1}$ or on a irregular basis Emam (2015).

Small units deployable at the well head using air and steam to partially oxidize methane to CO and H_2 are not commercially available and 60 % of the total capital investment is related to the reforming unit Mohajerani et al. (2018); Wright et al. (2003); Rostrup-Nielsen and Christiansen (2011). Therefore, the cost-effective design of compact reformers would have a tremendous impact on the commercialization of small field plant Wright et al. (2003).

In our approach, we produce syngas from associated CH_4 by catalytic partial oxidation (CPOX). The implementation of our proposed technology at the industrial scale includes additional advantages :

- The CPOX is exothermic, thus the heat generated decreases the energy requirements and the reformer can work adiabatically ;
- The products of the reaction, CO and H_2, are already in the optimal ratio (2 : 1) for the subsequent Fischer-Tropsch (FT) reaction to produce green diesel ;

— Air and not pure oxygen supplies the required reagent.

Even if the design of POX catalyst is a very well known, thoroughly investigated and a traditional subject, the improved synthesis procedures to achieve high reaction performance reported in the literature are usually complicated, economically demanding, and impractical on a large scale. This is also the reasonf why, even if some catalysts have shown outstanding performance, CPOX is still not used in industry.

We produced catalyst following a procedure that requires no modification for large scale synthesis. Thus, our lab scale product will have the same mechanical, physical, and chemical features that it will have during large scale application. So far, most of the catalysts activity tests has been completed at atmospheric pressure, which is uneconomic economically industrially. The subsequent FT stage requires pressure of around 2 MPa, and upstream CH_4 sweetening (sulphur removal) also requires high pressure. Carrying out CPOX at high pressure reduces equipment and overall process cost while challenging the thermodynamics and catalyst. Most of the studies have been done feeding stoichiometric methane and oxygen but, at this ratio producing coke is thermodynamically likely. It was proven that CPOX under kinetic control follows an indirect route consisting of full combustion followed by refroming, therefore short contact time (SCT) CPOX under these conditions are technically not feasible Chin and Iglesia (2011); Chin et al. (2011a). In other studies direct reaction mechanism was observed and tested in pilot and demonstration plants. On possible way to have an apparent direct reaction mechanism is to work under mass transfer limitation that avoids full CH_4 combustion as the oxygen is depleted from catalyst surface. This condition induces an apparent reaction mechanism that avoids downstream reforming of the products.

While it is know that a wide range of metals are active, noble metals in particular Pt, Rh and Ru have higher turnover rate and are more stable to carbon deposition. Our catalyst design involves low cost Ni promoted with noble metals on CeO_2 supported on FeCrAl. While ceria contains lattice oxygen that minimizes carbon depostion, it also reduces oxygen availability on the metal surface increasing syngas selectivity. FeCrAl is a suitable catalyst support for CPOX as it has high temperature resistance in oxidizing environment, high thermal conductivity compared to other ceramic support and is available in shapes that can be used for catalyst scale-up production. Combing all these materials and their respective features we have developed a catalyst, reactors, and process for the SCT-CPOX followed by FT in a unit deployable at the well head.

1.2 Objectives

The main objective of the project is to develop a a Ni based catalyst for methane SCT-CPOX at 20 bar. The final application is a mobile GTL unit that converts flared gas into synthetic fuels. In order to achieve this main objective, we have divided the project into four specific sub-objectives, that will result in four articles submitted to peer-reviewed journals. The specific objectives are :

1. Identify application of FeCrAl used as a catalyst support in high temperature reaction. The results of this objective are described in chapter 4, and submitted as comprehensive scientific article to **Chemical Reviews (I.F. 54.0)**
   - Mass and heat transfer in structured metal supports.
   - Identification and description of the synthesis techniques.
   - Summary of the various catalytic systems reported in the literature for a variety of high temperature processes.
   - Benefits and drawbacks with insight for necessary future work.
2. Develop a Ni/CeO_2 catalyst supported on FeCrAl gauze. Results are submitted as scientific article to **Applied Catalysis B : Environmental (I.F. 14.2)**
   - Preparation of Ni/CeO_2 on FeCrAl knitted metal fibers promoted .
   - Mechanical tests for coating stability.
   - CPOX redox process at reduced O_2 partial pressures for cycling reaction-regeneration steps.
   - Stability tests for most active and selective catalytic system.
   - Catalyst characterization via SEM-EDS, TEM-EDS, XRD and *in situ* XAS for the determination of Ni oxidation state during reaction.
3. Perform a techno economical analysis of a micro GTL unit and identify process process parameters. Results are submitted as scientific article in **Renewable & Sustainable Energy Reviews (I.F. 10.50)**
   - Thermodynamic of CPOX reaction with air from 0.2 MPa to 2.0 MPa.
   - Design of two tandem reactors working at 2.0 MPa.
   - Optimization of process conditions varying temperature, pressure and methane to oxygen ratio.
   - Identification of flammability ranges at 2.0 MPa and 800 °C to 950 °C for methane-air mixtures.
   - Techno economic analysis based on manufacturers' quotes.
4. Assemble and operate of a bench scale SCT-CPOX reactor operating 1.5 MPa. Results are submitted as scientific article to **Chemical Engineering Journal (I.F. 8.3)**

- CPOX at high pressure and apparent reaction mechanism.
- SCT-CPOX coupled with downstream reforming.
- Gas phase reaction identification and localization.
- Characterizations and comparison between CPOX and reforming catalysts.

CHAPTER 2 COHERENCE OF THE ARTICLES

Chapter 1 : this first section highlights the potential of converting methane, in particular stranded gas, to liquid product via a two step process involving first CPOX followed by FT. We introduced the benefits of CPOX, in particular related with the lower energy demand, compact size and proper H_2/CO ratio for the downstream FT synthesis. After enumerating the possible technologies to reduce gas flaring we introduce the concept of a micro GTL technology where flared gas first reacts in a SCT-CPOX reformer that feeds a downstream FT unit that produces transportable liquid fuels.

Chapter 2 : a brief description of the chapters of this manuscript, and the main links between them.

Chapter 3 : this section introduces the concept of syngas production via CH_4 conversion. After a summary of the technologies applied in industry to produce syngas, we report the state of the art on CH_4 CPOX, indicating the advantages and challenges that the process/reaction must overcome to find industrial applications. After the summery of the most relevant literature we focus on catalysts based on high temperature resistance FeCrAl. This material has high temperature performance and the improved mass and heat transfer partially overcomes current reaction problems. Design of a catalyst metal gauze will make it possible to easily scale-up the reactor design while converting CH_4 in a short contact time reactor, operating at pressure varying from 0.1 MPa to 2.0 MPa.

Chapter 4 : this section consists of comprehensive, authoritative, critical, readable review of FeCrAl with a particular emphasis on applications in catalysis. We cover all applications of FeCrAl that are commercial or under development, and describes the properties of the alloy considering the advantages that the metal structured support gives both on mass and heat transfer. We present, in depth, description of the catalysts preparation. We report the performance of the catalysts considering catalyst support shape and active phase ; while we connect catalyst performance with preparation techniques. We conclude shearing ideas for future research required for the final application of this material in catalysis.

Chapter 5 : design of Ni/CeO_2 on FeCrAl gauze catalyst for CPOX. After mechanical tests on the adhesion of the ceramic CeO_2 coating on the fibers, we tested this material with Ni promoted Pt and/or Ru. We compares the promoters effect during reaction and regeneration step. Comparison of the catalyst activity based on turnover frequency in C-H bond activation considering Ni metal loading, showed high catalytic activity in presence of Ru without initial pre-reduction step. We characterized catalyst morphology via scanning and transmission electron spectrometry and X-ray diffraction. Ni oxidation state during reaction was detected via *in-situ* XAS measurments at the 10-BM beamline at the Advanced Photon Source (APS) of the Argonne National Laboratory.

Chapter 6 : thermodynamic study relative to CH_4-air CPOX reaction operating from 0.2 MPa to 2.0 MPa. We have identified zero carbon region, maximum yield to CO, syngas with H_2/CO ratio as close as possible to 2, and preheating temperature. We varied operating pressure, temperature and CH_4/O_2 ratio. Starting from these equilibrium data we have developed CPOX and FT reactor designs and we have compleated a techo-economical analysis focusing on the possible operating process parameter. The goal of the design was a minimization of the capital costs that relied on manufacturer quotes. At the same time, based on these results we have built a process skid that will convert flared gas into liquid products that will be tested at an oil battery.

Chapter 7 : results of a bench scale reactor converts from $1\,\mathrm{l\,min^{-1}}$ to $4\,\mathrm{l\,min^{-1}}$ of methane. The reactor operating at 1.5 MPa and temperatures greater than 800 °C was used to correlate reaction performance and reaction mechanism. In this setup, we have also investigated the gas phase reaction that produced a considerable amount of soot during SCT-CPOX. We have also tested the combination of two different catalysts one for CPOX and one for reforming as the performance of a single CPOX step were unsatisfactory. This case proved that the trends of syngas selectivieties and methane conversion vs residence time were different with respect to the application of a single catalytic step. Characterization of the two Ni catalysts via *in-situ* XAS revealed different behavior and Ni oxidation states.

Chapter 8 : reports a general discussion of the work and summary of the results achieved.

Chapter 9 : summary of the project, focusing on the main hurdles and the limitations, providing recommendations for future work.

CHAPTER 3 LITERATURE REVIEW

3.1 Natural Gas Steam Reforming

Steam reforming produces 80 % of the world's H_2 Rostrup-Nielsen and Christiansen (2011). The process (Fig.4.2) involves CH_4 oxidation with water followed by the water gas shift reaction that further oxidizes CO to produce additional H_2 Fig. 4.2 Laosiripojana and Assabumrungrat (2005); Matsumura and Nakamori (2004); Holladay et al. (2009). The reactions involved in the hydrogen generation are :

$$\mathrm{CH_4 + H_2O \longleftrightarrow CO + 3\,H_2} \qquad \Delta H = 205\,\mathrm{kJ\,mol^{-1}} \tag{3.1}$$

$$\mathrm{CO + H_2O \longleftrightarrow CO_2 + H_2} \qquad \Delta H = -41\,\mathrm{kJ\,mol^{-1}} \tag{3.2}$$

$$\mathrm{C_nH_m + nH_2O} \longleftrightarrow n\mathrm{CO} + (n + 0.5m)\mathrm{H_2} \qquad \Delta H < 0\,\mathrm{kJ\,mol^{-1}} \tag{3.3}$$

The reforming process is endothermic and increases the mole number ; thermodynamically the process is favored at high temperatures and low pressure. Studying the equilibrium, high steam/methane (S/C) ratio (Eq. 3.4) pushes the reaction to the products' side as the partial pressure of the reagents (water) increases.

$$S/C = \frac{molar\ flow\ rate\ of\ steam}{\mathrm{C}\ molar\ flow\ rate\ in\ \mathrm{CH_4}} \tag{3.4}$$

The supply of the heat requires combustion of fuel gas, approximately 20 % of the used CH_4 is fired in the burners. Methane in the presence of excess air is burned in a fired furnace where tubes, containing the catalyst, are immersed. The position of the burners (top, bottom or side), characterize the reformer design and it depends on the suppliers (Halder Topsoe,

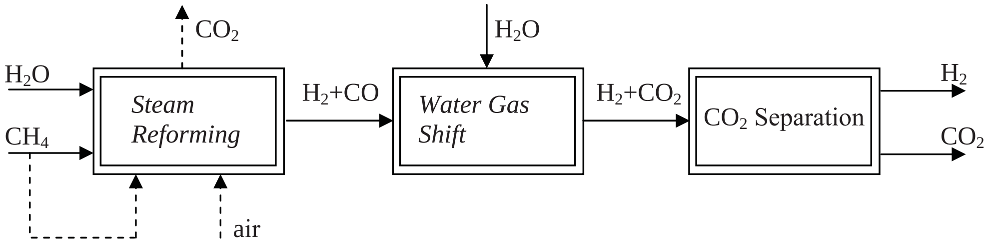

Figure 3.1 SMR process Seo et al. (2002).

Honeywell UOP, Air Liquide, Linde, Amec Foster Wheeler and Air Products). Top fired reformers are the most commonly used as they give the best temperature profile. Methane and steam are fed to the tubes that are filled with catalyst pellets and immersed in the fired furnace. These tubes are in direct contact with the flames of the burners. Because of mechanical constrains, SMR reactors cannot operate above 900 °C to 1000 °C, as the external skin temperature of the tube limits mechanical stability where 20 °C difference can drastically decrease the tubes lifetime. The most common industrial catalyst is Ni on calcium-aluminium oxide, that supports the active phase and minimizes sintering, favored by high temperatures Rostrup-Nielsen and Christiansen (2011). The high costs related to the management of the endothermic process come from the low reformer energy efficiency (less than 50 %) and from the high residence times required to approach equilibrium conversions. These reasons have pushed researchers to identify and study alternative syngas productions routes. Expensive energy recovery units increase the energy efficiency to value close to 90 % even if the reformer itself has value lower than 60 %. The low energy efficiency and the expensive fired furnace of the reformer prevent the use of this technology in small units, required for the production of decentralized syngas from flare CH_4 (often lower than $100\,m^3\,h^{-1}$). Currently SMR gives high synthesis gas yield as the technology has been developed and used in industry for more than 60 years.

3.1.1 Thermodynamics

Studies of the thermodynamics, to maximize H_2 yield, identified three independent reactions that represent the entire process Lutz et al. (2003); Rostrup-Nielsen and Christiansen (2011). The reactions are SMR (Eq. 5.1), water gas shift (WGS) (Eq. 7.1) and the reforming of higher hydrocarbons (Eq. 7.2) Seo et al. (2002). It is particular important to decrease as much as possible the S/C to minimize the amount of energy used. This, however, increases the probability of carbon deposition Rostrup-Nielsen and Christiansen (2011). Considering that the maximum temperature imposed by mechanical limitation of the reformer tubes is 1000 °C, the highest achievable performance are reported in Fig. 3.2.

In industry the ratio in the newest plants is close to 2.5, this is currently possible as a result of a deep industrial understanding. The old steam reformers used to have ratio close to 4-5 Rostrup-Nielsen and Christiansen (2011). Higher values increase CH_4 conversion and decrease the probability of carbon deposition, that often results in catalyst coking followed by clogging of the reforming tubes. Higher amounts of steam increase H_2 and CO_2 respect to CO as the availability of oxidizer (steam) is higher (Fig. 3.3). Experimental considerations have shown how the preheating temperature does not affect the performance because the heat capacity of the gases is negligible compared to the reaction endothermicity. An important value is

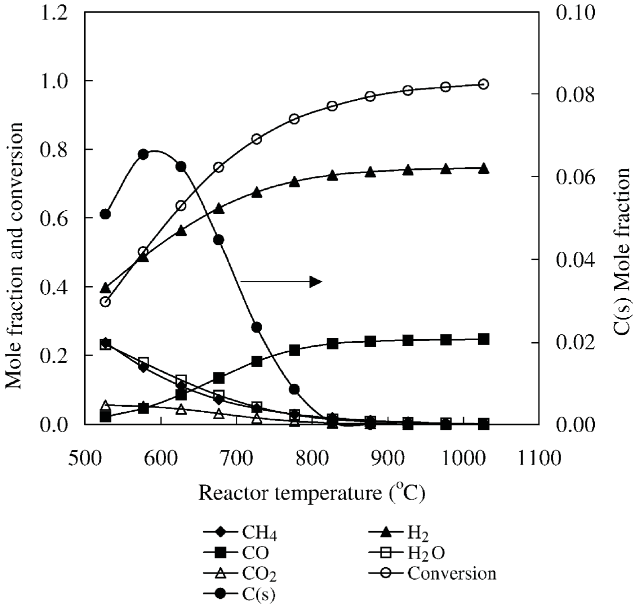

Figure 3.2 Effect of reactor temperature on the equilibrium composition and conversion in SMR at 1 bar, S/C=1 Seo et al. (2002).

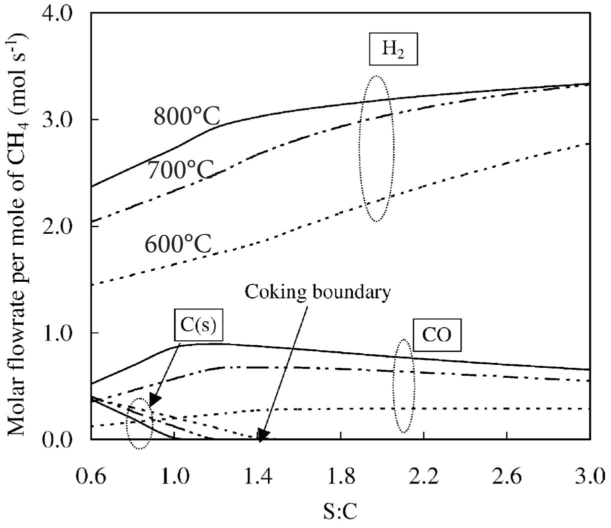

Figure 3.3 Effect of S/C on equilibrium composition at 1 bar and different Temperatures Seo et al. (2002).

the temperature of the catalyst that imposes the final reaction performance and approach to equilibrium. The catalyst effectiveness factor is often lower than 15 % and it is strongly dependent on radial temperature gradients within the reformer tubes Rostrup-Nielsen and Christiansen (2011).

3.1.2 SMR Mechanism

The kinetic mechanism of steam reforming that is currently accepted and mostly used in literature is the one proposed by Froment and Xu (1989). They studied the intrinsic kinetics of steam reforming on $Ni/MgAl_2O_3$ catalysts, in the range 0.3 MPa to 1.5 MPa. Between the possible reactions that occur on the substrate (L), only Eq. 7.3, 7.4, 7.5 were considered in the study of the kinetic model.

$$\mathrm{CHO{-}L + L \longrightarrow CO{-}L + H{-}L} \tag{3.5}$$

$$\mathrm{CO{-}L + O{-}L \longrightarrow CO_2{-}L + H{-}L} \tag{3.6}$$

$$\mathrm{CHO{-}L + O{-}L \longrightarrow CO_2{-}L + H{-}L} \tag{3.7}$$

Water is adsorbed and dissociated on Ni producing adsorbed oxygen and hydrogen gas. Methane adsorbed on the surface of the catalyst reacts with the oxygen or dissociates, giving radical species, such as $CH_3{-}L$, $CH_2{-}L$, $CH{-}L$, $C{-}L$. The adsorbed oxygen reacts with these components forming CH_2O, $CHO{-}L$, $CO{-}L$, $CO_2{-}L$. H_2, CO and CO_2, once formed, desorb in the gas phase.

The rate determining steps in the reaction mechanism are those that involve CO and CO_2 formation. Wei and Iglesia (2004) indicate methane (C-H bond) activation as the rate determining step but this discrepancy is consistent with the higher operating temperature Rostrup-Nielsen and Christiansen (2011).

3.2 Methane Partial Oxidation

To avoid heat transfer limitations and expensive fired reformers, exothermic reactions rather than SMR can be used for the production of syngas. Feeding methane and oxygen into an adiabatic reactor produces syngas following the methane partial oxidation (POX). In this case expensive pure O_2 is required to achieve operating temperature from 1000 °C to 1500 °C Rostrup-Nielsen and Christiansen (2011).

$$\mathrm{O_2/CH_4} = \frac{molar\ flow\ rate\ of\ \mathrm{O_2}}{molar\ flow\ rate\ of\ \mathrm{CH_4}} \times 0.5 \tag{3.8}$$

The most important parameter in POX is the O_2/CH_4 ratio (Eq. 3.8). The competing full combustion and partial oxidation determine the final adiabatic temperature :

$$\mathrm{CH_4 + 0.5\,O_2 \longrightarrow CO + 2\,H_2} \qquad \Delta H = -36\,\mathrm{kJ\,mol^{-1}} \tag{3.9}$$

$$\mathrm{CH_4 + 2O_2 \longrightarrow CO_2 + 2\,H_2O} \qquad \Delta H = -890\,\mathrm{kJ\,mol^{-1}} \tag{3.10}$$

If values close to 0.5 favor partial oxidation rather than combustion products, they fail to achieve high adiabatic temperatures thus conversions. Low temperatures favor unreacted methane to crack instead of reforming producing carbon and H_2. With POX, the problem of the reaction endothermicity is solved but the reaction is industrially used only for heavy hydrocarbons or for the production of synthesis gas for big GTL units. This process is used at Sasol's Oryx and Shell's Pearl plant in Qatar Hoek and Kersten (2004); Sichinga and Buchanan (2005). The plant requires air separation and difficult reaction control that can become unstable because of the one order of magnitude difference in the enthalpy of reactions between full combustion and POX. This problem together with the coke deposition on the reactor's walls and pipes make the process convenient and industrially applicable only to convert sulfured and possibly heavy hydrocarbons feed or when the syngas ratio H_2/CO must be equal to 2 (GTL).

3.2.1 Thermodynamics

Seo et al. (2002) studied also the thermodynamics of the partial oxidation. The ratio (Eq. 3.8) O_2/CH_4 varied between 0.0 to 1.2. The product compositions achieved at equilibrium in the adiabatic reactors are plotted as function of the air ratio in Fig.3.4. Ratios higher than 0.3 limits carbon black but a reduction in both H_2 and CO yield as competing full combustion becomes significant. Fig. 3.5 shows the trend of the CH_4 conversion, adiabatic temperature and H_2 yield (defined as product of methane conversion and hydrogen selectivity) versus air ratio. The yield of hydrogen has a maximum for air ratio of 0.3.

3.2.2 CPOX mechanism

POX in presence of a catalyst (CPOX) starts at temperature as low as 500 °C because the C-H bond activation is favored. Since 1989 constant and prolific research in the catalyst design resulted in more than 6000 publications (WoS).

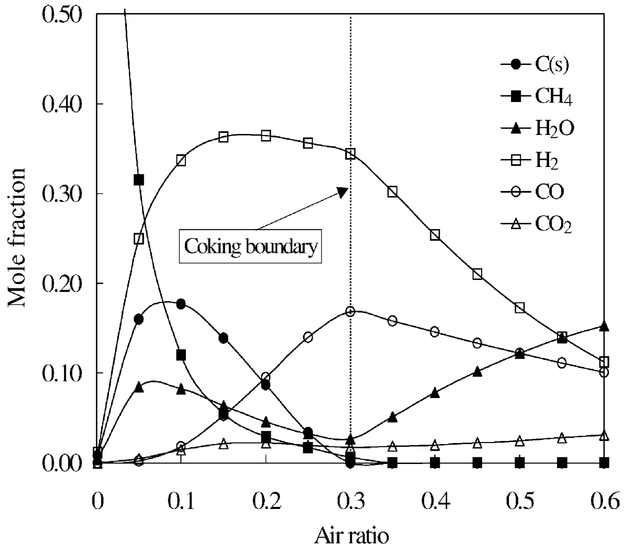

Figure 3.4 Effect or air ratio on equilibrium composition POX reactor. Preheat temperature of reactant 200 °C at 1 bar Seo et al. (2002).

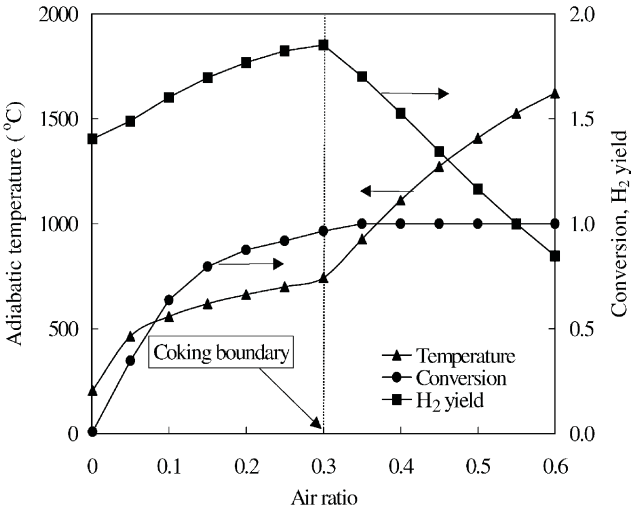

Figure 3.5 Effect of air ratio on adiabatic temperature, conversion and H_2 yield of POX. Preheat temperature of reactant 200 °C at 1 bar Seo et al. (2002).

Air instead of oxygen reaches lower temperatures also at high flow rates, that makes possible to reduce the size of the reactors and to avoid expensive heat exchangers or catalyst surface temperature greater than 1200 °C Bizzi and Saracco (2004); Bha (1995); Christian Enger et al. (2008). The use of air as oxidizer for CPOX makes possible to carry on reaction in decentralized sites where pure oxygen is normally not available Groote and Froment (1996). The mechanisms of the reaction that have been suggested and discussed for more than 30 years are :

- indirect mechanism proposed by Prettre et al. (1946), confirmed by Donazzi et al. (2008) and by the fundamental studies of Chin and Iglesia (2011); Chin et al. (2011a) ;
- direct mechanism proposed by Hickman and Schmidt (1993) still supported in the literature.

The direct mechanism makes possible to carry on reaction at short contact times (SCT) often in milli seconds reactors. Prettre et al. (1946) first studied the partial oxidation of methane on Ni catalysts. They measured the composition of the products and the temperature profiles inside the catalytic bed. The results were compared with equilibrium assuming that only POX reaction was taking place. They observed that, as soon as the reacting gases entered the catalytic bed, there was a rapid increase of the temperature, not compatible with the mild exothermicity of POX, followed by a gradual decrease, that they attributed to endothermic reforming reactions. Their results were suggesting an indirect mechanism where, after initial combustion, CO_2 and H_2O gradually reform with CH_4 into CO and H_2 Prettre et al. (1946). Hickman and Schmidt (1993) studied the oxidation of methane at high temperatures on alumina monoliths supporting Pt and Rh as well as on bulk noble metal gauzes. They compared the experimental results with those obtained from a model involving elementary steps. They proposed the direct CPOX mechanism to syngas that involved methane cracking on the catalyst surface followed by its oxidation. The hypothesis of irreversible adsorption of methane on the surface of the catalyst, proven also by Chin and Iglesia (2011) via isotopic scrambling, did not exclude the sequential dissociation of hydrogen, but eliminated $CH_x + O \longrightarrow CH_{x-1} + OH$ with consequent water formation through the reaction $H + OH \longleftrightarrow H_2O$. During experiments Hickman and Schmidt (1993) reached very high syngas selectivity but people in the literature attributed this performance to the specific fluid-dynamics, imposed by the metal gauze, that influenced the reaction kinetic by O_2 mass transfer limitations Hickman and Schmidt (1993); Chin and Iglesia (2011); Chin et al. (2011a).

The potential energy diagrams of Rh and Pt were obtained comparing the experimental results with the model. The higher activation energy for OH formation on Rh caused higher selectivity toward CO respect to Pt catalyst. Hydrogen desorption on Rh is faster than water formation thus it avoids hydrogen oxidation.

Yan et al. (2004) using Ru and Rh on SiO_2 showed that with the first combination the partial oxidation followed the indirect mechanism, while with the second the direct one. They suggested that the strong Ru−O bond inhibits the reduction of the metal during the partial oxidation process, favoring the formation of total combustion products. Being Rh−O bond weaker, it facilitates the reduction of Rh and it promotes the dissociation of CH_4. In this case superficial carbon leads to the production of partially oxidized products following the same mechanism proposed by Hickman and Schmidt (1993). In another publication they used Rh on either SiO_2 or Al_2O_3. They showed that the CPOX followed an indirect mechanism with Rh/Al_2O_3, because of the different interactions between active phase and support. Strong interaction between metal and support inhibits the reduction of the active phase, favoring the completed oxidation products.
Other studies concluded that the mechanism is always direct Veser et al. (2000). They concluded that the reason of initial large CO_2 and H_2O concentration is not the followed pathway but the different adsorption constants of oxygen and methane on the surface of the catalyst : at the inlet the catalytic surface is preferentially covered with O_2, that promotes the complete oxidation. When the partial pressure of O_2 decreases, this compensates the different absorption equilibrium and the resulting fuel rich reactive mixtures favor syngas products.
Groote and Froment (1996) tested Ni catalysts and supported the indirect mechanism. They also developed a model where they combined the kinetics of combustion with those of steam reforming. The presence of combustion followed by reforming lead to a peak in the temperature profile. This maximum is sharper when the overlap between the combustion and reforming zones decreases. Numerous additional studies showed that certain types of catalysts or reaction parameter favor O_2 mass transfer limitations that result in a direct CPOX Bizzi et al. (2003, 2002). Chin and Iglesia (2011); Chin et al. (2011a) showed that, if the reaction is carried out under kinetic regime, CO does not leave the reactor before all the O_2 is consumed. In their studies they showed that Pt, Ru, Ir, Pd, Ni, Rh catalysts partially oxidize CH_4 following the indirect mechanism.

Even if according to Groote and Froment (1996); Basile et al. (2001) temperature peak inside the catalytic bed inhibits the development of the partial catalytic oxidation, other researchers showed that high catalyst surface temperature enhances syngas production Basini et al. (2000, 2001); Basini and Guarinoni (2013). Basile et al. (2001) studied the feasibility of CPOX, considering the evaluation of the thermal stability of the catalytic system by measuring the temperature profiles within the catalytic bed. They measuremed with an IR camera the temperature profiles and they detected the presence of hot spots within the catalytic bed. These result from the consecutive behavior of the combined combustion-reforming reactions. Many researchers still believe that the reaction mechanism depends on the metal active phase

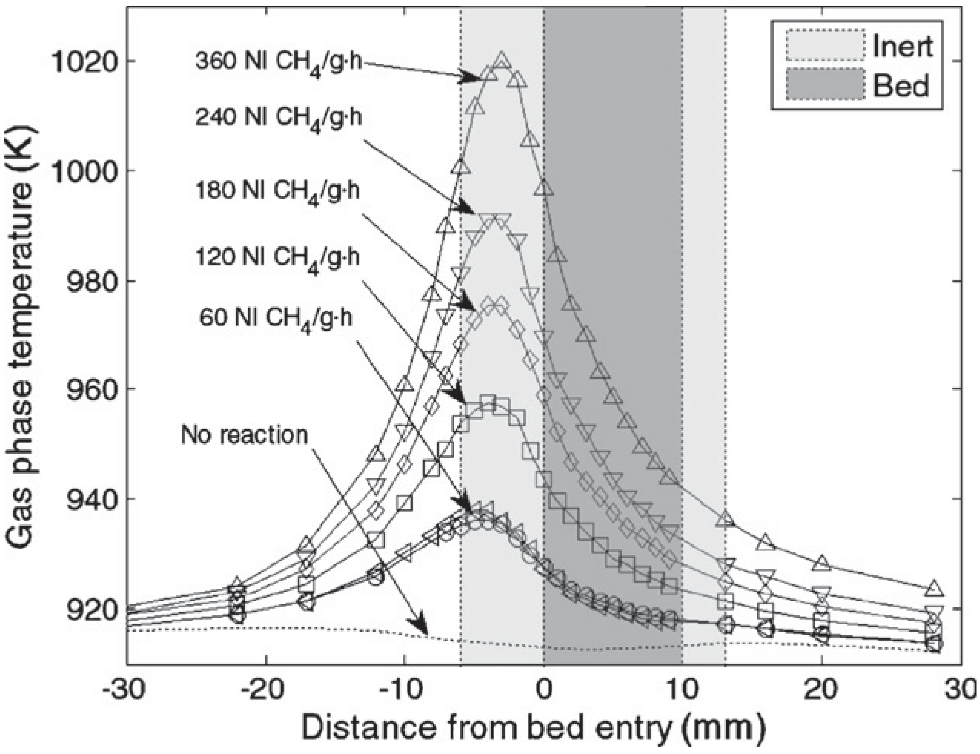

Figure 3.6 Catalytic partial oxidation on Ni/α-Al$_2$O$_3$ (25 mg) at $60\,\mathrm{l\,g^{-1}\,h^{-1}}$ to $360\,\mathrm{l\,g^{-1}\,h^{-1}}$ of CH$_4$ at 650 °C (furnace temperature). The apparent position of the temperature maximum in front of the catalyst was likely caused by catalyst fines present in the inert filling Christian Enger et al. (2008).

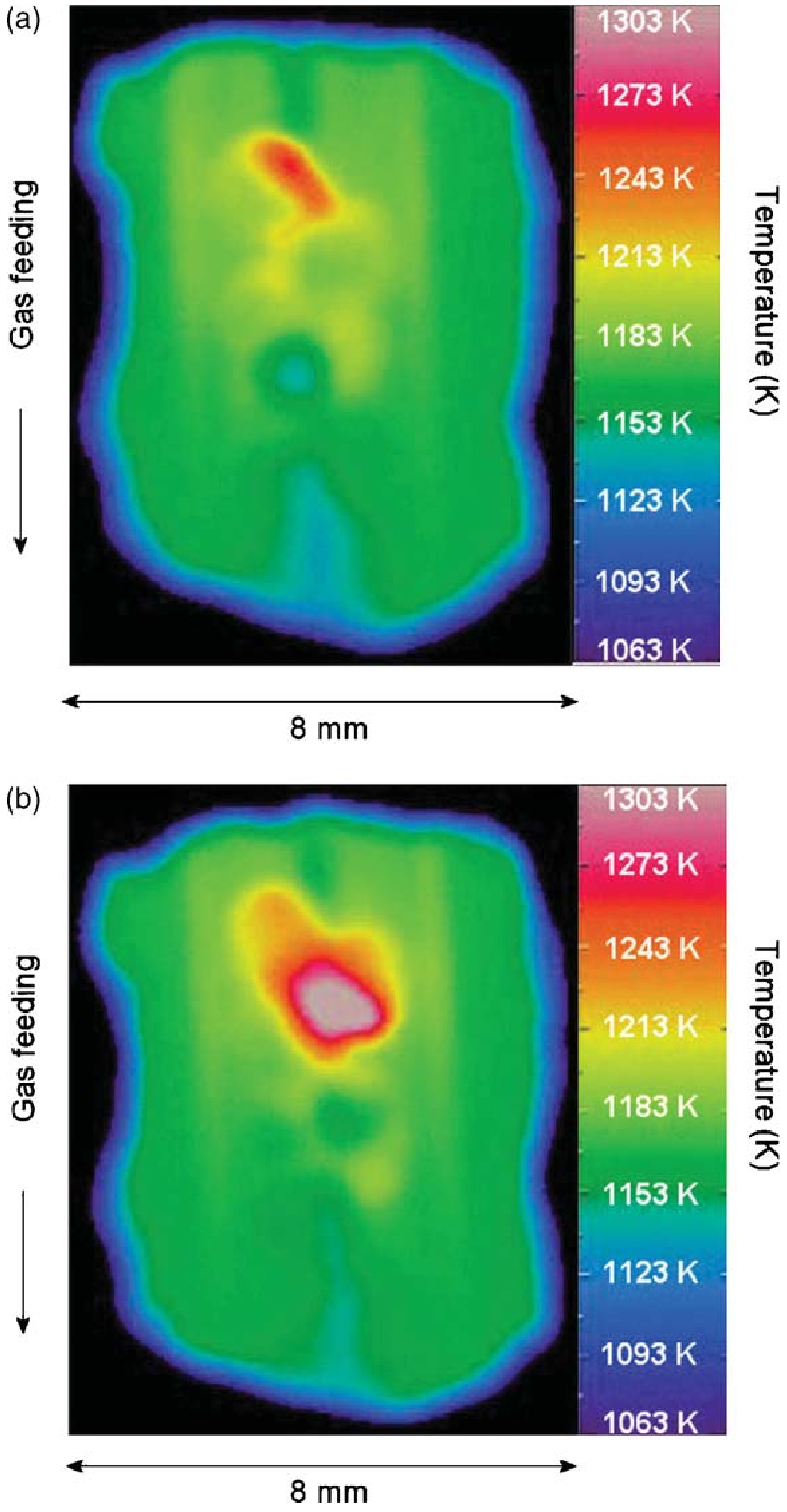

Figure 3.7 IR thermographic images of the catalyst bed during catalytic partial oxidation of methane at 850 °C, 2.5 mol g^{-1} h^{-1} (0.14 g catalyst), $CH_4/O_2/Ar=10/20/70$ and 1 bar. Catalyst bed temperature profile on (a) 0.3 g g^{-1} Rh/Al_2O_3 and (b) 0.6 g g^{-1} Pt/Al_2O_3 Li et al. (2004).

and on the type of support Christian Enger et al. (2008). Additional studies have also been completed using thermowell and pirometers inside the catalytic bed but similar conclusions and general non-agreement have been confirmed.

3.3 CPOX Catalysts

The main problems in the design of CPOX catalysts are Enger et al. (2008); Ghoneim et al. (2016) :

- high CO_2 selectivity ;
- catalyst stability ;
- catalyst deactivation coming form coke deposition on the catalyst surface ;
- and high temperature gradients within the catalytic bed.

Nobel metal have higher TOF, are less prone to oxidation and more resistant to coke deposition compared to other transition metals such as Ni Schulz et al. (2015).

However, Chin and Iglesia (2011); Chin et al. (2011a) proved using labeled C^{12} and C^{14} that as long as there is oxygen in the reactor Pd, Pt, Rh oxidize CO to CO_2 faster than CH_4 to CO. Shorter residence time leads to lower CO_2 selectivity but CH_4 conversion decreases and therefore it is not possible to increase CO yield. Only when O_2 is depleted from the catalyst surface the main oxidized product is CO but the reaction cannot operate at steady sate under these conditions. It is possible to operate the reactor in that way only when the systems limited by mass transfer.

Promising results are coming from supported metal nano particles catalyst or oxygen carriers. Nanoparticles together with improved supports have shown high reaction performance and coke stability Enger et al. (2008); Li et al. (2010a); Lou et al. (2017); Urasaki et al. (2018); Qin et al. (2018). They are stable and they catalyze the reaction with H_2/CO ratio equal to two Hotz et al. (2007); Lou et al. (2017); Wang et al. (2018); Singha et al. (2017). If on one hand metal nanoparticles lead to the desired products composition they also deactivate. Because of the unstable thermodynamic status of the nanoparticles, they tend to agglomerate in particular at increasing temperature necessary while regenerating the catalyst Gil-calvo et al. (2017); Somacescu et al. (2019).

CPOX via chemical looping in fluidized bed, where oxygen carriers are constantly regenerated to remove the deactivating carbon, has also given high performance but they require complex and expensive reactors Li et al. (2010a); Qin et al. (2018); Liu et al. (2019). CeO_2 is one of the most active catalyst in oxidation as it has low activation barrier in creating oxygen vacancies Paier et al. (2013); Yang et al. (2017).

Structured metal supports with thermal conductivity higher than traditional ceramics decrease temperature gradients and make possible to operate at high GHSVs in laminar regime Lofberg et al. (2011); Gascon et al. (2015). Because of the harsh reaction conditions, high temperature Ni−Cr stainless steel fails while FeCrAl is resistent under reaction condition and prevents deactivation blocking Cr migration to the surface Cairns et al. (1979); Reichelt et al. (2014); Kaltner et al. (2009). Foam and fibers of this alloy further enhance mass and heat transfer while maintaining low pressure drops Basile et al. (2009); Benito et al. (2015a); Neagoe et al. (2016).

3.4 Coke formation

Carbon formation is the biggest problem in the synthesis gas production. Carbon formation is higher at increasing methane/oxidizer ratio. In steam reforming this is avoided by appropriate catalyst and composition of the feed Rostrup-Nielsen and Christiansen (2011). The reactions that form coke are Trimm (1997) :

$$\mathrm{CH_4} \longleftrightarrow \mathrm{C} + \mathrm{H_2} \tag{3.11}$$

$$2\,\mathrm{CO} \longrightarrow \mathrm{C} + \mathrm{CO_2} \tag{3.12}$$

$$\mathrm{CO} + \mathrm{H_2} \longleftrightarrow \mathrm{C} + \mathrm{H_2O} \tag{3.13}$$

Eq. 3.11 is called methane cracking, Eq. 3.12 Boudouard reaction while Eq. 3.13 describes how carbon monoxide and hydrogen produces coke on the catalyst surface. All these reactions are reversible and can be used to remove carbonaceous deposits. The origin of the coke on the catalyst surface is well understood, even if some aspects have not found full explanation. It is suggested that the hydrocarbons fall apart on the catalyst surface and there form mono-atomic carbon (C_α) Wei and Iglesia (2004). Most of this carbon undergoes gassification via reaction with the coreactant but a marginal part can polymerize converting it into C_β, (Fig. 3.8). The resulting coke is commonly identified as whisker, encapsulating and pyrolitic carbon. Filamentous carbon is the most destructive, the long carbon nanofibres detach the metal particles from the support. Carbon diffuses from the surface of the metal to the interface metal-support and here build up. Continuous growth leads to full catalyst deactivation. Thermodynamically, filamentous carbon has higher free energy then graphite thus it is possible to operate at conditions that favor graphite rather than whiskers Amin et al. (2011). Coke formation depends on the metal particles size where the oxygen availability index, around the active phase, plays an important role Rostrup-Nielsen and Christiansen (2011); Lou et al. (2017). The smaller the crystals, the more resistant to coke formation showed that

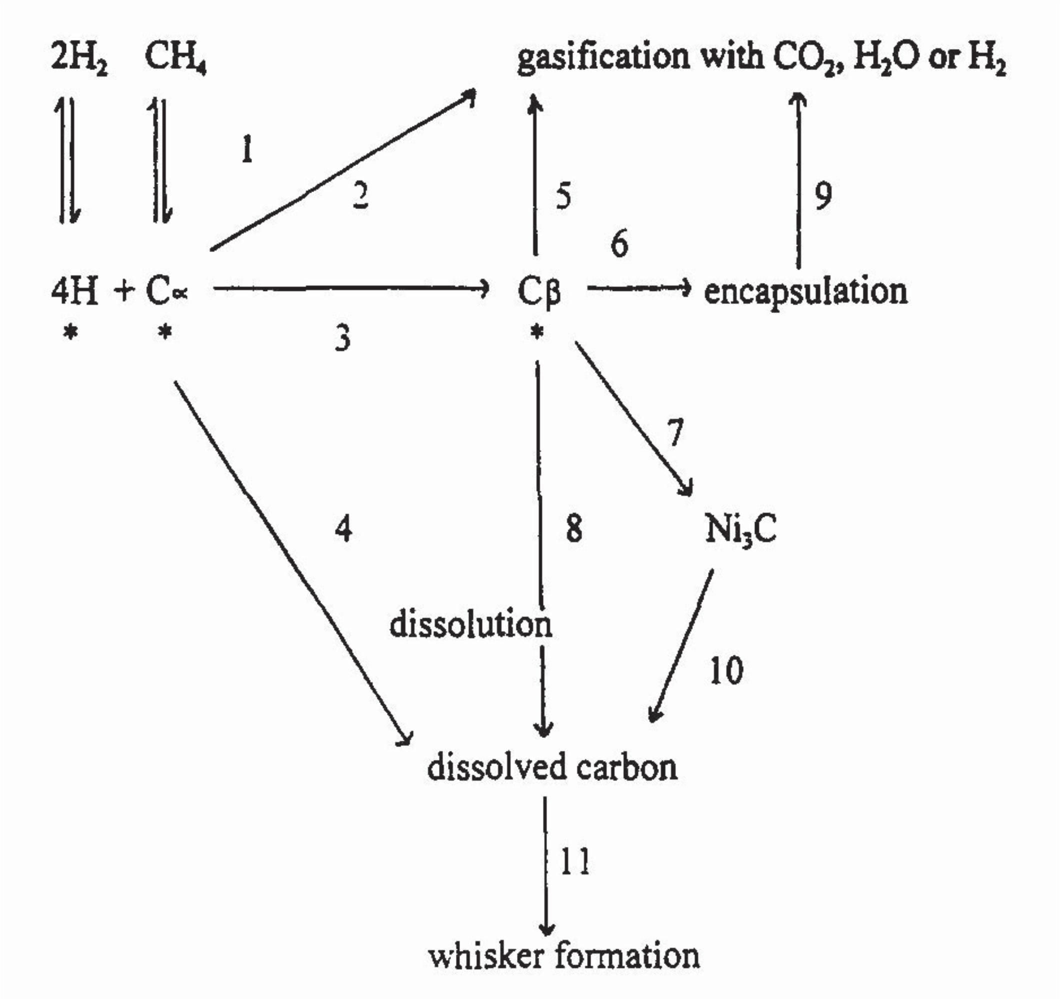

Figure 3.8 Mechanism of coke formation during SMR on Ni catalyst Trimm (1997).

the maximum temperature resistance to the formation of carbon black is 100 °C higher when crystallites of 7 nm are compared to 100 nm Rostrup-Nielsen et al. (2002). Encapsulating carbon easily forms with high molecular weight reagents or with aromatics. The probability of encapsulating carbon increases with the boiling temperature of the hydrocarbon mixture. Carbon results on a thin film of few atomic graphite layers, which cover the metal particles and leads to catalyst deactivation preventing the contact between active phase and reactants. This occurs when the amount of superficial carbon is too high and carbon removal together with diffusion do not manage to compensate its formation.

Pyrolytic carbon coming form thermal cracking is visible in tubular reformers on the walls of pipes called hot bands. These zones are often characterized by low catalytic activity as consequence they have high temperatures that activate CH_4 thermal cracking.

CHAPTER 4 ARTICLE 1 : FECRAL AS A CATALYST SUPPORT

Gianluca Pauletto, Angelo Vaccari, Gianpiero Groppi, Lauriane Bricaud, Patricia Benito, Daria C. Boffito, Johannes A. Lercher, Gregory S. Patience

Article published in Chemical Reviews (I.F. 54.0)

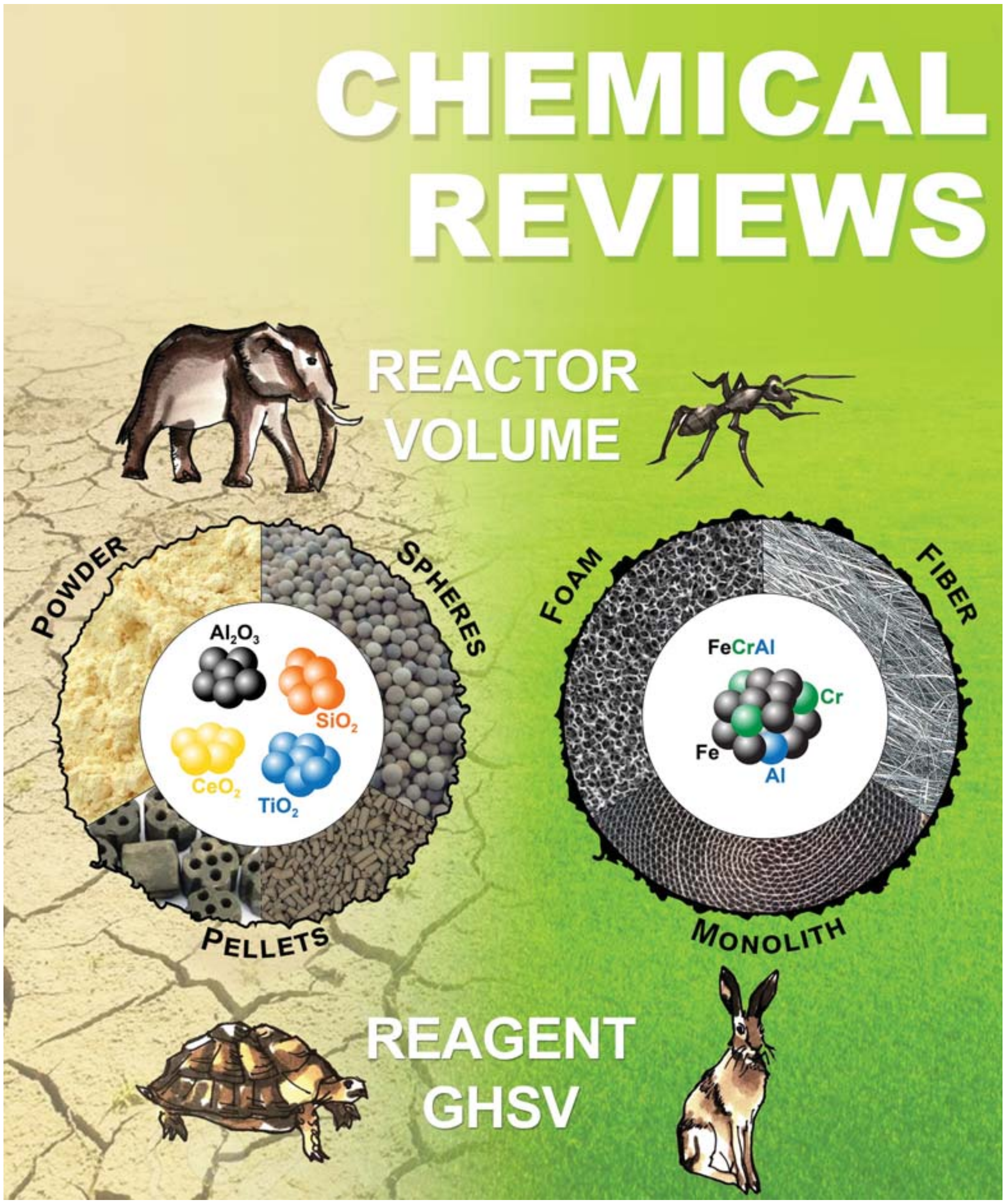

Figure 4.1 FeCrAl structures (foams, fibers, monoliths) minimize pressure drop and maximize heat and mass transfer. Al diffuses to the surface and after oxidation provides an adherent layer for catalyst. FeCrAl alloys resist oxidizing and corrosive atmospheres up to 1400 °C, which increases reaction rates and reduces reactor volumes-elements of process intensification.

4.1 Abstract

Fe, Cr, Al alloy (FeCrAl) is an exceptional support for highly exothermic and endothermic reactions that operate above 700 °C in chemically aggressive environments, where low heat and mass transfer rates limit reaction yield. FeCrAl two- and three-dimensional structured

networks—monoliths, foams and fibers—maximize mass transfer rates while their remarkable thermal conductivity minimizes hot spots and thermal gradients. Another advantage of the open FeCrAl structure is the low pressure drop due to the high void fraction and regularity of the internal path. The surface Al_2O_3 layer, formed after an initial thermal-oxidative, supports a wide range of metal and metal oxide active phases. This aluminum oxide that adheres to the metal surface protects it from corrosive atmospheres and carbon (carburization) thus allowing FeCrAl to operate at higher temperature. Top applications are industrial burners, in which compact knitted metal fibers distribute heat over large surface areas, and automotive tail gas converters. Future applications include producing H_2 and syngas from remote natural gas in modular units. This review summarizes the specific preparation techniques, details process operating conditions and catalyst performance of a several classes of reactions, and highlights positive and challenging aspects of FeCrAl.

4.2 Introduction

To meet societies aspirations of sustainable development requires innovation to substitute petroleum with renewable bio-sourced feedstocks and catalysis will figure prominently in this paradigm shift. Already, industry applies catalysis in over 80 % of the chemical processes, which represents 30 % of the global gross product C. Boffito and Van Gerven (2018); Toulhoat (2010). Solid catalysts have replaced harmful mineral acids and chloro-containing ones with the extra benefit of re-use compared to homogeneous systems. The incredible potential of heterogeneous catalysts, consists in their porous nature that can be optimized to meet reaction conditions—high temperature, pressure, and corrosive environments, for example. Consequently the share of solid catalysts in the chemical industry will continue to rise as a result of the growth in world population and the escalation of the global energy demand, which was forecast to double from 2000 to 2035 T. Mika et al. (2017); C. Boffito and Van Gerven (2018). Heterogeneous catalysis is a key component of new processes targeting green chemistry and sustainability Sudarsanam et al. (2018); Descorme et al. (2012). Indeed, in the last twenty years the field of environmental catalysts boosted the design of new solid materials capable of converting air and water pollutants generated by anthropogenic activities, as well as catalysts capable of converting heterogeneous substrates selectively—those derived from biomass Descorme et al. (2012); Sudarsanam et al. (2018); Jaber et al. (2018); Lotfi et al. (2015). Despite their numerous and indisputable advantages, heterogeneous catalyst design faces challenges to develop new sustainable processes and increase efficiency/decrease harmful and toxic byproducts in current processes. Catalyst comprising particles, pellets, and gauzes add complexity to plant operations ; mass and heat transfer resistance around the catalyst limits the reagent throughput and introduces uncertainty with respect to scale-up and modelling García-Bordejé et al. (2017) ; and, narrow pores limit applications to less bulky molecules Davis (2002). The latter limitation is particularly true for emerging biorefineries, which involves molecules such as lignin, polysaccharides and triglycerides. Synthesizing systems with interconnected micro- and mesopores, combining high specific surface area and improved mass transport remains major challenges in heterogeneous catalysis Perego and Millini (2012).

Process intensification (PI) principles suggest introducing structure or modular catalytic units to minimize spatial randomness and control preferential mass and heat transfer pathways C. Boffito and Van Gerven (2018); Gascon et al. (2015); Van Gerven and Stankiewicz (2009). The structure can fit molecular, micro-, meso- and macro-scales. In this context, besides choosing a material that is inert at the operating pressure and temperature, and act synergistically with the active component, selecting a support facilitates modularization. Industry requires high flow rates, short contact times, tight temperature control, and low pressure drop across the bed Forzatti et al. (2008). Pressure drop across structured catalysts are two orders of magnitude lower than across packed beds and radial and axial temperature gradients (local hot spots) are lower due to the higher effective thermal conductivity and the regularity of the internal path, which makes it possible to operate in the laminar regime Gascon et al. (2015).

Cordierite—a mixture of Mg, Si and Al oxides extruded as a monolith for automotive tail gas treatments—is the most common high temperature structured support.Weng et al. (2017) However, when hot spots affect the conversion and selectivity, materials with high heat transfer capacity, such as metallic supports, improve performance.

The metallurgy industry developed a Fe, Cr (up to 20 %), Al (0.5 % to 12 %) and Y (0.1 % to 3 %) alloy, which is commercialized under the name of FeCralloy® or Khantal®. Hans von Kantzow, engineer and CEO at Bultfabriks AB, discovered it in 1931, after a sample was left for years inside an oven in Hallstahammar, Sweden. FeCralloy® is a high temperature resistant steel in which Al diffuses to the surface above 800 °C. The surface Al oxidizes to Al_2O_3 in air and forms a resistant layer. The first applications were for furnaces, heating systems and electronic components. Yttrium prevents high temperature phase changes as it oxidizes first during the synthesis steps, therefore the melting steps require vacuum furnaces, which impacts the final cost of the material Cairns et al. (1979). The ductility of FeCrAl makes it easy to shape into monoliths, fibers, foams and porous materials Namkung et al. (2001); Koo et al. (2017b). The most common structures are monoliths followed by foams and fibers that are all suitable for fixed bed reactors (Figure 4.2). Changing temperatures (during process start-up and shut-down, for example) dilates the materials that would crack the surface coating if it were not for the mechanical characteristics that release the stress. This property confers its high stability Zhang (2009).

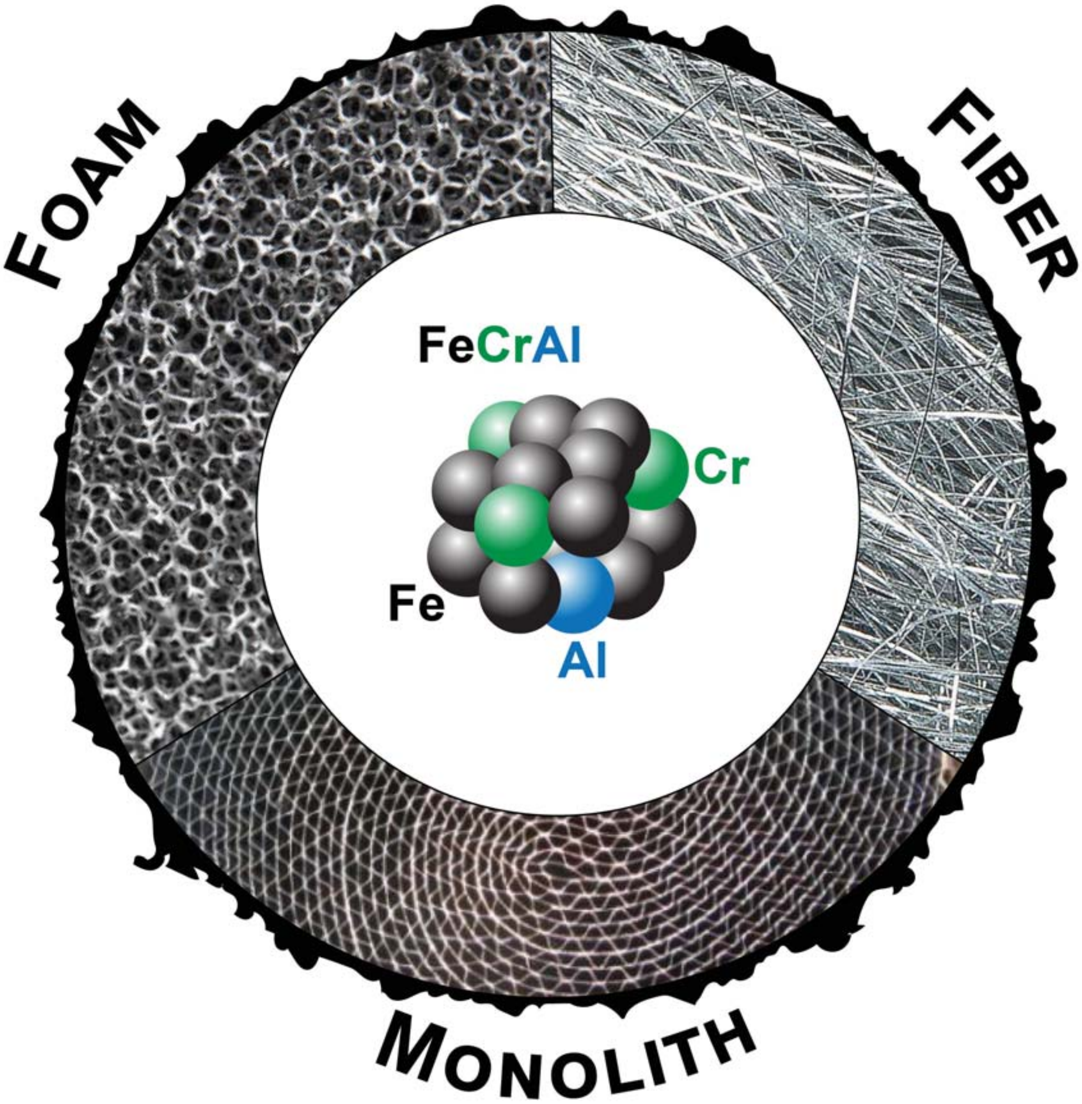

Figure 4.2 FeCrAl alloy. Structured supports : monolith, foam, fiber. External black coating Al_2O_3.

Since 1976, the automotive industry has been using this material as a catalyst support but FeCrAl burners remain the most common application. In this review, we summarize the state of the art of FeCrAl in catalysis. We have structured our review of the FeCrAl adopted as a catalyst support by type of chemistry and active phase supported.

Conductivity is the controlling radial heat transfer mechanism in the case of low void fraction systems (high solids fraction) that maximize contact between the catalyst and reactor wall Giani et al. (2005a); Bianchi et al. (2012, 2013). In traditional packed bed reactors, fluid dynamics contribute most to the heat transfer coefficient, h, while it contributes much less to structured beds. Since $h_{\mathrm{cond}} >> h_{\mathrm{conv}}$, structured beds transfer more heat in smaller volumes minimizing reactor dimensions, which respects the principles of process intensification.Aghaei et al. (2017) Even for highly exothermic and endothermic reactions, these beds operate isothermally, which is ideal to study reaction kinetics Lofberg et al. (2011).

Carbon preferentially forms on α-Fe Caplovicova et al. (2010); Altin and Eser (2001), but the Al_2O_3 surface layer minimizes contact between the gas phase and Fe thus minimizing coke deposition and carbon erosion Bauman et al. (2016); 158 (2007). Branched and bamboo nanotubes (carbon filaments) growing perpendicular to the surface of the FeCrAl indicate the presence of exposed reduced iron Chesnokov and Buyanov (2000). During methane pyrolysis, a strong reducing environment together with the carbon deposition on the surface destabilize the protective Al_2O_3 coating. As result the reduced Fe is exposed and carbon diffusing through the particle detaches the metal from the bulk and carburizes the support with deleterious consequences Borisov et al. (2014). Temperature also has an influence and the optimal growth appears at 700 °C. Less coke forms above 700 °C Longson et al. (2015). Additional and different coatings make FeCrAl a versatile material and in some cases they enhance the thermal resistance but influence carbon deposition, which carburizes the substrate with consequences on the mechanical behavior Liu and Chen (2007). Stainless steel supports for heterogeneous catalysts are sufficient for low temperature reactions (less than 700 °C), while at higher temperatures the steel degrades with time as it has no stable protective superficial oxide Frías et al. (2007); Vázquez-Gómez et al. (2012). The similar problem is also encountered in austenitic NiCr and NiCrAl form superficial chromia rather than Al_2O_3 layers and have higher density, lower electrical resistivity compared to ferretic FeCrAl. Superficial Al_2O_3 doping by Cr_2O_3 and Fe_2O_3 further stabilizes the stable alfa phase Cao et al. (2004). The maximum operating temperature of FeCrAl approaches 1400 °C, 200 °C higher than Ni containing alloys ; superficial alumina protects the bulk metal better than chromia against sulfur and carbon diffusion Jönsson et al. (2004). While traditional Ni-based materials have higher strength and creep resistance, important in the manufacturing of structural parts, the new generation of FeCrAl now have comparable mechanical properties. As little as 0.15 % by mass of Y, Zr, Mo, Mn and Si reduce elongation caused by the interaction between bulk metal and superficial ceramic layer that are, however, less important when the material has reached high hot strength as in the case of commercial Kanthal® APM or APMT. Moreover, the higher density Ni-based alloys deform more at high temperature. Aluchrom is the commercial name of another FeCrAl alloy containing 70 %, 25 % Cr, and 5 % Al. However, micro-alloying with yttrium and zirconium is absent Czyrska-Filemonowicz et al. (1995); Jönsson et al. (2012). Only in the last decade has the scientific community begun to apply FeCrAl beyond furnace elements (Figure 4.3). From 1990, the number of articles has been increasing linearly from 50 per year and now exceeds 250 per year with about 80 dedicated to catalysis Analytics (2018). The most prominent research cluster relates to microstructure and mechanical properties (red cluster in Figure 4.3), followed by oxidation (green cluster), metal composition (blue cluster with keywords Fe, Cr, Al, and Ni), and alloys, coatings, and steel (yellow cluster). Web of Science assigned 2424 journals with articles referencing FeCrAl to multidisciplinary materials science followed by metallurgy & metallurgical engineering (2225), physical chemistry (546), applied physics (418) nanoscience & nanotechnology (318), coatings & films materials science (311), and condensed matter physics (307). The most prolific journals were *J. Alloy. Compd.* with 170 articles, *Corrosion Sci.* with 100, and *Acta Mater.* with 98. Three articles, published in the 1990s, have garnered over 500 citations. Ballhaus et al. (1991); Pint (1996); McCafferty and Wightman (1998)

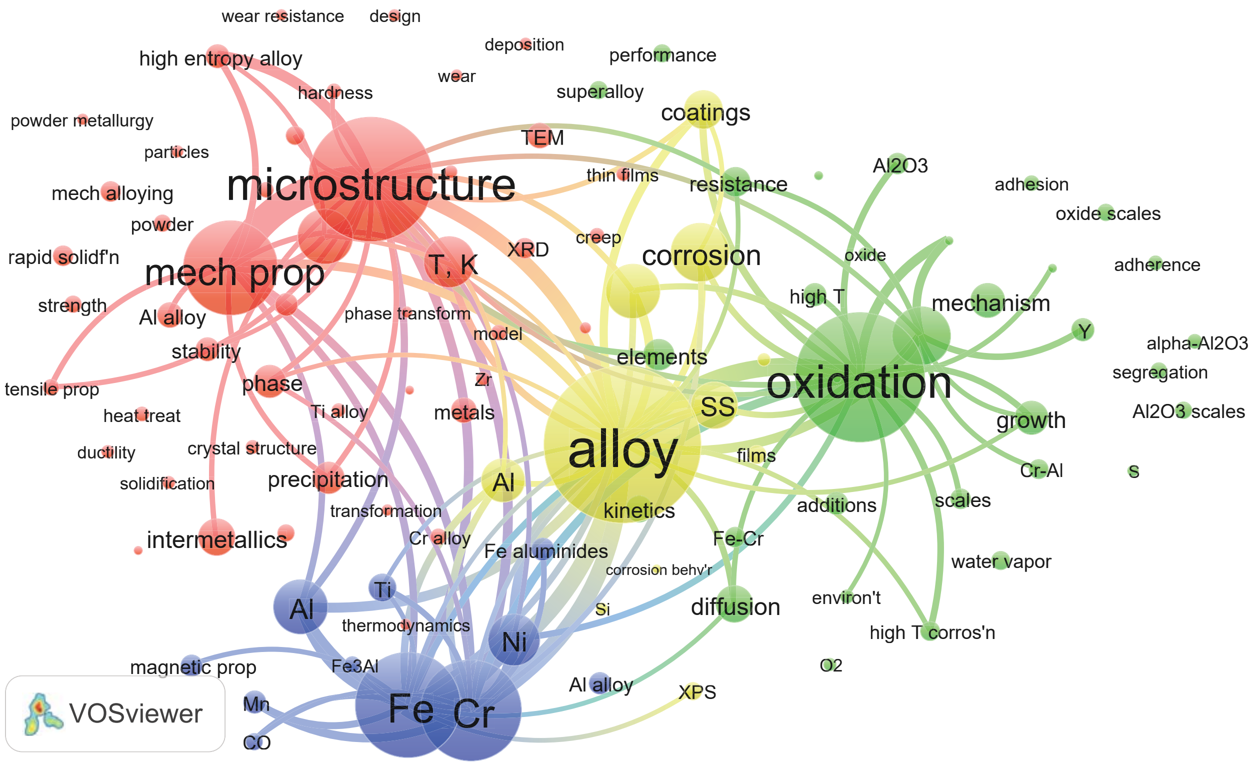

Figure 4.3 Bibliometric map generated by VOSviewer based on Web of Science Core Collection.van Eck and Waltman (2010); Analytics (2018) Keywords were FeCrAl, Kahntal and Fe Cr Al alloy. The size of each circle correlates with the occurrences in 4350 articles WoS indexed from 1989 to September 2018. VoSViewer groups the research into four clusters : microstructure (562 occurrences), oxidation (479 occurrences), Fe (476 occurrences), and alloy (709 occurrences) The smallest circles corresponds to 50 occurrences.

4.3 Heat and mass transfer in FeCrAl structures

Metal oxides as Al_2O_3, SiO_2, TiO_2, CeO_2, ZrO_2, CaO_2 are chemical resistant substrates for the synthesis of supported catalysts that operate at temperatures higher than 300 °C in the format of powder, sphere or pellet (Figure 4.4) Mizuno and Misono (1998); Chen and Mao (2007); Paier et al. (2013); Munnik et al. (2015); Montini et al. (2016); Liu and Corma (2018).

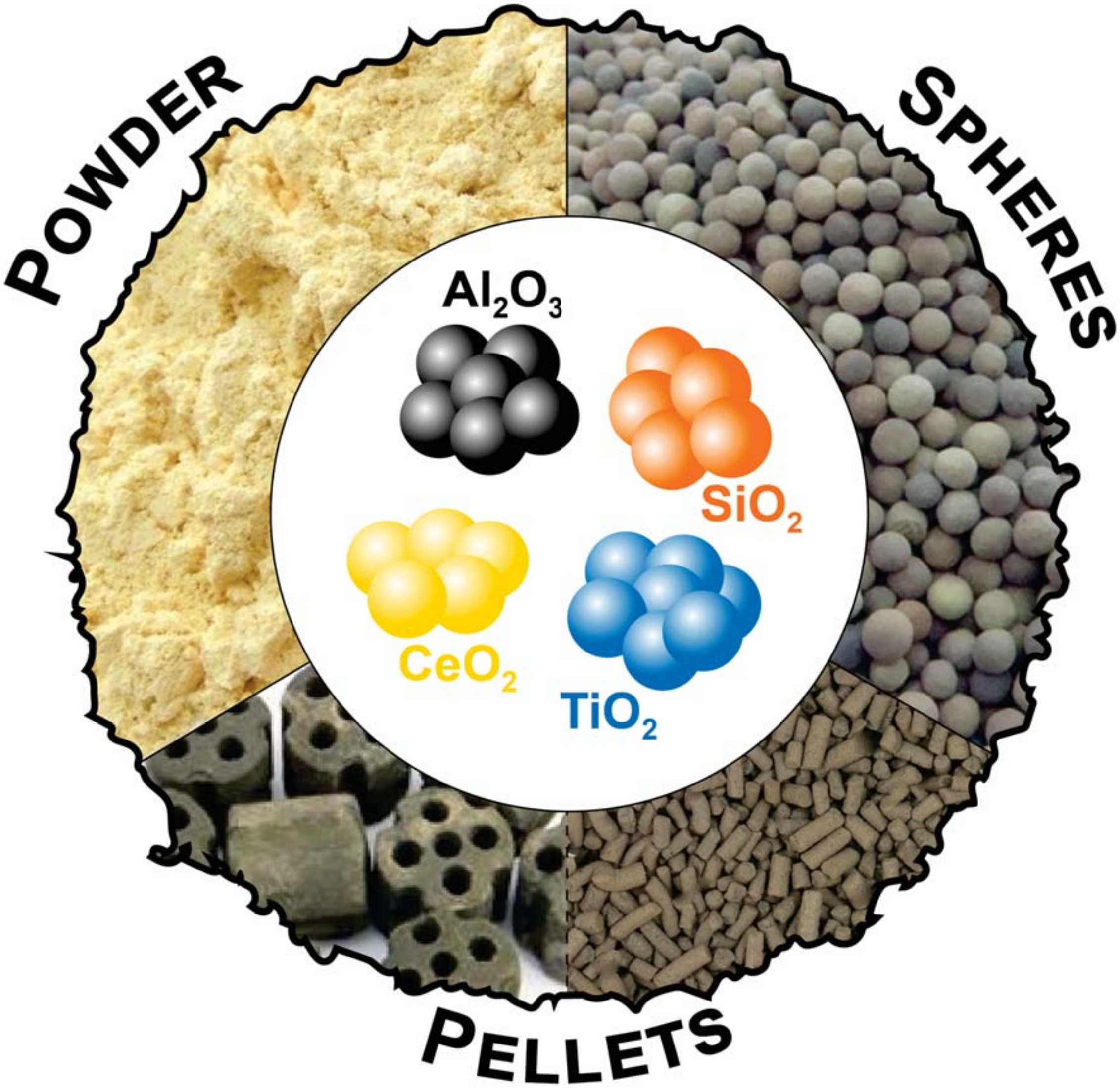

Figure 4.4 Most common ceramic supports.

During catalyst design, before hypothesizing synergies between support and active phases, considerations on the reaction such as temperature, pressure, energetic requirements, chemical properties of reagents and products help in identifying possible supports. The format of the substrates is a relevant parameter to consider, but usually in a second step, at scale larger than the lab one. However, when high flow rates, short contact times, tight temperature control, low pressure drops across the bed, high heat and mass transfer are required, traditional packed bed reactors are unsuitable Heck et al. (2001); Twigg and Richardson (2007); Gascon et al. (2015). Moreover, when the reaction conversion and selectivity suffer from hot spots and temperature gradients, high heat transfer capacity of metallic supports improves the performance. FeCrAl is the reference material for the manufacture of structured substrates (Figure 4.5) for catalytic applications at high temperatures in oxidizing environments. One feature of these structured substrates is the possibility to fine tune heat and mass transfer properties to maximize catalyst performance. This is related both to thermal conductivity, specific heat and density of the material and to the geometrical characteristics of the substrates.

4.3.1 Geometrical properties

Honeycomb structures have been the benchmark solution for after-treatment catalytic technologies over the last several decades. They consist of a multiplicity of identical parallel channels through which gas passes in a straight path, typically in the laminar flow regime. Metal FeCrAl honeycombs are manufactured by rolling a crimped sheet coupled with a flat foil around a mandrel, while ceramic substrates are extruded. Standard cell densities range from 400 cpsi to 600 cpsi (cell per square inch) with 40 µm to 50 µm thick foils Brück et al. (1995), while advanced designs reach 900 cpsi to 1600 cpsi with 25 µm to 30 µm thick foils with an open frontal area in excess of 90 % Marsh et al. (2001).

Figure 4.5 Most common examples of FeCrAl structures. Monoliths, foams and fibers (random sintered or knitted). Adapted with permission from reference mon. Copyright 2020 Catalysis.

The geometrical properties of the assembly are evaluated based on a single channel. The surface to volume ratio, S_V, is the proportion (Eq. 4.1) of the void fraction (or open frontal area of the honeycomb), ε, and the hydraulic diameter d_h (typically a triangular or sinusoidal shape) and is the determining factor in gas-solid heat and mass transfer :

$$S_{\mathrm{v}} = \frac{4\varepsilon}{d_{\mathrm{h}}} \tag{4.1}$$

S_{V} up to $4000\,\mathrm{m}^{-1}$ to $6000\,\mathrm{m}^{-1}$ are standard in conventional and advanced designs, respectively.

Sintered metal fibers substrates have been applied in catalytic burners and particulate filters. Felts are manufactured starting from small diameter fibers ($d_{\mathrm{f}} = 10\,\mu\mathrm{m}$ to $50\,\mu\mathrm{m}$) that are sintered via high temperature diffusion bonding and reach porosities in the 80 % to 85 % range. The disordered structure creates a complex flow path, and assuming the base elements are infinitely long cylindrical fibres, the surface to volume ratio is Groppi et al. (2010); Reichelt et al. (2014) :

$$S_{\mathrm{V}} = \frac{4\,(1-\varepsilon)}{d_{\mathrm{f}}} \tag{4.2}$$

With $25\,\mu\mathrm{m}$ fibers and $\varepsilon = 85\,\%$, S_{V} exceeds $20\,000\,\mathrm{m}^{-1}$ Groppi et al. (2010).

Open cell metal foams consist of cavities (cells) accessible through windows (pores) in an interconnected 3D solid matrix made of struts that intersect in nodes. In FeCrAl foams, porosity reaches 95 % with pore densities in the range of 10 ppi to 100 ppi (pore per inch). Geometrical models assume that the structure consists of repeating unit cells—cubic Lu et al. (1998), dodecahedral Huu et al. (2009), and tetrakaidecahedral Inayat et al. (2011). The latter polyhedron, also called a Kelvin cell, characterizes the foam geometry best Gibson and Ashby (1988). Refinements of the geometrical model include the shape of the strut cross-section that, due to minimum surface energy reasons, changes from circular to triangular and to triangular concave with increasing void fraction Inayat et al. (2011) and the node-strut distribution of the solid material Ambrosetti et al. (2017). In general, S_{V} increases with pore density and solid fraction of the foam : $S_{\mathrm{V}} > 5000\,\mathrm{m}^{-1}$ for a 100 ppi foam at $\varepsilon = 0.9$ Ambrosetti et al. (2017).

4.3.2 Gas-solid heat and mass transfer

Gas-solid heat and mass transfer rate coefficients, h and k_{m}, like S_{v}, depend on structure substrate geometry. Researchers apply the Colburn analogy for heat and mass transfer in ducts of honeycomb monoliths. The classical Hawthorn correlations relate the non-dimensional Nusselt number (N_{Nu}) for heat transfer and Sherwood number (N_{Sh}) for mass transfer to the Reynolds number (N_{Re}), Schmidt number (N_{Sc}) and Prandtl number (N_{Pr}), assuming that the characteristic length is d_h Hawthorn (1974) :

$$N_\mathrm{Nu} = 3.66 \left(1 + 0.095 \frac{N_\mathrm{Re} N_\mathrm{Pr}}{z} d_\mathrm{h}\right)^{0.45} \tag{4.3}$$

$$N_\mathrm{Sh} = 3.66 \left(1 + 0.095 \frac{N_\mathrm{Re} N_\mathrm{Sc}}{z} d_\mathrm{h}\right)^{0.45} \tag{4.4}$$

The coefficient 3.66 represents the asymptotic solution for fully developed laminar flow in ducts, while the N_Re term accounts for the development of the velocity, temperature (Eq. 4.3), or concentration profiles (Eq. 4.4), which decrease along the channel coordinate, z. These Hawthorn correlations apply to average transfer coefficients in circular channels but have been adapted to local heat transfer coefficients Tronconi and Forzatti (1992) and alternative geometries including triangular and sinusoidal channels typical of FeCrAl honeycombs Bhattacharya et al. (2004). Correlations mainly refer to laminar flow conditions which cover most of the practical applications, however, advanced configurations have been developed for FeCrAl honeycombs, which enhances heat and mass transfer coefficients by repeated disruption of the laminar flow structure Downey et al. (2007).

The assessment of the gas-solid heat and mass transfer performance of open cell foams is still debated in the literature. The choice of the characteristic length to be adopted in N_Nu and N_Sh correlations is a key issue. Originally, the equivalent channel diameter was assumed to be the pore size Richardson et al. (2003). Later, the mean pore diameter was defined as the size of the internal pore window and the strut diameter Garrido et al. (2008). For metallic foams, Giani et al. (2005b,a) stated that the average strut diameter, $d_\mathrm{s,av}$, was a more representative characteristic length when considering the flow path in the foam structure and they developed a correlation based on the analogy with convective heat transfer in bundles of tubes. The approach was further refined by combining experimental tests on CO oxidation with computational fluid dynamic simulations (CFD) developing a correlation (Equation. 4.5) based on the combination of asymptotic contributions associated with creeping and turbulent flow, respectively Bracconi et al. (2018a) :

$$N_\mathrm{Sh} = \varepsilon^{-2} \left(0.566 N_\mathrm{Re}^{0.33} + 0.039 N_\mathrm{Re}^{0.8}\right) N_\mathrm{Sc}^{\frac{1}{3}} \tag{4.5}$$

Few studies have been performed on sintered metal fibers Hawthorn (1974); Reichelt and Jahn (2017) but foam and fiber felt performance correlate with the same equation with

Sauter mean diameter, d_{sauter} as the characteristic length :

$$d_{\mathrm{Sauter}} = \frac{6\left(1-\varepsilon\right)}{S_{\mathrm{V}}} \tag{4.6}$$

$$N_{\mathrm{Sh}} = 1.26\left[\frac{1-\left(1-\varepsilon\right)^{\frac{5}{3}}}{2-3\left(1-\varepsilon\right)^{\frac{1}{3}}+3\left(1-\varepsilon\right)^{\frac{5}{3}}-2\left(1-\varepsilon\right)^{2}}\right]^{\frac{1}{3}}\left(0.991N_{\mathrm{Re}}^{\frac{1}{3}}N_{\mathrm{Sc}}^{\frac{1}{3}}+\frac{0.037N_{\mathrm{Re}}^{0.8}N_{\mathrm{Sc}}}{1+2.44N_{\mathrm{Re}}^{-0.1}\left(N_{\mathrm{Sc}}^{\frac{2}{3}}-1\right)}\right) \tag{4.7}$$

Internal mass transfer in the porous washcoat is as important as external mass transfer because the effective intraporous diffusivity is low. However, it is negligible when considering heat transfer : the gas phase boundary layer is much larger than the porous washcoat thickness and its thermal conductivity is one order of magnitude lower ($0.05\,\mathrm{W\,m^{-1}\,°C^{-1}}$ for air vs. $0.2\,\mathrm{W\,m^{-1}\,°C^{-1}}$ for a porous ceramic layer).

4.3.3 Heat transfer in FeCrAl structures

The effective conductivity, k_{eff} is a sum of the contributions from conduction, $k_{\mathrm{eff,cond}}$, convection, $k_{\mathrm{eff,conv}}$, and radiation, $k_{\mathrm{eff,rad}}$:

$$k_{\mathrm{eff}} = k_{\mathrm{eff,cond}} + k_{\mathrm{eff,conv}} + k_{\mathrm{eff,rad}} \tag{4.8}$$

Referring to the cross sectional direction of a honeycomb structure, the convective term is absent as the flow path is segregated in the parallel channels. Also radiation is negligible because the channel wall shielding and the large aspect ratio of the channel geometry, results in very low view factors along the axial direction. With respect to conduction, geometric anisotropy of the honeycomb structure must be considered. In the axial coordinate heat flows along the gas and the solid phases, so the axial effective thermal conductivity $k_{\mathrm{eff,ax}}$ is the sum of the intrinsic gas conductivity, k_{g} and solid conductivity k_{s} weighted by their geometrical fraction Groppi and Tronconi (1996) :

$$k_{\mathrm{eff,ax}} = k_{\mathrm{g}}\varepsilon + k_{\mathrm{s}}\left(1-\varepsilon\right) \tag{4.9}$$

Because of FeCrAl's relative high thermal conductivity, which increases from $12\,\mathrm{W\,m^{-1}\,K^{-1}}$ at room temperature to $25\,\mathrm{W\,m^{-1}\,K^{-1}}$ at 1200 °C (Figure 4.6), the solid term dominates Field et al. (2015).

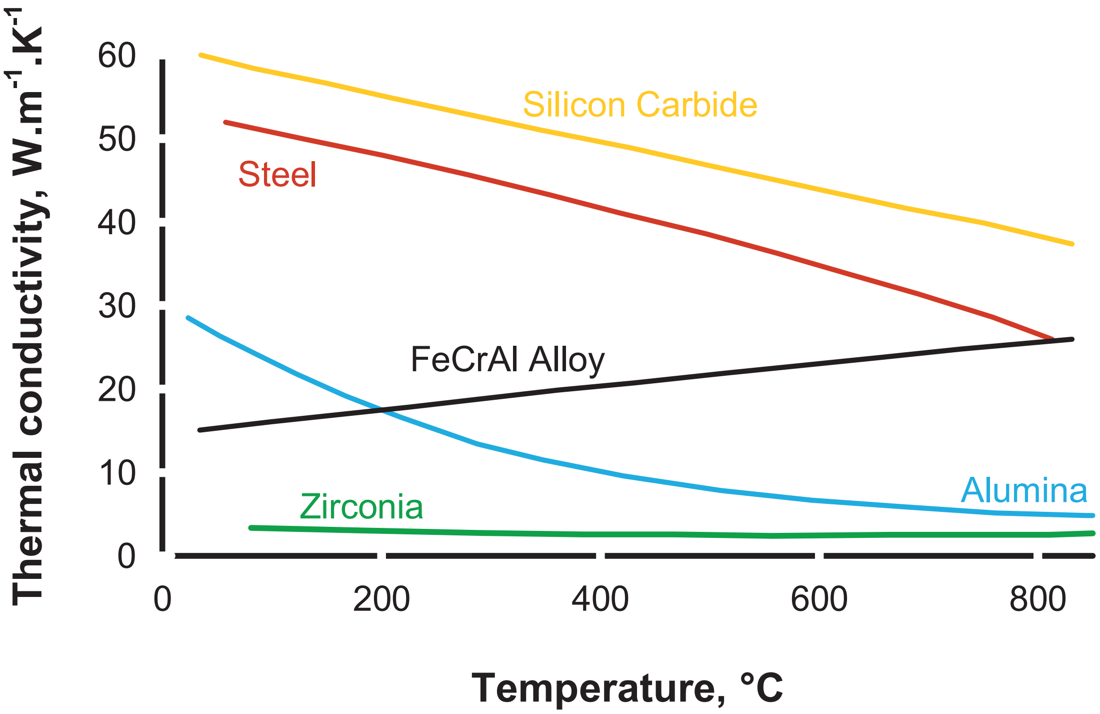

Figure 4.6 Thermal conductivity vs temperature of some of the most used catalyst supports kyo.

On the other hand, heat conduction along the cross sectional direction is limited due to the more tortuous path along the solid walls and, mainly, to the lack of continuity of the structure associated with the manufacturing process of FeCrAl monoliths. The equations developed for extruded honeycombs are inapplicable since the lower contact points between the rolled layers result in a major resistance to heat transfer along the transversal coordinate Groppi and Tronconi (1996); Visconti et al. (2013).

As opposed to honeycombs, open cell foams are isotropic, which guarantees the same effective conductivity in all directions. Two approaches account for the heat transport term : one approach, adapted from porous media literature, assumes that the effective conductivity is a weighted average of in-series in-parallel heat conduction paths in the solid and gas phases :

$$k_{\mathrm{eff,cond}} = b k_{\mathrm{serial}} + (1-b)\, k_{\mathrm{parallel}} \tag{4.10}$$

where

$$k_{\mathrm{parallel}} = k_{\mathrm{g}} \varepsilon + k_{\mathrm{s}} (1-\varepsilon) \tag{4.11}$$

and

$$k_{\text{serial}} = \left(\frac{\varepsilon}{k_{\text{g}}} + \frac{(1-\varepsilon)}{k_{\text{s}}} \right)^{-1} \tag{4.12}$$

Several studies report that b varies from 0.63 to 0.65 for metallic Bhattacharya et al. (2002) and ceramic foams Edouard et al. (2010); Wallenstein et al. (2014).

The second approach considers the tortuosity, τ, of the heat flow path along the solid interconnected structure :

$$k_{\text{eff,ax}} = k_{\text{g}}\varepsilon + \frac{k_{\text{s}}\,(1-\varepsilon)}{\tau} \tag{4.13}$$

where τ depends on void fraction according to Bracconi et al. (2018b) :

$$\tau = \left(\frac{1}{3} + \frac{2}{3}\,(1-\varepsilon) \right)^{-1} \tag{4.14}$$

which respects the theoretical asymptotes, $\tau = 3$ as $\varepsilon \to 1$ and $\tau = 1$ as $\varepsilon \to 0$ Lemlich (1978).

Because foams are open, both convective dispersion and radiation contribute to Eq. 4.8. For the convective dispersion terms, the few available literature correlations include the Peclet number, N_{Pe} :

$$\frac{k_{\text{eff,conv}}}{k_{\text{g}}} = \frac{N_{\text{Pe}}, x}{K_{\text{r}}} \tag{4.15}$$

where x is the characteristic length and K_{r} is the radial dispersion coefficient. The square root of the permeability Calmidi and Mahajan (2000), the cell sizeEdouard et al. (2010) and the mean pore diameter Wallenstein et al. (2014) have been used as characteristic lengths, with K_{r} equal to 16.67, 14.5 and 8, respectively. Considering air as the flow medium, the convective dispersion term is comparable with the conductive term at $10\,\text{m}\,\text{s}^{-1}$ in a 60 ppi FeCrAl foam with $\epsilon = 0.9$. The Rosseland approximation applies for the radiation term :

$$k_{\text{eff,rad}} = \frac{16\sigma_B T^3}{3E_{\text{r}}} \tag{4.16}$$

where σ_{B} is the Stefan-Boltzmann constant and E_{r}, the Rosseland extinction coefficient, which is a function of the foam geometrical properties where d_{c} is the diameter of the foam cell :

$$E_{\text{r}} = C_{\text{r}}\frac{(1-\varepsilon)^{0.5}}{d_c} \tag{4.17}$$

with $C_{\text{r}} = 2.65$ as proposed by Bianchi et al. Bianchi et al. (2012), the radiation term is negligible with respect to the conduction and convection except for FeCrAl foams with high void fraction ($\epsilon > 95\,\%$) and low pore density 10 ppi to 20 ppi operating below 500 °C.

When honeycomb and foams are loaded in a tube casing, the local resistance at the wall-structure interface contribute to the overall heat transfer rates towards the external environment Bianchi et al. (2012); Groppi and Tronconi (2005).

4.4 Catalyst preparation

Nijhuis et al. (2001); Avila et al. (2005); Meille (2006); Mehla et al. (2019) reviewed structured catalyst support preparation, including FeCrAl. The two main approaches to coat a catalytic layer on a 3D support include (Figure 4.7) :

- **i)** deposition of a ready-made catalyst (and/or support), and
- **ii)** in situ growth of the catalyst (and/or support)Alm (2010); Montebelli et al. (2014); Laguna et al. (2016a).

Catalytic films comprise metal oxides containing the active phase, metallic particles, or zeolites ; in situ syntheses of hydroxides form a layer of metal oxides after calcination.

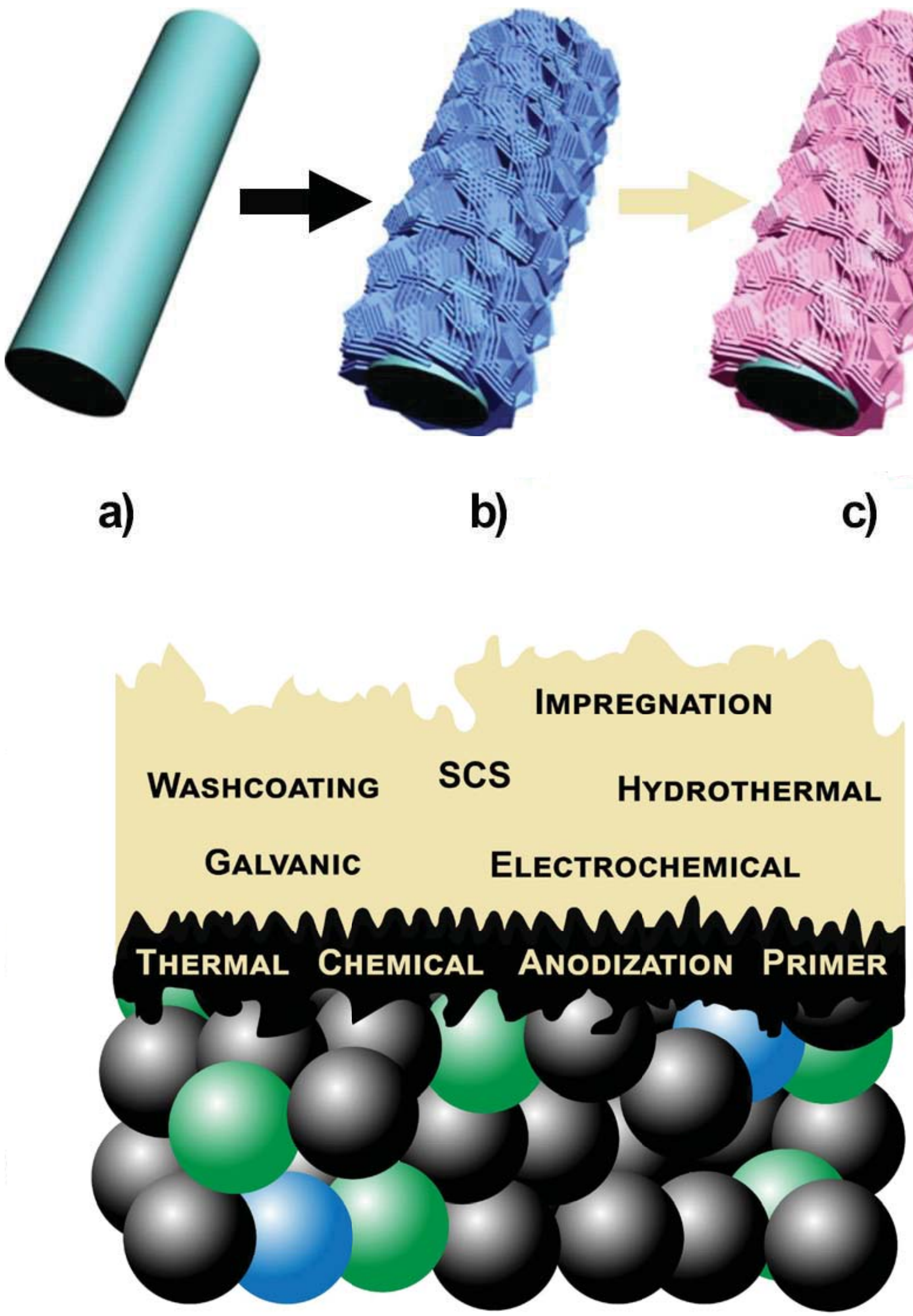

Figure 4.7 FeCrAl catalyst preparation : a) FeCrAl, b) FeCrAl after pretreatment, c) FeCrAl after coating of catalytic layer. Pretratments (black layer) : thermal and chemical treatment, anodization and primer deposition. Coating of catalytic layer (ochre) : i) washcoating ; ii) impregnation followed by calcination, solution combustion synthesis (SCS), hydrothemal methods, galvanic displacement and electrochemical processes. Adapted with permission from reference Chai et al. (2017a). Copyright 2017 American Chemical Society.

Herein, we describe methods to coat FeCrAl materials—honeycomb monoliths, fibers, meshes and open-cell foams—and focus on the in situ synthesis techniques developed in the last few years. In the sections dealing with the application of the structured catalysts, we report the specific preparation technique and its effect on the catalytic activity.

4.4.1 Pretreatment of the FeCrAl

Low surface area, low chemical interaction, and a mismatch between thermal expansion coefficients of the ceramic coating and the metallic support compromise the stability of structured catalyst on metallic supports. Consequently, the catalytic film creeps and peels during preparation and under reaction conditions. Pretreating and preoxidizing the metallic supports increase the available surface area and improve coating adhesion, which protects the metal chu (2002); Zhang (2009); Reichelt et al. (2014); Cairns et al. (1979). The parent FeCrAl surfaces are smooth on a µm length scale and chemical species bind poorly to it (Figure 4.8). After the preoxidation step, the surface has a rough sandpaper like quality with ridges and valleys. Thus, preoxidition produces a surface Al_2O_3 layer that promotes chemical interactions between the substrate and active phase.

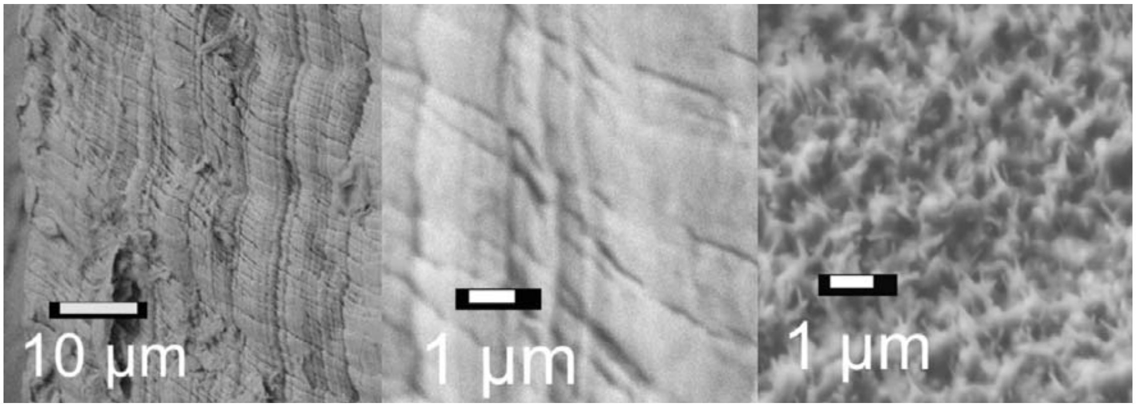

Figure 4.8 FeCrAl fiber surface before preoxidation (two picture on the left) and after (right).

Aluminum oxide is a common support because of its versatility to stabilize catalytically active materials for a variety of reactions. Production procedures consists of the thermal dehydration of aluminum hydroxide that produces eight Al_2O_3 allotropes but only the α, γ, δ and θ phases are common. Temperature influences the physical conformation and the transitions from one phase to the other Cai et al. (2003).

Thermal and chemical treatment

In the case of FeCrAl metal support, the thickness and homogeneity of the Al_2O_3 produced during the initial thermal pretreatment is important but insufficient for every chemical system where precise catalyst formulations are required, as is the case of environmental reactions Martínez Tejada et al. (2013). In a 500 h stability experiment for preferential CO oxidation operating between 100 °C to 300 °C Fe, Cr and Y migrated from the bulk to the wash coating and there deactivated the catalyst Laguna et al. (2016b). A 22 h-preoxidation treatment at 950 °C was insufficient to create an Al_2O_3 barrier between the metal support and washcoat so cations continued to migrate from the bulk Martínez Tejada et al. (2013). Cr from a FeCrNi support migrated within 24 h on-stream operation after a 650 °C peroxidation step, while migration in a FeCrAl was undetected Kaltner et al. (2009). During thermal pretreatment of FeCrAl (above 800 °C), Al migrates to the surface and oxidizes to create a Al_2O_3 coating (Figure 4.9) Cairns et al. (1979); Jönsson et al. (2004); Rallan et al. (2015a); Rallan and Garforth (2014). This coating binds compounds and has high heat shock resistance without shelling after 5000 cycles at 1000 °C (Figure 4.10(a)) Tran et al. (2007).

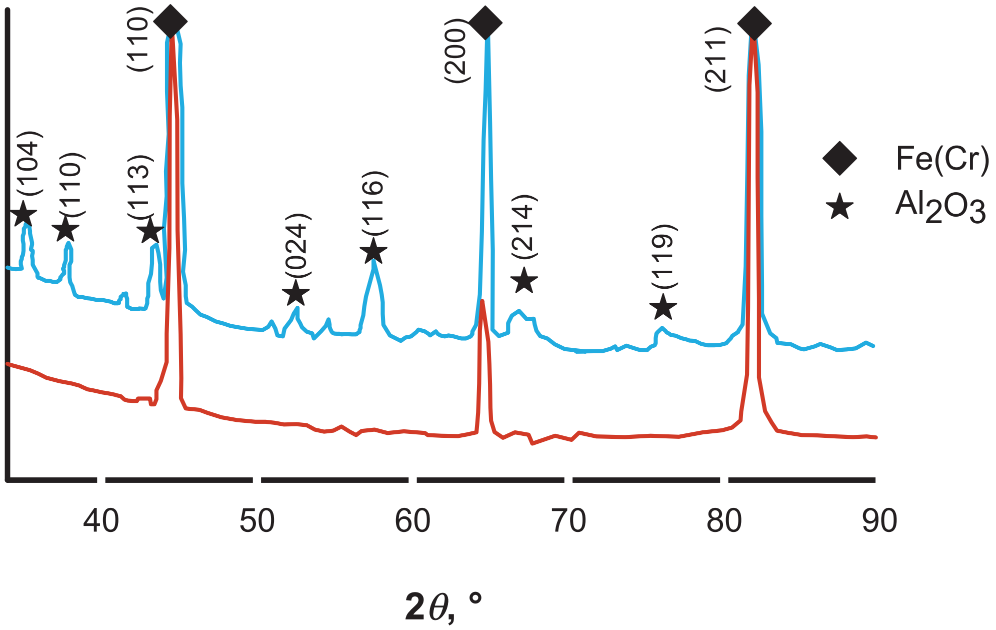

Figure 4.9 X-ray diffraction (XRD) analysis of FeCrAl before (red) and after (blue) preoxidation. Adapted with permission from reference Kim et al. (2012). Copyright 2012 Elsevier.

Additional FeCrAl pretreatment is however necessary, because the Al_2O_3 layer (after preoxidation) is rarely thick enough to protect the metal, and the surface area is too low for catalysis (Figure 4.10(b)). Chemical pretreatment of FeCrAl increases the oxidation rate as well as the superficial roughness that creates mechanical junctions (Figure 4.10(c)) Zhang et al. (2009). Thermal pretreatment is more effective than the chemical, but combining both is best (Figure 4.10(d)) Wu et al. (2017).

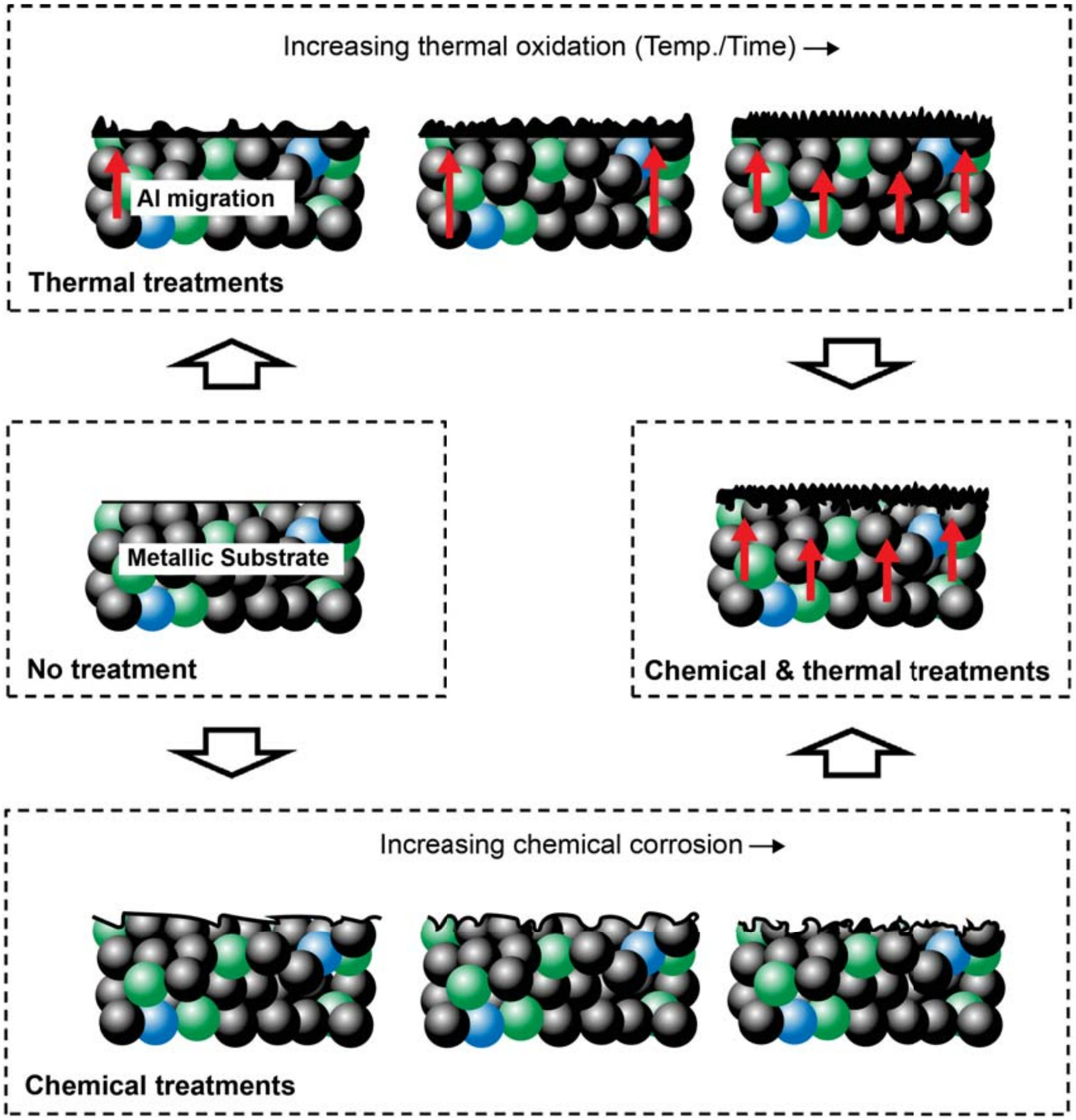

Figure 4.10 Morphological changes as a function of thermal pretreatment time and temperature (a), chemical pretreatment and corrosion (c) on the untreated FeCrAl (b). Al migration to the surface (red arrows) and Al_2O_3 (black). Adapted with permission from reference Wu et al. (2017). Copyright 2017 Elsevier.

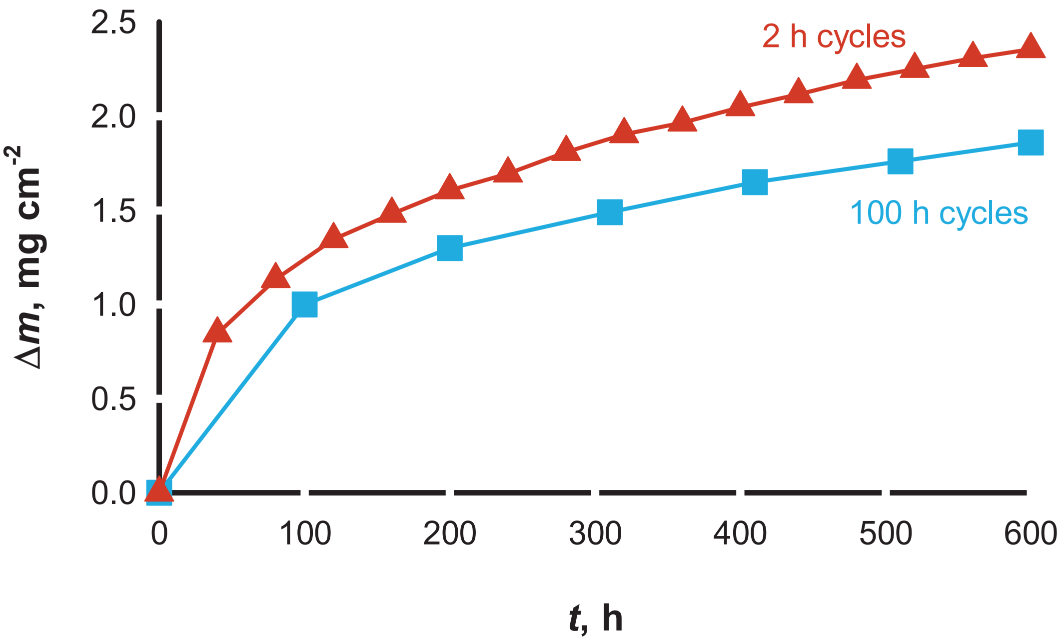

Figure 4.11 Mass increase depending on the air oxidation cycle duration at 1200 °C. Adapted with permission from reference Quadakkers et al. (2004). Copyright 2004 Springer Nature.

FeCrAl preferentially begins to degrade at points where the Al_2O_3 surface has defects or inhomogeneities Chadli et al. (2009). Cr_2O_3 between the bulk metal and alumina coating provides additional stability to the support, but the mass fraction of Al in the alloy is the determining factor for life-time Nicholls et al. (2003). α-Al_2O_3 preserves the metal better than γ, δ, and θ phases, because it minimizes oxygen diffusion Reszka et al. (2006).

α-Fe, body-centered cubic, in the FeCrAl bulk determines the morphology of the Al_2O_3 formed during oxidation. Folding, stretching, and bending (mechanical deformations) of the support changes the shape and the orientation of Fe and therefore the thickness of the final Al_2O_3 Białas et al. (2008). The oxidation rate, and thus the nature and thickness of the coating, varies with the oxidative environment composition—air, H_2O, O_2, and O_2 plus SO_2—temperature, time, substrate origins, and geometry. The chemical composition of the superficial coating changes with temperature : below 900 °C mixtures of Fe, Cr and Al oxides form. At 900 °C the coating consists mostly of α-Al_2O_3 with some γ or θ- Al_2O_3 and a rich intra layer of Cr oxide. The mass fraction of Al metal hovers at 80 % up to a depth of 350 nm then drops to below 10 % at 600 nm. H_2O in the oxidizing mixture favors metastable phases

Engkvist et al. (2009). The α phase forms in the range of 900 °C to 1100 °C while several allotropes co-exist at lower temperatures. Chadli et al. (2009)

The oxide layer grows following a cubic time dependence even if possible discrepancies might appear as a result of thermal cycling cracks and support inhomogeneity Quadakkers et al. (2004). Higher quantities of Al in the alloy increase the thermal stability of FeCrAl, because Al oxidizes into a thicker protective layer Bennett et al. (2005). However, not all Al diffused to the surface oxidizes because the growing Al_2O_3 thickness blocks metal-oxygen contact.

In short-time thermal cycles, the oxide layer cracks and exposes additional Al (Figure 4.11) that reacts and forms a Al_2O_3 grain. More Al_2O_3 increases oxidation resistance but, on the other hand, a higher number of grain boundaries decreases it as O_2 diffusion increases. After H_2 annealing, La-Zr and La-Hf in the bulk reduce the oxidation state of the alloy and they reduce the presence of both Fe and Cr in the oxide layers Fukuda et al. (2003).

Thermal oxidation in O_2 and SO_2 atmospheres, or deposition of active catalyst and alumina via magnetron sputtering creates acid and basic sites that change the catalytic activity Reszka et al. (2011, 2006). Even though the magnetron radio frequency (RF) is six times more efficient than direct current (DC), it operates on a small surface area limited by the geometry of the source Reszka et al. (2005). Magnetron sputtering supplies superficial Al_2O_3 that helps to control the morphology but powder embedded techniques also increase superficial aluminium that produces nanowires during oxidation. In this case, thermal stress does not crack the additional alumina washcoat that is often added Wu et al. (2005).

Anodization

Anodic oxidation applies an electric field to an electrolyte, usually an acid (H_2SO_4), in contact with a material that generates a porous oxide layer at the surface, while dissolving the support. Time, current density, temperature, type of electrolyte, and its concentration determine morphology, porosity, and thickness of the oxide layer. This result is different from that produced by calcination. During anodization of FeCrAl, the metals component dissolve generating channels of ca. 1 µm to 4 µm perpendicular to the surface and simultaneously an amorphous oxide film develops with cavities at the nanometeric scale ; iron preferentially dissolves compared to chromium Li et al. (2017b,a).

Deposition of a primer

Calcined substrates coated with an intermediate layer (primer) have higher chemical affinity between the coating and FeCrAl. Boehmite (AlOOH) sol, the precursor for Al_2O_3, can be prepared by dispersion of DisperalTM in an HNO_3 aqueous solution. The viscosity of the slurry depends on the concentration of the acid, the HNO_3/Al_2O_3 ratio, pH and particle dimensions ; the concentration of the solid phase in the slurry influences the adhesion of the particles on metal fibers Valentini et al. (2001). Alternatively, an AlOOH sol is produced by direct reaction between aluminum foils and an HCl solution (a mass fraction of 10 % HCl) Zhao et al. (2003). A dip-coating methodology (vide infra), controlling the withdrawal rate, is used to deposit the sols on foams or plates.

Some authors reported the synthesis of metal supported catalysts after the intermediate deposition of enamel layers that creates a barrier between metal support and superficial coating. This technique, normally used in the manufacturing of steel reactors for corrosive atmosphere, has mainly been reported for metals structures that do not form a protective superficial Al_2O_3 layer Serres et al. (2012). Even if the barrier properties of dense enamel to cation migration are higher compared to Al_2O_3, the final stability of the coating is negatively affected by a low thermal expansion coefficient of the enamel Smeacetto et al. (2011). Syngas type reactions are to be avoided as the Si in the enamel reacts with hydrogen. This is a similar challenge that the refractory industry solved with applying high purity alumina Wright and Wolff (1948); Herbell et al. (1998); Laguna et al. (2016b). Enamel coatings work best at lower temperatures but lack mechanical stability above 800 °C Jönsson et al. (2004, 2012). Coating surfaces with enamel introduces interesting barrier properties for precise catalyst formulations. Annealing enamel requires precise operating conditions to minimize Cr migration as the enamel densifies Laguna et al. (2016b); Domínguez et al. (2014); Laguna et al. (2016a).

4.4.2 Washcoating of a ready-made catalyst or support

Washcoating with ready-made catalysts and supports has evolved over time to improve adhesion and loading and to preserve the properties of the powder catalysts. This process includes :

i) filling the voids of the structured support with a powder slurry or a sol-gel dispersion (liquid-like material) by dipping it for seconds ;

ii) removing the excess fluid ;

iii) drying and calcining ;

iv) repeating the procedure to reach the desired catalyst loading.

The resulting film thickness depends on the balance between fluid viscosity (rheology), and the slurry removal procedure Meille (2006); Laguna et al. (2016a); Montebelli et al. (2014). Final cladding adhesion depends on preoxidation, binder and slurry composition (Figure 4.12) Jia et al. (2007a); Zhao et al. (2003).

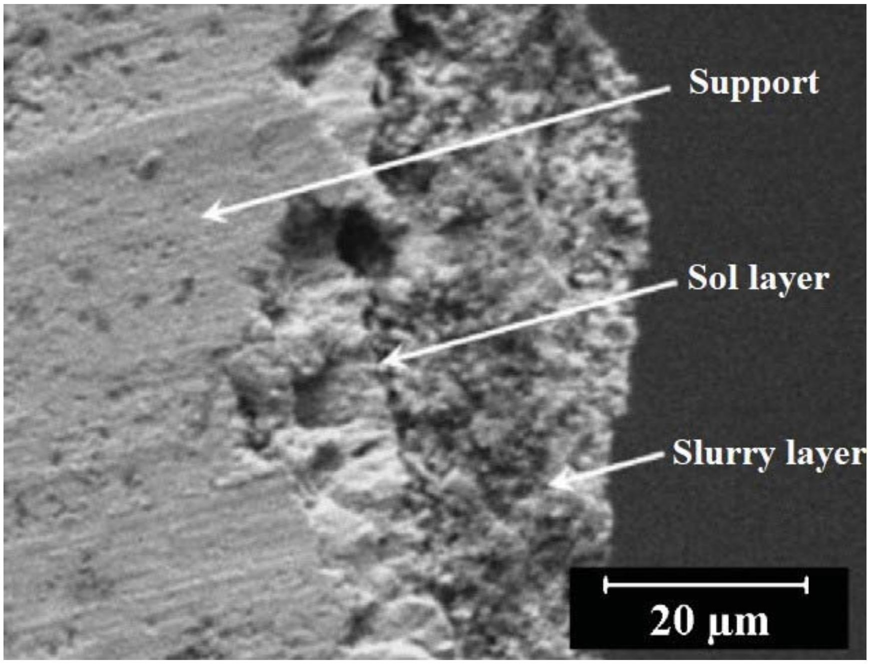

Figure 4.12 Scanning electron microscope (SEM) image of sample section after 10 h preoxidation at 900 °C, sol layer 2 % g g^{-1} and slurry 25.3 % g g^{-1} deposition. Adapted with permission from reference Jia et al. (2007a). Copyright 2017 Elsevier.

High temperature decreases the BET surface area and changes the Al_2O_3 phase. However, porosity and superficial area remain constant with stabilizers like CeO_2, La_2O_3, ZrO_2 (Figure 4.13). Wu et al. (2001) Adding $Ce_{0.68}Zr_{0.32}O_2$ in Al_2O_3 increases the binding strength with the support and inhibits the phase transformation of the Al_2O_3 giving a high and stable surface area Jia et al. (2007b); Shen et al. (2006).

Sample	Slurry formulation	Solid content
A	35% γ-Al_2O_3	35%
B	30% γ-Al_2O_3 5% $Ce_{0.68}Zr_{0.32}O_2$	35%
C	28% γ-Al_2O_3 7% $Ce_{0.68}Zr_{0.32}O_2$	35%
D	17.5% γ-Al_2O_3 17.5% $Ce_{0.68}Zr_{0.32}O_2$	35%

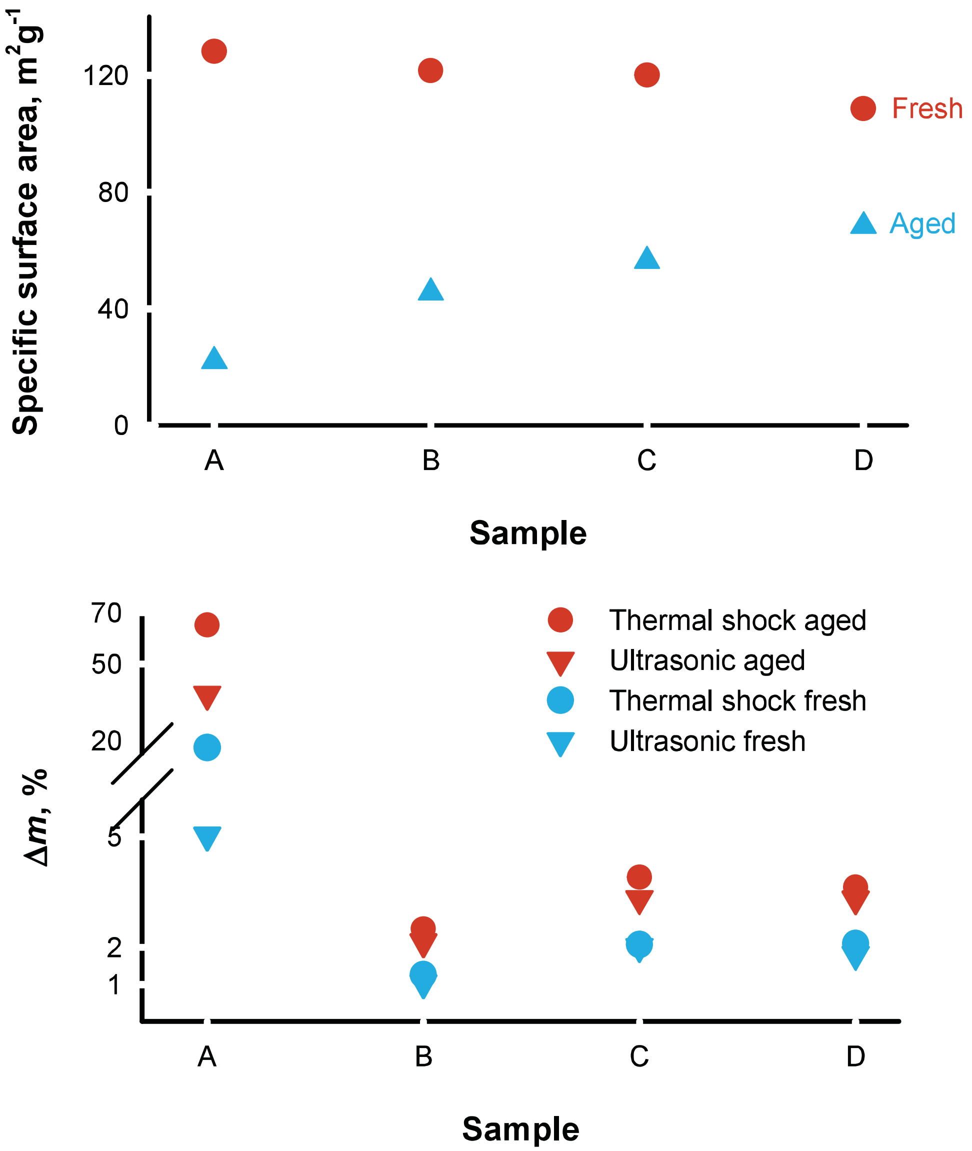

Figure 4.13 Specific surface area before and after washcoat aging. Percentage mass loss of the washcoat before and after aging for thermal shock and ultrasonic tests. Sample composition reported on the table.

Thermal shock tests at 700 °C and mechanical test under sonication in petroleum ether demonstrated that the support geometry has a stronger influence than pretreatment. The adheshion of the protective layer was best on the high porosity foam compared to preoxidized foils, coated foils and coated foams (Figure 4.14) Kim et al. (2012); Zhao et al. (2003); Wu et al. (2005); Zhang et al. (2011); Jia et al. (2007a). In any case, pretreatment increases the interfacial forces between support and coating. Sol gel coating of fibers with Al_2O_3 behaves differently compared to flat foils and alcohol, as a solvent, is better for fibers because of its lower surface tension and boiling point compared to water Zhang et al. (2011); Fei et al. (2003).

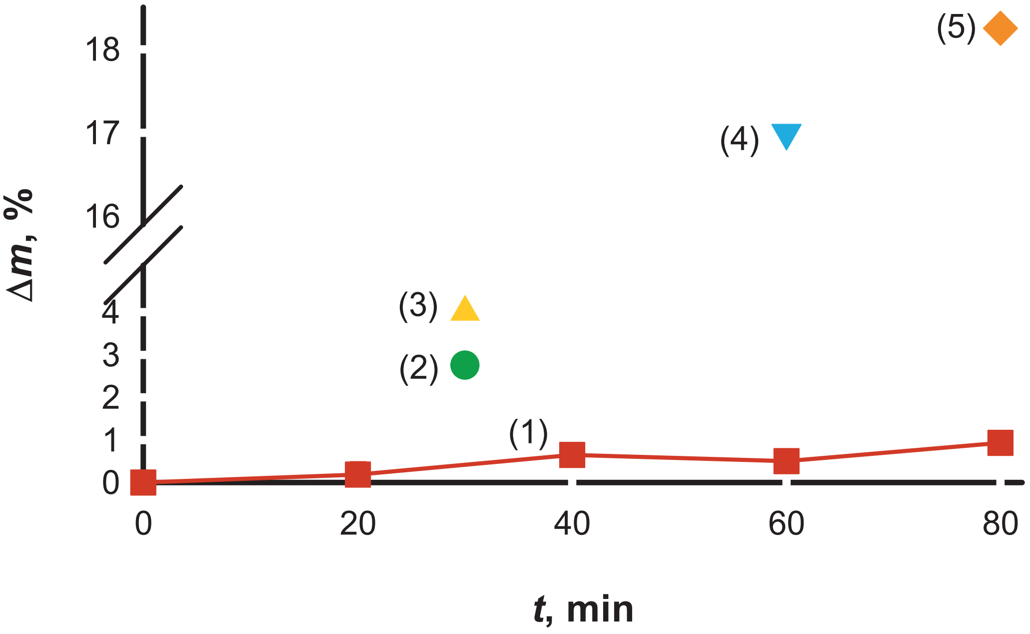

Figure 4.14 Weight loss comparison during mechanical stress test at 40 kHz in ultrasonic bath. (1) Kim et al. (2012), (2) Zhao et al. (2003), (3) Wu et al. (2005), (4) Zhang et al. (2011) and (5) Jia et al. (2007a). Adapted with permission from reference Kim et al. (2012). Copyright 2012 Elsevier.

A mass fraction of 2 % $g\,g^{-1}$ La in the Al_2O_3 slurry stabilizes the metastable phase at 950 °C. La also minimizes cracks in the cladding and reacts with the metal substrates enhancing the adhesion (Figure 4.15) Ozawa and Araki (2015). Introducing a $LaMnAl_{11}O_{19}$ hexaaluminate (HA) in Al_2O_3 layer on FeCrAl foil enhances the adhesion stability of the catalyst and maintains its high activity Chen et al. (2014). The HA is vertically embedded in Al_2O_3

intermediate layer Chen et al. (2013).

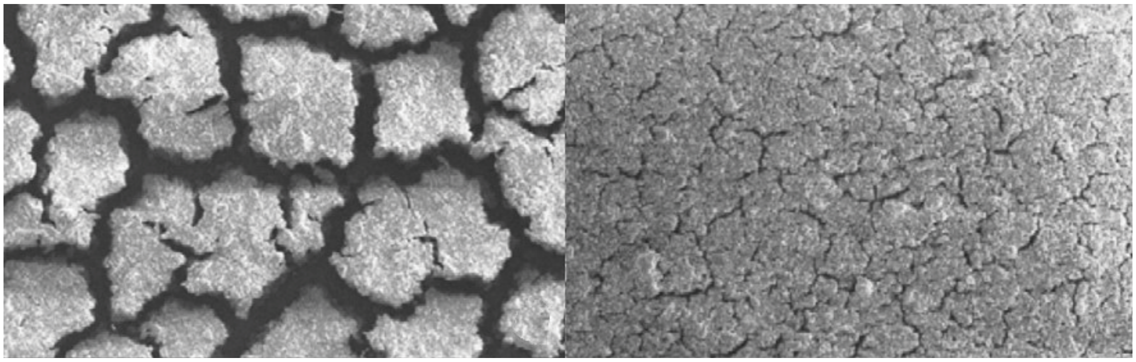

Figure 4.15 FeCrAl surface micrographs after 2 h at 1200 °C. With (right) and without (left) 2 % g g^{-1} La. Adapted with permission from reference Ozawa and Araki (2015). Copyright 2015 Elsevier.

Adhesion of plasma sprayed Al_2O_3 and TiO_2 is superior to that of traditional dip coating. Plasma electrolytic oxidation is a promising technique, because it creates a protective cladding without any pretreatment although the dispersion remains more heterogeneous than traditional deposition methods Yang et al. (2015a). Silica SBA-15 is an alternative to alumina as a protective layer, but requires colloidal silica rather than Al_2O_3 as a binder to favor the interaction between cladding and the metal support Pérez et al. (2010).

The elements of the slurry that affect its rheology include : solvent type (usually water), particle size and distribution, binder (e.g. colloidal silica/alumina), dispersant (mainly acids), and additives (e.g. long-chain surfactants containing hydrophilic and hydrophobic groups).

The recipe depends on the type of powder to be coated and determines the amount, homogeneity, and adhesion of the film. Low slurry viscosity lead to low loading and high adhesion, while high-viscosity formulations generate thicker washcoat layers that adhere poorly Montebelli et al. (2014). A drawback to the coating method is that it modifies catalyst morphology Bobadilla et al. (2019). For instance, SBA-15 agglomerates with a wheat-like appearance break down under magnetic stirring into rods Pérez et al. (2010).

The preparation method of a colloidal dispersion of a ready-made catalyst is similar to the binder deposition step. Driving out liquid is easy for simple shaped supports since only viscous force resists the fluid movement. Blowing (dip-blowing) and centrifugation (spin-coating) are appropriate for complex shapes like open-cell foams, especially with a high pore density. Air jets and centrifugation complement gravitational forces to overcome capillary forces in draining liquid from the channels and cells Giani et al. (2006); Pérez et al. (2010); Ambrosetti et al. (2018). For instance, spin coating controls the $Pd-CeO_2$ coating formation on FeCrAl open cell foams with cell diameters down to 500 µm. The higher shear stresses induced by rotation during wet film deposition reduces clogging and increases the film homogeneity with respect to ordinary dip-coating (Figure 4.16) Ambrosetti et al. (2018).

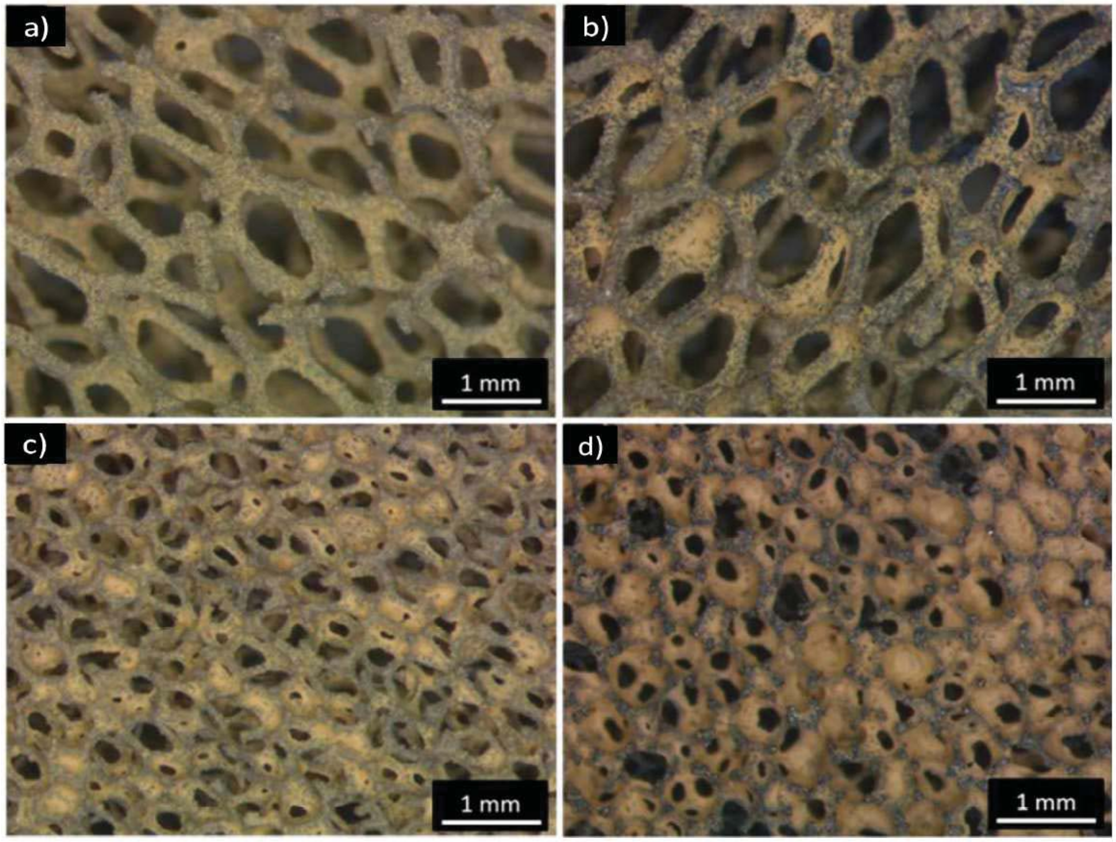

Figure 4.16 Optical microscope images of spin-coated (a,d) and dip-coated (b,e) foams of 1200 µm (a,b) and 580 µm (d,e) cell diameters. Adapted with permission from reference Ambrosetti et al. (2018). Copyright 2007 Elsevier.

4.4.3 In situ-growth of active phases

In direct deposition routes, catalyst (metal particles, metal oxide, and zeolites) and precursor (hydroxides) grow directly on the surface of the structured support. These methods can be considered as a heterogeneous precipitation where the growing seeds form on the metal support surface rather than in the liquid phase. While in-situ growth techniques avoid modifications of the catalyst during slurry preparation, producing materials like those from conventional synthesis methods (without a structured metal support), requires special attention.

Impregnation followed by calcination

The simplest way to develop in situ catalytic materials is to impregnate a solution of a precursor (mainly metal salts) on a pretreated FeCrAl, i.e with a porous alumina coating, followed by calcination, like in the conventional preparation of powder catalysts. The immersion of a pretreated foil in a solution containing La^{3+} and Mn^{2+} leads to their adsorption on the porous Al_2O_3 layer, which generates a firmly adhered $LaMnAl_{11}O_{19}$ hexa-aluminate after calcination due to solid state reactions. Chen et al. (2013, 2014) Alternatively, when dealing with more complex shapes, such as fibers, wherein the immersion may lead to inhomogenous species adsorption, the precursor solutions can be sprayed on the support, which oxidizes to Al_2O_3 or Al_2O_3-CeO_2 during calcination Neagoe et al. (2016).

Solution combustion synthesis

Solution combustion synthesis (SCS) produces adhesive coatings of inorganic nanomaterials. It is a self-propagating redox reaction between metal precursors (oxidizers) and organic fuel in aqueous solution Specchia et al. (2017); Thoda et al. (2018). The solution heated until 300 °C to 600 °C initiates reaction that rises to temperature from 750 °C to 1500 °C, for a very short time. Consequently, a highly crystalline and pure film develops consisting of nanosized powder with relative high specific surface area and low tendency to sinter. The fuel-to-oxidizer ratio, φ (elemental stoichiometric coefficient), controls the heat released and the crystalline structure of the final product. Metal nitrates are common oxidizers while urea and glycine are conventional fuels. Compared to washcoating, in SCS crystal lattice parameters can be regulated and reactants are cheaper.

CuO-CeO_2 on FeCrAl monolith thermally pretreated are prepared from Cu/Ce nitrate and urea. The solid loading increases with the concentration of the solution but the detachment of the film is also more noticeable—$200\,\mathrm{g\,L^{-1}}$ concentration balances both phenomena. Pr and La improve the adhesion of the catalytic film as Nd and Zr influence copper and CeO_2 dispersion Zeng et al. (2011); Zeng and Liu (2008).

The aqueous solution of the nitrate precursors with glycine as fuel is sprayed over the gauze surface at 400 °C. One step in situ spray pyrolysis SCS on pre-oxidized gauzes produces a highly corrugated and porous $Pd(LaMnO_3 \cdot 2ZrO_2)$ catalytic layer (Figure 4.17) Specchia et al. (2010). Pt-Rh/MgO on pretreated woven fibers are prepared by a two-step SCS ; MgO first deposits from a $Mg(NO_3)_2$ and urea solution and afterwards the SCS of Pt-Rh is done using $Pt(NH_3)_4(NO_3)_2$, $RhCl_3$ with the same fuel Ma et al. (2016a). Usually after SCS the material is calcined to confer additional stability. To achieve the desired catalyst loadings, the deposition cycles are repeated several times, as in the case of washcoating.

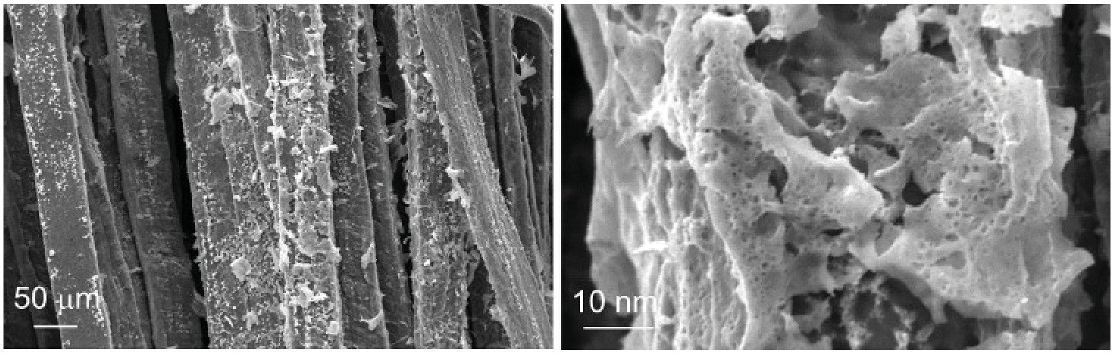

Figure 4.17 SEM micro-graphs of FeCrAl fibers supporting Pd($LaMnO_3 \cdot 2ZrO_2$) prepared by in situ SCS Specchia et al. (2010).

Hydrothermal methods

The synthesis and deposition of catalytic species under hydrothermal conditions is typically used to prepare zeolites or the urea assisted co-precipitation of single or mixed hydroxides on structured supports. Its main advantage is the control of the crystal growth and, therefore, the orientation of the particles on the coating. On the other hand, yield on the support is low, since the solids precipitate in the bulk solution at the same time as on the support. This is particularly costly when dealing with noble-metal catalysts.

The in situ synthesis of zeolites on the surface of structured supports generates a binderless and oriented microporous film of zeolite crystals, while washcoating forms a disordered meso- (due to the binders) and microporous zeolite film Meille (2006); Eleta et al. (2009); Mehla et al. (2019). The coating procedure consists of immersing the pretreated support in a zeolite gel that is hydrothermally treated at 140 °C to 160 °C. The gel is prepared from an aqueous solution containing zeolite precursors (e.g. sodium silicate, SiO_2, $Na_2Al_2O_4$), a structure directing or pore filling agent and a base mobilizing agent (e.g. OH^-, F^-). Zeolite nucleates and grows homogeneously in the mother liquid while nucleation and nuclei growth on the support surface, relevant for the in situ zeolite synthesis, is heterogeneous. The subsequent calcination step removes structure directing agents and binders.

Likewise for conventional (homogeneous) preparation of zeolites, type of precursors, Si/Al and H_2O/Si ratio, pH, type and amount of additives as well as crystallization temperature and time determine the growth kinetics and, therefore, the properties of the zeolitic materials. These parameters control the shape and size of crystals and, as a consequence, the coating stability. Zeolitic material properties depend on Si/Al ratio, which also determines nucleation and crystallization rates Rebrov et al. (2009). The concentration of the gel controls the ratio homogeneous/heterogeneous precipitation ; the hydrothermal treatment pH can dissolve the Al_2O_3 from FeCrAl Pérez et al. (2013); Eleta et al. (2009).

The surface accessibility and the support pretreatment affect the synthesis of the zeolite, but in micro-channels and pores, diffusive limitations of the gel may create non-homogeneous coatings with unstable over-growths. The FeCrAl pretreatment provides chemical compatibility, increases hydrophilicity and irregularities (roughness) on the surface that favor the zeolite growth and promote coating adhesion. At the same time α-Al_2O_3, formed during pretreatments, acts as an Al precursor in the zeolite synthesis Rallan et al. (2015b); Eleta et al. (2009); Ochonska et al. (2013); Rallan et al. (2015b); Włoch et al. (2006); Pérez et al. (2013).

Crystals of ferrierite are synthesized on foils pretreated at 800 °C starting from alumina, silica and piperidine. Nucleation time and temperature are two factors that control crystal size, small crystals improve contact with the metal foil Włoch et al. (2006).

Seeding pretreated supports avoid organic templates. Ochonska et al. (2013); Zamaro et al. (2008) In the synthesis of ZSM-5 over sheets, the alumina layer increases the amount and stability of zeolite. Similarly, ZSM-5 and SSZ-13 bind to the Al_2O_3 layer developed on open-cell foams pretreated at 1000 °C Kryca et al. (2016a,b).

In the synthesis of mordenite, the preoxidized surface at 700 °C of corrugated foils is impregnated with a cationic polymer (poly-diallyldimethilammonium chloride) prior to seeding—charge reversion procedure Pérez et al. (2013). Deposits are polycrystalline, dense, continuous, adherent, and producible quickly with a *c*-axis orientation perpendicular to the support surface. A marked preferential growth on the metallic surface at the expense of a negligible growth within the synthesis solution is an advantage of seeding, but the type and concentration of the seed as well as the calcination temperature influence the properties of the film (Figure 4.18) Pérez et al. (2013). To obtain Cu-Ce/mordenite coatings, Cu is introduced by ionic exchange, while Ce by impregnation.

Table 4.1 Zeolite synthesis performed on FeCrAl foils pretreated at 900 °C.

Catalyst name	**Synthesis time** h	**Seeding suspension** $g\,L^{-1}$	**Mass variation** $\%g\,g^{-1}$
F900-1	3	5	0.3
F900-2	6	5	1.5
F900-3	24	5	14.3
F900-4	24	10	8.4

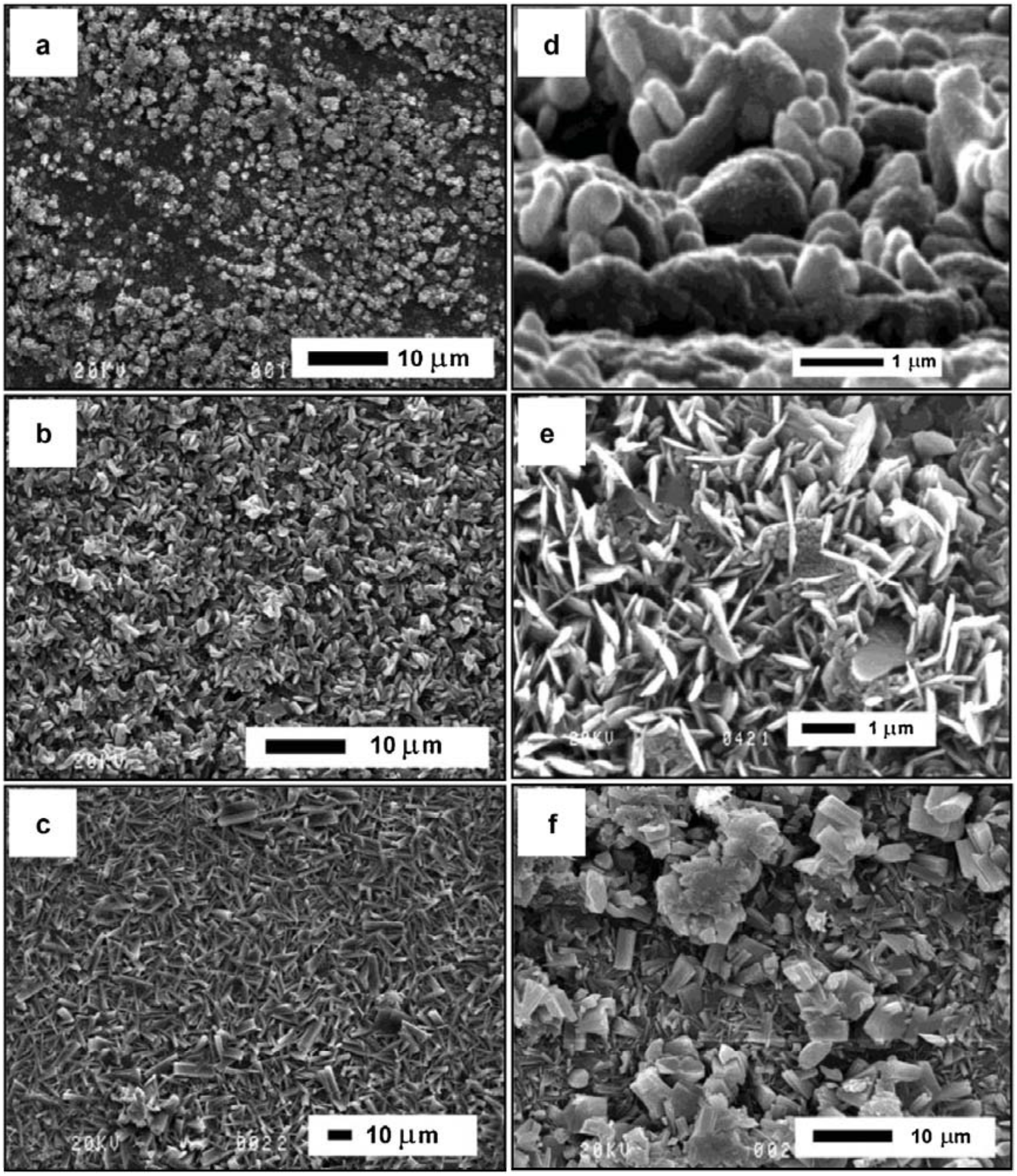

Figure 4.18 Growths obtained under various syntheses conditions (Table 4.1) : (a) F900-1, (b) F900-2, (c) F900-3, (d) close view on sample F900-1, (e) seeding of nanocrystals on substrate with alumina whiskers and (f) F900-4 Pérez et al. (2013). Copyright 2013 Elsevier.

The precipitation of hydroxides on FeCralloys with urea as a homogeneous base is also conducted under hydrothermal conditions. Like for zeolite synthesis, the pretreatment of the support plays a key role. Ni/Mg/Al layered double hydroxides (LDHs), catalyst precursors, do not crystallize onto pristine FeCrAl-fiber, while through a $\gamma-Al_2O_3$/water interface-assisted method homogeneously distributed and vertically aligned LDH nanoplatelets deposit. Chai et al. (2017a) The process involves :

- **i)** FeCrAl preoxidation ;
- **ii)** hydrothermal reaction to embed AlOOH nanosheets on the $\alpha{-}Al_2O_3$ film and calcination from 450 °C to 600 °C ;
- **iii)** LDHs synthesis under hydrothermal conditions at about 150 °C for several hours (∼12 h) starting from nitrate salts and urea later calcinated above 500 °C.

The method strongly depends on the Al_2O_3 nanosheets, which are grown from a solution of sodium aluminate and urea at 160 °C for 12 h. Increasing the amount of Al_2O_3 nanosheets improves the LDH growth. AlOOH can also be obtained starting from a suspension of Al powder in a NaOH aqueous solution, while the in situ growth of LDH can be performed in the absence of Al in the mixture, since the Al_2O_3 layer acts as an Al source (Figure 4.19) Chai et al. (2017a).

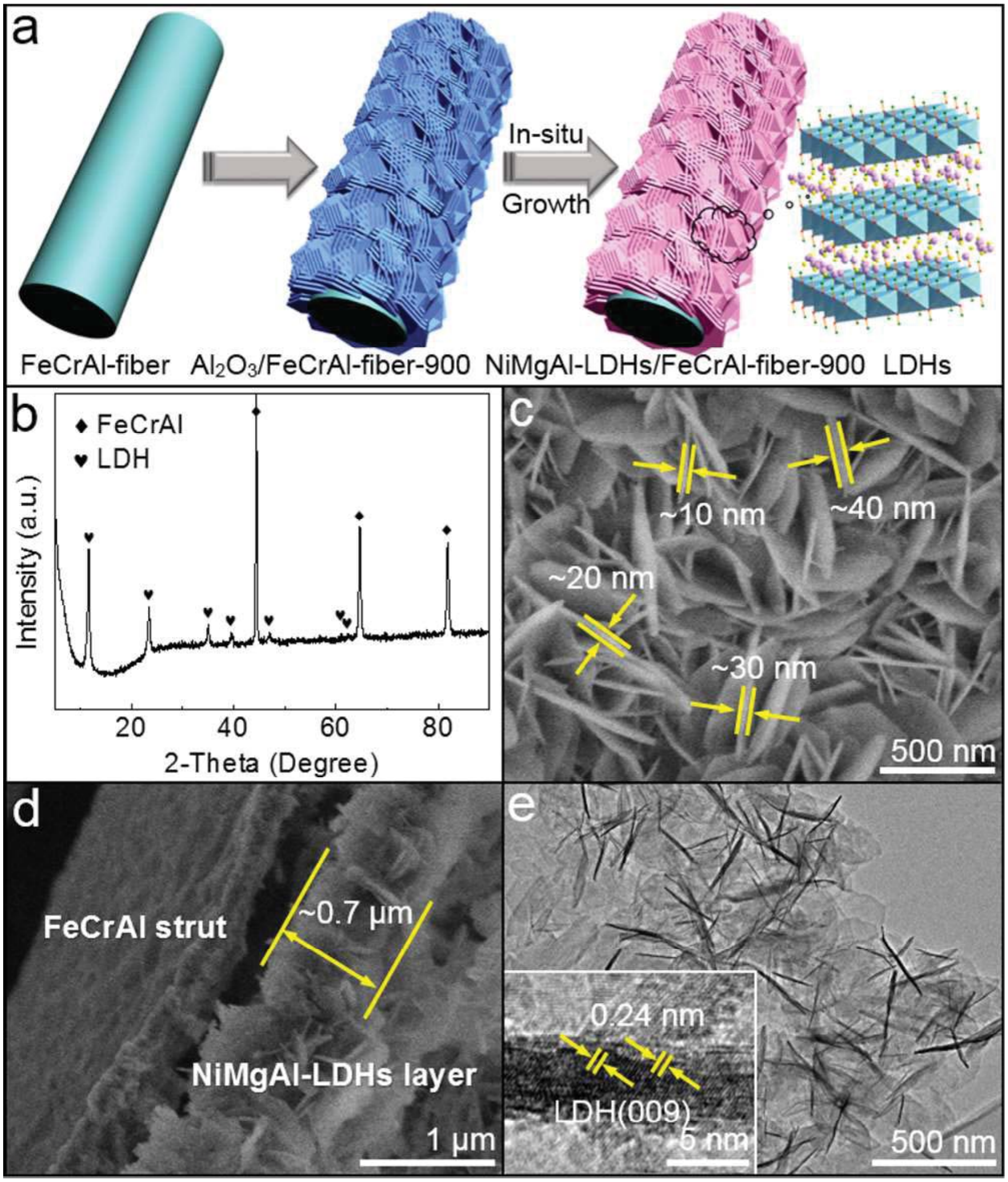

Figure 4.19 Fabrication strategy (a) of the NiO−MgO−Al_2O_3/FeCrAl-fiber-900 catalyst derived from the NiMgAl−LDHs/FeCrAl-fiber-900 precursor. XRD pattern (b), SEM (c,d) and TEM micro-graphs (e) of the NiMgAl−LDHs/FeCrAl-fiber-900 precursor Chai et al. (2017a). Copyright 2017 American Chemical Society.

The method is modified to synthesize Ni@SiO_2/Al_2O_3/FeCrAl-fiber core shell catalysts. A "top-down" from "macro-micro-nano" self-assembly strategy adds to the two first steps (oxidation and AlOOH nanosheet deposition), the wet impregnation with Ni^{2+} using 3- aminopropyltriethoxysilane as bridge molecules and as a source of SiO_2, after hydrolysis in water. Calcination at 550 °C is finally necessary to obtain the actual catalyst Chai et al. (2017b).

Galvanic displacement and electrochemical processes

The methods explained in previous sections are also applied to coat ceramic supports. Indeed, besides the treatment of the FeCrAl and the migration of alloy elements into the coating, the other preparation parameters can be considered support-independent. On the contrary, in galvanic displacement and electrochemical deposition, the spontaneous reactivity of the support and its electrical conductivity are exploited to deposit catalysts or precursors.

Galvanic displacement occurs when a less noble metal template contacts a more noble metal cation and it begins as soon as the support is immersed in the solution (also called spontaneous deposition). The morphology and mass of particles deposited depends on time, precursor, concentration, and pH of the solution. The method is effective to deposit noble metals on FeCrAl, because the galvanic potentials of reductant/oxidant between two pairs are different.

Pd deposits on foam surfaces in an O_2-free aqueous solution of $PdCl_2$ in HCl ; Fe, Cr, and Al are all displaced by Pd^{2+}. Concentration of the precursor, time, passive oxides on FeCrAl surface, and pH influence the Pd loading and the particle size (Figure 4.20) Vázquez-Gómez et al. (2012); Cimino et al. (2013). At pH= 3, Pd loading increases with time from 5 min to 120 min, nonetheless the metal nucleates in a rather low number of sites that preferentially keep growing, resulting in large Pd particles Vázquez-Gómez et al. (2012). Decreasing the pH to 1, reduces the Pd particle size and improve the dispersion Cimino et al. (2013).

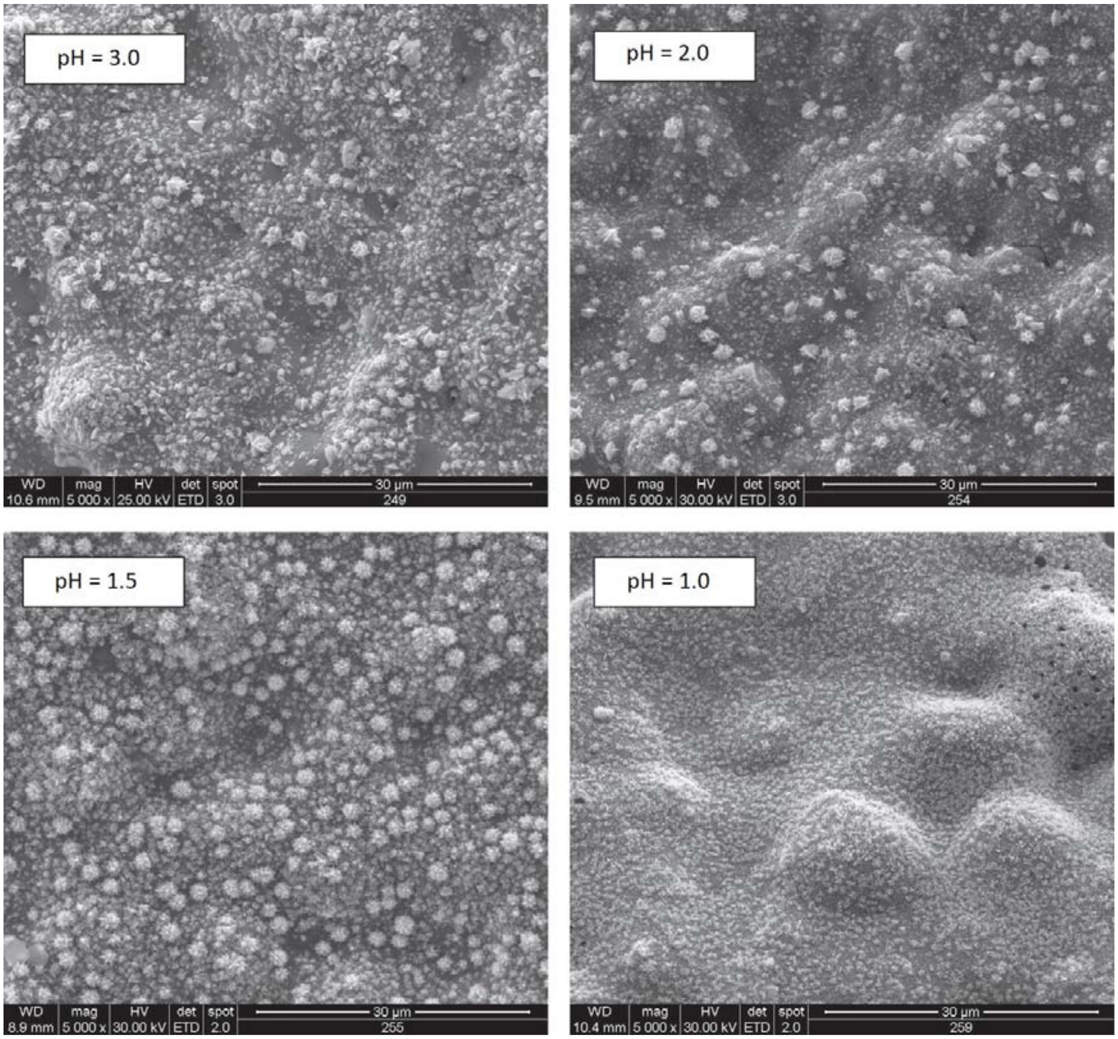

Figure 4.20 SEM micrographs of FeCrAl foams obtained by spontaneous deposition of Pd as a function pH. Adapted with permission from reference Cimino et al. (2013). Copyright 2013 Elsevier.

Coating of foam surfaces with nanometric Rh requires 24 h starting from an O_2-free $RhCl_3$ in HCl aqueous solution at pH 2 ; however, these conditions deteriorate the mechanical properties of the foam Verlato et al. (2014).

Electrochemical deposition coats conductive FeCrAl supports with metallic particles, hydroxides and oxides, and their combinations in one-step, at room temperature. A cathodic potential is applied in continuous or pulse mode to the metal substrate to be coated (working electrode). Rh and Pt metallic particles are deposited on bare foams (untreated) as an alternative to galvanic displacement Verlato et al. (2014); Cimino et al. (2016). Metal precursors are electrochemically reduced at a selected cathodic potential. The concentration of the salts, applied potential, deposition charge, and roughness of the support control the nucleation and growth of metallic deposits, and therefore the particle size and distribution. Diluted chloride baths (mM concentrations) promote nucleation, while acidic pH (around 2-3) minimizes the hydrolysis of the ions of noble metals. The deposition charge controls the noble metal loading ; however, under these electrodeposition conditions hydrogen evolution reaction is favored, decreasing the current efficiency.

Electroreduction of $RhCl_3$ at $-0.4\,\mathrm{V}$ vs saturated calomel electrode (SCE) forms Rh particles of ca. 25 nm, homogeneously deposited on the surface, even if in 2.44 mL foam cylinders the local Rh loading at peripheral positions is higher than in the center. The loading and the morphology are better compared to galvanic displacement (Figure 4.21) Verlato et al. (2014).

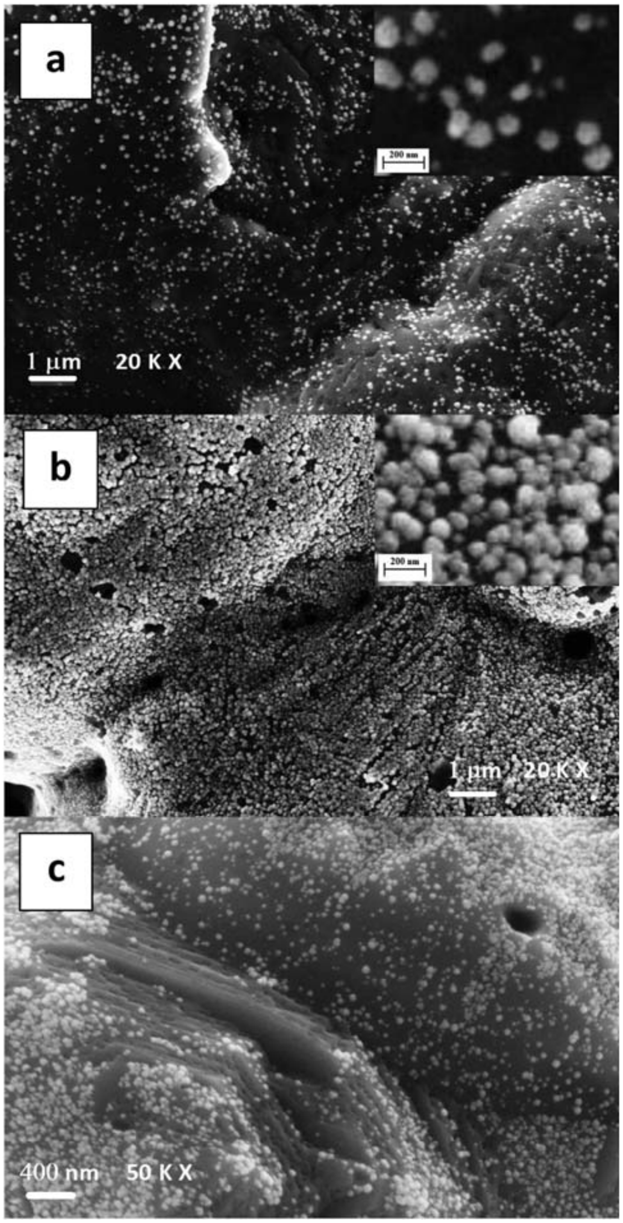

Figure 4.21 SEM micro-graphs of Rh-FeCrAl samples prepared following electro-deposition (a,b) or spontaneous deposition (c) Verlato et al. (2014). Copyright 2014 Elsevier.

Starting form H_2PtCl_6, the inhomogeneous reactivity of the FeCrAl surface produces a low surface density of large Pt particles (0.1 µm to 1 µm), which are composed of assemblies of small and spiky crystallites ; Pt loading grows with the deposition charge Cimino et al. (2016). Like Pd particles obtained by galvanic displacement, most Pt particles simultaneously nucleate on reactive positions and keep growing without generating new ones when increasing the noble metal loading and/or upon prolonged electrolyses.

The electrodeposition of hydroxides or oxides occurs through the electro-base generation method—the generation of a basic medium at the electrode-electrolyte interface provokes the chemical precipitation of cations on the electrode surface. This method, consisting of applying a cathodic pulse at the foam dipped in a solution containing nitrates and cations, was developed to coat untreated open-cell foams of small pore sizes. LDHs (Ni/Al Basile et al. (2010a) and Rh/Mg/Al Ho et al. (2018a)) and $PdCeO_2$, coatings are prepared avoiding pore blockage Ho et al. (2018b). Nitrate, water and O_2 reduction contribute to the pH increase Ho et al. (2016) while OH^- generated from dissolved O_2 has a minor contribution. Although H_2O and $NO_3{}^-$ reduction increase the pH, the former produces H_2 bubbles that detach the coating and the pH generated is low Ho et al. (2020). The quality of the electrodeposited catalysts is determined by :

i) the support, including electrical conductivity and roughness Ho et al. (2016) and geometrical parameters (size and shape Benito et al. (2012); Ho et al. (2020)) ;

ii) electrochemical set-up, namely electrical contact between the working electrode and the potentiostat Benito et al. (2015a) and type of cell Ho et al. (2018a)

iii) type and concentration of metal precursors, pH of the electrolyte, applied potential, and synthesis time Benito et al. (2012); Basile et al. (2010b, 2009); Benito et al. (2015b); Ho et al. (2019).

The potential applied controls the electrochemical reactions, though the presence of precipitating cations catalyzes the reduction processes. Prolonging the synthesis time usually increases the solid loading, but it can change the composition of the precipitates. Reaching 15 µm to 20 µm Rh/Mg/Al LDHs layers with controlled properties also depends on the size of the foam piece. For highly reducible Rh^{3+} adjusting the initial pH minimizes Rh metallic precipitation. For $PdCeO_2$ catalysts, selecting a suitable Pd^{2+} complex precursor like $(Pd(NH_3)_4(NO_3)_2$ or $PdCl_2$ in HCl), minimizes precipitation. In the synthesis of Rh/Mg/Al-LDHs, modifying the total metal concentration determines the amount of solid deposited, composition, and crystalline phases. However, as in the case of Rh/Mg/Al films with coprecipitated-like features (Figure 4.22), it is required to optimize potential (−1.2 V vs SCE), time (2000 s), total metal concentration (0.06 M), number of electrical contacts, replenishment of the solution, and separation of working and counter electrode with a double-compartment flow cell. However, since actual catalysts only develop after calcination at 900 °C the properties of the materials also depend on the interaction of the coating with the metallic support Benito et al. (2014). Cubic fluorite CeO_2 forms on the surface and is highly reproducible (compact and platelet-like), while the task is more challenging for $PdCeO_2$ coatings. Adjusting the Pd precursor, $PdCl_2$ concentration (0.15 M), applied potential and time (−1.1 V vs SCE for 500 s) disperses well Pd species on the CeO_2 coating ;

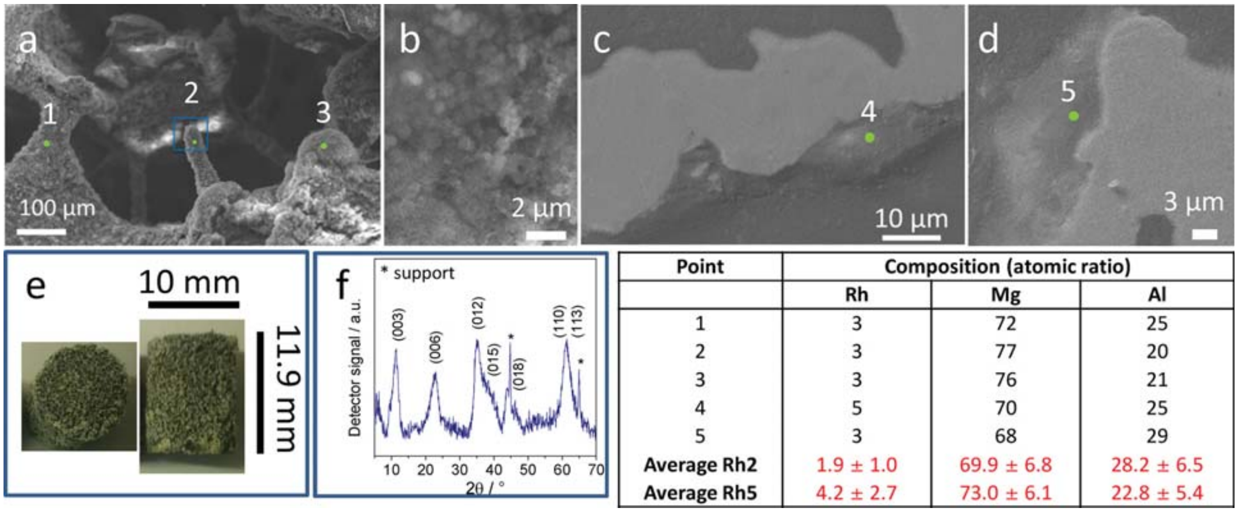

Point	Composition (atomic ratio)		
	Rh	Mg	Al
1	3	72	25
2	3	77	20
3	3	76	21
4	5	70	25
5	3	68	29
Average Rh2	1.9 ± 1.0	69.9 ± 6.8	28.2 ± 6.5
Average Rh5	4.2 ± 2.7	73.0 ± 6.1	22.8 ± 5.4

Figure 4.22 SEM micro-graphs and composition of Rh5 catalyst precursor : a) medium magnification ; b) high magnification ; c and d) cross-section of an embedded foam ; e) of the prepared coated foam ; f) XRD of the fresh coating. In the table EDS composition of the spots identified with the numbers 1, 2, 3, 4, 5 Ho et al. (2018a). Copyright 2018 Elsevier.

depositing of Pt-CeO_2 on foams faces similar challenges too Verlato et al. (2017). Pulsed deposition, instead of constant-potential electrodeposition, controls size and surface distribution of nanoparticles (ca. 30 nm to 50 nm at -1.0 V and 100 nm at -0.7 V vs SCE).

In variance to electrochemical processes, electroless plating relies on redox reactions to deposit metals on objects without an electric current. The metal substrate is immersed in a solution of the metal precursor and a reducing agent is added. For the deposition of Pd and Pt on FeCrAl wire mesh substrate with robust adhesion and uniform dispersion, electroless plating is applied after an initial galvanic displacement step on a cleaned surface to remove passivated oxides Li et al. (2012, 2017c).

4.5 Applications in emission control

Catalytic devices drastically reduce CO, NO_x, uncombusted hydrocarbons, and particulate emissions from gasoline and diesel engines Lambert et al. (2018); Johnson (2016); Lee et al. (2019). Gas hourly space velocities (GHSV) in the catalytic converters approach 1 000 000 h^{-1}. They operate with noble metals (active phase) and structured supports with a high void volume, such as honeycomb monoliths, to minimize pressure drop. Cordierite ($Mg_2Al_4Si_5O_{18}$) has the added benefit of negligible thermal expansion. In the last 10 years, most research has focused on replacing ceramic supports with metallic ones that withstand 1000 °C, expand catalytic functionality and reduce noise. This configuration is easier to manufacture and it is more facile to recover precious metals. Fibres, monoliths and foam of FeCrAl have been tested and most being coated with an Al_2O_3 layer (Figure 4.23). Coatings are more prevalent for monoliths and include ZSM5, SBA15, modenite, bentonite, ZrO_2, CeO_2, and TiO_2. They promote the interaction with the active phase, reduce sintering and supply lattice oxygen.

Cost remains a limiting factor Kaltner et al. (2009); Andersen et al. (2000); Govender and Friedrich (2017). During the metallic support preparation Ni coming from the brazing material modifies the structure of FeCrAl. Transition metals enters the alloy and creates regions of Ni_xAl_y, that strength the support in a similar way to the precipitation hardening technique Leone et al. (2006). Although the deactivation strongly depends on the nature of the support, FeCrAl supporting Pt behaves in the same way as Pt supported on cordierite (Figure 4.24), while the same active phase on FeCrNi is poorer Kaltner et al. (2009).

FeCrAl wire meshes supporting K, from vapor chemical deposition, suppress soot emission. It combusts soot above 330 °C and remains active with a difference in the CO_2 peak of only 25 °C between the first and the fifth cycle. Qi et al. (2017) Catalytic converters with diesel particulate filters, currently also made of cordierite, trap the particulate matter by physical separation; when the pressure drop increases, ceria catalytically oxidizes the carbon and temperature increases.

4.5.1 Automotive tail gas treatment

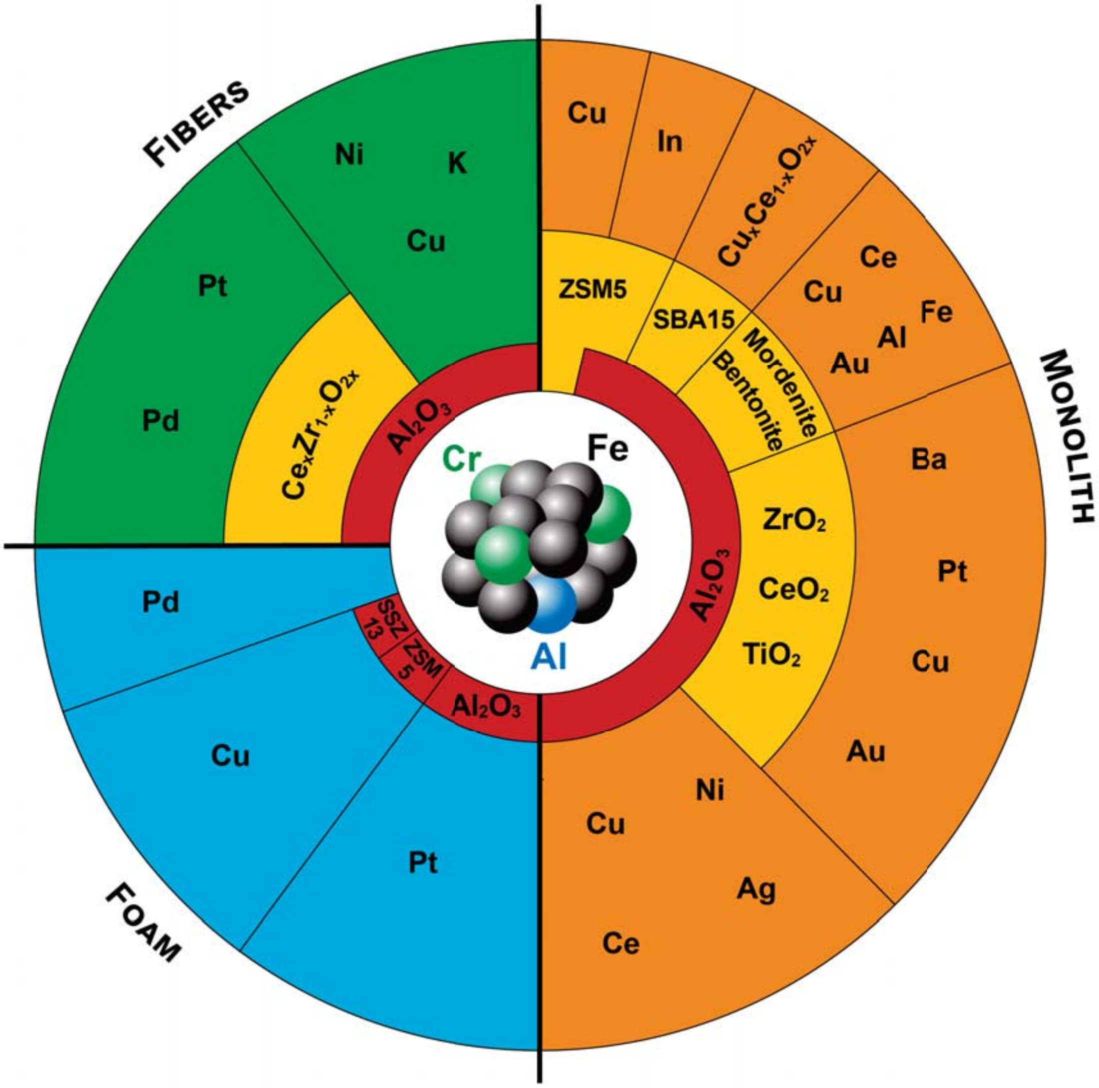

Figure 4.23 Catalyst structure, formulation and active phase for automotive tail gas treatment.

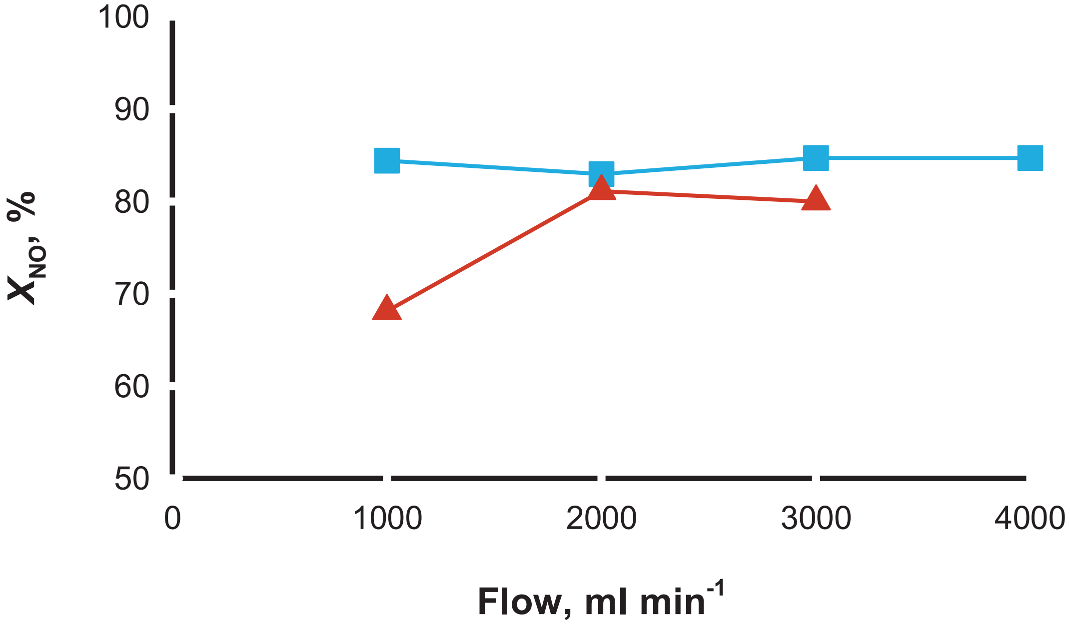

Figure 4.24 Conversion of NO as function of the residence time for FeCrAl hollow sphere structured bed (blue) and ceramic monolith (red). Adapted with permission from reference Kaltner et al. (2009). Copyright 2009 Elsevier.

In FeCrAl the alumina layer, formed on the surface, blocks the negative effect of the Cr that otherwise diffuses or migrates from the bulk to the active phase Kaltner et al. (2009). With Al−Fe pillared bentonites or CeO_2 coatings, cations move between external and protective oxide layers, which is deleterious in the case of precise catalyst formulations. These movements vary with elements, protective coating, ions, and the process/reaction conditions Martínez Tejada et al. (2013); Martínez T et al. (2009). When supported on bentonites, Au blocks Cr in the alloy, while the contrary occurs with CeO_2 as the intermediate layer Martínez Tejada et al. (2013). In-situ combustion synthesis produces $Cu-CeO_2$ on FeCrAl catalysts for the preferential oxidation of CO. Adding Pr or La improves the stability of the catalyst but La decreases CO oxidation.Zeng et al. (2011)

Oxygen treatment of silver nanoparticles on FeCrAl plate with a diameter smaller than 3 nm creates AgO_x that are active in transforming nitrite to nitrate. When the metal particles are bigger, the grains are more stable ; the activation of O_2 and its consequent interaction with the active phase does not occur, that is why only particles with a certain maximum diameter are active in the nitrogen reduction Centeno et al. (1998). Ba and TiO_2 or ZrO_2 are active at room temperature in the reduction of NO_x and their interactions generate superficial nitrites followed by the oxidation of superficial barium or carbon. The formation of these components is more efficient in presence of zirconia Smirnov et al. (2014).

Noble metals

Noble metals are the most active component in catalytic automotive converters. In cycling NO_x storage-reduction (NSR) catalysts to treat diesel tail gases, Pt particles deposited on external coating of BaO, work both in lean and rich conditions. In the first case, Pt catalyzes the full oxidation of nitrogen oxides to NO_2 while forming $BaNO_3$; in the second, it catalyzes the reaction between nitrates and excess fuel Johnson (2016); Lambert et al. (2018); Lee et al. (2019); Johnson and Joshi (2018); Takahashi et al. (1996); Centi et al. (2003); Fornasiero et al. (2008). With time, $\mathrm{NO_x}$ oxidizes Pt, but thermally treating the system produces coarse particles, which minimizes the oxidation rate Smirnov et al. (2015). Activity and thermal stability are higher for Pt−Pd and Pt−Rh bimetallic particles or three way catalysts (TWC) and where successfully deposited by ionic exchange on γ-Al_2O_3 or on a mixture CeO_2-ZrO_2-γ-Al_2O_3 on preoxidized FeCrAl fibers Johnson (2016); Lambert et al. (2018); Lee et al. (2019); Cooper and Beecham (2013); Wang et al. (2015); Fornasiero et al. (2008). Together with the design of the geometry of the mesh, it combines high catalytic and filtration ability without affecting the pressure drop at high flow rate Fornasiero et al. (2008).

In the preparation of metallic foams, like TWC supports, spontaneous deposition of Pd avoids problems during the preparation. The specific surface area, s_A, of the active metal increases at pH= 1 (Figure 4.20) but s_A is higher on Ni-based foams. However, with FeCrAl the interaction with the substrates preserves the activity and the final efficiency is 10 times higher than the traditional Pd alumina washcoating Cimino et al. (2013).

Copper-Indium

Although Cu has not been applied industrially in pollution control devices for vehicle exhaust, Cu is an alternative to precious metals for CO oxidation or selective catalytic reduction (SCR) of $\mathrm{NO_x}$, as it is inexpensive, has acceptable mechanical properties, and is relatively stable to poisoning Lukiyanchuk et al. (2018). SCR use ammonia or urea to reduce NO_x and are usually combined with oxidation catalysts to prevent prevent leakage after the reduction step Block et al. (2005). Cu is forbidden in North America because it produces traces of dioxin but bulk Cu, while activates both carbon and nitrogen species, is constrained by it low melting point Marklund et al. (1990). When on FeCrAl fibers prepared via chemical and electrochemical methods, it has comparable performance to bulk copper fibers (Figure 4.25) but can operate at higher temperatures. A spinel phase forms between the Cu and fiber under layers that stabilizes Cu/CuOx nanoparticles in or on its crystallites Lukiyanchuk et al. (2018). Corrugated FeCrAl metal foils coated with 30 % ($g\,g^{-1}$) Ce/mordenite impregnated with 2 % ($g\,g^{-1}$) Cu efficiently oxidize CO in micro reactors Pérez et al. (2013).

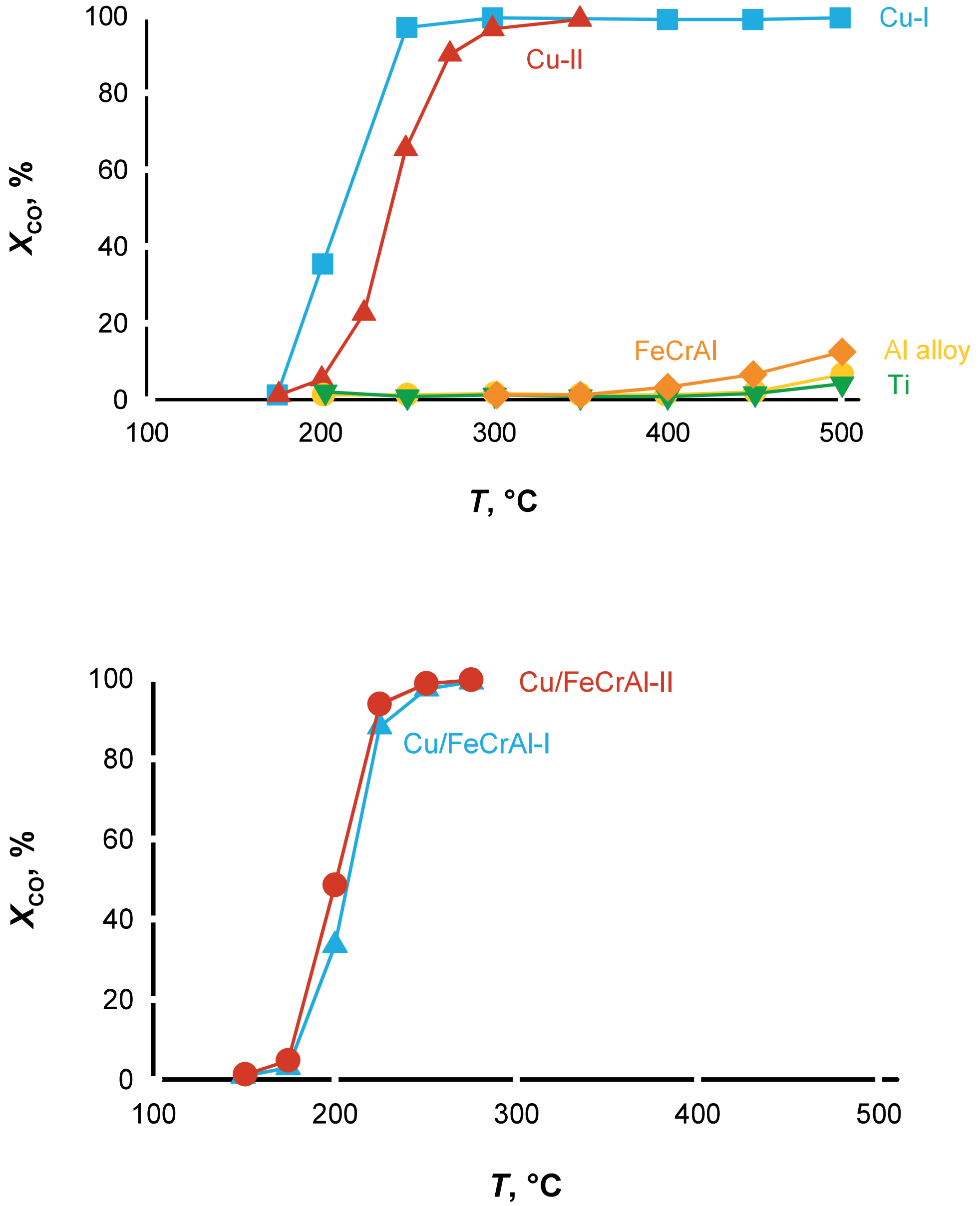

Figure 4.25 CO conversion vs. temperature : for bulk metal fibers (above) and for Cu-coated FeCrAl fibers (below). Adapted with permission from reference Lukiyanchuk et al. (2018). Copyright 2018 Elsevier.

Monolithic catalysts on FeCrAl foils are pretreated with basic, acidic, and ethanol solutions; boehmite primer sol improved the adhesion between the calcined metallic support and the washcoat layers of SBA-15 (mesoporous silica) co-impregnated with Cu and Ce nitrates. The strong interactions between CeO_2, CuO and the metallic substrate improve catalytic activity such that CO oxidizes completely at 160 °C Zhao et al. (2009).

Pressure drop in FeCrAl converters are lower and the catalytic beds are shorter than ceramic monoliths for the SCR of NO_x in stationary applications Ochonska et al. (2013); Kryca et al. (2016b). Mechanical stability of short channel structured converters prepared by in situ synthesis of Cu-exchanged ZSM-5 zeolite on FeCrAl was superior to dip-coating. The high activity and selectivity confirm the active phase is highly dispersed Ochonska et al. (2013). FeCrAl foams (Table 4.2) are very active (Figure 4.26) in the SCR of NO_x because the deposited thin zeolite layer enhances the mass transfer. Pressure drop was 200 times lower than in traditional packed beds operating at the same conversion and catalyst loading Ochonska-Kryca et al. (2013).

Table 4.2 Preparation conditions and composition of ZSM-5 supported on FeCrAl plate. C calcined, N no calcined metal support. S in-situ, D dip-coating.

Catalyst name	**Support**	**Deposition**	**Si/Al**	**Cu/Al**	**Loading**, $\mathrm{g\,m^{-2}}$
25 CSO	C	S	25	0.25	14
25 NSO	N	S	25	0.35	101
15 CSO	C	S	15	0.13	10
15 CSI	C	S	15	0.25	13
37 CDO	C	D	37	1.06	4

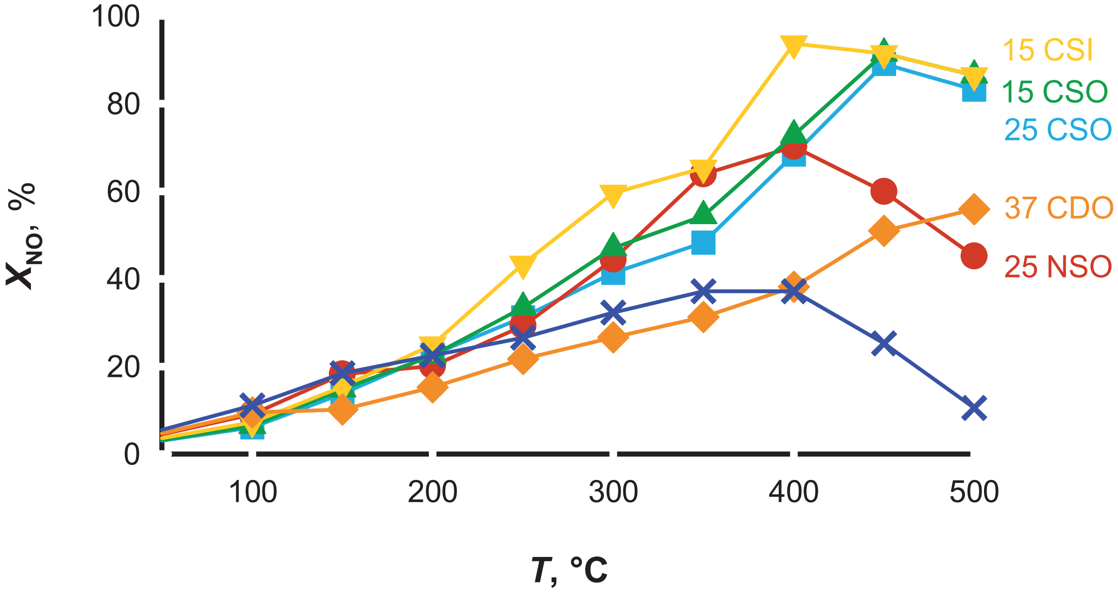

Figure 4.26 NO conversion vs temperature of samples (Table 4.2). Adapted with permission from reference Ochonska et al. (2013).

Polycrystalline ZSM5 as a dense and continuous phase on FeCrAl has *c*-axis preferred orientation orthogonal to the support surface. After In ion-exchange, it becomes less active in the SCR reaction compared to the same powdered catalyst. The orientation of the channels decreases the accessibility of the active sites with a consequent drop in performance. At the same time, the selectivity increased due to a decrease of the non-selective In and to the presence of oxidized Fe Zamaro et al. (2008). Similar results have been reported from the test of a mordenite grown on monolithic support. In this case, the b-axis was orthogonal to the surface ; the metal support gives better results not only because of the orientation of the zeolite but also of the nature of In active sites compared to the results with a cordierite monolith Zamaro et al. (2006). Cu/SSZ-13 zeolite on a foam, synthesized in situ via hydrothermal synthesis, was as active as in a packed bed reactor. This system operates at higher temperature (to the point where mass transfer rather than kinetics limits reaction rates), while maintaining a pressure drop two orders of magnitude lower than a packed bed at the same flow rate Kryca et al. (2016b).

Nickel

NiO catalysts obtained by electroplating combined with ultrasonic treatment of FeCrAl washcoated γ-Al_2O_3 were proposed as catalytic converters for exhaust emission control. Oxidation exhaust gas tests at 1100 °C for 100 h in a tube demonstrated the potential of Ni as the active phase Leman et al. (2016a). It not only catalyzed the reaction but also improved the thermal stability of the FeCrAl. Al_2O_3 deposited at the same time as the electroplating, as an ultrasonic bath effectively replaces a magnetic impeller. The final material had a homogeneous layer of alumina with higher superficial roughness Feriyanto et al. (2017). The mass of a FeCrAl monolith support after three 20 h cycles in a furnace at 1100 °C changed marginally, indicating it is resistant toward support oxidation. Combined coating and electroplating in the catalyst preparation performed best Leman et al. (2016b).

4.5.2 CH_4 oxidation

The global warming potential of CH_4 is 21 times greater than CO_2 Setiawan et al. (2017); Yang et al. (2015b), so it has stricter emission limits for natural gas power plants, automotive engines, chemical industry flares, landfills, and oil operations Setiawan et al. (2017); Yang et al. (2015b). Standard flares operate readily at methane concentrations above ~30 % ($L\,L^{-1}$) but generate NO_x because of the high temperature flame. Reacting low methane concentrations requires catalysts, which, coincidentally, reduces the operating temperature thus minimizing NO_x Prasad et al. (1984); Zwinkels et al. (2006); Hayes and Kolaczkowski (1997); Chen et al. (2015). Active metals include Pd and Pt supported on SiO_2 or Al_2O_3, but also rare earth oxides and perovskites have proven high effictive at lower cost Choudhary et al. (2002); Yang and Guo (2018); Gélin and Primet (2002).

Below 800 °C, intrinsic surface kinetics control the reaction rate in coventional packed bed reactors and at higher temperature, mass-transfer limits the activity. Structured beds operate better at both low and high CH_4 concentration. In the first case, pressure drop is lower at high volumetric flow rates, and in the second case adapting the structured bed geometry to the reaction conditions increases heat transfer rates Cybulski and Moulijn (2005); Gascon et al. (2015). FeCrAl as fibers and a monolith have been applied more than foams to support both noble and and transition metals for such applications (Figure. 4.27).

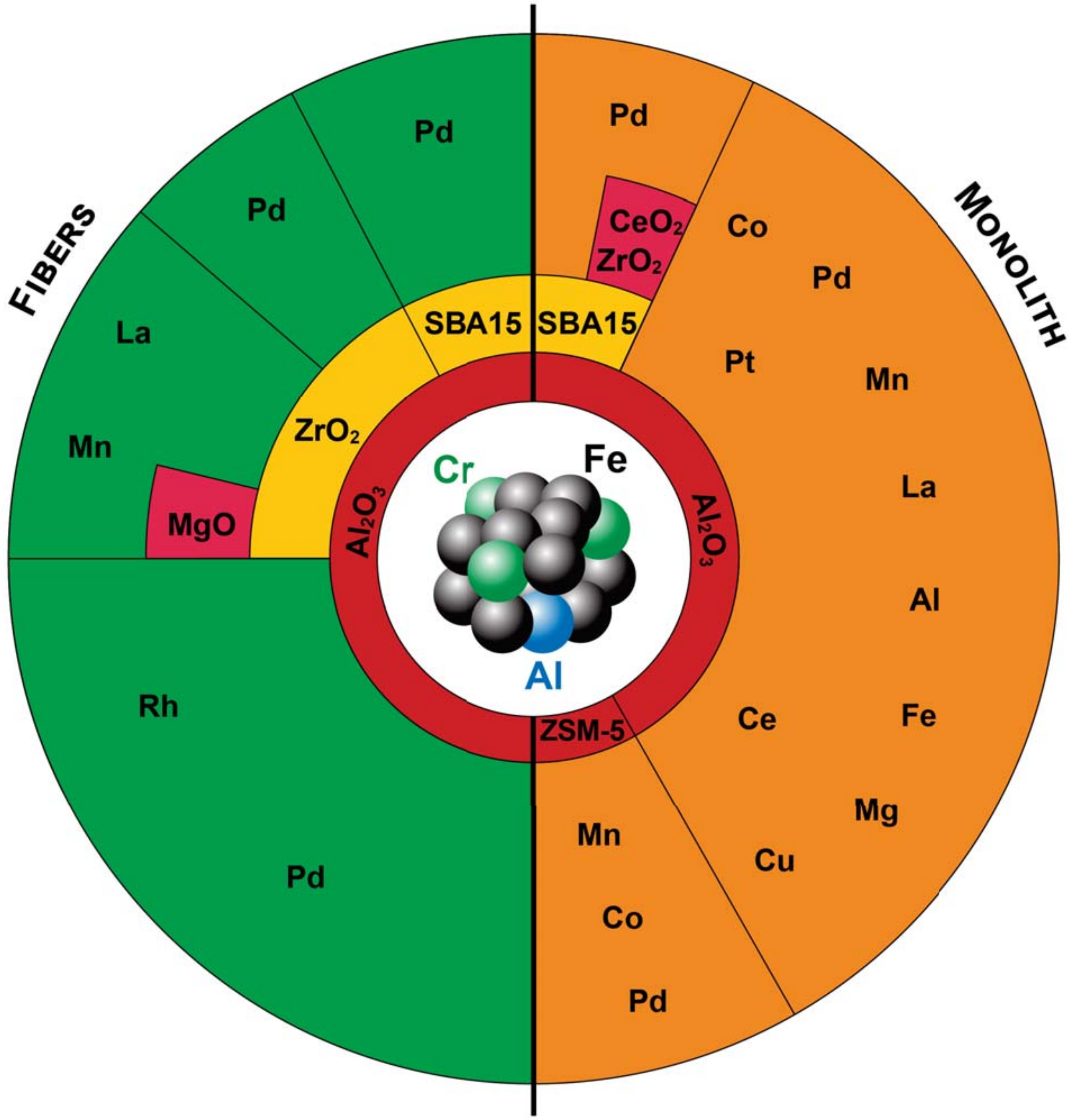

Figure 4.27 Catalyst structure, formulation and active phase for CH_4 oxidation.

Pd and Pt-based catalysts

Catalytic FeCrAl fibers supporting perovskite/zirconia ($LaMnO_3$-2 ZrO_2) with and without Pd synthesized via in situ SCS with glycerine have a higher specific surface area than samples prepared using urea Civera et al. (2003). The combustion with these catalytic converters—burners— is more stable, maximizes heat transfer by radiation, and improves natural gas combustion performance Specchia et al. (2010, 2004).

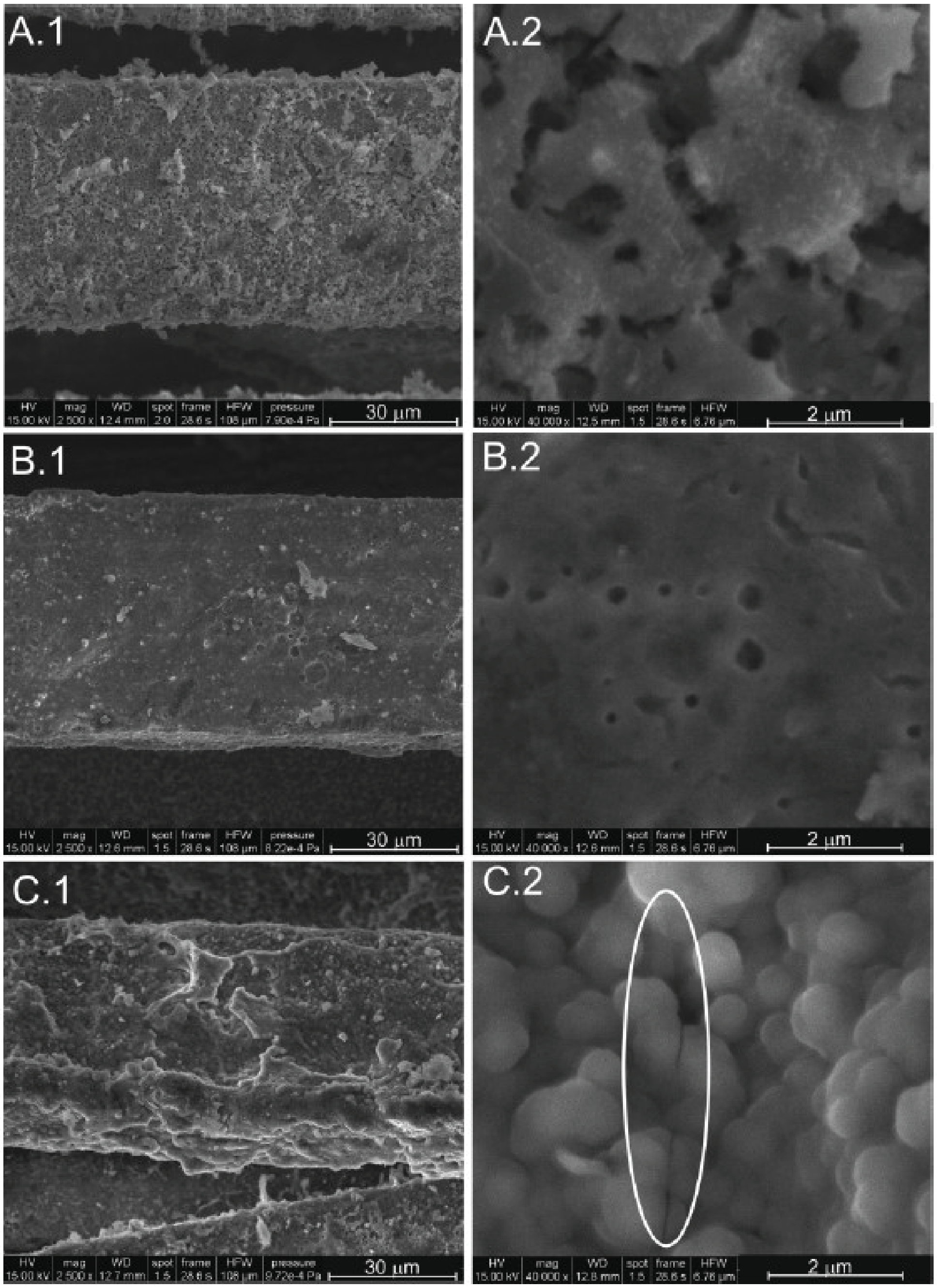

Figure 4.28 SEM micrographs of fresh (A.1/A.2), 1 week old (B.1/B.2), and 3 week old (C.1/C.2) aged burners at 2500 × magnification (.1 fig) and 40 000 × (.2 fig). Micro-fractures are evident in the oval region of C.2. Adapted with permission from reference Specchia et al. (2007). Copyright 2007 American Chemical Society.

Burner aging study demonstrated that after 3-weeks under a flow of 200 ppm SO_2, corresponding to one-year of routine operation, CO and NO emissions remained acceptable : the burner resisted poisoning and catalytic activity was constant. Cracks (Figure 4.28) in the coating that formed with time exposed more β-type oxygen desorption sites Specchia et al. (2007). Spray pyrolysis disperses catalyst better compared to wash-coating thus NO and CO emissions are between 25 % to 50 % lower Ugues et al. (2004).

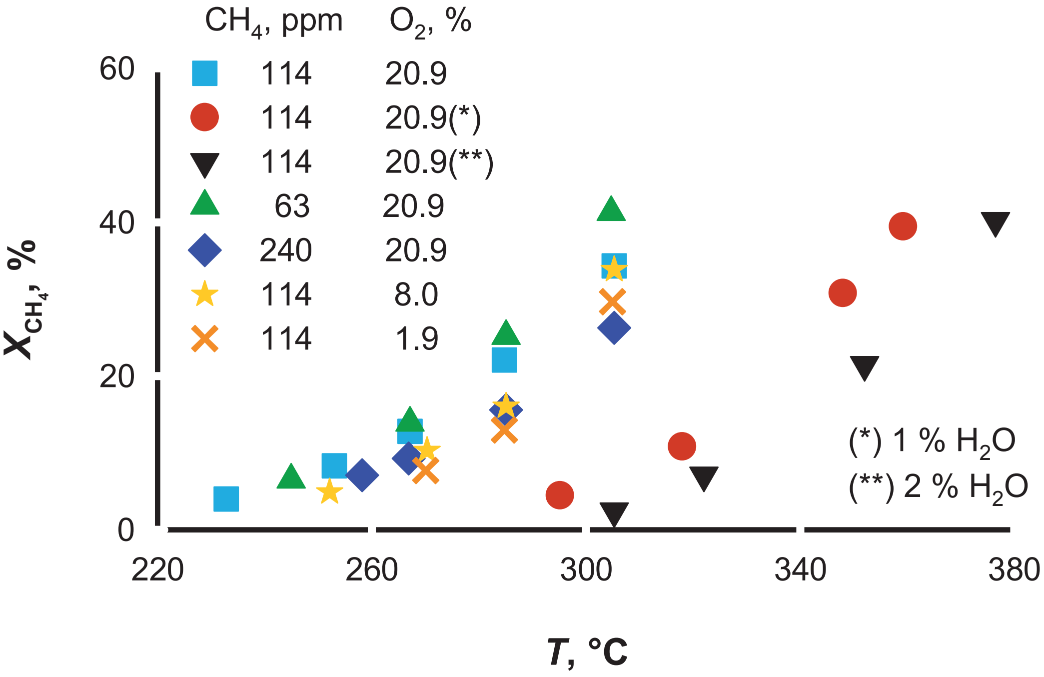

Figure 4.29 CH_4 conversion vs temperature as a function of co-reactant (O_2 and H_2O) concentration. Adapted with permission from reference Stefanov et al. (2015). Copyright 2015 Elsevier.

Pd-Co/α-Al_2O_3 catalyst was highly active and stable in CH_4 combustion, because surface Co oxides stored O_2 and stabilize Pd oxides. Adding 1 % ($L\,L^{-1}$) water to the gas mixtures delays the light off temperature by 50 °C. CH_4 conversion decreases with increasing inlet concentration, but is relatively insensitive to O_2 concentration (Figure 4.29) Stefanov et al. (2015).

ZrO_2 improves activity and stability of Pd-based FeCrAl monolithic catalyst. With Pd/ZrO_2/SBA-15/Al_2O_3 on FeCrAl, the methane conversion is complete at 450 °C even after 700 h operation Yin et al. (2008). At low temperature, CH_4 oxidation activity increases with pre-calcination temperature and washcoat loading as the amount of Al_2O_3, promoter for Pd, changes ; Pd/Al_2O_3 activity was higher than Pd/SnO_2 Kikuchi et al. (2003).

ZSM-5 with isolated metal ions supported on FeCrAl monoliths promote heterogeneous-homogeneous reactions. The most active metals are Pd, Mn, and Co. Increasing either the temperature or the residence time improves conversion. The final performance depends not only on the catalyst composition, but also on physical properties like surface area and reactor volume. Because of the high heat transfer rates in these monoliths, reactants reach a higher temperature faster, thus, initiating homogeneous reactions Slovetskaya and Kustov (2003). Bimetallic Pd-Rh/γ-Al_2O_3 dip-coated felts with at least 1 % Pd are insensitive to oxidizing or reducing gaseous pretreatments, since they exhibit higher CH_4 conversion than monometallic Rh and Pd Maione et al. (2007). Pd-Pt bimetallic catalysts are also more active than the monometallic catalysts. Impregnated Pd/SBA-15 dipcoated on fibers combust methane entirely below 400 °C ; activity is greater in the presence of Ce−Zr oxide Fan et al. (2012). Pt deposited on FeCrAl honeycombs is suitable for CH_4 oxidation. The reaction rate depends mainly on the Pt loading rather than on the mesh density, which is incongruous with the metal ions on ZSM-5 catalyst that promote heterogeneous-homogeneous reactions Uda et al. (2008, 2005).

La and Ce based catalysts

CO and hydrocarbon emissions are 3 to 5 times lower with catalytic burners based on perovskite-type catalyst ($LaMnO_3$) compared to non catalytic burners operating below 800 $kW\,m^{-2}$ Cerri et al. (2000). Contrary to a La_2O_3 layer, an intermediate layer of Al_2O_3 interacts with the dipcoated LaMn-hexaaluminate catalyst on FeCrAl foil Zhang et al. (2011). The conversion is highest (at constant temperature) when the mole fraction of Fe equals that of Mg ($x = 0.5$) in $LaFe_{1-x}Mg_xO_3/Al_2O_3$/FeCrAl catalyst, where Fe and Mg components enhance the thermal stability (Figure 4.30).

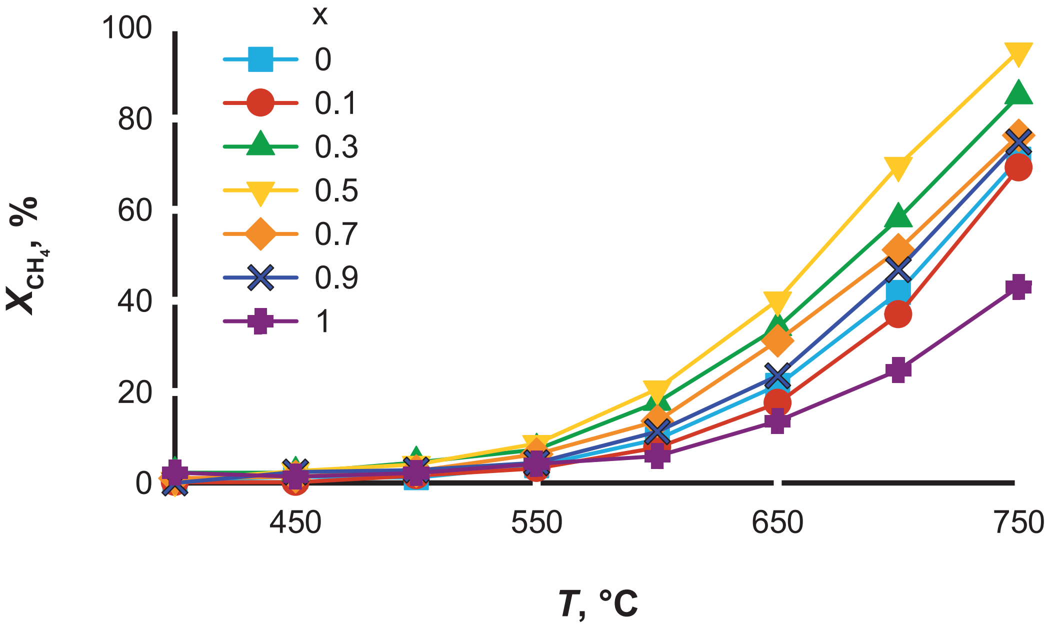

Figure 4.30 Methane conversion vs temperature over $LaFe_{1-x}Mg_xO_3/Al_2O_3/FeCrAl$ catalysts. GHSV $= 36\,000\,mL\,g^{-1}\,h^{-1}$. Adapted with permission from reference Yin et al. (2006a). Copyright 2006 Elsevier.

With this catalyst, CH_4 combustion to CO_2 is complete at 640 °C and $9000\,mL\,g^{-1}\,h^{-1}$ Yin et al. (2006a). In the context of catalytic micro-combustors using a FeCrAl catalyst support with $LaMnO_3/\gamma\text{-}Al_2O_3$ paintbrushed on alloy foils better oxidize CH_4 than $Pt/\gamma\text{-}Al_2O_3$. Co-feeding CH_4 with H_2 enhances the combustion because H_2 activates CH_4 radicals above 700 °C Scarpa et al. (2009).

Varying the cerium and lantanium ratio in $Ce_{1-x}La_xO_{2-x/2}/Al_2O_3/FeCrAl$ dipcoated monolithic achieves the best activity at $x = 0.3$; at this value, the surface is homogeneous and the particles are smaller than 0.1 µm. The strong interaction among the rare earth solid solutions, the Al_2O_3 washcoats and the FeCrAl support improves the redox properties of the catalysts, and therefore their activity Yin et al. (2006b). After replacing La with Cu, the final catalytic system maintains similar behavior Yin et al. (2005).

4.5.3 VOC oxidation—Volatile organic components

Volatile organic compounds (VOC), besides being the main contributor to the tropospheric ozone levels, are hazardous for human health.Stucchi et al. (2018); McDonald et al. (2018) Thermal and catalytic combustion oxidize VOC, limiting their emissions. Traditional VOC combustion catalysts are noble metals, such as Pt and Pd supported on Al_2O_3 or TiO_2. Supported transition metal oxides offer an alternative, because they are less expensive and more resistant to Cl_2 and HCl than noble metals Everaert and Baeyens (2004); Li et al. (2009a). Not only they are more tolerant towards poisons but they exhibit the same or higher activity than noble metals : MnOx Lahousse et al. (1998), Mn in combination with Fe Morales et al. (2007), Ni Morales et al. (2007), Cu Barbero et al. (2008); Morales et al. (2011), are examples.

Because of the high volume of exhaust gases to treat linear velocities are high in industrial processes, therefore catalysts geometries must minimize pressure drop. Catalyst supports include ceramic honeycomb monoliths, and metal supports. The latter has the extra advantage of having high mechanical properties, material ductility and electrical resistance. Indeed, the Joule effect makes the temperature of the catalyst more easily controllable, and introduces an additional process design variable that minimize capital and operating costs. In this context, FeCrAl is an active catalyst support for VOC oxidation (Figure 4.31) : Pt, for example, is deposited either on the base FeCrAl (foam and fibre) or on FeCrAl with a CeO_2 layer Li et al. (2017c, 2018); Cimino et al. (2016).

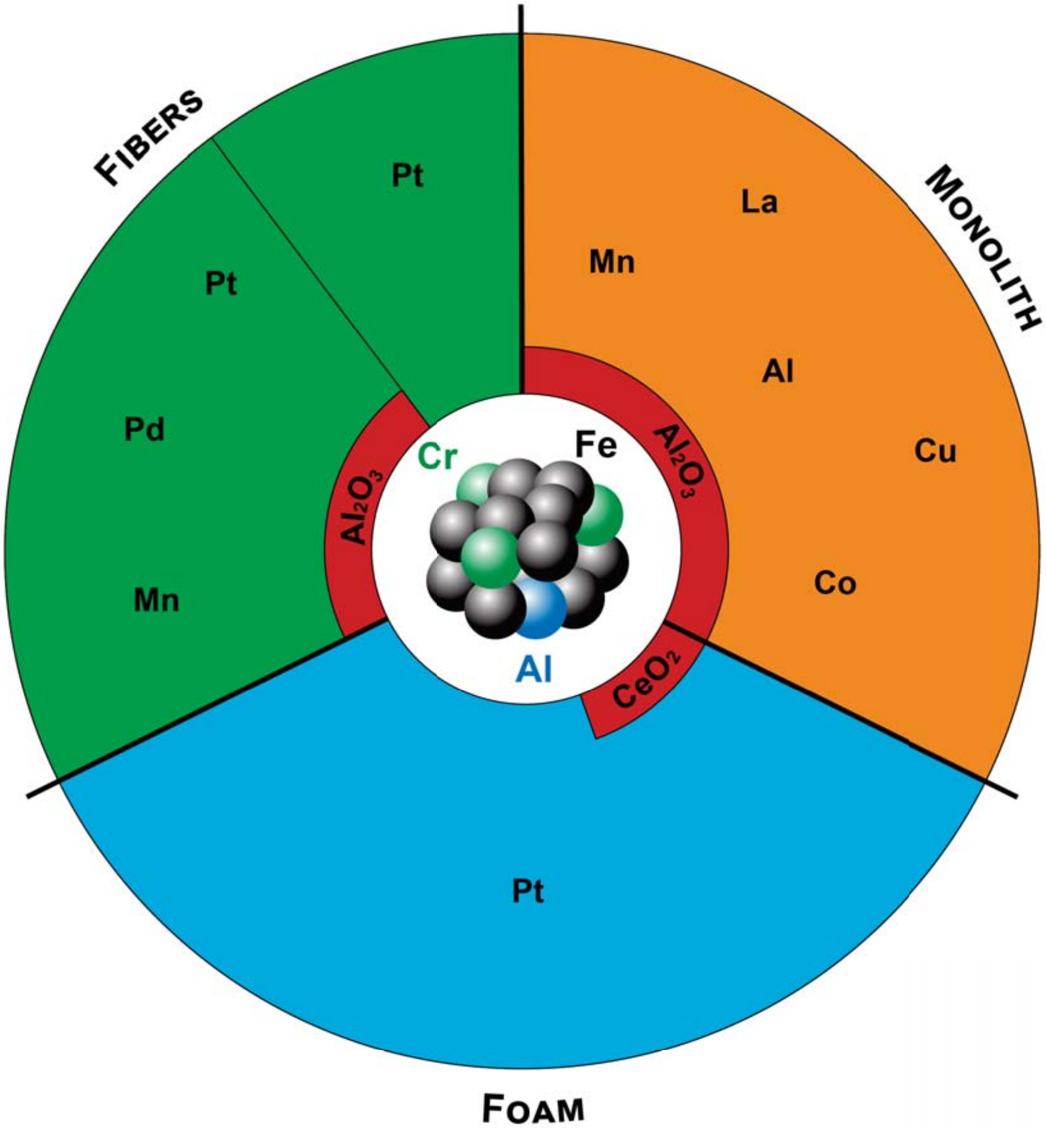

Figure 4.31 Catalyst structure, formulation and active phase for volatile organic components oxidation.

Pt-based catalysts

Pt electrodeposited cathodically on FeCrAl foams oxidize methanol. The reaction starts at 80 °C at the highest Pt loading ($> 13\,\%$) and at about 140 °C with the lowest metal loading ($< 1\,\%$). Yield of CO was negligible at all conditions during multiple oxidation cycles while even loading of $0.8\,\mathrm{mg\,cm^{-3}}$ approached 100 % yield to CO_2 above 320 °C (Figure 4.32).

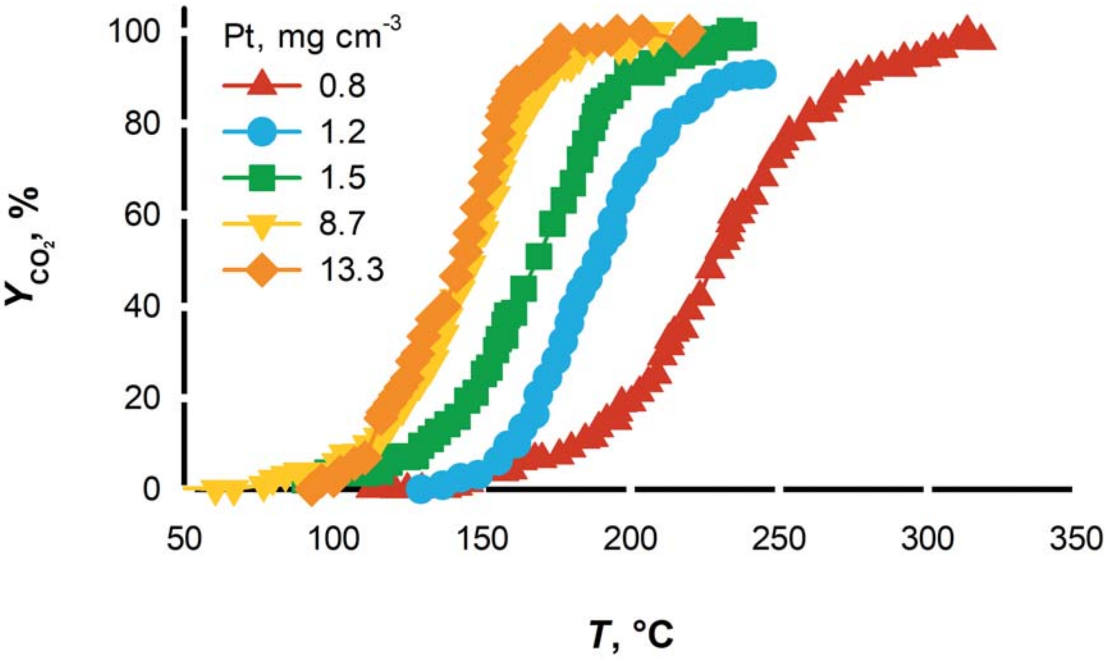

Figure 4.32 Methanol yield to CO_2 vs reaction temperature over Pt/FeCrAl foam catalysts at increasing Pt loading. Feed conditions : CH_3OH 0.5 % in air, GHSV = 16 500 h^{-1}. Adapted with permission from reference Cimino et al. (2016). Copyright 2016 Elsevier.

Cimino et al. reported no correlation between Pt surface area and CO_2 formation rate, characterized by constant apparent activation energy (independing of Pt loading and methanol concentration). It is indeed the FeCrAl support that plays an important role in the oxidation : in particular, the metal oxides next to the noble metal particles activate oxygen, thus, favoring oxygen spillover Cimino et al. (2016).

Although the addition of a CeO_2 film onto the Pt-FeCrAl decreases the surface area of the active metal, the activity of the catalyst in methanol oxidation improves, because additional active sites located at the CeO_2–Pt nanoparticle interface are formed. This confirmed previous results that underlined the importance of the interaction support-active phase. Moreover, at the same Pt loading, FeCrAl with CeO_2 produces 10 % more CO_2 at 10 °C lower than Pt-FeCrAl (Figure 4.33) Verlato et al. (2017).

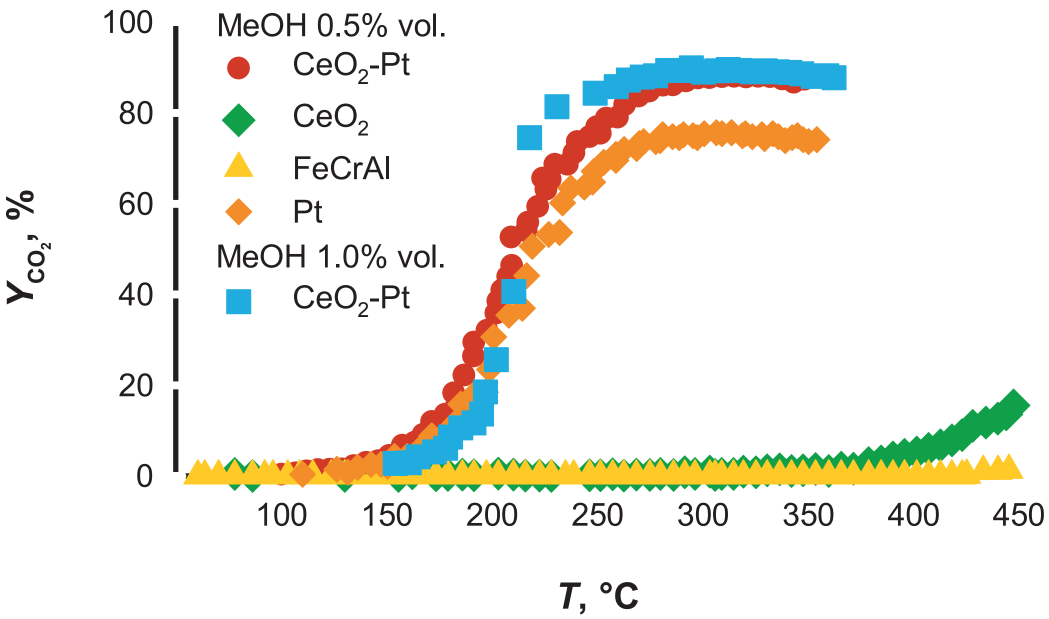

Figure 4.33 Methanol yield to CO_2 vs reaction temperature over several catalysts. Feed conditions : GHSV = 16 500 h^{-1}, CH_3OH = 0.5 % to 1 % in air. Adapted with permission from reference Verlato et al. (2017). Copyright 2017 Elsevier.

Despite the fundamental role of ceria in increasing catalytic performance, the metal support has a much greater influence. This suggests that not only the promotion of the active sites is beneficial to the final catalyst performance but also the structures itself that can also be characterized by different thermal conductivity. Changing the batch or supplier of the metal support maintaining the same alloy composition, apparent density and pores per inch, not only the specific surface can strongly change but also the temperature to achieve the same performance Cimino et al. (2016); Verlato et al. (2017).

Electroless plating deposits 0.15 % to 0.20 % (g g^{-1}) Pt active particles on the wire mesh substrate. The resulting sample after calcination at 450 °C has homogeneously distributed micro particles that enhances the transformation of Pt and PtO and completely oxidizes toluene at 180 °C Li et al. (2017c) ; simply spraying a solution of Pt precursor on preoxidized metal fibers result in lower activity catalyst that requires between 50 °C to 100 °C to achieve complete toluene conversion Li et al. (2018).

Pd-based catalysts

Pd deposited via electroless plating on non-oxidized FeCrAl wire mesh completely oxidizes toluene at temperatures just above 200 °C. The activity comes from 0.3 % to 0.4 % ($g\,g^{-1}$) PdO particles formed during catalyst calcination at 800 °C Li et al. (2012), and results more active compared to catalyst with Pt Li et al. (2017c, 2018). Electroplated Pd catalyst was also used as Joule-heated reactors to combust ethylene. The FeCrAl calcined structure usually gives better activity and promotion to the active phase (Figure 4.34(b)) compared to catalysts deposited on anodized or untreated supports (Figure 4.34(a)), even though resulting noble metal particles are often bigger. This is attributed to the surface oxides that supply active oxygen species to the neighbor Pd.

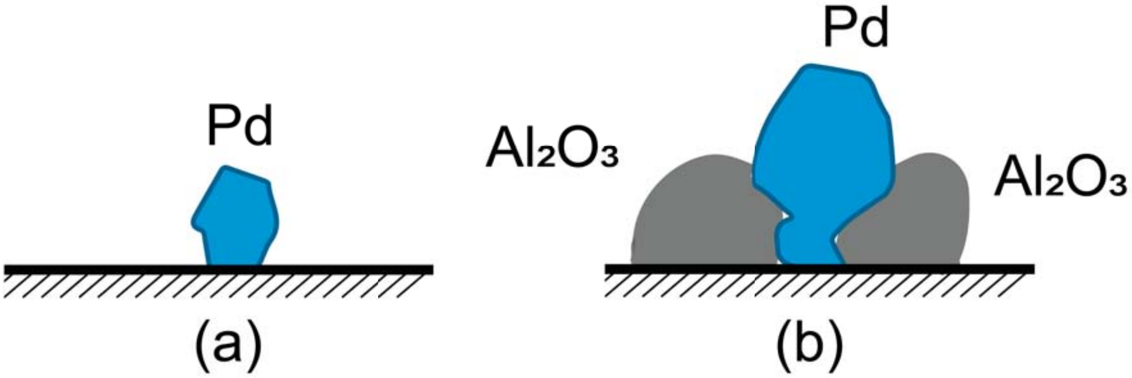

Figure 4.34 Electroplated palladium particles on virgin (a) and oxidized (b) FeCrAl substrate. Adapted with permission from reference Li et al. (2017a). Copyright 2017 American Chemical Society.

Electroplated catalysts on a calcined surface is the most active combination after comparing the noble metal on an anodized or untreated surface ; in this case both intimate contact between Pd and Al_2O_3 and small particles of active species improve supply of oxygen species that facilitates VOC oxidation Li et al. (2017a).

Mn and Cu based catalysts

FeCrAl wires dipcoated with MnO and heated up exploiting their electrical resistance also catalyze the oxidation of toluene. Anodized FeCrAl supports are more active than oxidized ones to increase MnO loading. Precoating with Al_2O_3 further favors active metal oxide loading and dispersion. The mechanical stability increases adding Zr in the Mn precursors.Li et al. (2017b) Heating these catalyst above 14 $kW\,m^{-2}$ oxidizes CO completely and toluene above

90 % (Figure 4.35). Even though Oshima et al. (2014); Li et al. (2017b) suggested that the electric field affects the chemical equilibrium, in this case, this difference comes from an incongruence between measured and real temperature, given the different heating method.

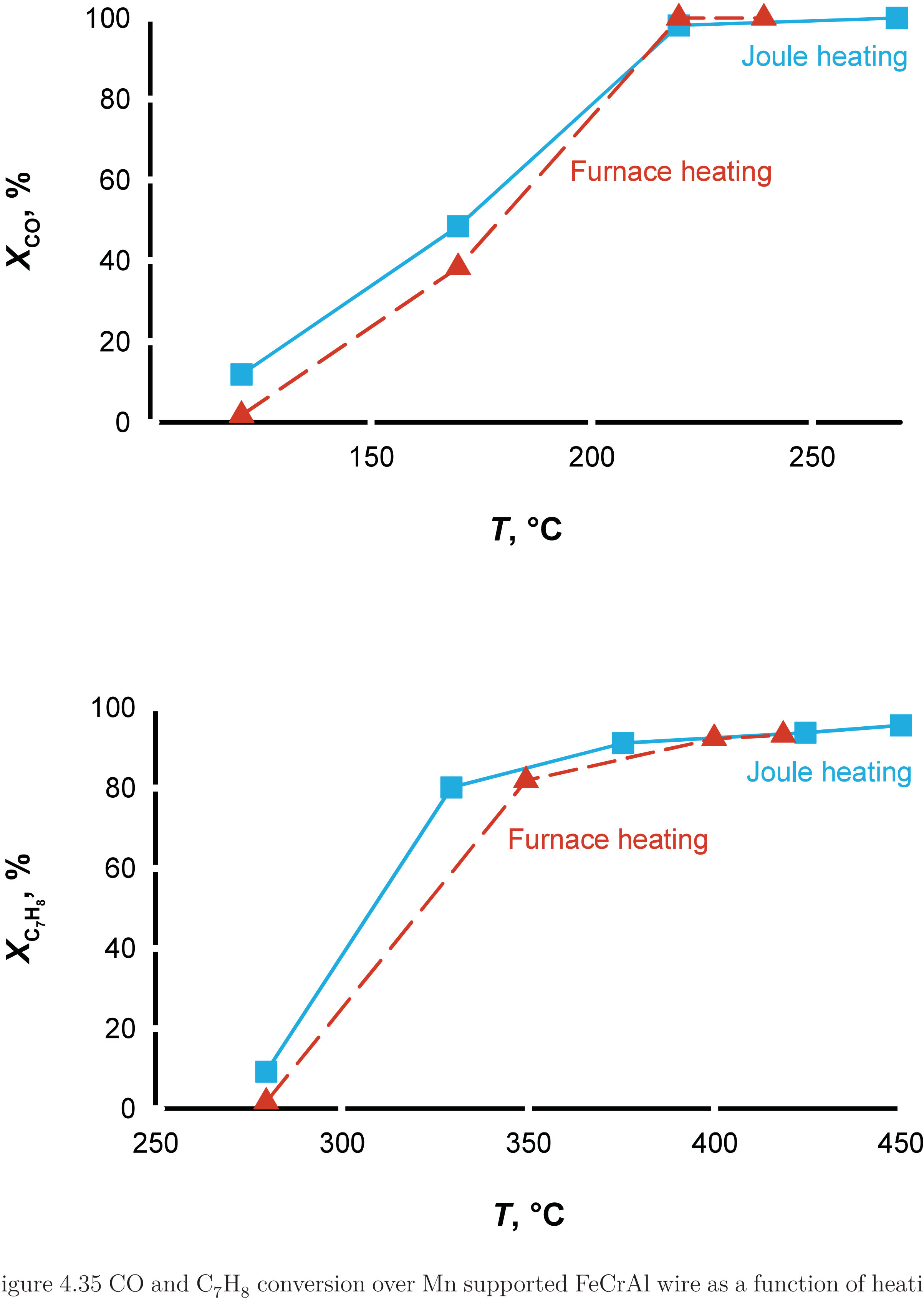

Figure 4.35 CO and C_7H_8 conversion over Mn supported FeCrAl wire as a function of heating methods. Adapted with permission from reference Li et al. (2017b). Copyright 2017 Elsevier.

FeCrAl monoliths with Mn and MnCu also combust ethyl acetate and toluene. Multiple dipcoating steps increase the amount of Mn and MnCu, thus increasing the catalytic activity but decreasing the adhesion of the active species Peluso et al. (2013); Barbero et al. (2008). Powder catalysts, prepared via co-precipitation, with a Mn :Cu ratio of 9 :1 have higher conversion compared to FeCrAl structured cataysts Morales et al. (2011). While washocated and impregnated monoliths have similar yield in the oxidation of a variety of VOC, anodized monoliths are more active at the same temperature (Figure 4.36).

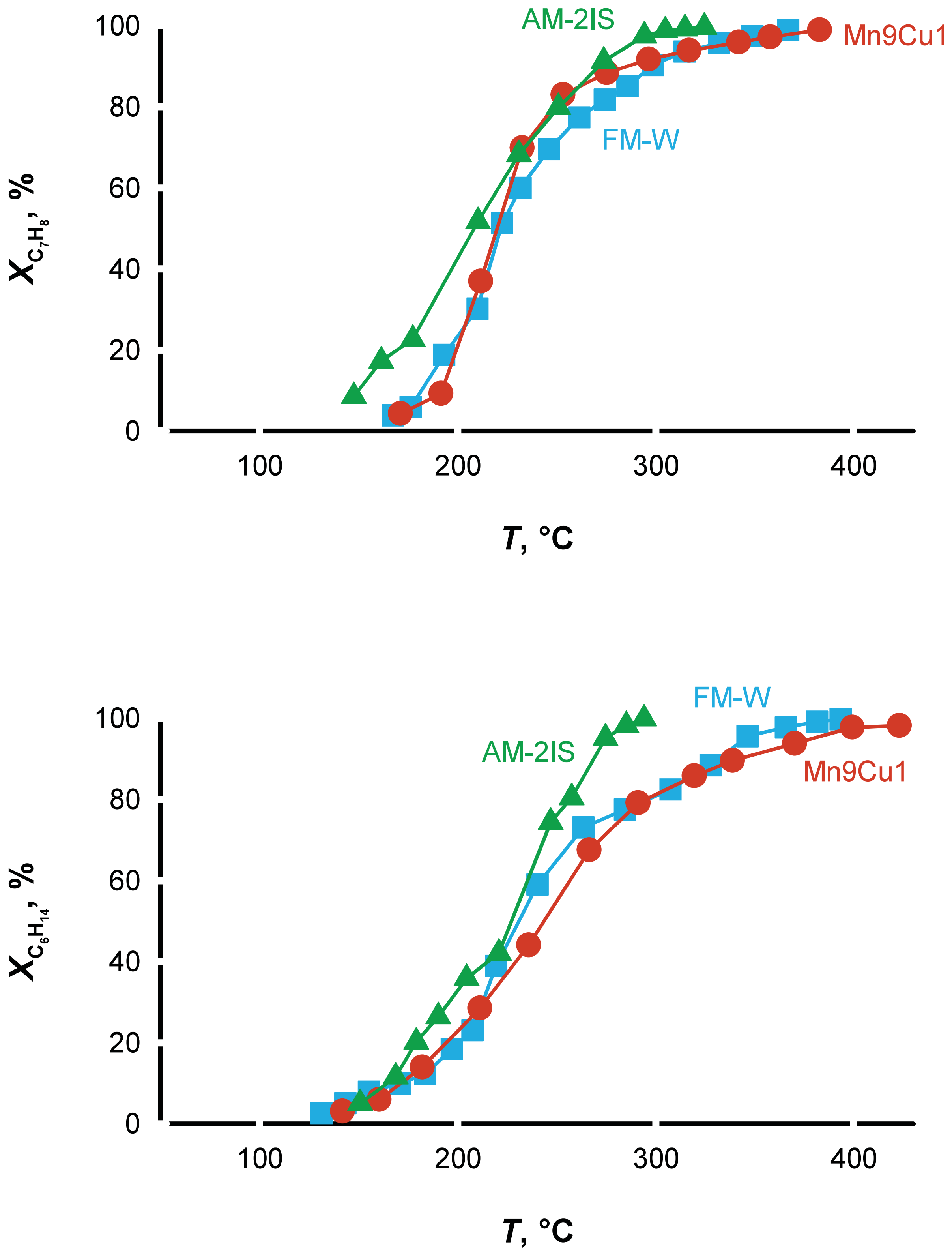

Figure 4.36 Conversion of toluene (top) and n-hexane vs. reaction temperature on FeCrAl washcoated monolith, impregnated AM-2IS and powder Mn_9Cu_1 catalyst. Adapted with permission from reference Morales et al. (2011). Copyright 2011 Springer Nature.

4.6 Syngas

Syngas production via steam methane reforming (SMR), auto-thermal reforming (ATR), dry methane reforming (DMR), and catalytic partial oxidation (CPOX) operate above 700 °C, for which the thermal and mechanical properties of FeCrAl are well suited. Methane reacting under extreme conditions destabilizes high temperature resistant metals as $Fe-Cr$ and $Ni-Cr$ alloys Cairns et al. (1979). In FeCrAl, the superficial segregated Al_2O_3 isolates the reactive atmosphere and the support, while the thermal conductivity of the bulk material (higher than the majority of the usual ceramic supports) reduces the temperature gradients within the catalytic bed, limiting secondary reactions that decrease selectivity. In the case of CPOX, the heat transfer coefficients of structured bed catalysts is sufficient to dissipate energy and to minimize local hot spots. To keep adiabatic conditions, the gas velocity must not exceed a threshold value to maintain an ignited steady state Maestri et al. (2005).

Metal supports with low porosity, induced by thin coating layer, minimize internal mass transfer resistance, one of the governing factor for fast reactions.

4.6.1 SMR—Steam methane reforming

SMR is the most common chemical process to produce H_2 and is highly endothermic : $CH_4 + H_2O \rightleftharpoons CO + 3\,H_2$ ($\Delta H_R = 205\,\mathrm{kJ\,mol^{-1}}$). Multi-tubular reactors operate from 700 °C to 1000 °C, 5 bar to 30 bar, and with a steam to carbon ratio (S/C) from 2.5 to 5.0. Industrially, the catalyst consists of Ni supported on cylindrical hollow pellets 1 cm to 3 cm in diameter Rostrup-Nielsen et al. (2002). The high capital costs, related to the large reactor volume and energy recovery units, discourage applying this technology to small decentralized production facilities. FeCrAl mitigates drawbacks of heat exchange rates in current technology Sadykov et al. (2010), but this single improvement is insufficient for shut-down economics for existing facilities. Exploiting its high resistance ($1.45\,\Omega\,\mathrm{mm^2\,m^{-1}}$ at 20 °C) and thermal conductivity minimize energy consumption, reactor volumes, start-up time, and replace burners and heat exchange reactors using the Joule heating effect Wismann et al. (2019a). All these advantages are more appealing and might push forward current technology retrofit ; these have already led to the synthesis of more than 20 different catalysts supported on FeCrAl (Figure 4.37).

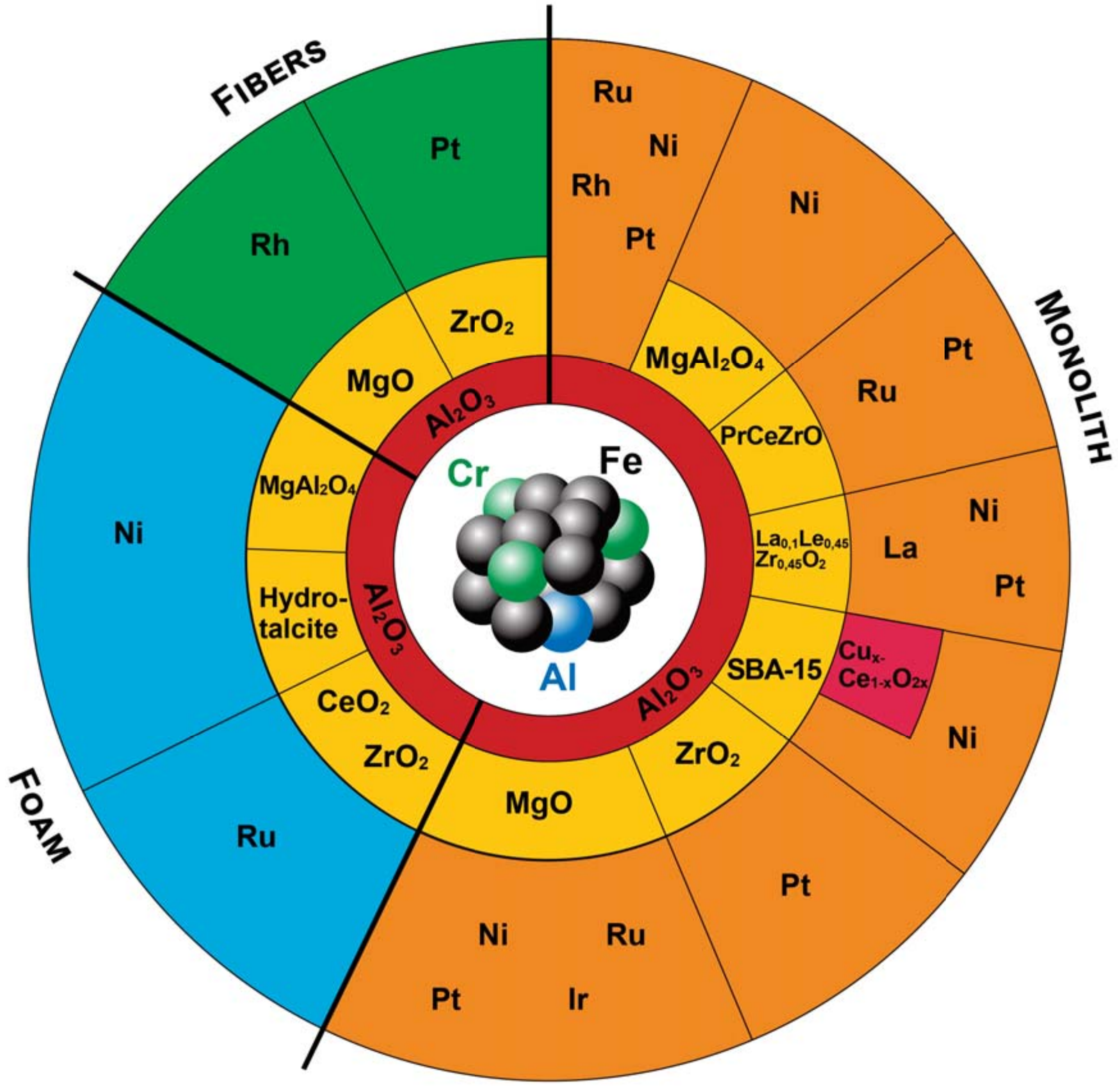

Figure 4.37 Catalyst structure, formulation and active phase for natural gas steam reforming and water gas shift.

Ni-based catalysts

Ni/$MgAl_2O_4$, a well-known catalyst for SMR, coats the surface of a metal monolith previously preoxidized and electrochemically pretreated. Addition of binders in the milled catalyst slurry modifies the physico-chemical properties of the catalyst like surface area, degree of reduction, and effective dispersion. These changes decrease the conversion (from 5 % to 10 %) of a FeCrAl structured bed compared to the traditional fixed one that uses the same catalyst Katheria et al. (2017). In contrast deposition-precipitation produces a 1 µm thick uniform and highly dispersed nanosheet that increases the availability of surface active metal sites on the FeCrAl monolith (Figure 4.38), leading to higher activity and stability compared to catalyst pellets Koo et al. (2016).

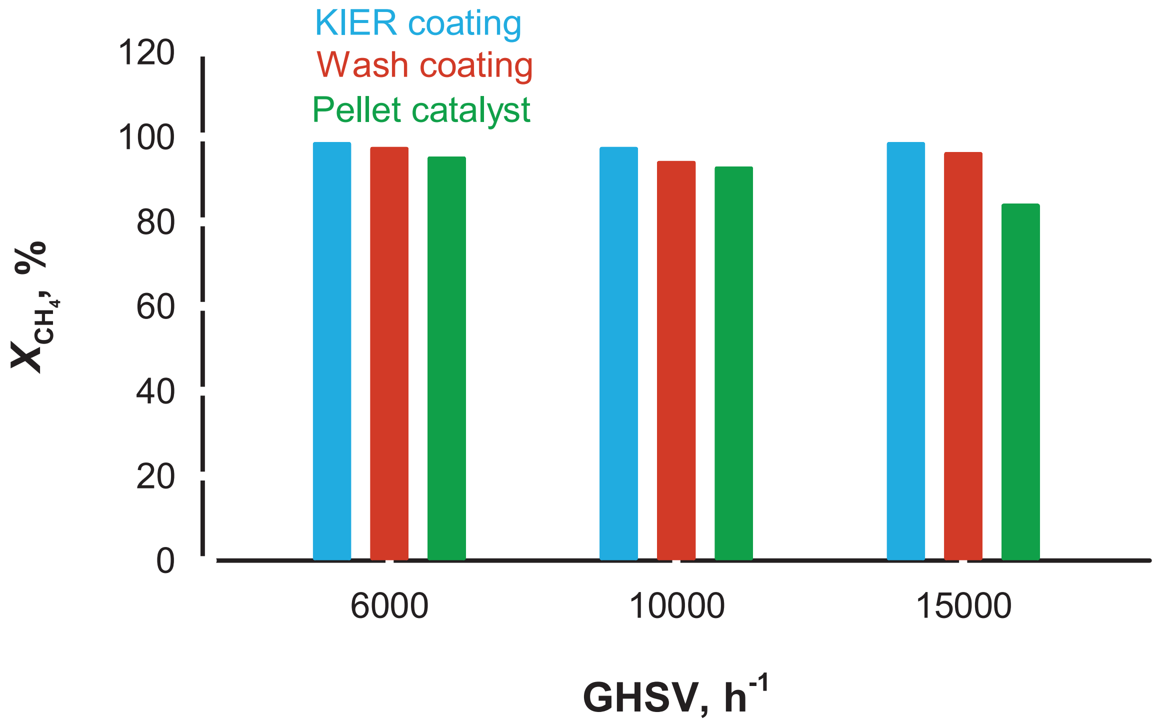

Figure 4.38 CH_4 conversion vs GHSV for Ni/$MgAl_2O_4$ catalyst. Adapted with permission from reference Koo et al. (2016). Copyright 2016 Elsevier.

Percolation-blowing deposition of Ni/$MgAl_2O_4$ on FeCrAl foams is more reproducible compared to dip-blowing Cristiani et al. (2010), which is important for industrial applications. Above 450 °C the catalyst operates at 130 000 mL h^{-1} g^{-1} reaching equilibrium performance.Cristiani et al. (2012) Thermally sprayed Al_2O_3 on FeCrAl, afterward impregnated with Ni, is suitable for millisecond SMR micro-channel reactors and is stable for 500 h at a S/C ratio of 3.0 above 700 °C.Cheng et al. (2011) A metal-monolith with anodic alumina and Ni promoted Pt catalyst was Joule-heated : the start-up time decreased from 30 min to 30 s (Figure 4.39) Guo et al. (2011).

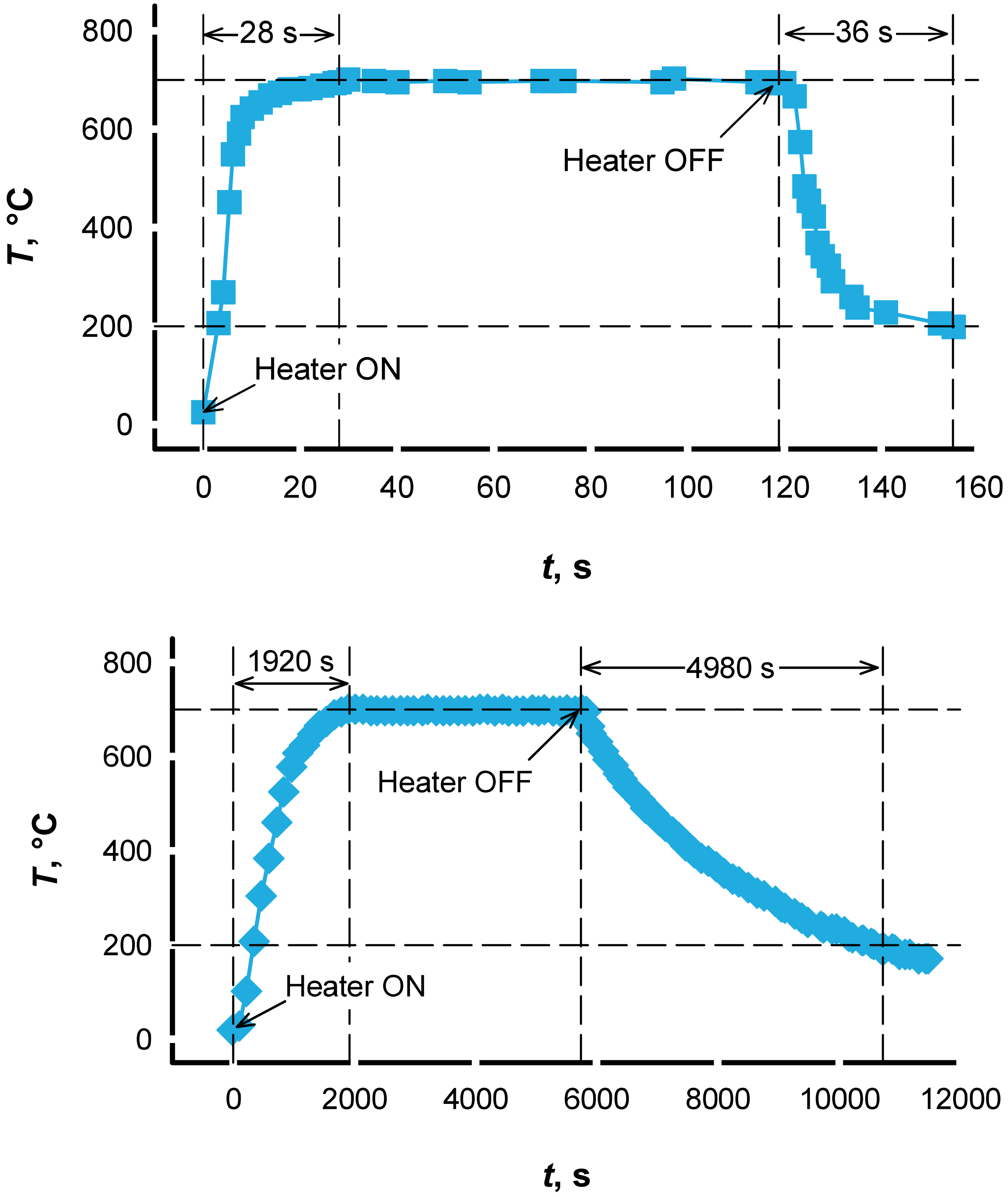

Figure 4.39 Catalyst temperature profile vs time for electrified support (top) and outside heated (bottom) Guo et al. (2011). Copyright 2011 Elsevier.

Ni-Al_2O_3 on microchannel FeCrAl was more active and stable compared to Ni on MgO or

CeO_2/Al_2O_3 De Miguel et al. (2010). 10 % Ni/$Ce_{0.5}Zr_{0.5}O_2$/SBA-15 was the most active and stable among the Ni/SBA-15 monolith catalysts. All the CH_4 reacts at 800 °C for 110 h of time-on-stream Wu et al. (2009). Calcination of Ni/Al hydrotalcite-like compounds electrodeposited on FeCrAl foams at −1.2 V, optimum synthesis conditions Basile et al. (2009), vs. SCE for 1000 s produces a thin and strongly adherent film that has higher density of active sites per unit of mass. Ni metal crystallites dispersed on α-Al_2O_3 prove the catalyst layer is stable after reduction and catalytic tests. Coating stability is related to the intermediate Al_2O_3 scale developed from the foam during calcination. Compared with a commercial pelletized Ni catalyst, under industrial conditions, coated foams reacts more CH_4 even though the catalyst loading is lower Basile et al. (2010a, 2008). Methane conversion was also higher over monolith wash-coated Ni compared to powders because of the better heat transfer and catalyst effectiveness factor Ryu et al. (2007).

Ru and Pt-based catalysts

Ru FeCrAl monolith, prepared via deposition-precipitation, outperforms commercial Ru/Al_2O_3 at higher GHSV (Figure. 4.40) even when the active metal content is 14 times lower. These outstanding results come from the high availability of Ru that leads to long-term stability of the structured bed Koo et al. (2017a).

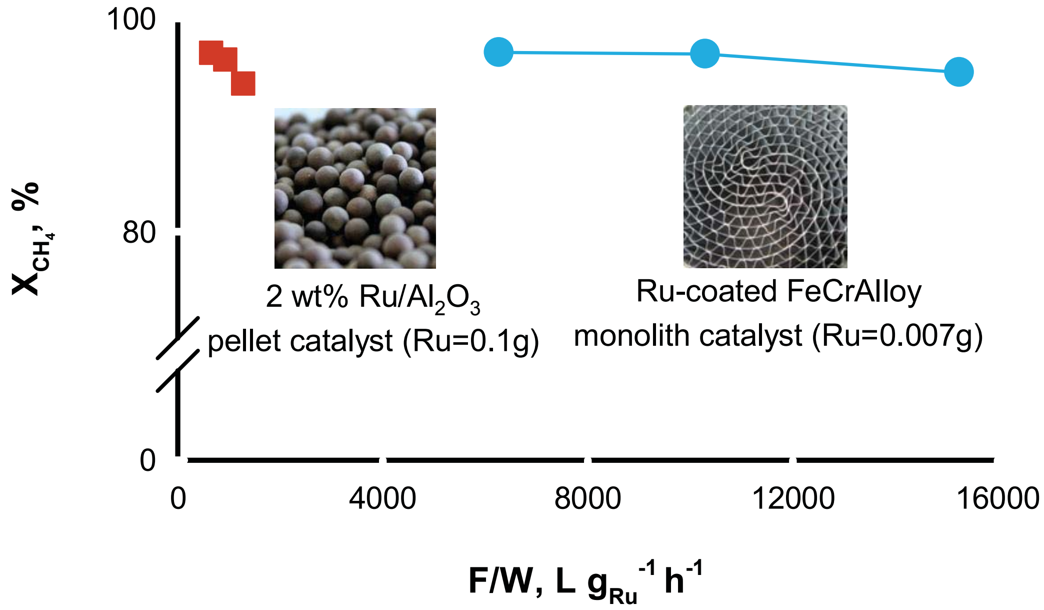

Figure 4.40 Conversion vs space velocity (flow over weight F/W) over commericial 2 % Ru/Al_2O_3 pellet and Ru-coated FeCrAl monolith in SMR at 700 °C, S/C = 3.0, F/W = 430 L g^{-1} h^{-1} to 15 100 L g^{-1} h^{-1} Koo et al. (2017a). Copyright 2017 Elsevier.

Pt-Zr on FeCrAl mesh ignited hydrogen in a microchannel reactor, in which hydrogen provides the start-up fuel. This configuration increases both SMR capacity and energy efficiency without an external energy source from a furnace or burner Ryi et al. (2006). Another type of reformer uses metallic heat exchangers coated with catalyst. Compared to conventional reformers, this design minimizes reactor dimensions, heat transfer resistance, and pressure drop Shi et al. (2008a). These types of operation are possible because of the high temperature stability and the low heat capacity of the FeCrAl structured catalyst.

4.6.2 CH_4 CPOX—Catalytic partial oxidation

The partial oxidation of CH_4 to syngas is mildly exothermic $2\,CH_4 + O_2 \rightleftharpoons 2CO + 4H_2$ ($\Delta H_R = -36\,kJ\,mol^{-1}$) and is suitable for Fisher Tropsch (gas to liquid technologies) because it produces syngas with a H_2/CO ratio of two Christian Enger et al. (2008); Ghoneim et al. (2016). Even if the reaction mechanism and kinetics are widely accepted in the literature, the economics remain unfavourable because the catalyst deactivates or produces CO_2 at high selectivity while hot spots irreversibly damage the catalyst Christian Enger et al. (2008); Chin and Iglesia (2011); Chin et al. (2011a,b). Metal supports minimize hotspots and in the case of FeCrAl the superficial α-Al_2O_3 not only protect the material but also stabilizes the active sites reducing the deactivation rate. Noble metals are more active and less prone to oxidation and carbon deactivation than Ni but both have been supported on FeCrAl (Figure 4.41) Lou et al. (2017); Urasaki et al. (2018); Qin et al. (2018); Wang et al. (2018); Singha et al. (2017).

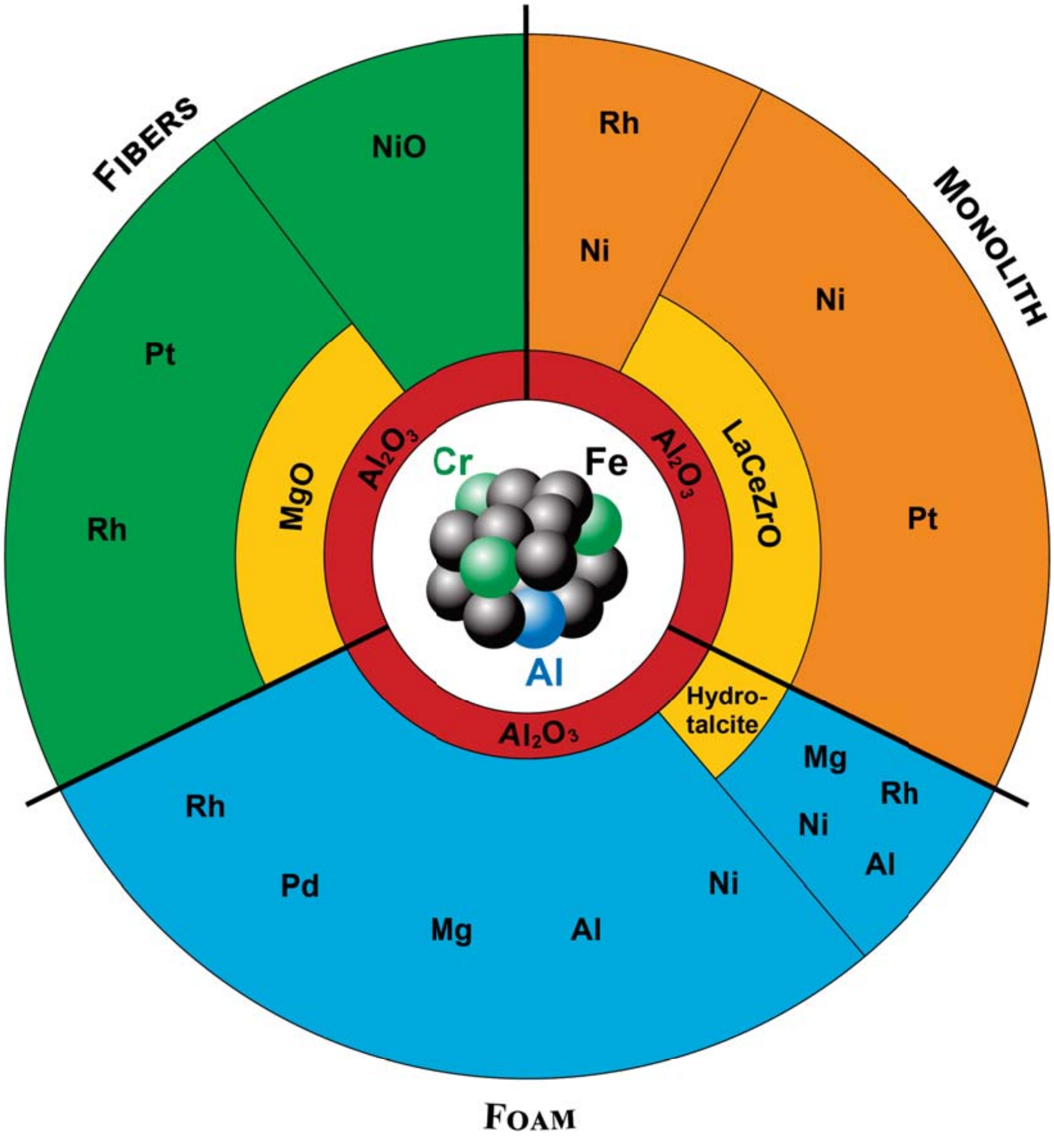

Figure 4.41 Catalyst structure, formulation and active phase for catalytic partial oxidation of methane.

Rh-based catalysts

Because of their higher surface area (compared to monoliths), electrical conductivity, efficient heat transfer, and resistance to oxidation, FeCrAl foams are excellent supports for methane

CPOX Musiani et al. (2015). The in situ synthesis of Rh/Mg/Al hydrotalcite-type (HT) compounds on foams by electrodeposition is as an alternative to the conventional washcoating Benito et al. (2015a); Basile et al. (2010b,c).

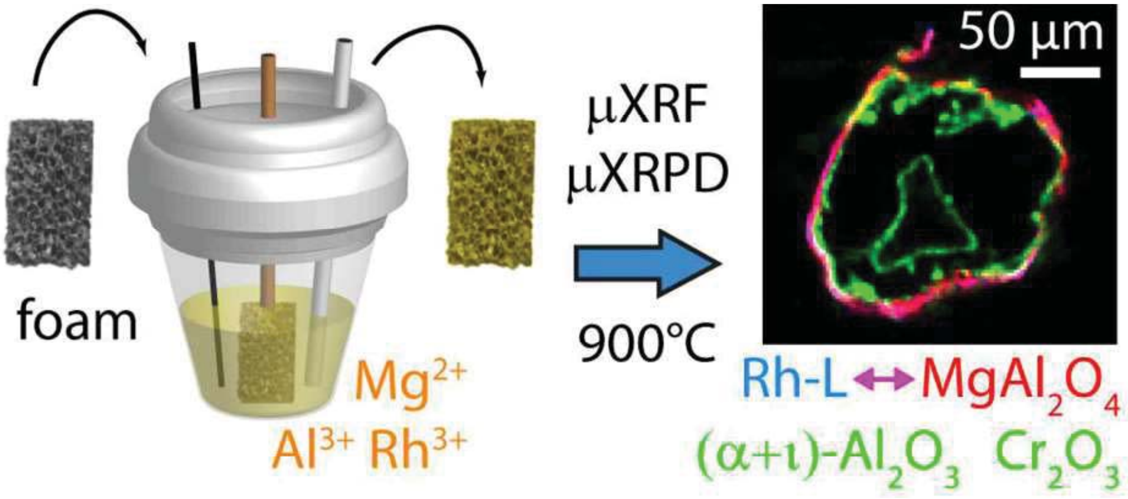

Figure 4.42 Production method and micrograph of electrosynthesized Rh foam. Adapted with permission from reference Benito et al. (2014). Copyright 2014 American Chemical Society.

These catalysts combine the properties of HT compounds and open cell foams. Thermally stable nano MgO and spinel-type phases contain Rh highly dispersed and stabilized against sintering, with better mass and heat transfer. $MgAl_2O_4$ thin films in the support-coating interface, formed via chemical reaction between Mg^{2+} from the coating and Al^{3+} from the support during calcination, improves catalyst adhesion (Figure 4.42) Ho et al. (2016); Benito et al. (2014). After 50 h on-stream, the coat is stable and the 2 nm Rh nanoparticles are still well dispersed Benito et al. (2015b). Partially substituting Mg^{2+} with Ni^{2+} in the synthesis solution produce an active bimetallic Rh/Ni catalyst with CH_4 conversion and selectivity to syngas higher than 90 % Benito et al. (2015b).

Complementary to the electro-base generation method, direct cathodic electrodeposition of Rh on foams produces an active phase that undergoes constant deactivation mainly coming form the growing Al_2O_3 layer. In this case the catalyst stability result lower compared to a washcoated catalyst sample Verlato et al. (2014). Traditional methods impregnate the thermally grown Al_2O_3 on the surface of a microchannel reactor, where dispersed Rh on the porous surface improves H_2 selectivity Aartun et al. (2004). Washcoating of a Nicrofer reactor with alumina via a sol-gel technique forms a surface coating with low stability ; during operation, Cr species cover the Rh particles and channel surface Enger et al. (2008). Even if hydrocarbons ignition at the entrance of the monolith leads to lower syngas production, higher GHSV limits this phenomenon Aartun et al. (2005).

Catalytic modules based on Rh/θ-Al_2O_3/FeCrAl fiber mesh with both radial and axial intermixing (Figure 4.43), as an alternative to open-cell foams, increase heat transfer. This configuration, coming from a FeCrAl nets, is less expensive and more accessible in the market. Strongly bound θ-Al_2O_3 coating create a porous support for incipient wetness impregnation of Rh. The composite architecture maintains Rh highly dispersed with good adhesion despite operating above 900 °C for 20 h on stream with 4 start-up/shut-down cycles Rogozhnikov et al. (2019).

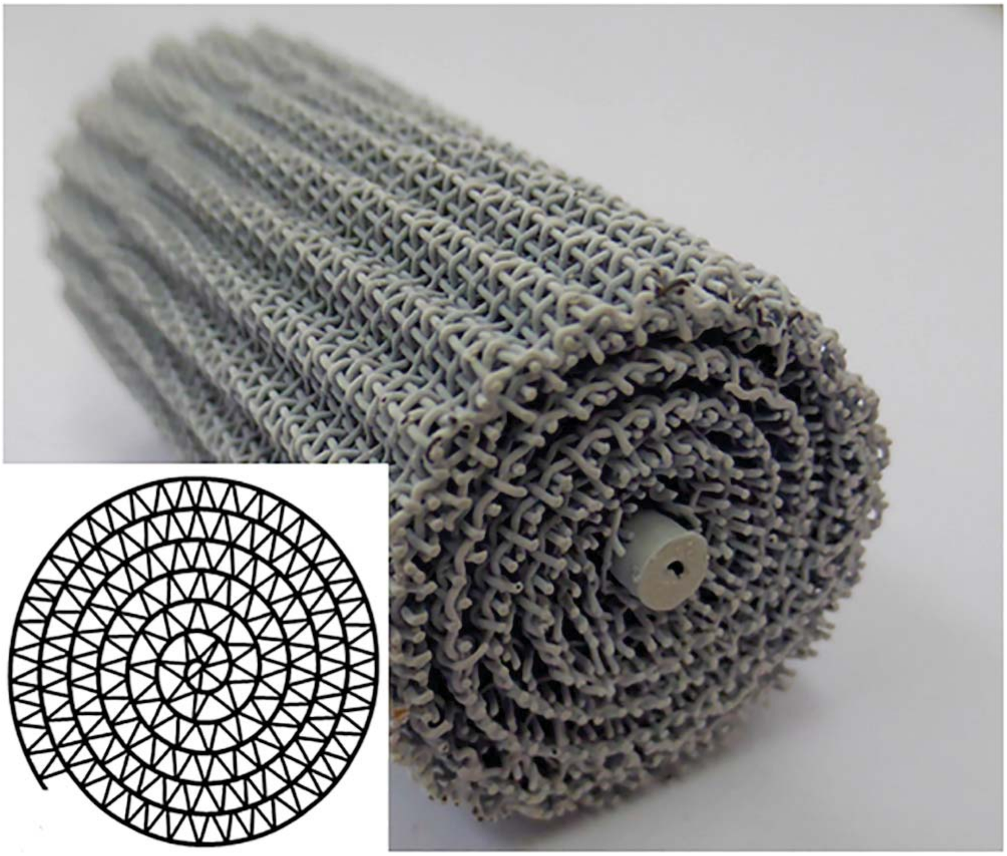

Figure 4.43 Structured catalyst overview and cross section Rogozhnikov et al. (2019). Copyright 2019 Elsevier.

Rh impregnated on γ-Al_2O_3 support on FeCrAl foam performed as good as a packed bed in the partial oxidation of dimethyl ether at a catalyst loading 10 times lower for 1200 h Kim et al. (2015).

Pt and Ni-based catalysts

Pt-catalyst deposited on woven fibers partially oxidize CH_4, reaching almost equilibrium performance at 20 bar and 800 °C. Compared to commercial Pt-gauzes, H_2 and CO selectivities were higher Neagoe et al. (2016). CPOX forms more coke with increasing pressure and deactivates the catalyst. MgO layers, produced via SCS on the alloy fibers, supports a 1 % mass fraction of Pt-Rh that adheres to the support based on an ultrasonic stress test Ma et al. (2016a).

Bimetallic Ni-Pt/$La_{0.2}Zr_{0.4}Ce_{0.4}O_x$ partially oxidizes methane in a microchannel reactor containing ten corrugated FeCrAl foil plates. The efficiency of this reactor type is proportional to the number of plates, as both CH_4 conversion and CO selectivity remain constant. All the methane combusts at the inlet and corrodes the plate ; complete oxidation in these zones suggests that the oxide layer cracks and exposes Fe. Despite the corrosion, after 40 h on-stream at 840 °C hydrogen yield only dropped by 10 % Makarshin et al. (2015). Preoxidized FeCrAl fibers supporting Ni-$CeAlO_3$-Al_2O_3 synthesized via hydrothermal growth of LDHs achieving CH_4 conversion higher than 85 % while reacting at 700 °C. Decomposition of NiAl-LDHs stabilizes Ni nanoparticle for more than 350 h on stream, while the presence of $CeAl_2O_3-CeO_2$ minimizes carbon Zhao et al. (2019).

4.6.3 DMR—Dry methane reforming

In DMR methane and carbon dioxied react to form carbon monoxide and hydrgen : $CH_4 + CO_2 \rightleftharpoons 2CO + 2H_2$ (ΔH_R=247 kJ mol^{-1}). The high concentration of carbon favors coke and the reaction rate to coke increases with increasing pressure, particularly above 10 bar, which is required to achieve attractive process economics Schulz et al. (2015). Even if Pt and Ru are more active and resist coke better, the low cost of base metals like Ni are preferred industriallly Lercher et al. (1996); Lou et al. (2017); Aziz et al. (2019). Cold spots (rather than hot spots), reduce conversion and promote coke, while a highly conductive, permeable 3-D metal support minimizes thermal gradients Zhang and Li (2015); Cao et al. (2010); Peng et al. (2017). 3-Aminopropyltriethoxysilane facilitates creating a macro-meso-nano scale structure in a single step, starting from a fiber felt. The resulting Ni on SiO_2/Al_2O_3/FeCrAl contains cross links that are active, selective, and stable even after operating 500 h at 800 °C and a gas hourly space velocity of 5 L g^{-1} h^{-1} Chai et al. (2017b).

At these conditions, another promising FeCrAl-fiber-structured nanocomposite, NiO-MgO-Al_2O_3, maintained CH_4 conversion constant at 90 % during the initial 90 h, but decreased to 10 % over the following 180 h Chai et al. (2017a). Among the various Ni/SBA-15 catalysts synthesized via wet impregnation and waschoated on FeCrAl monolith, the ones with a Ni loading of 8 % was active and stable at 800 °C for over 1400 h time on stream. The hexagonal mesoporous structure of SBA-15, which minimizes coke formation, together with the benefits coming from the higher thermal conductivity of the support enhance the performance Wang et al. (2008a, 2007).

A laboratory-scale tubular reactor, consisting of two coaxial monolith cylinders, combines two reactions : the heat produced by the catalytic combustion of CH_4 over $LaFe_{0.5}Mg_{0.5}O_3/Al_2O_3$/FeCrAl (inner monolith) moves to the endothermic CO_2-CH_4 reforming over Ni/SBA-15/Al_2O_3/FeCrAl. The conversion of methane and carbon dioxide exceeds 90 % while the energy efficiency reaches 82 % Yin et al. (2009). FeCrAl's ability to be shaped allows creative shapes to create flow paths in reactors to achieve the performance prescribed by process intensification. An electrically heated reactor with $LaNi_{0.95}Ru_{0.05}O_3$ catalyzed CH_4 conversion ; conversion increased with temperature but plateaued at 900 °C Rieks et al. (2015).

4.6.4 ATR—Autothermal reforming

While SMR is strongly endothermic and CPOX is mildly exothermic, oxygen is co-fed together with steam so that the ATR operates isothermally and absent of a external heat source or cooling. Like SMR, CPOX, and DMR, ATR requires catalyst supports that operate at high temperature in the presence of H_2O and O_2 rich atmospheres. FeCrAl and traditional ceramic supports are among the few materials that meet these conditions. Methane conversion reaches 88 % over a NiO-Al_2O_3/FeCrAl-fiber catalyst at a H_2/CO selectivity of 90 % at 700 °C. NiO was highly dispersed on Al_2O_3/FeCrAl-fiber prepared via incipient wetness impregnation. Overall the catalyst was stable for more than 30 h, which was 24 h more than a washcoated NiO on FeCrAl-fiber Chai et al. (2017c). Rh particles, prepared through sorption-hydrolytic deposition, on $Ce_{0.75}Zr_{0.25}O_{2-\delta}$ mixed with alumina powder show 100 % conversion during the first 6 h on stream that afterward decreases following carbon deposition. When supported on FeCrAl, it achieved 100 % conversion for 12 h without forming coke on the surface Shoynkhorova et al. (2018). Ni/$Ce_{0.75}Zr_{0.25}O_2$ washcoated on FeCrAl foams autothermally reform iso-octane in stainless steel and quartz microreactors. Quartz and insulated (no contact between reactor walls and catalyst support) reactors reached light off at 150 °C and 100 °C, respectively, lower than the standard assembly configurations, which demonstrates the strong effect of the heat transfer through the reactor walls Tadd et al. (2005).

4.6.5 Methanol steam reforming

The advantages of methanol versus methane as a fuel to produce syngas via steam reformning $CH_3OH + H_2O \rightleftharpoons CO_2 + 3H_2$ (ΔH_R=49 kJ mol^{-1}) relates to logistics and infrastructure capital investment Palo et al. (2007). The major catalyst systems for this process include Cu, Pd/ZnO, Ir and Pd-Zn. A 2.5 % Pd on ZnO prepared via wet impregnation is more active than the same catalyst washcoated on FeCrAl monolith. The catalyst appeared homogeneous and adheres well to the surface, but its activity suffers because of the additional aqueous dissolution and re-precipitation process occurring during washcoating (surface area decreases). Impregnating and washcoating the monolith simultaneously with an aqueous soultion of the ZnO support, colloidal zinc oxide, and palladium nitrate overcome these drawbacks. This all-in-one strategy eliminates also the intermediate calcination step Echave et al. (2014). Performance of aluminum and brass supports were higher than the FeCrAl which was imputed to the formation of cracks or Fe migration that deactivates the active phase but also because of the higher thermal conductivity of the two materials. The surface Al_2O_3 coating dehydrates methanol to dimethyl ether but none was detected during the tests with the Pd/ZnO coated FeCrAl monolith, which suggests the catalyst homogeneously covered the Al_2O_3 Echave et al. (2013).

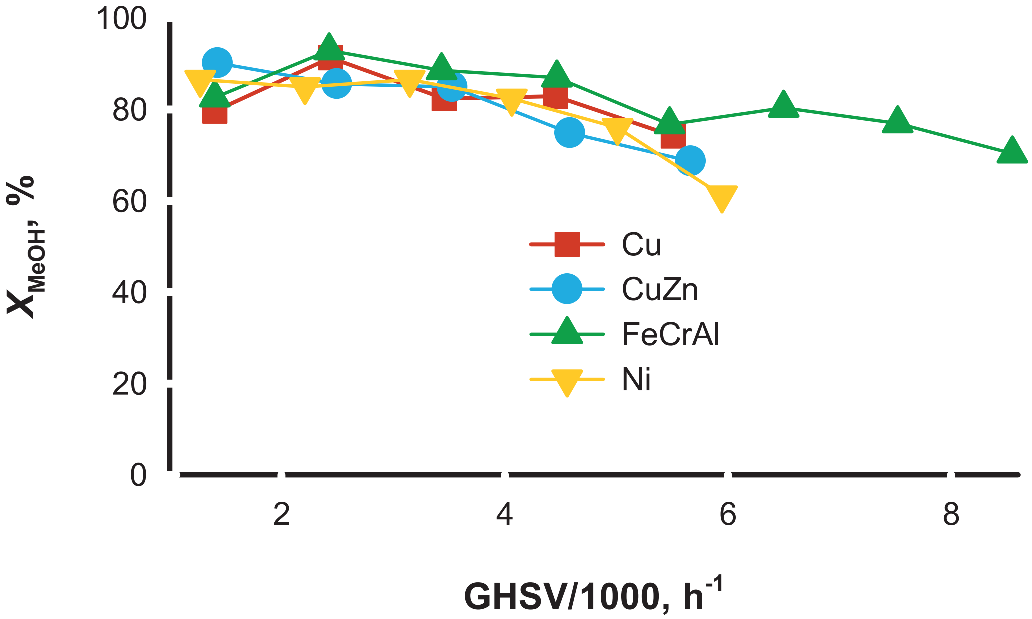

Figure 4.44 Methanol conversion vs of GHSV on different metal foam Yu et al. (2007). Copyright 2007 Elsevier.

Catalyst poisoning by metal support elements is also reported for Cu/Zn/Al/Zr active phases on foams tested in microcatalytic reformers at 600 °C (Figure 4.45, 4.44). The calcination temperature during preparation was too low to form a stable and uniform superficial protective alumina coating ; however, interactions between active metals and support minimize the WGS, resulting in a higher CO selectivity Yu et al. (2007).

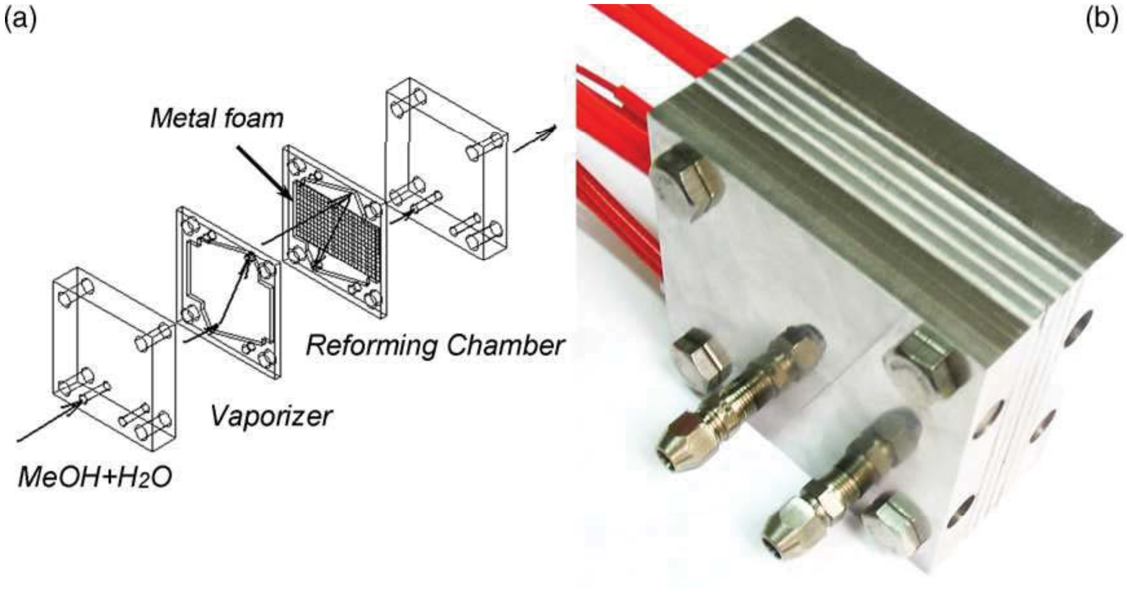

Figure 4.45 Reactor mechanical drawing : (a) integrated operative reactor (b) Yu et al. (2007). Copyright 2007 Elsevier.

Pd/Zn have also activity similar to Cu/Zr Wang et al. (2008b). Ir on Al_2O_3 or on $Ce_xZr_{1\text{-}x}O_2$ with or without Al_2O_3 are active in the production of H_2 from methanol. Washcoating with boehmite as primer for the combination of these metal oxides as superficial layers well resisted ultrasonic vibration mechanical tests ; the final catalyst was active for more than 120 h Jia et al. (2008).

4.6.6 WGS—Water gas shift reaction

Hydrogen is the desired product in SMR and to increase yield carbon monoxide and water present in the syngas further reacts following the water gas shift reaction (WGS) $CO + H_2O \rightleftharpoons CO_2 + H_2$ ($\Delta H_R = -42\,kJ\,mol^{-1}$) Rostrup-Nielsen et al. (2002). Industry applies Cu promoted Fe−Cr or Cu−Zn at 250 °C to 400 °C Holladay et al. (2009). The interests of FeCrAl for this reaction come for the tighter temperature control combined with a lower pressure drop across the catalytic bed. The possibility of electrifying syngas synthesis introduces novel reactor designs with multiple zones and catalysts simultaneously. In this way it is possible to both reform CH_4 and shift CO in the same unit to intensify the process, decreasing capital cost and making it possible to scale down H_2 production avoiding expensive fired furnaces and decreasing the land footprint Basini et al. (2012); Wismann et al. (2019a). Alternate layers of plasma-polymerized precursors form an active layer with Pt and zirconia. During the calcination step, catalyst detaches from the surface and the remaining fraction forms cubic phases and thus requires higher temperatures to activate the WGS Dhar et al. (2005). 3 % Ru/TiO_2 and 6 % Ru/CeO_2-ZrO_2 supported on microchannel FeCrAl convert 78 % of the CO_2 in the revers WGS at 365 °C and a GHSV of 30 500 h^{-1} Hu et al. (2007a).

4.6.7 CO PROX—CO preferential oxidation

The increasing demand of H_2 to replace fossil fuel triggers the interest in preferential CO oxidation. In the case of fuel cells for automotives, the upper CO limit, to minimize catalyst deactivation, is 5 ppm Korotkikh and Farrauto (2000). FeCrAl is suitable for this reaction as it is stable at the maximum operating temperatures (400 °C) with a minimal pressure drop. CuO-CeO_2/Al_2O_3 prepared by sol-pyrolysis adheres well to FeCrAl monolith surfaces based on ultrasonic and thermal stress tests. While in this case the catalytic activity is independent of the nature of the support (FeCrAl monolith), the interaction and distribution of the active phase depends on it Zeng et al. (2007). Nd and Zr improve the catalytic performance in the selective oxidation of $CO-H_2$ mixtures. They influence CeO_2 and CuO, decreasing the oxidation of H_2 in favor of CO ; the higher thermal properties of FeCrAl decrese temperature gradients limiting the reverse water gas shift reaction Zeng and Liu (2008). Pt on metal foam is also active in the selective oxidation and the results are similar to those of Pt/Al_2O_3. Fe impurities on the surface creates peculiar features that can be reproduced in the Al_2O_3 powders when Fe is added. Considering the two different materials the metallic foam was more active because of its physical properties (low porosity and low surface area) and of Fe impurities Sirijaruphan et al. (2005). At 72 000 $cm^3\,g^{-1}\,h^{-1}$ bimetallic Pt-Co impregnated on η-Al_2O_3 on FeCrAl gauze activate CO oxidation at 140 °C, 75 % conversion was achieved at 200 °C Potemkin et al. (2019).

4.7 Other applications

Other than for high temperature oxidation (TWC, SMR, CPOX, CO and CH_4 oxidation) FeCrAl structured supports catalyze reactions like oxidative coupling of methane (OCM), Fischer-Tropsch (FT) or mild exothermicity as transesterification and hydrogenation. The excellent mechanical properties, the easy support functionalization, and the benefit of shaping have brought FeCrAl to these lower temperature and non-oxidative applications.' FeCrAl supports improve micro channels reactors, that Velocys® has already exploited in the design of FT production units Lerou et al. (2010); LeViness et al. (2014). The wide variety of producible geometries of FeCrAl tune mass and heat transfer increasing yield toward desired products.

4.7.1 OCM—Oxidative coupling of methane

An alternative to high-temperature processes based on syngas is the oxidative coupling of methane (OCM) ($2\,CH_4 + O_2 \rightleftharpoons C_2H_4 + 2H_2O$, $\Delta H_R = -165\,kJ\,mol^{-1}$) Galadima and Muraza (2016); Lunsford (1995). Catalyst development stalled because of the poor yields and the research community shifted their focus towards Fischer-Tropsch, with world-scale plants built by Shell and Sasol Hoek and Kersten (2004); Sichinga and Buchanan (2005). Recently new studies on OCM are underway Weinberger et al. (2012).

Na_2WO_4, Mn_2O_3, and PbO catalysts on FeCrAl foil coated with Al_2O_3 and SiO_2 are candidates for the oxidative condensation of methane. SiO_2 is sensitive to calcination conditions and less stable than Al_2O_3 coating, given the chemical affinity Kustov and Tkachenko (2013). Bulk Mn-Na_2WO_4/SiO_2 catalyst converts 12 % CH_4, this performance was matched by electrophoresis-deposition of the bulk catalyst on SiO_2/FeCrAl monolith. Structured catalyst shows 50 % lower activity compared to bulk catalyst because of the modification induced during electrophoresis deposition Greish et al. (2009). Placing 5 % ($g\,g^{-1}$) Na_2WO_4-2 % Mn/SiO_2 in tandem with Ce/Na_2WO_4/SBA-15/Al_2O_3 as a dual bed reactor increased conversion when a tube fed oxygen at the interface between the two beds. Optimized temperature distribution of this configuration improved C_2H_4 selectivity (2 %) compared to the powder fixed bed Wang et al. (2012).

Joule heated fibers convert methane to acetylene either in the absence of oxygen or at $CH_4:O_2$ ratios greater than 9 Sigaeva et al. (2013). Zirconia or alumina (on FeCrAl) together with silicon carbide catalyzed the reaction. Activation started at 600 °C producing ethane and ethylene. FeCrAl (without any active metal) reached 45 % selectivity at 1200 °C which is 7 times higher compared to the results with carborundum Sigaeva et al. (2017) ; this is stable but do not contribute to the catalyst activity.

4.7.2 FT—Fischer Tropsch

Fe and Co are the active catalysts to polymerize CO to hydrocarbons ($n\mathrm{CO} + (2\,n+1)H_2 \longrightarrow C_nH_{2n+2} + nH_2O$, $\Delta H_R = -165\,kJ\,mol^{-1}$) in the range 200 °C to 350 °C and 10 bar to 25 bar Speight (2014). Slurry reactor technology has displaced Sasol's synthol reactors because of their higher productivity and yield. Recent work, on the other hand, has explored fixed bed reactors with inserts to increase the thermal heat transfer to remove the high amount of heat released during the reaction Frost et al. (2016). FeCrAl and microfibrous structures increase heat transfer from the centre of the bed towards the walls. A new type of engineered catalyst based on multilayer thin film of Al_2O_3 and carbon nanotube arrays over FeCrAl foam showed noteworthy catalytic performance in an associated microchannel reactor (Figure 4.46). This catalyst enhanced Fischer-Tropsch (FT) synthesis activity by a factor of 4 compared to a catalyst structure without the carbon nanotube arrays. Because of the superior thermal conductivity, carbon nanotubes enhance the heat removal from catalytic active sites during the highly exothermic reaction, the reactor operates at 265 °C without runaway phenomena Chin et al. (2005).

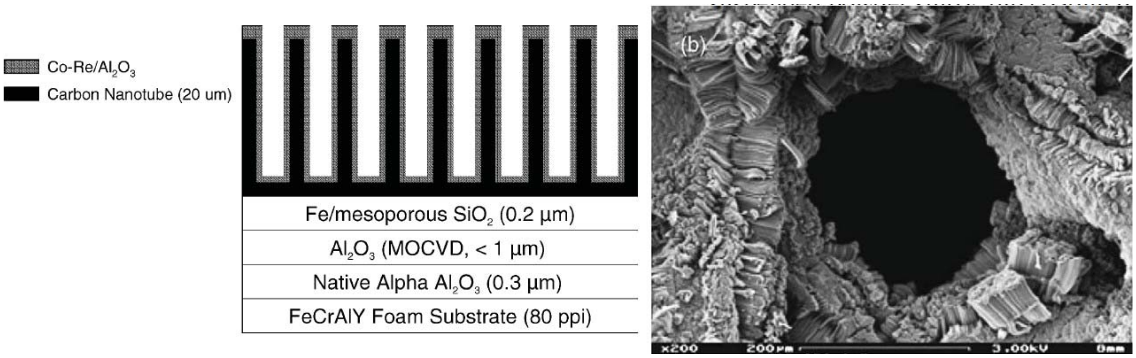

Figure 4.46 Schematic of engineered catalyst based on multilayer carbon nanotube arrays for Fischer-Tropsch synthesis in a microchannel reactor (left). Micrograph of the prepared foam (right) Chin et al. (2005). Copyright 2005 Elsevier.

Activity and selectivity with 20 % (g g^{-1}) Co/γ-Al_2O_3 catalyst washcoated on monolith operating at 250 °C, 10 bar and H_2/CO=2 were the same as the powder sample Almeida et al. (2007). Washcoated Co-Re/Al_2O_3 on monolith catalyzed the FT reaction at 20 bar and 220 °C. Higher average catalyst layer thickness resulted in higher CH_4 and lower C^{5+} selectivities ; the local heat removal capacity decreases as the heat transfer in the porous ceramic layer decreases. Overall reactor thermal conductivity, both on a micro and macro scale, must be tuned to remove the heat from the active sites (via coating layer) and to transfer it through the reactor wall (via metal support). In the case of foams, the thermal properties are proportional to cell density and tuning this parameter together with the catalyst activity plays an important role in the reaction yield Merino et al. (2017).

4.7.3 Biodiesel

Heterogeneous catalysts for biodiesel synthesis and post-treatment potentially decrease operating cost and waste ; however, the main challenge is slow mass transfer of the bulky triglycerides and leaching. Anchoring the catalytic active phase on a structured support with tunable pores size addresses both mass transfer and leaching. Ca/Ce oxides on FeCrAl monoliths activate the transesterification of sunflower oil to biodiesel. Metal citrated as precursors and isopropanol as solvent produced the most active catalyst Reyero et al. (2016). Transesterification with 2 % Mg-Al HT compounds on a similar support reached 62 % to 77 % triglyceride conversion after 10 h in a monolithic stirred reactor at 60 °C. The main challenges for the washcoating are the low surface area coming form the low porosity, and adhesion. Reyero et al. found that a binder is essential to limit the leaching of the active phase : the mass loss of catalyst prepared with a 0.05 $\mathrm{g\,g^{-1}}$ to 0.10 $\mathrm{g\,g^{-1}}$ methanol washcoating slurry was only 4 % after a 30 min ultrasonic stress test Reyero et al. (2013). FeCrAl catalyst have yet to achieve commercial activity for biodiesel where commercial technologies convert 95 % of the triglycerides after 2 h. Often, biodiesel derived from unsaturated triglycerides is unstable to oxidation ; a mild hydrogenation of the double bonds increases its stability and FeCrAl can be adopted also as a support for hydrogenation catalysts. FeCrAl monolith washcoated with $\mathrm{Pd/Al_2O_3}$ partially hydrogenated sunflower oil at 100 °C and 4 bar. Compared to powder catalysts, the structured ones had lower selectivity to trans-isomers, while the equivalent ceramic monoliths were stable, FeCrAl based catalyst lost 10 % in activity after 3 reaction cycles, because of the active phase leached Sánchez M. et al. (2009). Multiple FeCrAl oxidation steps formed $\mathrm{Al_2O_3}$ whiskers (Figure 4.47) ; the advantage of this micro structure support is the improved mass transfer and reduced catalyst pore mouth blocking Samad et al. (2011).

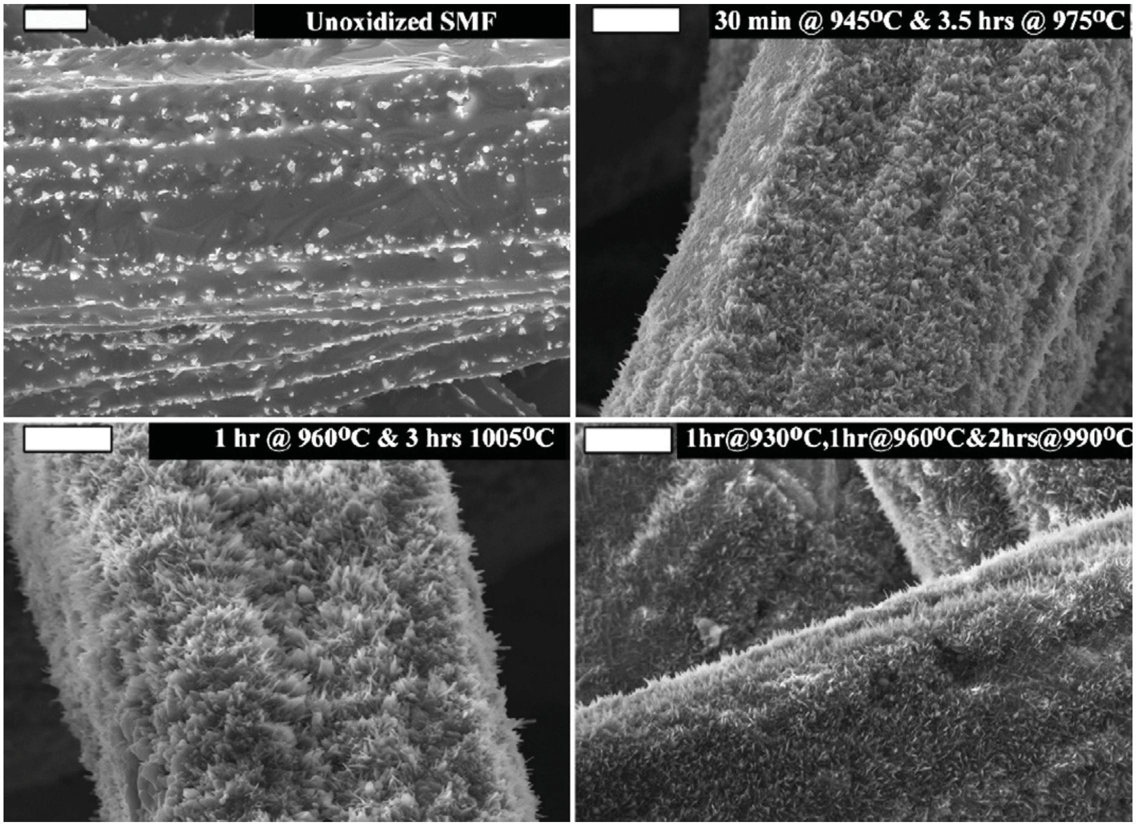

Figure 4.47 SEM micrograph of sintered micro fibers oxidized at various temperatures Samad et al. (2011). Copyright 2011 Elsevier.

4.7.4 Miscellaneous

Cr/SBA-15/Al_2O_3 on a FeCrAl monolith oxidatively dehydrogenated ethane with CO_2 for over 1130 h. Ethane conversion and ethylene selectivity were respectively 66.5 % and 99.5 % at 750 °C with a 5 % Cr loading. Cr^{6+} species were the most likely reason the activity was so high Shi et al. (2008b). Well adhered catalytic films of zeolites (ZSM-5 and Y) and alumina pre-impregnated with 1 % Pt on metal fibers cracked n-heptane and dehydrogenated methylcyclohexane, respectivel. Yield was comparable to traditional pellet and powder catalyst but these coated structure improved temperature distribution and mass transfer.

Rh in microchannel reactors is active to produce alcohols and C_{2+} oxygenates from biomass-derived syngas. CH_4 formation is suppressed at low temperature, high pressure and low H_2/CO ratio. A hybrid catalyst of CuZnAl and Rh-Mn/SiO_2 showed increasing activity after redox cycles. Rh-Mn/SiO_2 coated on FeCrAl doubles the catalyst activity considering the moles of CO converted Hu et al. (2007b).

Mo and W oxides coated FeCrAl for the thiophene hydrodesulfuration reaction at 400 °C and 1 atm. The slurry of Mo implied higher catalytic activity than the W slurry. Oxidizing atmosphere or concentration of electrolytic solution, long time and high temperature treatment fostered the roughness of the coated layer. In addition to fixing the catalyst, the oxidizing layer contributes to the thiophene conversion Diaz et al. (2013).

Gas phase propylene epoxidation on gold catalysts exhibits high selectivity. However, propylene conversion was low and the catalyst deactivated rapidly. These issues led to the design of new microchannel reactors, allowing catalyst regeneration thanks to a fast electric heating. Exploiting FeCrAl resistance, Au/TiO_2 dip-coated on alloy served as catalyst for the reaction Yuan et al. (2005). Application of FeCrAl materials has also been reported in the methanation of CO as this metal fibers and monolith offer additional benefits like higher thermal conductivity and mechanical resistance compared to other ceramic supports noz Murillo et al. (2018); Konishcheva et al. (2019, 2020). Washcoating a FeCrAl monolith after preoxidation at 900 °C with RuO_2/Al_2O_3 produced a more active structure compared to the primary particles. The preparation of the slurry and the calcination of the structured catalyst after washcoating modified the active phase. Conversion was higher than 93 °C and the optimal temperature of the metal supported catalyst was shifted to a lower temperature compared to RuO_2/Al_2O_3 noz Murillo et al. (2018).

4.8 Future applications

One of the most promising applications of FeCrAl supported catalysts is the possibility of exploiting the electrical resistance of the support Dou et al. (2020); Mortensen et al. (2018). This will make it possible to switch from fuel combustion as a heat source to renewable electricity in the chemical industry Van Geem et al. (2019). Only recently SMR electrification has been reported in the scientific literature Wismann et al. (2019a,b), while a similar technology has been reported in the patent literature Basini et al. (2012). The high mass and heat transferring properties of FeCrAl structures, combined with the in-situ generation of heat, would reduce land and carbon footprint of the chemical industry. The remaining problems limiting these applications are :

- unsatisfactory stability and adhesion of the catalyst coatings with the bulk metal support that limits operating lifetime ;
- low electrical resistance of the macroscopic structure given the considerable cross section that requires prohibitive currents at low potential to achieve required wattage per volume.

Different high resistivity and high temperature materials such as SiC and tungsten could also be used but in this case their ceramic-behaving mechanical properties limit their application and transformation into macroscopic structures Dyos (2012). Achieving a more environmentally friendly chemical industry through electrification will require tighter collaboration between chemical engineering, catalysis, surface science, metallurgy and electrical engineering

4.9 Conclusions

FeCrAl as a catalytic support has a tremendous potential for energetic reactions operating in challenging environments not only because of its exceptional thermal characteristics and superior mechanical properties but also because it is flexible and can be formed into many shapes. 3-D printing represents an opportunity to optimize reactor configuration and flow patterns to minimize mass transfer resistance and maximize heat transfer area ; FeCrAl offers similar flexibility but with the advantage of economies of scale in the manufacturing process. Pressure drop across FeCrAl structured supports are orders of magnitude lower than in packed beds. Exploiting Joule heating in SMR minimizes reactor volume and catalyst mass and would decrease the annual world wide CO_2 emission by 1 % Wismann et al. (2019a). Mobile micro-gas-to-liquids units that convert flared natural gas to fuel and chemicals exploit FeCrAl features to partially oxidize methane to syngas at 1000 °C and milli-second residence times.

The potential of FeCrAl relates to it ability to operate at high temperature—Three-Way-Catalysts and syngas production, for example—but also for Fischer-Tropsch synthesis, transesterification, and hydrogenation. The bulk of the published literature is still mainly focused on the metallurgical aspects of the material and uptake in the chemical field is lagging. Austenitic FeNiCr covered with Al combines mechanical and oxidation resistance features Hattendorf et al. (2008), but requires an additional step in the production process that increases further the cost of this high temperature alloy ; adhesion between Al_2O_3 coating and bulk metal also requires additional improvement. FeCrAl has already been applied to more than 10 chemical processes and improved yield while reducing the physical footprint. The possibility of washcoating and even more of synthesizing in situ zeolite, hydrotalcites, bentonites and metal oxides will further enhance the application of this material in the chemical industry and in the development on new catalysts and processes.

Operating at higher temperature increases reaction rates and by controlling heat transfer and mass transfer, yield improves. Introducing structure to reactor design reduces spatial randomness and these features correspond to the principles of process intensification to reduce the equipment scale by improving efficiency while meeting the goals of sustainability.

CHAPTER 5 ARTICLE 2 : Ni/CeO$_2$ SUPPORTED ON FECRAL GAUZE FOR CYCLING METHANE CATALYTIC PARTIAL OXIDATION—CPOX

Gianluca Pauletto, Nicole Libretto, Daria C. Boffito, Jeffrey T. Miller, Andreas Jentys, Gregory S. Patience, Johannes Lercher

Article submitted to Applied Catalysis B : Environmental (I.F. 14.2)

5.1 Abstract

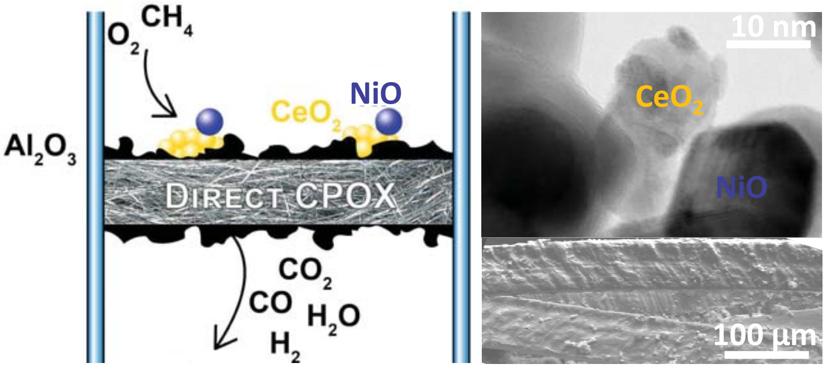

Stranded natural gas is economically unattractive due to high operating and investment costs necessary to bring it to market but promoted Ni-based catalysts supported on a FeCrAl knitted gauze partially oxidize CH$_4$ in air to syngas at a GHSV up to 200 000 h^{-1}. High syngas selectivities at 1 bar, 700 °C and CH$_4$/O$_2$ ratios of 2.5 to 5 suggests an apparent direct reaction path to CO and H$_2$ selectivities. Ru promoted catalysts had higher turnover rates in CH$_4$ activation compared to Ni, Ni-Pt and Ni-Pt-Ru. All catalysts containing Pt formed carbon species refractory to air regeneration at 700 °C. 2.25% Ni with 0.1% Ru had the highest CH$_4$ turnover rate (155 mol s^{-1} mol^{-1}) and CO selectivity (80 %) at CH$_4$/O$_2$ ratio 2.5. CH$_4$ conversion and CO production were constant after 50 reaction-regeneration cycles that involved 25 min methane/air followed by an equal dosing time in air at the same reaction temperature.

5.1.1 Keyword

CPOX, FeCrAl, Gauze, Natural gas, Flaring, Ni/CeO$_2$, Syngas

5.2 Introduction

Stranded natural gas from oil extraction (predominantly CH_4) represents an unexploited revenue stream, while at the same time contributes greenhouse gas emissions. The volume of CH_4 flared worldwide corresponds to the volume Germany and France combined consume every year Elvidge et al. (2016); Ismail (2012). The main impediment to exploiting this resource is high cost to build infrastructure with respect to its low value, particularly for remote oil wells Ma et al. (2016b). Rather than investing in pipelines or liquefaction projects, companies vent and flare the associated gas, or shut-in wells when required by legislation Emam (2015).

Micro-refinery gas-to-liquid units (μGtL) at the well head could meet the economic constraints by reducing cost of the first step in the process—methane to syngas (CO and H_2), which represents 40 %-50 % of the total capital investmentMohajerani et al. (2018); Wright et al. (2003).

Water, CO_2 and O_2 are oxidants for the syngas reaction—steam methane reforming (SMR), dry reforming, and partial oxidation (POX), respectively. POX produces a H_2 :CO ratio of 2 :1, which is optimal for the downstream Fischer-Tropsch (FT) reaction of the μGtL Trevisanut et al. (2016). POX operates above 1200 °C, but catalyst activates the reaction as low as 500 °C (CPOX). Challenges remaining for the CPOX process include Christian Enger et al. (2008); Ghoneim et al. (2016) :

i) coke formation that deactivates the catalyst surface ;

ii) high CO_2 selectivity ;

iii) local hotspots that sinter the metal particles because heat transfer is poor and favor thermodynamically the complete rather then the partial oxidation.

The advantages of CPOX (optimal H_2/CO ratio and reaction exothermicity) continues to motivate research groups who have published over 6000 articles since 1989 Clarivate Analytics (2019). Noble metals are more active, less prone to oxidation and more resistant to coke deposition than transition metals such as Ni Schulz et al. (2015). However, C^{12} and C^{14} labelling studies demonstrate that as long as O_2 is present, Pd, Pt, Rh oxidize CO to CO_2 faster than CH_4 to CO. Shorter residence times lead to lower CO_2 selectivity, but CH_4 conversion decreases as does CO yield. CO is the main reaction product only when O_2 is depleted from the catalyst surface Chin and Iglesia (2011); Chin et al. (2011a,b).

Nanoparticles of Ni, Pt, Ph and Ru with improved supports are the most active (turnover frequency) catalysts and produce syngas with H_2 :CO ratio equal to two Hotz et al. (2007); Lou et al. (2017); Wang et al. (2018); Singha et al. (2017); Christian Enger et al. (2008); Li et al. (2010a); Lou et al. (2017); Urasaki et al. (2018); Qin et al. (2018). Even if catalysts with nanoparticles give equilibrium conversion, high syngas selectivites, and decrease carbon deposition, their stability is negatively affected by the low thermodynamic stability of the metal nanoparticles. In the case of high turnover frequency, the surface temperature is higher than the the gas phase and the local excess of heat results in sintering and support failure Gil-calvo et al. (2017); Urasaki et al. (2018); Somacescu et al. (2019). Because of this, the final catalytic support not only requires high temperature stability but also improved thermal conductivity and heat transfer properties as the case of structured FeCrAl.

Chemical looping partially oxidizes CH_4 in fluidized beds or cycling feeds in parallel fixed beds via direct mechanism Li et al. (2010a); Chiron and Patience (2011); Qin et al. (2018); Rifflart et al. (2018); Li et al. (2009b). Moreover, the improved heat transfer coming from the more efficient mixing in fluidized bed reactors minimizes hotspots Hossain and de Lasa (2008). CeO_2 is one of the most active oxidation catalysts because of its low activation barrier for creating oxygen vacancies and, as a consequence, it is the base component for many oxygen carriers Paier et al. (2013); Yang et al. (2017).

The main focus in the catalyst design was to find a stable catalyst, that minimizes CO_2 production rather than coke. We evaluated catalyst stability after multiple deactivation cycles and a highly exothermic regeneration step. Adsorbed O_2 on the surface of active metals produces CO_2, but in presence of CeO_2 oxygen reacts CH_4 maintaining high activity and low CO_2 selectivity.Structured metal supports are suited for industrial operations and with their shape and high thermal conductivity increase heat transfer rates, reduce hotspots, and operate at higher GHSVs Lofberg et al. (2011); Gascon et al. (2015); Giani et al. (2005b); Bianchi et al. (2012). Because of the harsh reaction conditions, traditional high temperature Ni−Cr stainless steel supports fail, while FeCrAl allows operating above 1000 °C and minimizes deactivation due to Cr migration Kaltner et al. (2009); Cairns et al. (1979); Reichelt et al. (2014). In addition, when adopting open structures such as foam and fibers of this alloy, they reduce pressure drop, enhance mass and heat transfer eliminating hotspots Basile et al. (2009); Benito et al. (2015b); Neagoe et al. (2016). In this work we report :

i) a new catalyst formulation and activity results of CeO_2 impregnated Ni, Ru, and Pt supported on a FeCrAl gauze

ii) CH_4 reaction at under-stoichiometric ratio with O_2 in presence of CeO_2 to decrease oxygen coverage on the metal surface and to favor CO and H_2 selectivity.

iii) a clycling (under stoichiometric POX/air regeneration) FeCrAl structured gauze reactor supporting Ni/CeO_2 promoted Pt and /or Ru.

5.3 Experimental

5.3.1 Synthesis

All chemicals were bought from commercial suppliers and used as received : Ni(II) nitrate hexahydrate (Sigma Aldrich, 98.5 %), Ru(III) chloride hydrate (Sigma Aldrich), tetraammineplatinum(II) nitrate (Sigma Aldrich, 99.995 %), Ce(III) nitrate hexahydrate (Laboratoire Mat), and FeCrAl knitted gauze.

We pretreated FeCrAl gauze in air at 600 °C for 10 h with a heating rate of 0.5 °C $\mathrm{min^{-1}}$. $Ce(NO_3)_3{\cdot}6H_2O$ was dissolved in deionized water to coat the metal fibers with 9.5 % or 14 % (% g $\mathrm{g^{-1}}$) of CeO_2. The gauze was dipped in the solution while a magnetic impeller stirred the liquid together with the alloy at 40 °C until complete water evaporation. We placed the samples in a furnace that ramped the temperature to 600 °C at a heating rate of 0.5 °C $\mathrm{min^{-1}}$ and the impregnated gauze calcined in air for 2 h. We synthesized twelve gauze catalysts all having Ni, Pt and/or Ru. Ni loading was 0.5 %, 2.25 % and 4.5 % (g $\mathrm{g^{-1}}$) while noble metal promoters were either 0 % or 0.1 % (g $\mathrm{g^{-1}}$). The metal precursors dissolved in deionized water and the impregnation procedure was the same for cerium oxide. At this point, the catalyst calcined in air at 800 °C for 2 h (heating rate of 0.5 °C $\mathrm{min^{-1}}$). We synthesized 12 catalysts and labeled each according to the following nomenclature (Table 7.2) : first two letters are the metal (active phase), the following two digits represent the metal loading, the next digit is the loading of Ru promoter, where 1 represents 0.1 %, and the last digit represents Pt promoter loading, again where 1 represents 0.1 %.

Table 5.1 Metal loading on FeCralloy gauze coated with 9.5 % g $\mathrm{g^{-1}}$ CeO_2.

Sample name	Ni, g $\mathrm{g^{-1}}$	Ru, g $\mathrm{g^{-1}}$	Pt, g $\mathrm{g^{-1}}$
Ni0500	0.50	0	0
Ni0510	0.50	0.10	0
Ni0501	0.50	0	0.10
Ni0511	0.50	0.10	0.10
Ni2500	2.25	0	0
Ni2510	2.25	0.10	0
Ni2501	2.25	0	0.10
Ni2511	2.25	0.10	0.10
Ni4500	4.50	0	0
Ni4510	4.50	0.10	0
Ni4501	4.50	0	0.10
Ni4511	4.50	0.10	0.10

5.3.2 Catalyst characterization

We tested the adhesion of CeO_2 on the metal fibers by immersing the catalyst for 10 min to 35 min in an ultrasonic bath operating at 120 W and 40 Hz. We calculated the adhesion based on a mass balance around the initial mass, m_i, and the final mass after the treatment, m_o :

$$\Delta m_{\mathrm{CeO_2}} = \frac{m_\mathrm{i} - m_\mathrm{o}}{m_\mathrm{i}} \tag{5.1}$$

Field emission scanning electron microscope (FE-SEM) Jeol JSM-7600TFE produced images of the gauze and the dimensions of the particles. Energy dispersive X-ray spectroscopy (EDS) detector mapped the superficial elemental composition. A Philips PW3040/60 X-ray diffractometer (XRD) with CuKα radiation at 45 keV and 10 mA analyzed the sample from 5° to 70° (2θ) at 0.01° intervals and a $5\,^\circ\,\mathrm{min}^{-1}$ scanning rate. A Jeol 2100-F FEG-TEM transmission electron microscope (TEM) operated at 200 keV to identify morphology, structure, and particle dimensions of the powder removed after the ultrasonic bath. An Oxford X-ray detector acquired EDS images in specific areas. In situ X-ray absorption spectroscopy (XAS) experiments were performed at the 10-BM beamline at the Advanced Photon Source (APS) of the Argonne National Laboratory. Measurements were performed at the Ni K (8.333 keV) edge for the Ni/CeO_2 sample, which was pressed into a stainless-steel holder and placed in a quartz tube cell. The cell was sealed and treated at 700 °C in a CH_4/O_2 of 2, cooled to room temperature in the reaction gas mixture, and then transferred to the beamline. The measurements were conducted in transmission mode in fast scan from 250 eV below the edge, to 550 eV above the edge, which took approximately 10 min per scan.

A Mettler Toledo TGA/DSC1 - OmniStar GSD 320 O series thermogravimetric analyzer coupled with an online mass spectrometer (TGA-MS) and a UNICHEM 939 AA-Spectrometer atomic absorption spectroscope (AAS) quantified and identified the coke deposited on the used catalyst. The TGA heating rate was $5\,^\circ\mathrm{C\,min}^{-1}$ until 800 °C. The temperature program consisted of 8 steps : In the first 5, the feed gas was N_2 at $20\,\mathrm{mL\,min}^{-1}$, while in the last 3, $20\,\mathrm{mL\,min}^{-1}$ of air was added. Only the 2.25 % Ni, 0.1 % Ru/CeO_2 (highest yield of the 12 samples) was characterized with the above procedure. The coke on the Pt promoter was also analyzed. We prepared samples for TEM, XAS, TGA-MS and AAS measurements after manual mechanical stretch followed by 2 h treatment in an ultrasonic bath. 85% of the coating considering the mass of CeO_2 and Ni was removed.

5.3.3 Catalytic activity tests

Reaction : methane partial oxidation was carried out in a fixed bed reactor : 0.16 g to 0.35 g of catalyst was loaded as a one or two layer gauze with a total height of 3 mm to 6 mm in a 6 mm ID quartz reactor. A thermocouple was sandwiched between the outside wall of the quartz reactor and a metal jacket. The side of the reactor wall was constant at 700 °C. A 99.99 % pure CH_4 stream at $6\,\mathrm{mL\,min^{-1}}$ to $45\,\mathrm{mL\,min^{-1}}$ reacted with air at 700 °C and atmospheric pressure. An Online Shimadzu GC2010 with TCD detector analyzed the reaction products. The catalyst activity was calculated based on CH_4 conversion (Eq. 7.1), CO, CO_2 and H_2 selectivity (Eq. 7.2,7.3,7.4) and yield (Eq. 7.5), where n represents molar rates of each species, i indicates inlet while o indicates outlet flow. Average reaction rates were calculated in the first 2 min (Eq 7.6).

$$X_{\mathrm{CH_4}} = \frac{n_{\mathrm{i,CH_4}} - n_{\mathrm{o,CH_4}}}{n_{\mathrm{i,CH_4}}} \tag{5.2}$$

$$S_{\mathrm{H_2}} = \frac{n_{\mathrm{o,H_2}}}{2 \times \left(n_{\mathrm{i,CH_4}} - n_{\mathrm{o,CH_4}}\right)} \tag{5.3}$$

$$S_{\mathrm{CO}} = \frac{n_{\mathrm{o,CO}}}{n_{\mathrm{i,CH_4}} - n_{\mathrm{o,CH_4}}} \tag{5.4}$$

$$S_{\mathrm{CO_2}} = \frac{n_{\mathrm{o,CO_2}}}{n_{\mathrm{i,CH_4}} - n_{\mathrm{o,CH_4}}} \tag{5.5}$$

$$Y_i = X_{\mathrm{CH_4}} S_i \tag{5.6}$$

$$r = \frac{n_{\mathrm{i,CH_4}} - n_{\mathrm{o,CH_4}}}{n_{\mathrm{Ni}}} \tag{5.7}$$

Since the activity of the catalysts varies with time as carbon builds up on the surface and the Ce becomes reduced (particular at low O_2 ratio), the GC protocol consisted of sampling the effluent at 2, 4 and 6 min after initiating the feeds. *Catalyst regeneration* : after reaction the catalyst was regenerated in the reactor at the same process conditions with a flow of $30\,\mathrm{mL\,min^{-1}}$ air. A $75\,\mathrm{mL\,min^{-1}}$ stream of N_2 purged the reactor for 3 min between reaction and regeneration.

5.4 Results and discussion

5.4.1 Catalytic performance

Blank tests over the FeCrAl demonstrated that the gauze was inert before and after pre-oxidation step. Contrary to conventional activation procedures, we never reduced the catalyst with H_2 neither after the initial calcination nor in between regeneration cycles. Early explo-

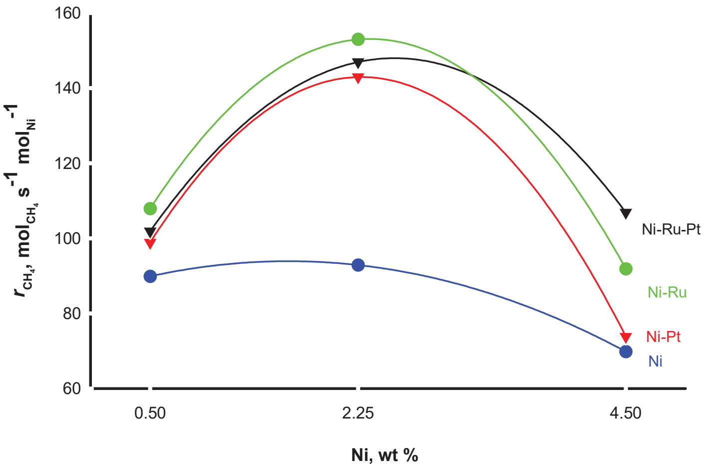

Figure 5.1 Reaction rate of CH_4 cracking versus Ni loading promoted Ru, Pt at 700 °C.

ratory experiments assessed how much the catalyst cracked CH_4 in the first 2 min (Fig. 5.1). The average reaction rate reached a maximum when the Ni loading was equal to $2.25\,\mathrm{g\,g^{-1}}$. Ni2510 converted 53 % of the CH_4 and conversion was higher with Ru compared to Pt because it reduces Ni better via H_2 spillover Choudhary et al. (1995). Moreover, the higher stability of Ni-Ru compared to Ni-Pt, proved by an higher CH_4 conversion after reacting the same about of methane, corresponds to a more efficient usage of lattice oxygen coming from the oxygen carrier that produced preferentially CO respect to CO_2. All catalysts promoted with Pt showed visible residual coke after 2 h on stream (8 min reduction—8 min regeneration) at 700 °C. Otsuka et al. (1998) reported that Pt increases the extent of reduction of CeO_2 and decreased the activation energy of CPOX, but others showed that it produces CO_2 rather than CO Ma et al. (2020). Otsuka et al. also suggested that only 10 % of the oxygen lattice is available for the redox cycle. Above this threshold, coke forms and the catalyst become permanently over reduced. During our experiments only samples containing Ru would fully regenerate after multiple cycles. Because of the superior catalyst stability and activity, we completed a series of tests varying CH_4/O_2 with Ni0510, Ni2510, and Ni4510.

At a ratio of 5, CO yield over Ni2510 was the highest and reached 34 % while with Ni4510 it was the lowest at 30 % (Fig. 5.2) ; selectivity to CO_2 was negligible. At a ratio of 3.4, CO yield increased for all catalysts (Fig. 5.3) while CO_2 remained low except for Ni4510, 3 %. With 4.5 % Ni promoted Ru, the reoxidiation of Ce^{3+} (Eq. 5.9) becomes the slow step, favoring reaction 5.8 that leads to more CO_2. Adsorbed oxygen reacts with CH_4 following an indirect mechanism that leads to the production of CO_2 and therefore gives lower CO selectivity.

$$C\cdot + 2\,O\cdot \longrightarrow CO_2 \tag{5.8}$$

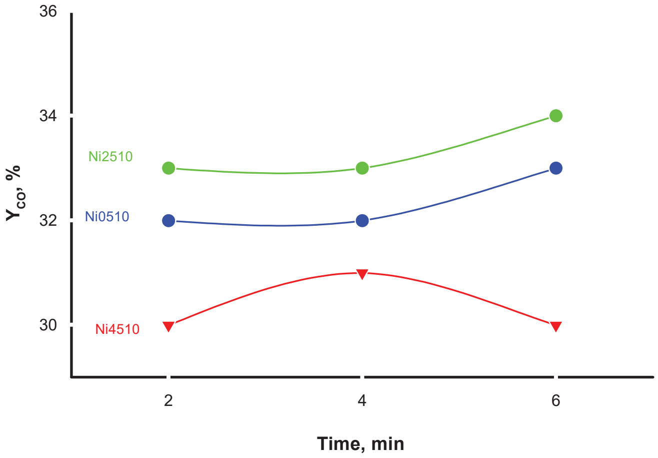

Figure 5.2 CO yield of Ni0510, Ni2510 and Ni4510 at CH_4/O_2 ratio equal to 5 and 700 °C.

$$CeO_{2-x} + \frac{1}{2}xO_2 \longrightarrow CeO_2 \tag{5.9}$$

Increasing O_2 partial pressure from 0.10 bar to 0.12 bar led to an higher oxygen coverage of the Ni particles and consequently CO_2 selectivity increases.

Ni0510 and Ni2510 at a 2.5 ratio completely oxidized CH_4 into H_2O and CO_2, because the increased O_2 partial pressure increased the O_2 availability on the surface that react absorbed species as carbon and CO. Experiments at half the volumetric flow rate (6 mL min^{-1}), corresponding to double residence time, at 2.5 CH_4/O_2 ratio) produced mostly syngas. Increasing the CH_4 flow rate from 12 mL min^{-1} to 45 mL min^{-1}, keeping the same reagents partial pressures, produced also syngas. Differently, feeding stoichiometric CH_4 and O_2 forms syngas with high CO_2 yield and an excessive amount of heat that in some case damaged the catalyst itself Urasaki et al. (2018). Furthermore, adsorbed and lattice O_2 present after switching from regeneration to methane may also initiate combustion at the beginning of the reaction. Heat released during the reaction can account for the high CO_2 selectivity Bianchi et al. (2012). Temperature gradients and multiple reaction zones during CPOX develop in typical fixed bed reactors of ceramic supported catalysts, several dozens of mm in length. In the 6 mm FeCrAl bed, the increased thermal conductivity minimizes temperature gradient thus the possibility to have distinct reaction zones. Comparing Ni0510 to Ni2510 (Fig. 5.4) only the latter achieves equilibrium conversion at GHSV=200 000 h^{-1}, confirming that it is the the most active catalyst composition. Moreover, Ni2510 had also higher CO and lower CO_2 selectivity (Fig. 5.5) that results in higher catalyst stability as oxygen is more efficiently used to remove C via CO production. Catalytic activity during a long stability test (Fig. 5.6) was constant and close to equilibrium : it was active for 50 reaction-regeneration cycles where each cycle consisted of 25 min, demonstrating that the catalyst was physically and chemically

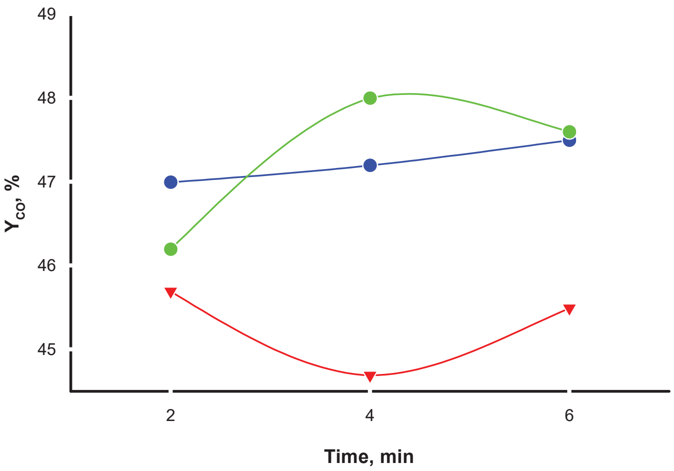

Figure 5.3 CO yield of Ni0510, Ni2510 and Ni4510 at CH_4/O_2 ratio equal to 3.4 and 700 °C.

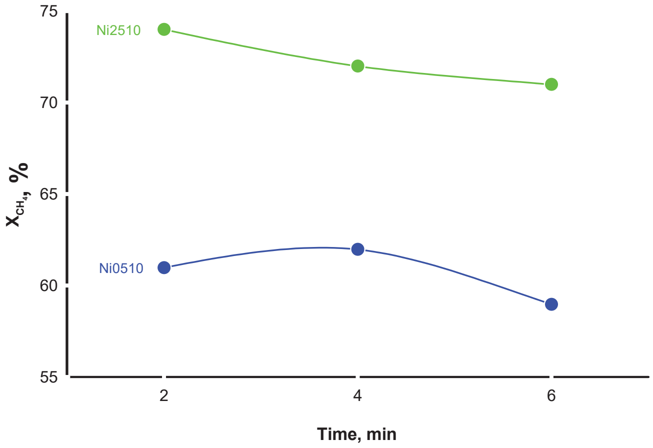

Figure 5.4 CH_4 conversion of Ni0510 and Ni2510 at CH_4/O_2 ratio equal to 2.5 and 700 °C.

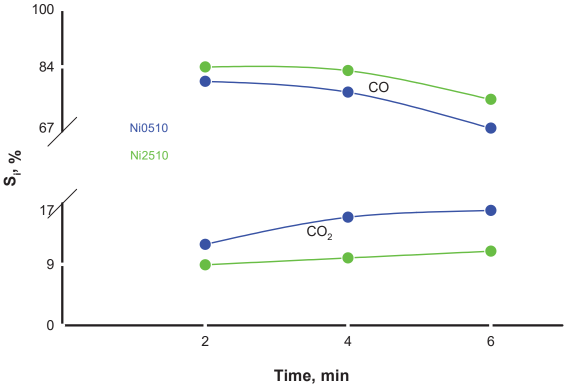

Figure 5.5 CO and CO_2 selectivity of Ni0510 and Ni2510 at CH_4/O_2 ratio equal to 2.5 and 700 °C.

stable.

The variations of CO_x selectivity and CH_4 conversion showed a direct correlation between mass of loaded Ni/CeO_2 and reaction performance, in agreement with Otsuka et al. Otsuka et al. (1998). Urasaki and al. also showed from CH_4 pulse tests that $Rh/CeO_2{-}ZrO_2{-}MgO$ supported on ceramic foam followed a direct oxidation route, which is consistent with our experimental data Urasaki et al. (2018). The indirect oxidation route first combusts methane (to CO_2 and H_2O) at the beginning of the bed and then reforms CO_2 with CH_4 (dry reforming) and H_2O (steam reforming). Under CPOX fed conditions when methane combustion prevailed (at 12 mL min^{-1} at CH_4/O2 ratio 2.5), CO and H_2 were not detected. The formation of two separate reactive zones within the 6 mm FeCrAl catalytic bed was not possible and therefore the catalyst was incapable of activating reforming. This was also the reasons why H_2O was not detected during experiments (except for tests where only CO_2 and H_2O formed), which supports the hypothesis that CPOX during experiments follows a apparent direct mechanism. In the case of indirect mechanism water should have been present in the exit stream. The experimental evidence showed that when H_2O was produced it did not reform with CH_4 into H_2 within the 6 mm FeCrAl catalytic bed. DeGroote et al., Basini et al. and Basile al. showed that the temperature changes within the bed when combustion followed by reforming take place Groote and Froment (1996); Christian Enger et al. (2008); Basini et al. (2000); Basile et al. (2001, 2002).

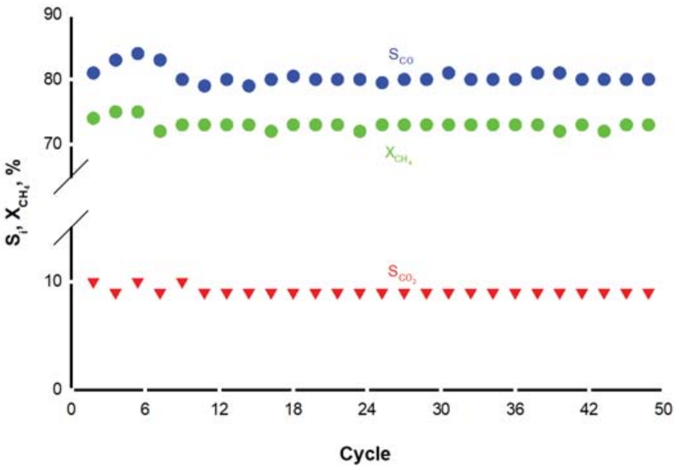

Figure 5.6 CH_4 conversion, CO and CO_2 selectivity of Ni2510 at CH_4/O_2 ratio equal to 2.5 in 50 cycles experiment at 700 °C.

5.4.2 Catalyst characterization

Weight loss from 14% and 9.5% $g\,g^{-1}$ CeO_2 on FeCrAl fibers were measured after 10 min to 35 min of mechanical stress test (Fig. 5.7). The weight loss depended on the initial loading and varied with time. After 20 min the weight loss from the sample with 9.5 % CeO_2 was constant at 12 % while it increased linearly without stabilizing for the sample with 14 % in the same time frame. Based on these data, we chose 9.5 % as the target composition. SEM images of the catalyst showed that the initial mass loss was due to the loss of CeO_2, which was only weakly bond to the surface and/or trapped between the fiber mesh (Fig. 5.8). The remaining particles were well anchored to the metal support and the protective Al_2O_3 layer. In all samples CeO_2 was present as non-uniformly distributed agglomerates on the surface.

Reactor performance dropped with time as CeO_2 escaped from the system ; CO selectivity and CH_4 conversion decreased in the first 30 h (Fig. 5.6). During the first six cycles, CH_4 conversion and CO selectivity rose and then fell to a steady value after 12 cycles and remained stable thereafter. CeO_2 activated during the induction period (first 6 cycles) as already reported form Dai et al. Dai et al. (2006). The loss of impregnated CeO_2 accounted for the drop in activity rather than from sintering or a change in its structure . SEM-EDS images also showed that Ni was heterogeneously dispersed on the metal fibers and concentrated in regions together with CeO_2 (Fig 5.9). The fibre had low surface porosity and surface area and the CeO_2 offered a better anchor for Ni. Based on geometric considerations the fibre surface area varied from 0.7 $m\,g^{-2}$ to 0.9 $m\,g^{-2}$ (a rectangular section of 80 µm per 30 µm). Its lack of porosity made difficult to support and impregnate the active phases, but conferred catalyst

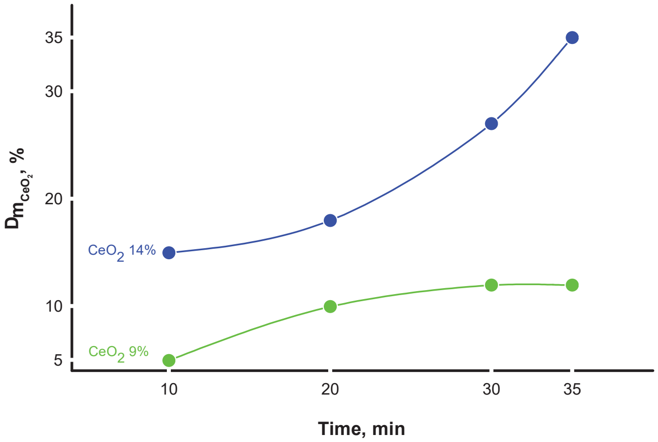

Figure 5.7 CeO_2 mass loss after ultrasonic mechanical test versus time of 14% and 9.5% CeO_2 on FeCrAl gauze.

stability against phase transformation, particle coalescence and pore blockage.

Preoxidation of the reduced support at 600 °C generated a non-uniform Al_2O_3 coating Ugues et al. (2004), but sufficient superficial roughness for the adhesion of CeO_2 precursors. The additional 800 °C oxidation step during the last calcination produced additional alumina that incorporated CeO_2 and NiO particles creating Ce-Ni-Fe oxides in tight contacts. The EDS analysis (Fig. 5.9) showed that the CeO_2 clusters contained Ni, Al, and Fe oxides. Because of the higher final calcination temperature, additional Al diffused from FeCrAl bulk to the surface and there oxidized. In this way the additional superficial Al_2O_3 not only incorporate the deposited active species but also confer additional stability also to coke formation as shown by Lu et al. (2012).

The primary particle size, determined by SEM, ranged from 10 nm to 50 nm, which agreed with the TEM images (Fig 5.9). Secondary particles (agglomerates of primary particle) on the fibre were generally less than 20 µm (Fig 5.8). The primary particles comprised two types with independent and well defined structures (Fig. 5.10) : the larger particles were oval, while the smaller particles were spherical. At higher magnification, these difference were more visible and the bigger particles corresponded to CeO_2 while the smaller were NiO (Fig. 5.11) ; nickel oxides contained Fe.

The structures of the as-synthesized catalysts were verified by XRD (Fig 5.12). Ni2510 and Ni2501, which contained traces of Ru and Pt, respectively, were selected to provide insights of the excellent catalytic activity of the former compared to the lower activity of the latter. Prior to reaction, XRD peaks assigned primarily to the CeO_2 and FeCrAl gauze support were observed. The high crystallinity of the support led to sharp peaks that reduceed the

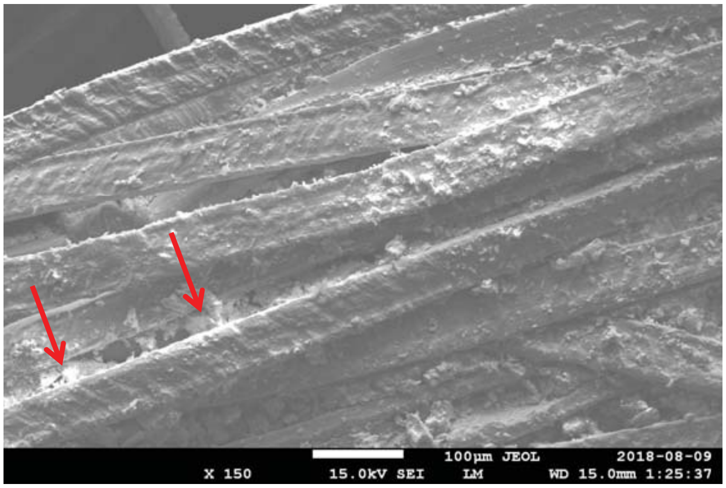

Figure 5.8 SEM image of Ni2510. Accumulation spots of Ni/CeO$_2$ between the fibers of the preoxidized FeCrAl gauze.

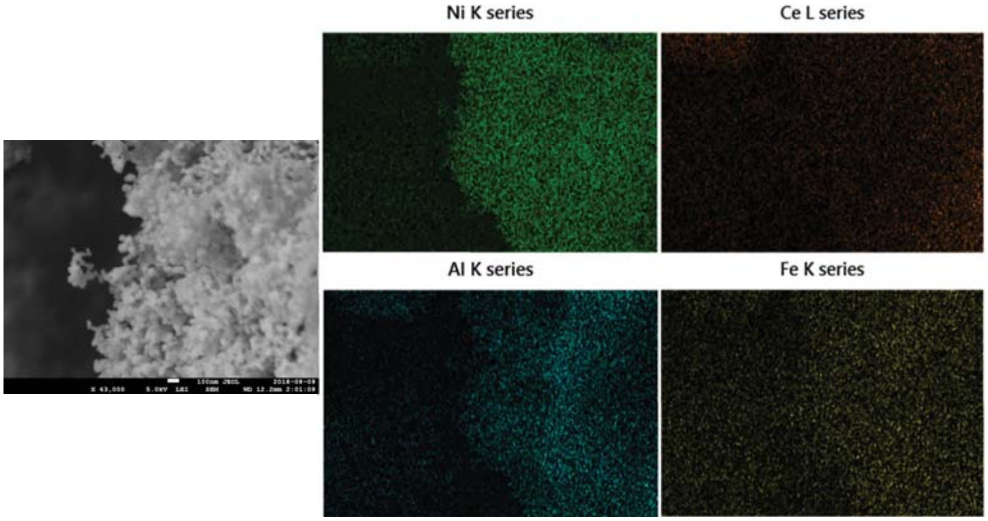

Figure 5.9 SEM-EDS analysis of powder cluster support on FeCrAl gauze, coexistence of Ni$_{\mathrm{C}}$e$_{\mathrm{A}}$l$_{\mathrm{F}}$e.

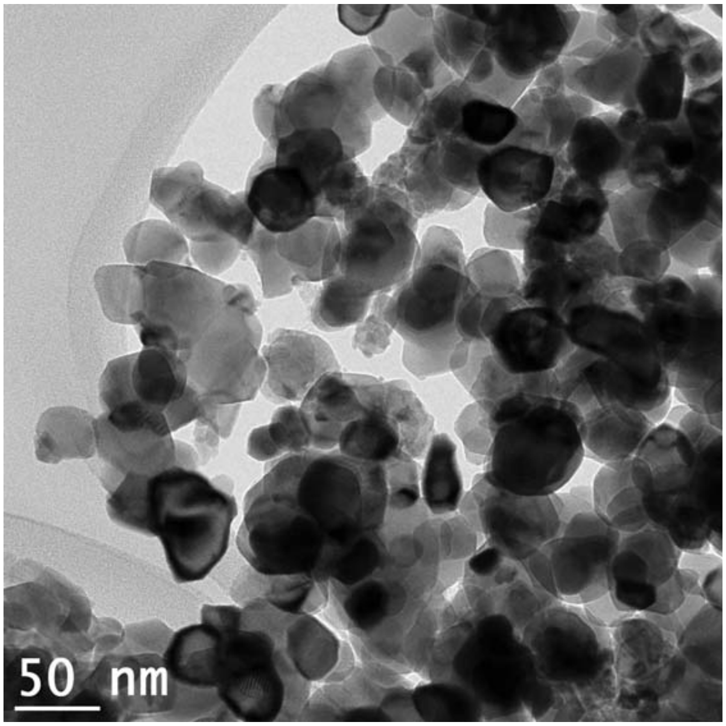

Figure 5.10 TEM image of the powder catalyst removed from the metal support. Presence of two types of particles.

intensity of metal nanoparticles present. In addition, the XRD of Ni2501 suggested that NiO was present before the reaction, but its amorphous nature led to broad diffraction peaks that were difficult to detect. This ultimately showed that the CeO_2—supported nanoparticles were present on the gauze, though the specification of Ni remained unclear. In situ XAS, after treatment in reaction conditions ($CH_4:O_2$=2 :1), identified the specific structure of Ni during reaction conditions. The normalized XANES spectra (Fig 5.13) showed a pre-edge feature at 8.334 keV, consistent with predominantly Ni^{2+}. The XANES was consistent with that of NiO, the shape was nearly identical to bulk NiO. The data were fit using standard fitting procedures using WinXAS 3.1 software Ressler (1998). Feff6 was used to develop a model to fit these samples at the Ni K Rehr et al. (1994). Theoretical phase an amplitude files were created for Ni-Ni (CN=12, R=2.49 $Å^{-1}$) and Ni-O (CN=1, R=2.09 $Å^{-1}$) scattering pairs. The $S_o{}^2$ at each edge was calibrated by fitting the metal foil and was found to be 0.77 for Ni. A least squared fit the first shell of r- space was performed on the k^2 weighted Fourier transform data over the range from 2.7 $Å^{-1}$ to 11.0 $Å^{-1}$ in each spectrum to fit the magnitude and imaginary components. The position of the features along the x-axis indicated the scattering pairs present (Tab 7.5). The sample contained Ni-O bonds and was nearly identical to NiO. The FT mag of the Ni foil was plotted for Ni−Ni reference (Fig. 5.14). It was suspected that

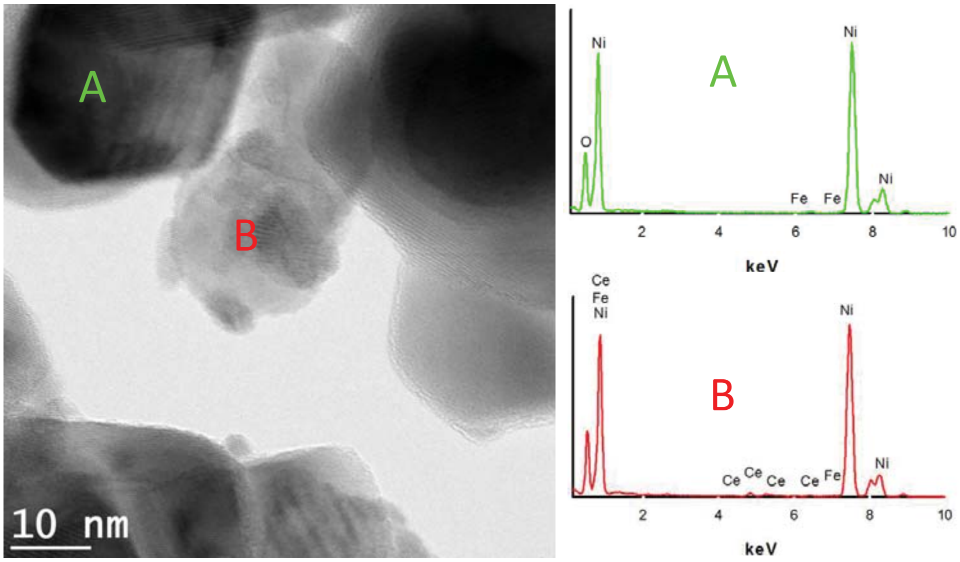

Figure 5.11 TEM detailed image of two particles with their relative EDS : left CeO_2, center NiO.

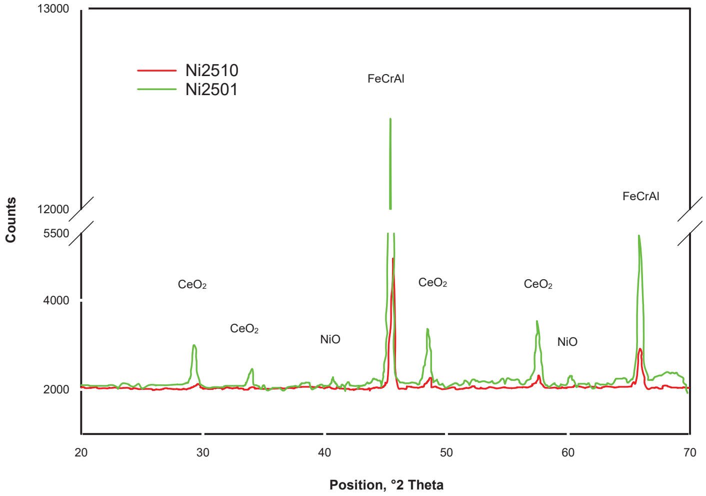

Figure 5.12 XRD of Ni2510 and Ni2501 using Cu k radiation (keV).

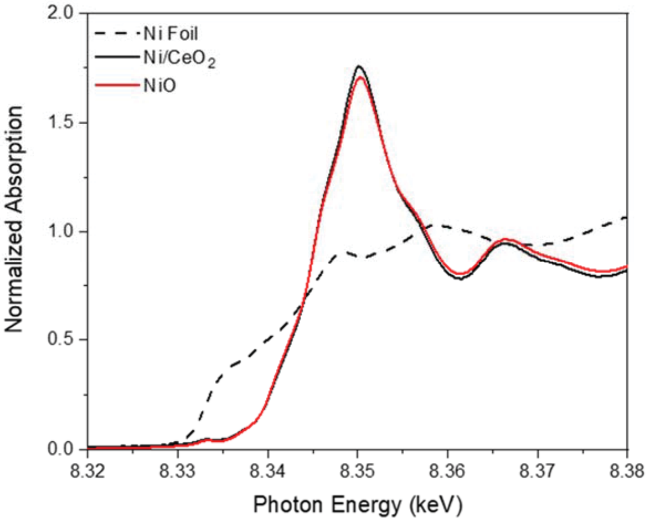

Figure 5.13 Normalized XANES of Ni2510 at the Ni K edge of Ni/CeO_2 compared to Ni foil and NiO.

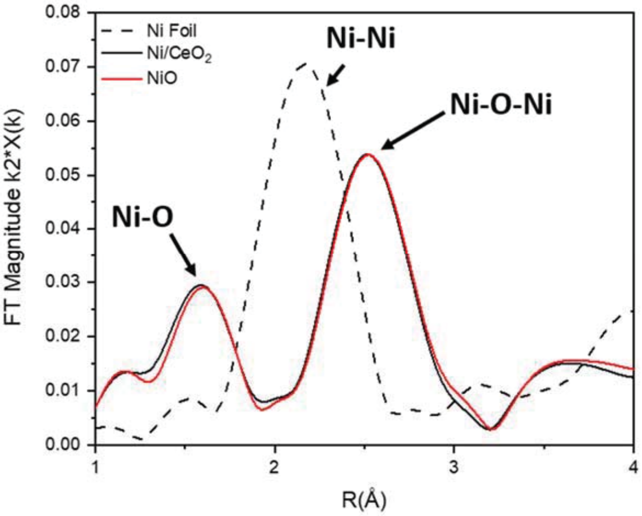

Figure 5.14 Ni-edge magnitude of the Fourier transforms after samples were treated in reaction conditions at 700 °C in a 2 :1 ratio of CH_4 :O_2.

a mixture of metallic Ni and NiO would be present under reaction conditions. The pre-edge feature in the XANES was consistent with Ni^{2+} and the XANES closely matched that of NiO. In the EXAFS, only Ni-O scattering was observed. Because XAS is a bulk averaged technique, it measures only the average arrangement of Ni atoms. The XANES and EXAFS are both consistent with bulk NiO, indicating that the majority of Ni atoms contain only Ni-O bonds. No Ni-Ni bonds were observed on Ni/CeO_2.

Table 5.2 EXAFS fitting parameters over a Fourier transform range of 2.7 to11 Å at the Ni K edge for sample Ni2510 treated at 700 °C in CH_4 :O_2 ratio 2 :1.

Sample	Pre-edge, keV	XANES, keV	Pair	CN	R, Å	σ^2, Å	ΔE, eV
Ni foil		8.333	Ni-Ni	12	2.49		
NiO	8.334	8.345	Ni-O	6	2.07	0.005	-5.7
			Ni-O-Ni	12	2.94	0.005	
Ni/CeO_2	8.334	8.345	Ni-O	6	2.06	0.005	-6.0
			Ni-O-Ni	12	2.94	0.005	

5.4.3 Coke

The composition (C/O ratio) of the reaction is in the thermodynamic range where coke deposition occurs. As a result, activity drops with time and to maintain productivity requires an intermittent regeneration step. The regeneration step was insufficient to remove coke from any of the catalysts containing Pt. Not only the amount of coke formed on Ni promoted Pt was higher compared to Ru but it was also refractory to on stream air oxidation. Even after prolonged regeneration at 700 °C in air, Ni2501 had visible residual carbon. Elemental analysis via atomic absorption spectroscopy of the powders from Ni2510 and Ni2501 measured respectively 0.19% and 0.37% $g\,g^{-1}$ carbon. TGA-MS analysis in O_2-N_2 of the two samples confirmed the measurements of the AAS. Both samples initially decreased their mass because of the coke removal but afterward the mass of the Ni2501 began increasing, ending up with a final weight 0.7% higher then the initial as the material got oxidized. This variation of the mass corresponded to the low oxidation state of Ce_Ni_Fe and absence of lattice oxygen. Ni2501 at the end of the TGA analysis was no longer dark and the the final aspect of both powders

Table 5.3 Mass composition of coke on Ni2510 and Ni2501 sample after catalyst regeneration.

Sample	AAS C, % $g\,g^{-1}$	TGA ΔmI, % $g\,g^{-1}$	TGA ΔmII, % $g\,g^{-1}$
Ni2510	0.19	0.18	0.05
Ni2501	0.37	0.39	-0.70

was the same.

5.5 Conclusions

Promotion of Ni on CeO_2/FeCrAl gauze with Ru and Pt resulted in at least 40 % higher activity in C-H bond activation. Pt facilitates CH_4 activation but produces carbonaceous species that could not be removed during catalyst regeneration on stream. Pt promotion of Ni or Ni-Ru prevented reoxidation of the catalyst reduced during sub-stoichiometric methane CPOX. We hypothesize that this inhibition to the reoxidation of the catalyst, in particulare CeO_2, is related to the lower binding energy of Pt to oxygen compared to Ru and Ni Madey et al. (1975); Stampfl and Scheffler (1996); Wellendorff et al. (2015); Silbaugh and Campbell (2016). Pt preferentially adsorbs O_2 and prevents carbon removal via oxidation. A the same time, during reaction, Pt gives higher O_2 coverage that, while increasing CO_2 selectivity, prevents carbon oxidation produced via CH_4 activation on CeO_2 and NiO. For this reason, CPOX reaction produces carbonaceous deposits on the catalyst that also resulted refractory to regeneration with air.

The most active catalyst contained 2.25% Ni and 0.1% Ru. The catalyst gave constant reaction performance even after 50 cycles of carbon deactivation followed by on stream air regeneration. We attribute the outstanding catalyst stability not only to the Ru promotion and the adhesion of CeO_2 to the metal fibers, but also to the low catalyst porosity that limited deactivation via pore blocking. The FeCrAl metal supports, with improved thermal conductivity, homogenizes the temperature within the catalytic bed, decreasing the temperature gradients exploiting its thermal conductivity ($25\,\mathrm{W\,m^{-1}\,{}^{\circ}C^{-1}}$) at least three times higher than traditional Al_2O_3. This made possible to feed methane and air without introducing any additional dilutant and to obtain high syngas yield at 700 °C. It was possible to work under this condition even if the contact between catalytic bed and reactor walls were limited to a cylindrical surface of 3 mm height. The high void fraction of the structured support improved the capacity of accumulating coke without preventing contact between reagent and surface of the active phases, giving negligible pressure drop even after full catalyst deactivation. The reduced bed heat capacity, bed height and pressure drop favors cycling reactions, high GHSV ($200\,000\,\mathrm{h^{-1}}$) and therefore reduced reactor dimensions.

CHAPTER 6 ARTICLE 3 : TECHNO ECONOMIC ANALYSIS OF A MICRO GAS-TO-LIQUID UNIT FOR ASSOCIATED NATURAL GAS CONVERSION

Gianluca Pauletto, Paolo Mocellin, Alice Gaillardet, Federico Galli, Gregory S. Patience

Article submitted to Renewable & Sustainable Energy Reviews (I.F. 10.5)

6.1 abstract

Flared and vented gas in remote regions of the world contribute >1 % of the total CO_2 emissions. High investment costs to build facilities to treat this gas and labor costs to operate the infrastructure are deterrents. Here we report a techno-economic analysis of a commercial mobile manufacturing plant that processes $100\,\mathrm{m^3\,h^{-1}}$ of methane via a tandem short contact time catalytic partial oxidation (CPOX) gauze reactor and a single-pass Fischer-Tropsch fluidized bed to produce 7 bbl $\mathrm{d^{-1}}$. Starting from methane and air, a thermodynamic analysis identified the optimized operating conditions considering both carbon yield, CO/H_2 ratio and adiabatic conditions. We studied the flammability limits of the mixture at operating pressures and temperatures. The economic analysis itemizes costs for all equipment rather than applying scale-up power law or factors. The greatest contributors to direct costs are the compressors and the CPOX reactor. Operating CPOX at 2.0 MPa reduces reactor volumes but to achieve 90 % conversion and selectivity requires operating this unit above 900 °C. Avoiding syngas compression and upstream syngas conditioning reduces capital costs. The capital cost (CAPEX) reaches 570 000 USD when the whole process operates at 2.0 MPa. Considering numbering-up, the price of the 100th unit approaches 360 000 USD thus the MRU increases profitability. We demonstrate how thermodynamics constrains methane conversion and syngas selectivity. A large part of achieving low CAPEX is operating a single pass process, building multiple units, and replacing the methane to heat the treater with the incondesable leaving the three phases separator downstream the Fischer-Tropsch.

6.1.1 keyword

Catalytic partial oxidation, Numbering up, Techno-economic analysis, Gas-to-Liquids, Fischer-Tropsch, Flared gas

6.2 Introduction

Gas-To-Liquid (GTL) processes convert light hydrocarbons like natural gas from oil production, landfills, and bio-sources, to liquid fuels and chemicals—methanol, diesel, dimethyl ether, and gasoline. Often, the first step produces syngas, a mixture of hydrogen and carbon monoxide, and the most common second step is the polymerization/hydrogenation of CO to high molecular weight hydrocarbons via Fischer Tropsch synthesis (FT), which was discovered in the 1920s (Schulz, 1999; Dry, 2002). To compete with petroleum, GTL products must be cost effective, particularly when the price of oil drops or the price of natural gas rises. In the last thirty years increasing oil price, abundance of stranded natural gas, and stricter regulations on volatile organic compounds, CH_4, and CO_2 emissions increased the interest for GTL.

FT is profitable when the gas price is greater than 7 $USDGJ^{-1}$ while, at 2.8 $USDGJ^{-1}$, other products like dimethyl ether are economic (Lee and Han, 2009). These constrains have limited the expansion and application of FT technology to large volume production like Sasol's Oryx plant and Shell's Pearl unit in Qatar (Hoek and Kersten, 2004; Sichinga and Buchanan, 2005). Micro refinery units (MRU) to convert natural gas in remote regions have yet to meet economic hurdles but they have been scaled down by Velocys® and Infra® to produce synthetic fuels down to 100 barrel per day (Hargreaves, 2017; Infra, 2020).

Even when the investment of a GTL unit, that is 100 % efficient, costs 280 000 USD/10 bbl d^{-1} (1/3 of existing cost estimates) with no constraints on CO_2 emissions, GTL market penetration is expected to be limited in the United States. Including a carbon tax on CO_2 emissions, linked to the syngas production, aggravates the profitability (Ramberg et al., 2017). However, the Environmental Protection Agency is poised to repeal methane emissions restrictions applied during the Obama administration. Plants with an output greater than 20000 $bbld^{-1}$ are profitable at 0.32 $USDL^{-1}$ (~46 USD/bbl) (Mohajerani et al., 2018).

Alberta Energy Regulator (AER) published directives to minimize venting and flaring of associated gas. The World Bank is supporting this strategy with the Global Gas Reduction program whose goal is to eliminate all routine flaring by 2030. Together with the AER mandate for lower emissions, they limit flaring during well commissioning to 72 h. These initiatives, together with the Paris agreement on global warming, challenge developed countries, like Germany, to reduce CO_2 emissions by 55 % by 2030 (Denchak, 2018). As results over the years, oil companies have abandoned 170 000 oil wells only in Alberta, Canada (AER, 2019). In 2019, the annual methane consumption in France and Germany amounted to that flared worldwide—1 % of the annual world CO_2 emission comes from the combustion of associated natural gas at oil sites (Ismail, 2012).

While it is clear that GTL is incapable of displacing oil, converting this wasted natural gas into synthetic fuels remains the most attractive solution. Power generation, production of liquid natural gas, and methanol or dimethyl ether are unable to address the problem Chen and Xu (2019). Techno-economic analysis of small scale FT-GTL considering air and methane as co-reactants are unavailable in the literature or report capital cost estimates based on correlations rather than detailed process design and manufacturer's quotes (Herz et al., 2017; Christian Enger et al., 2008; Valle et al., 2013; Yang et al., 2020). In this study, we report :

i) a thermodynamic analysis that minimizes carbon formation that maximizes syngas selectivity for a high pressure air blown SCT-CPOX

ii) a safety analysis based on flammable limits for the SCT-CPOX operating with CH_4 and air at 2.0 MPa and 800 °C to 1000 °C

iii) an innovative integration of a small scale GTL unit, comprising a single pass FT reactor, in the existing oil battery facility

iv) a CAPEX estimation based on manufacturers quotes.

6.3 Process description

GTL processes comprise desulphurization, compression, syngas generation, liquid fuel production, product separation, and upgrading (and those based on autothermal reforming require oxygen separation). Our process considers compression, syngas, FT, and product separation : syngas produced via catalytic partial oxidation enters a FT fluidized bed where it reacts to synthetic fuel. Heat transfer rates in fluidized bed are close to an order of magnitude greater than fixed bed reactors at $>700\,\mathrm{W\,m^{-2}\,°C^{-1}}$, which minimizes heat transfer surface. Solids back-mixing in fluidized beds ensures iso-thermal conditions reducing catalyst deactivation due to hot spots typical of fixed bed reactors. FT reactors with iron catalyst operate at 2.0 MPa and above 300 °C, Cobalt catalyst operate below 240 °C but newer formulations operate as high as 280 °C (Bitter and Torres, 2012; Tucker and van Steen, 2018). A three-phase-separator knocks-out water from the FT hydrocarbons and non-condensable gases—a mixture of light $C_{3\text{-}}$ products, unreacted syngas, and N_2.

In low pressure CPOX, a compressor pressurizes H_2, CO, un-reacted CH_4 and N_2 downstream the reformer before FT synthesis (Fig. 6.1). When CPOX operates at high pressure, compressors elevate CH_4 and air pressure upstream of this vessel but downstream any desulphurization unit (Fig. 6.2). In the case of a stoichiometric mixture of methane and pure oxygen, total gas volumes of reactants are half of the effluent volumetric flow rate. With air, the volumetric expansion is less pronounced because of the nitrogen ballast and so the total volumetric flow rate is close to the effluent of the low pressure process (Trevisanut et al., 2016) :

$$2CH_4 + O_2 \longrightarrow 4H_2 + 2CO \qquad \Delta H^\circ = -36\,\mathrm{kJ\,mol^{-1}} \tag{6.1}$$

Therefore, compressing energies upstream and downstream CPOX are comparable as the volumetric flows. We ignore configuration where CPOX operates from 5 bar to 15 bar while FT at 20 bar as in this case, three compressors are required, which increases capital investment.

6.3.1 Catalytic partial oxidation—CPOX

The SMR process produces syngas with a H_2/CO ratio of 3 :1, while the ratio from POX is ideal for Fischer-Tropsch at 2 :1 but require pure O_2. Furthermore, POX is exothermic (Eq. 6.1) while SMR is endothermic and requires as much as 10 % to 20 % excess methane to supply heat to maintain the endothermic reaction (Smith and Shekhawat, 2011). POX was first reported by Liander et al. in 1929 who coupled it to ammonia synthesis (Liander, 1929). At the same time, also Padovani et al. described the reaction (Padovani and Francetti Giorn, 1929), but only (Prettre et al., 1946) reported Ni catalyst activity at 700 °C to 900 °C and 1 bar. Thermal activation of methane starts above 900 °C but, catalyst can decrease it to below 500 °C (Choudhary et al., 1995).

Normally CPOX operates below 1000 °C where the reaction sequence depends on catalyst and process reaction and follows either the direct (Eq. 6.1) or the indirect pathway in which methane combusts to CO_2 and H_2O first (Eq. 6.2) and afterward reforms with the excess of CH_4 (Eqs. 6.3,6.4) (Chin and Iglesia, 2011; Chin et al., 2011a,b; Velasco et al., 2015; Urasaki et al., 2018; Lyubovsky et al., 2005).

$$CH_4 + 2O_2 \longrightarrow 2H_2O + CO_2 \qquad \Delta H^\circ = -802\,\mathrm{kJ\,mol^{-1}} \tag{6.2}$$

$$CH_4 + H_2O \longrightarrow 3H_2 + CO \qquad \Delta H^\circ = 206\,\mathrm{kJ\,mol^{-1}} \tag{6.3}$$

$$CH_4 + CO_2 \longrightarrow 2H_2 + 2CO \qquad \Delta H^\circ = 247\,\mathrm{kJ\,mol^{-1}} \tag{6.4}$$

$$2CO \longrightarrow C + CO_2 \qquad \Delta H^\circ = 171\,\mathrm{kJ\,mol^{-1}} \tag{6.5}$$

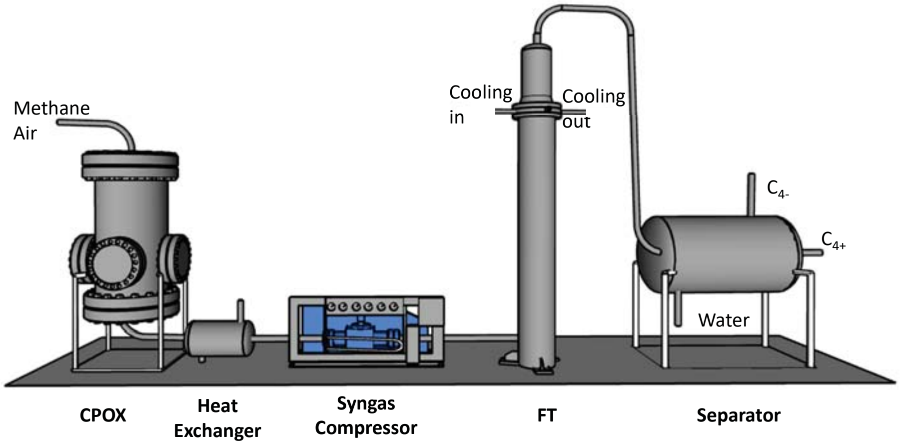

Figure 6.1 Low pressure CPOX configuration.

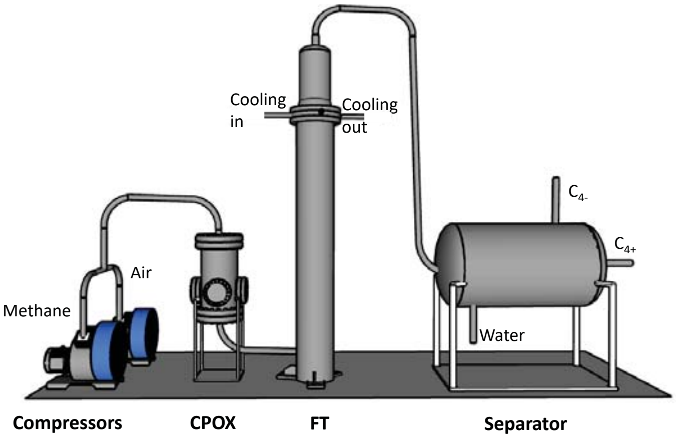

Figure 6.2 High pressure CPOX configuration.

Regardless of the reaction mechanism, the equilibrium reaction between air and methane at 0.2 MPa and 800 °C is thermally auto-sustainable (adiabatic) when the reactants enter above 300 °C at a CH_4/O_2 ratio of 1.67 (Seo et al., 2002). At this ratio, 85 % of the methane reacts at 0.2 MPa, and 700 °C while at 2.0 MPa, the temperature must reach 900 °C (Christian Enger et al., 2008; Chein and Hsu, 2018).

In 1998, ConocoPhillips developed a CPOX process and built two pilot plants and two demonstration scale facilities in Ponca City. They showed that low pressure reactors, typically studied in academia were unrepresentative of commercial conditions and thus unhelpful for scale-up (Wright et al., 2003). At the same time, Eni S.p.a. studied and developed the first industrial short contact time CPOX unit (Basini et al., 2001; Basini and Guarinoni, 2013).

6.3.2 Fisher Tropsch

Fischer-Tropsch synthesis is a highly exothermic reaction that polymerizes CO to alkanes and produces water (Eq. 6.6). FT synthesis requires tight temperature control to minimize hot spots that reduce product selectivities (Mohajerani et al., 2018). To increase heat transfer rates, fixed bed configurations comprise multi-tubular reactors 25 mm in diameter, while recent designs include inserts and foams to increase contact between the walls and catalyst but also increase reactor complexity (Frost et al., 2016). Fe and Co are commercial catalysts : Fe is less active and much less expensive and toxic compared to Co (Dry, 2002). It operates best at 300 °C to 360 °C (in a fixed-bed or fluidized bed reactor configuration), while Co catalysts operate best at 220 °C to 250 °C (Bitter and Torres, 2012).

$$n\mathrm{CO} + (2n+1)\mathrm{H_2} \longrightarrow \mathrm{C_nH_{2n+2}} + n\mathrm{H_2O} \qquad \Delta H^\circ = -165\,\mathrm{kJ/mol} \tag{6.6}$$

Industrial FT reactors convert less than 60 % to 80 % of the CO to minimize CH_4 and CO_2 selectivity that increases with H_2O partial pressure (Ostbye Pedersen and Blekkan, 2018). The axial partial pressure profile of water is more uniform using air rather than oxygen in the synthesis gas step therefore it improves selectivity ; higher single pass CO conversions are possible. Pt−Co catalysts promoted with Mn convert up to 90 % of the CO while maintaining the C_{5+} yield greater than 75 %, which alleviates the need for syngas recycle, which is impossible in presence of inerts like N_2 (air-blown CPOX) (Tucker and van Steen, 2018).

In this study, the statistical description for the formation of carbon bonds was replaced by product selectivities from bench scale experiments (Tab. 6.1).

Table 6.1 FT reaction performance

Temperature	300 °C
Pressure	20 bar
CO conversion	>0.80
$C_{4\text{-}}$	0
C_{4+}	0.64

6.3.3 MRU integrated into an existing oil battery

Oil production facilities include multiple wells that with pump jacks that draw petroleum, water, and gas from the reservoir and sends this mixture to a battery unit (Figure 6.3). The battery unit includes a treater that separates gas from liquids and breaks the water-oil emulsion. To break the emulsion takes chemical, temperature, and time. These units are large to afford sufficient residence time for the demulsifer to work and are up to 8 m in diameter and at least as tall. Methane burners heat the fluids to around 60 °C. Water from the treater is often treated with clarifiers and bactericides, for the case of sour wells, to kill sulfur-reducing bacteria that produce H_2S, which eventually reacts with iron in pumps to form FeS. The natural gas is flared and the water is pumped back down-hole through one of the wells to maintain the oil-field pressure.

As in the case of in the region of Swan Hills, Alberta, wells are often several kilometers from the battery. Installation cost to lay pipe depends on the terrain but start at 100 000 USD/km/inch diameter. The investment in pipelines feeding the battery unit in Figure 6.3 is several 1 000 000 USD. Integrating the MRU with a battery unit, rather than treating the stranded gas at the well-head reduces the number of unit operations (heat exchangers, separator, flare, turbines) and thus investment. Furthermore, overall yield is maximized by substituting the the off-gas from the 3-phase MRU separator (containing H_2, ${C_4}^-$, and CO) for the methane that heats the treater. In many oil fields, the water load exceeds 90 % of the total mass extracted from the reservoir. Other potential heat integration strategies are possible with the energy generated in the FT-reactor. Since electricity is already available at battery sites, no provision is required to generate electricity to supply energy to compressors. While sour wells require an additional pretreatment step to remove H_2S, in this analysis we assumes to use sweet gas only.

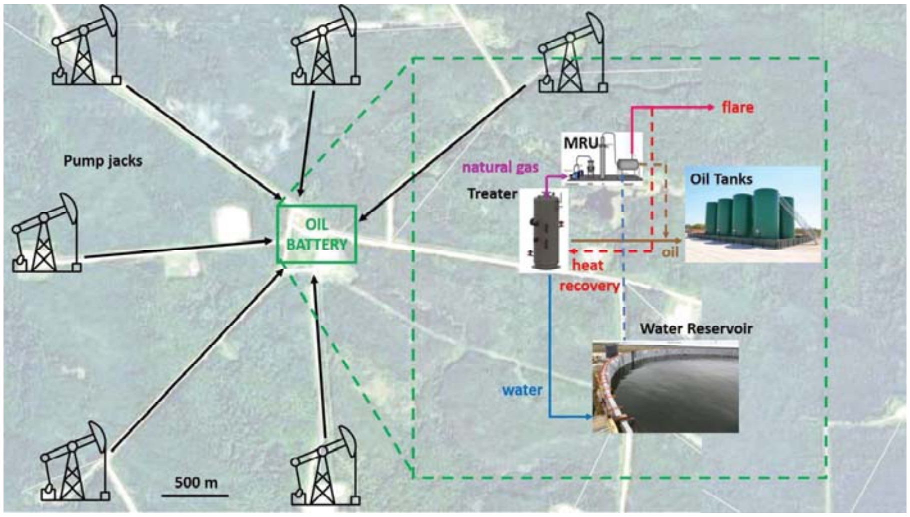

Figure 6.3 Overview of the process concept on a google maps image of an oil field located north of Swann Hill, Alberta.

This techno-economic analysis considers equilibrium performance, consistent with bench scale reformers : 60 % of the total capital investment is attributable to the reformer and therefore optimizing its performance has the largest impact on economic feasibility (Dybkjaer and Aasberg-Petersen, 2016; T. et al., 2017; Rostrup-Nielsen and Christiansen, 2011). Since the water content in the syngas is less than 10 %, water removal step between CPOX and FT is unnecessary. Here we compare the economics of a FT-GTL process with either a high pressure or a low pressure CPOX step.

6.4 Methodology

The economic analysis relies on equipment and instrumentation suppliers quotes and neglect operating parameters except ordinary maintenance and gas compression cost for the plant to produce 7 bbl d^{-1}. Integration of MRU in the existing facility maintains the usual operating procedures that include a slip stream of flared gas that is fired in the oil treater to accelerate the demulsification. Even when the flared gas is entering the MRU a certain amount of fuel gas, in this case coming from the three phase separator downstream the FT, remains available. The only difference is the higher flow rate as the heating value of this gas is lower as considerable amount of N_2 is diluting.

6.4.1 CPOX

The design of the CPOX is based on scaling-up a 15 mm diameter bench scale-reactor. Considering a 3 mm gauze bed height (the catalyst support), the reactor diameter is 61 cm when operating at 0.2 MPa and 22 cm at 2.0 MPa. Adding a second gauze layer while maintaining the same contact time, reduces by factor of two the reactor diameters to 30.5 cm and 11 cm. Pressure drop is below 0.1 bar, which is suitable for industrial operation (Hohn and Schmidt, 2001).

Electrical elements preheat the reactor/catalyst to light off the reaction. Alternatively, hydrogen or methane combustion with air raises the temperature of the catalyst during start-up. The reactor materials specification depends on pressure, skin temperature, and gas composition. Hydrogen operations require steel with higher concentrations of chromium to minimize diffusion and embrittlement and pure Al_2O_3 as isolation. Hot wall reactors insulate the exterior, which exposes the metal to the reaction environment, but the reactor diameters are smaller. In our case, we add Al_2O_3 ceramic insulation to the interior (cold-wall operation), which increases the reactor diameter and unit lifetime but is operational with a lower grade of steel since the skin temperature is maintained below 125 °C. A 304 L stainless steel shell is suitable for its mechanical, oxidation resistance and lower cost compared to 316 Stainless Steel, Fe-Cr-Al alloy, Ni-Cr alloy, or Hastelloy.

6.4.2 FT design

The minimum fluidization velocity, U_{mf} of the FT catalyst is $3\,\mathrm{mm\,s^{-1}}$. Considering a gas velocity approaching $0.20\,\mathrm{m\,s^{-1}}$ ($P = 2.0\,\mathrm{MPa}, T = 300\,°\mathrm{C}$) the resulting reactor diameter is 0.4 m. Gas residence time of 10 s requires a bed height of 2 m.

For the design of the cooling coils we calculated the enthalpy of reaction, flow rate, conversion and products selectivities. The exchange surface area consider inlet cooling water at 25 °C. We verified the design considering the cooling coils effect on linear velocity and residence time when they are immersed in the bed.

Calculating the height and the width of the jets, which have to avoid contact between reactor walls and cooling coils, we chose a sparger instead of a grid with a windbox. This solution was more suitable for a MRU : lower pressure drop, 80 % cheaper and easier to change and modify according to the fluid-dynamics that was not investigated when the heat exchanger is immersed in the catalytic bed. The gas stream above the transport disengaging height (TDH) flows across two filters in parallel. The filters, which replace cyclones, provide a cheaper, more compact and robust solution for small scale fluidized bed reactors. The filtration system removes the catalyst particles entertained in the gas flow and uses two differential pressure transducers that measure the pressure drop across the filter (Fig. 6.4). This difference in pressure, given by the filter, indicates clogging and therefore activates the cleaning system. Changing the position of two valves, N_2 burst flow inside the filter and in counter-current removes the particles from the surface. FT reactor, cooling coils and filtering system are manufactured in 316 stainless steel.

6.4.3 Control, instrumentation and safety

The lower flammability limit (LFL) of methane in air is 4.4 % and the upper flammability limit (UFL) is 16.4 % at ambient pressure and temperature. It expands to about 40 % at 2 MPa (Table 6.2) (Zlochower, 2012). The stoichiometric feed concentration of methane and oxygen, fed as air, is 2 :1 (17 %) but this value is not applicable as only ratios between 1.4 to 1.8 minimizes carbon formation. Since at the process temperature the feed conditions lie above the the auto-ignition temperature, mixing methane and air represents a safety hazard (Wierzba and Wang, 2006; Laviolette et al., 2011). The inlet gas composition for low pressure CPOX lies above the UFL that corresponds to a CH_4/O_2 ratio of 1.2 at 1000 °C. Limiting-oxygen-concentration (LOC) is the volume fraction of oxygen required to sustain a flame (Table 6.2).

Table 6.2 Flammability features of CH_4, CO and H_2 in air at 20 bar

Species	LFL, vol%	UFL, vol%	LOC, mol%
CH_4	5.0	>40.0	11.1
CO	12.5	>90.0	5.1
H_2	4.0	>75.0	4.8

Presence of CO and H_2 increase the safety hazard of the process. To minimize risk associated with these gases and the possibility of a deflagration requires that the oxygen volume fraction after CPOX reaction remains below $0.06\,\mathrm{mol\,mol^{-1}}$ (the LOC). Based on these considerations, appropriate control strategies are required in an inherently safer design (ISD) perspective.

The final operating version of the plant requires detailed studies to track the flammability behavior of evolving CH_4-CO-H_2 mixtures in the reaction stage and identification of possible flammable pockets (Wierzba and Wang, 2006).

Safety loops that detect and prevent possible failures and hazardous scenarios and detailed operating start-up and shut-down protocols are necessary for the high temperature and pressure operation. Monitoring the reactor with high frequency thermocouples coupled with gas sensors ensure safe operation while minimizing false negatives : a thermal excursion—a rapid increase in temperature due to an uncontrolled reaction—trips an interlok only when a thermocouple measures a sudden rise in temperature possibly accompanied by a change in the gas composition (Hutchenson et al., 2010; Patience and Bockrath, 2010). Two mass flow controllers (fail-close), maintain a tight control of the feed gases and an additional valve (fail-open) controls the flow of inert that purges the system in case an interlok is tripped.

Two thermocouples, at distinct radial positions, with a temperature range from 0 °C to 1200 °C monitor the temperature of the catalytic bed. A proportional integral logic controls the supply of heat through the heating elements inside the CPOX reactor. Two additional thermocouples, near the heating elements ensure the integrity of the ceramic insulation : a temperature exceeding 1050 °C triggers an interlok. Two pressure transducers measure the pressures in CPOX and FT reactor that trip an interlok if the pressure exceeds 2.2 MPa. Both reactor have safety valves and rupture disks in case the control system is inadequate to respond to a sudden increase of the pressure.

Three thermocouples monitor the temperature in the Fischer-Tropsch reactor that operates up to 350 °C at three different axial position with 0.5 m distance. The transmitters are linked to a proportional integral and derivative (PID) controller that modulates the control valve downstream the cooling coils. Two diaphragm differential pressure transducers monitor bed density, bed height and any abnormal operations like defluidizations. An additional pressure transducer measures the pressure drop across the sparger. Four gas sensors next to the units operation detect H_2, CO, LFL, and smoke and trip the interlok in case gas thresholds are reached.

The emergency interlok :

i) turns off the furnace inside the CPOX reactor,

ii) shuts down the flows first air then CH_4,

iii) purges the system with inert,

iv) activates acoustic and visual alarms.

All instrumentation is intrinsically safe and certified to operate in zone 1 division 1 (Engineer, 2019). Operators manipulate process variable from a control panel or remotely based on *LabView*® loaded on a cRIO controller.

6.4.4 Modeling

We completed mass and energy balances with AspenPlus®. The Peng-Robinson equation of state with the Boston-Mathias alpha function calculated fugacities and thermodynamic properties of the gas mixtures (Trippe et al., 2013; Sandvik et al., 2018). FactSage 7.3 equili-

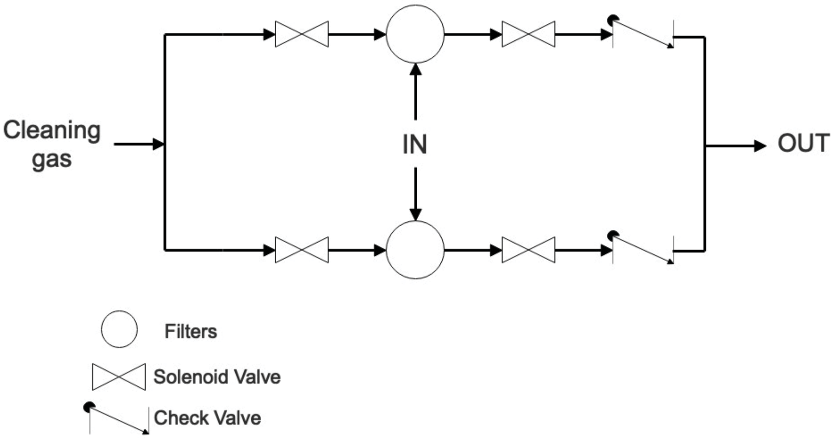

Figure 6.4 Control loop for filters cleaning

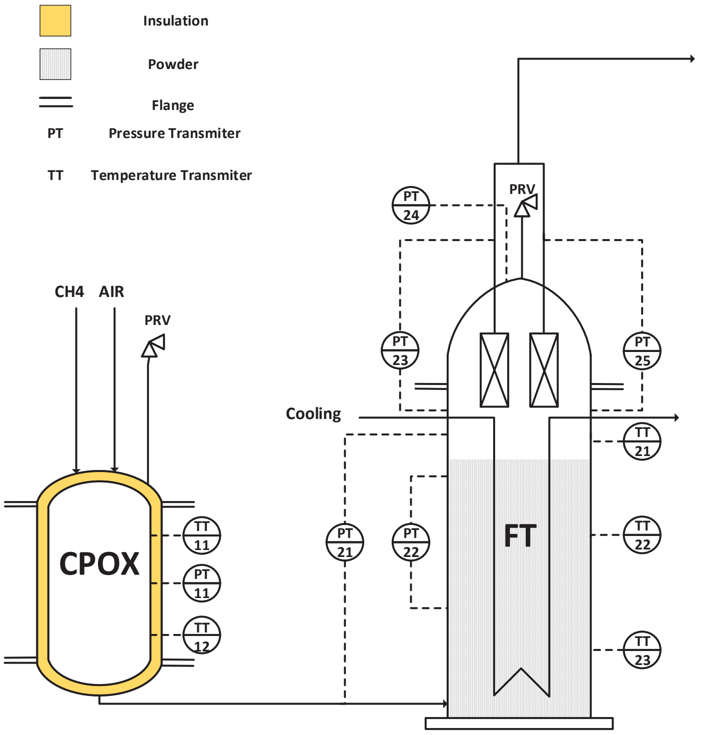

Figure 6.5 Process layout

brium calculations confirmed the AspenPlus® equilibrium calculations of the CPOX reactor. We identified methane and air flowrates to minimize coke build-up. We modeled the CPOX reactor with RGibbs and considered that it operated adiabatically. Furthermore, catalyst reacts methane and air to equilibrium (kinetics were not limiting), which is consistent with bench scale reactor performance.

The Fischer-Tropsch reactor is simulated as a stoichiometric reactor (Tab. 6.1). Vertical cooling coils withdraw the heat of reaction and maintain isothermal conditions. To minimize ancillary heat exchangers, the syngas in the case of high pressure CPOX enters the fluidized bed reactor hot (>600 °C).

Rather than compressor energy demand estimates based on *AspenPlus*Ⓡ, we used manufacturers specifications (Figs. 6.1 and 6.2).

6.4.5 Operation cost estimate

The economics of the process is based on 8000 h per year (Ric, 2013). While methane is available on the market at 0.38 USD/kg as stranded gas has no value (and in the future, countries may impose a cost to flare). The real and considered operating cost of the process is compression. Unreacted CO, CH_4, C_2H_6, C_3H_8 vent to the utility flare of the battery unit even if in remote locations, these gases can be used in the battery three phase separator or generate electricity to drive the compressors. Methane conversion in CPOX ranges from 85 % to 95 % while the Fischer Tropsch unit reacts more than 80 % of the CO. At the outlet, the three phase separator works at 2.0 MPa to recover C_{4+} hydrocarbons and we assume the value of this product is 0.55 USD/kg.

The production costs takes into account capital depreciation, taxes, and interest on working capital as well as ordinary maintenance. The process takes place on site at an existing oil battery unit and therefore transportation costs of raw materials and products are neglected. Costs related to handle the produced water from FT are zero as it will be pumped downhole with the water coming from the oil production.

The annual production costs is the sum of the Fixed Capital Investment, I_{FC} and compression costs :

$$C_{\mathrm{operation}} = I_{\mathrm{FC}}(p_{\mathrm{a}} + p_{\mathrm{m}} + p_{\mathrm{ti}} + p_{\mathrm{wc}}) + C_{\mathrm{compression}} \tag{6.7}$$

p_{a} is the percentage of annuity depending on the interest rate and the process lifetime, p_{m} is the percentage of the I_{FC} for maintenance, p_{ti} is percentage of I_{FC} for tax and insurances, and p_{wc} is the interest for the working capital. We assume an interest rate of 8 % and a 10-y amortization period. Combining mass and energy balances we calculated the economic potential of the process changing the operating condition of the CPOX reactor :

$$P = C_{\text{products}} - C_{\text{operation}} \tag{6.8}$$

The final output of the FT rector also change as function of the inlet syngas composition and flowrate.

6.5 Results and discussion

We first identified the maximum CH_4/O_2 ratio that minimizes carbon formation based on thermodynamic equilibrium. Independently of pressure, increasing the O_2 concentration decreases coke formation. A further increase of O_2 decreases CO yield because both CO_2 selectivity and CH_4 conversion increase. At 0.2 MPa, 800 °C and CH_4/O_2 ratios lower than 1.65 maximizes CO yield while minimizing carbon selectivity (Fig. 6.6). Increasing temperature (all other conditions being equal) reduces the tendency to form coke as the Boudouard equilibrium (Eq. 6.5) shifts toward the production of CO. All these results matches (Jaworski and Pianko-Oprych, 2018), that conducted a theoretical study on the equilibrium conditions for carbon deposition at 0.3 MPa and 3 MPa, from 773 K to 1273 K. CO yield approaches 1 at 1000 °C and a CH_4/O_2 close to 2, (stoichiometric value for CPOX, Eq. 6.1) (Fig. 6.7). We adopted this logic to identify the optimal conditions when the CPOX operates at 2.0 MPa. Here coke formation is negligible at $CH_4/O_2 = 1.45$ (Fig 6.8, Fig. 6.9) and the ratio of H_2/CO is almost 2. Aspen results agree with Factsage equilibrium calculations, with (Seo et al., 2002), who also studied optimal conditions for the CPOX at 1 bar and with Enger et al. at high pressure (Christian Enger et al., 2008).

At 0.2 MPa CPOX operates adiabatically as long as the CH_4/O_2 ratio is equal to 1.65. Increasing reaction temperature requires pre-heating the feed gases more (Tab. 6.5) because the higher selectivity toward CO generates less heat since combustion to CO_2 is lower. To reach 1000 °C requires a feed gas temperature of 580 °C but lowering the CH_4/O_2 (which lowers the heat requirement) decreases CO yield. CPOX yield to CO rises from 0.90 at 800 °C to 0.94 above 900 °C while H_2/CO ratio decreases from 2.00 to 1.94 ; CO selectivity increases faster than H_2 at increasing temperature (Fig. 6.6).

CPOX operating at 2.0 MPa and 800 °C and requires cooling the feed gas to −20 °C at a 1.45 CH_4/O_2 ratio (Table 6.6) as the competitive methane combustion releases excessive heat : increasing the CH_4/O_2 ratio decreases the amount of heat released by combustion but carbon builds up on the catalyst. Operating above 800 °C adiabatically is feasible. Starting up the reactor with a low ratio would avoid investing in start-up heaters. CO yield increases from

50 % to 90 % increasing temperature from 800 °C to 1000 °C. At this high pressure, the ratio H_2/CO drops from 2.04 to 1.87 because of the improved CO selectivity.

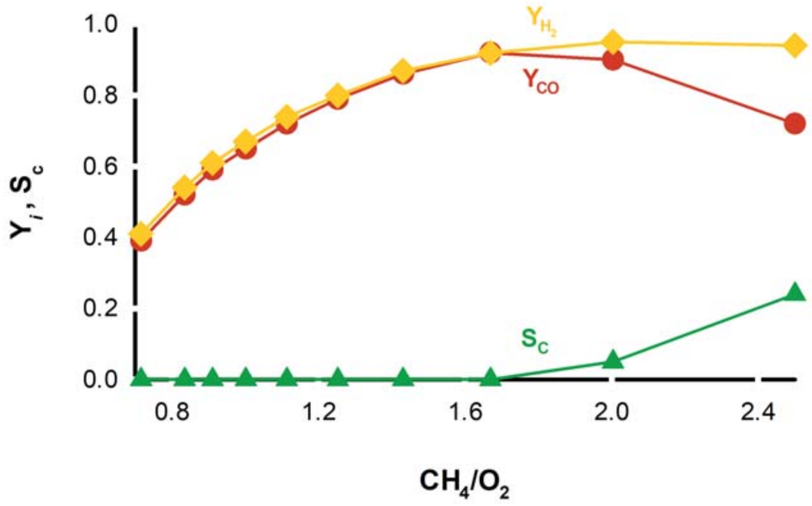

Figure 6.6 Carbon selectivity, CO and H_2 yield as function of CH_4/O_2 ratio for CPOX at 0.2 MPa and 800 °C.

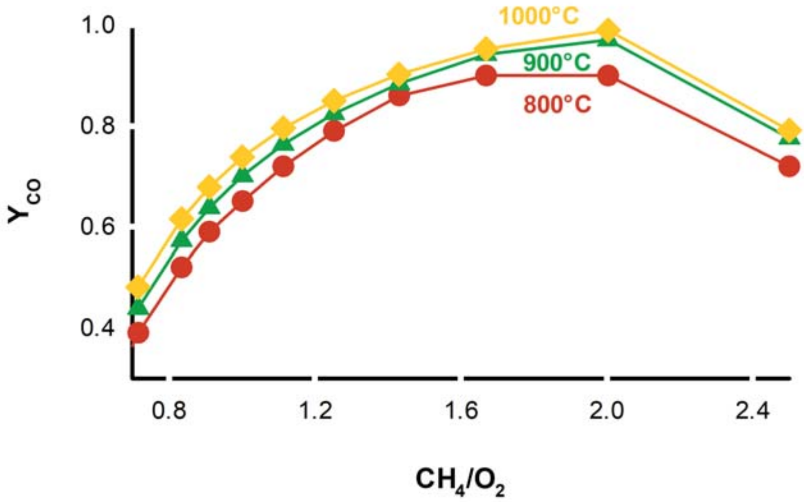

Figure 6.7 CO yield vs CH_4/O_2 ratio for CPOX at 0.2 MPa and 800 °C to 1000 °C.

6.5.1 Capital investment estimate

The economic assessment compares low and high pressure process costs, where FT operating parameters are constant at 300 °C and 2.0 MPa. We define the capital investment as the sum of all the direct costs and includes engineering, building (customize container and electrical

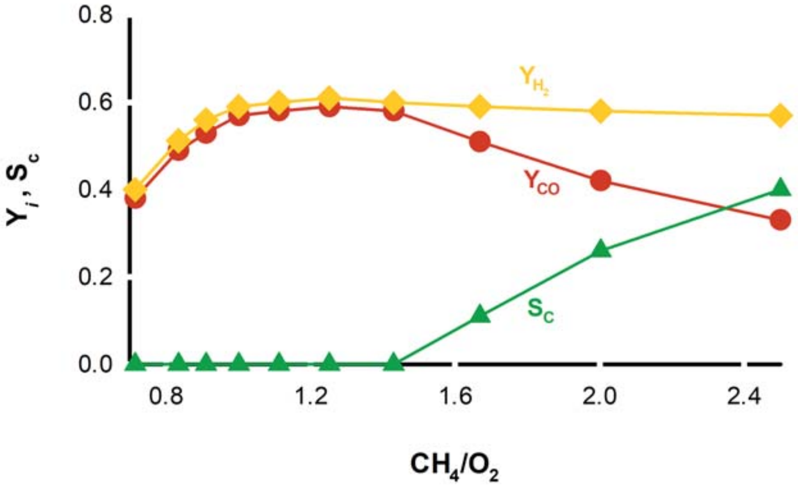

Figure 6.8 H_2/CO ratio, carbon selectivity and CO yield as function of CH_4/O_2 ratio for CPOX at 2.0 MPa and 800 °C.

system), piping and plumbing, process instrumentation and control code programming additionally to reactors, separator and compressors costs but we excluded R&D. The indirect ones consider management, insurances and interest on capital.

The equipment prices are 78 000 USD for CPOX at high pressure and 180 000 USD for low pressure while FT reactors cost 45 000 USD. Downstream, the high pressure three phase separator costs 45 000 USD. Syngas compressors cost 570 000 USD whereas both air and methane compressors are 230 000 USD (Tab. 6.3). The percentage of all additional items compared to the reactors and compressors total price agree with literature (Tab. 6.4) (Peters et al., 2003; Mohajerani et al., 2018).

Table 6.3 Equipment prices

	Price, USD
Low pressure	
CPOX reactor	185 000
FT reactor	50 000
Separator	20 000
Syngas compressor	570 000
High pressure	
CPOX reactor	80 000
FT reactor	50 000
Separator	20 000
Air compressor	64 000
CH_4 compressor	160 000

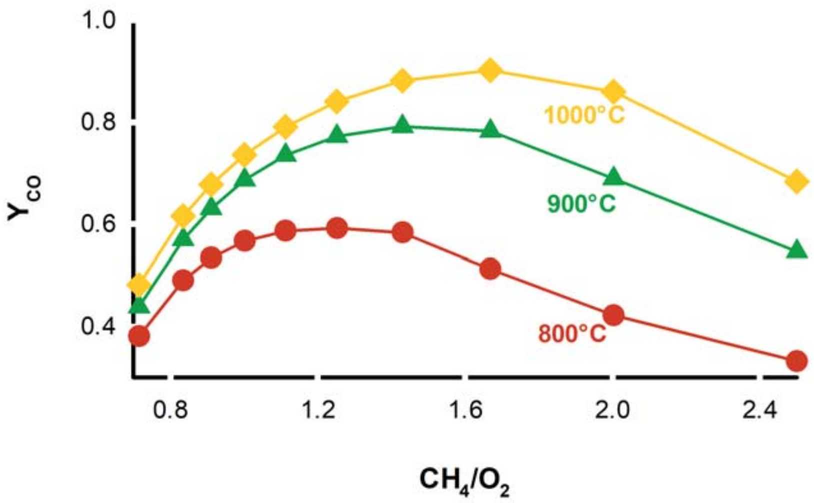

Figure 6.9 CO yield vs CH_4/O_2 ratio for CPOX at 2.0 MPa and 800 °C to 1000 °C.

We considered quotes and when not possible standard factors for the costs (Table 6.4). All values are in the range of those reported by Peters et al. (Peters et al., 2003).

Table 6.4 Percentage factor for direct and indirect costs for the MRU working with CPOX at 20 bar

Items		Source
Building	8 %	quotes
Electrical system	14 000 USD	
Container	14 000 USD	
Piping	1 %	quotes
Instrumentation and control	14 %	quotes
Control Programming	15 000 USD	
MFC and Valve	15 000 USD	
Safety equipment	7000 USD	
Transmitter	8500 USD	
Start up	12 %	(Mohajerani et al., 2018)
Maintenance	11 %	(Peters et al., 2003)
Engineering	12 %	(Peters et al., 2003)
Contingencies	8 %	(Mohajerani et al., 2018)

6.5.2 Production cost

Assuming a project life of 10 years, equipment depreciation together with insurance and maintenance contributes 65 % to overall $C_{\text{operation}}$ for both low and high pressure cases, while compression represents the other major contribution. At 0.2 MPa, syngas yield is reasonably independent of operating temperature but uneconomic. Operating at 800 °C is preferable as the material and manufacturing costs will be lower as the reactor shell diameter will be smaller. Disregarding the lower capital costs coming from lower temperature operation, the low pressure GTL loses over 70 000 USD y^{-1}.

At all conditions, the economics of operating the CPOX at high pressure is better than at low pressure (Fig 6.10). Cost of syngas compressor and CPOX reactor are twice higher at 0.2 MPa compared to 2.0 MPa (Table 6.3). The compression cost for the low pressure configuration is 1.4 times higher. An important capital costs we neglected in the low pressure CPOX is the extra heat exchanger and gas conditioning to remove any condensables (H_2O) before entering the syngas compressor. High pressure GTL profitably improves with operating temperature due to the increasing syngas yield.

6.5.3 Energy integration

The influence of heat integration improves the economic potential as the energy efficiency increases but this is more important for large scale units (Rostrup-Nielsen and Christiansen, 2011; Basini and Guarinoni, 2013). In our case, heat losses are greater and the economies of scale are poorer and the hurtle to justify additional capital is greater. Total capital investment is indeed the limiting stop to the implementation of decentralized and intensified plants. We can recover heat at the effluent of the CPOX reactor (900 °C) and/or in Fischer-Tropsch but this would require additional expensive gas heat exchangers. Alternatively, the reagent methane and air could cool the FT effluent, but the preheating temperature in this case would be maximum 300 °C. Radiation and conduction within the catalyst together with absence of thermal equilibrium between product stream and catalyst surface, coming from short contact time, will reduce the required preheating temperature (Weinberg, 1971). This non-equilibrium state helps in achieving adiabatic conditions even when gas preheating is lower than 200 °C when operating CPOX in equilibrium at 1000 °C.

The FT is best operated iso-thermally, which requires cooling coils. Generating steam from the cooling water could provide electricity to offset the compression costs (45 000 USD y^{-1}) but also in this case capital cost might be the hurtle. Future studies and process integration with oil batteries operators would help the MRU to penetrate the market.

6.5.4 Numbering up economics

Modular and mobile units are easy to build, quick to install but require capital cost minimization. Costs drop for each additional unit manufactured due to experience and learning

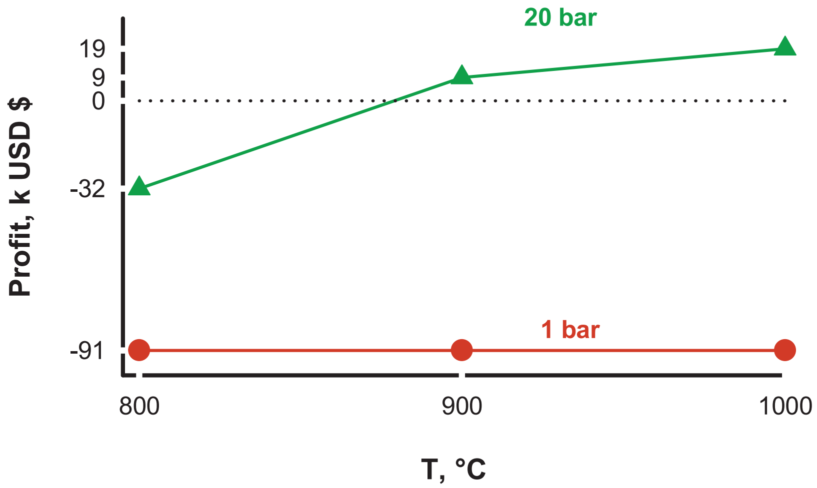

Figure 6.10 Profit of the MRU in 1000 USD$ as function of the operating temperture for 1 bar and 20 bar.

Table 6.5 Energy balance from Aspen simulation at 1 bar

T_R, °C	T_{Pre} , °C	Q_{Pre}, kW	Q_{FT}, kW
800	320	43	-150
900	450	66	-150
1000	580	89	-150

(Weber and Snowden-Swan, 2019; Gregory S. and Daria C., 2020; Garnett and Patience, 1993; Tsagkari et al., 2016). The capital cost of the 2.0 MPa unit is 550 000 USD and it corresponds to the 87 % for the 10th unit and 76 % for the 100th unit (Fig. 6.11) (Edward M Merrow, 1989). Construction costs drop 70 % and engineering costs to 41 % after the 5th unit, and so its costs will correspond to 75 % of the first unit. In the case of the MRU, cost normally considered for traditional chemical plant construction decreases or vanish as contingency, engineering and start-up given the learning experience.

Table 6.6 Energy balance from Aspen simulation at 20 bar. T_R= reaction temperature, T_{Pre}= preheating temperature, Q_{Pre}= heat for preheating, Q_{FT}= heat for the FT reactor

T_R, °C	T_{Pre} , °C	Q_{Pre}, kW	Q_{FT}, kW
800	-20	-	-90
900	70	6	-130
1000	300	44	-140

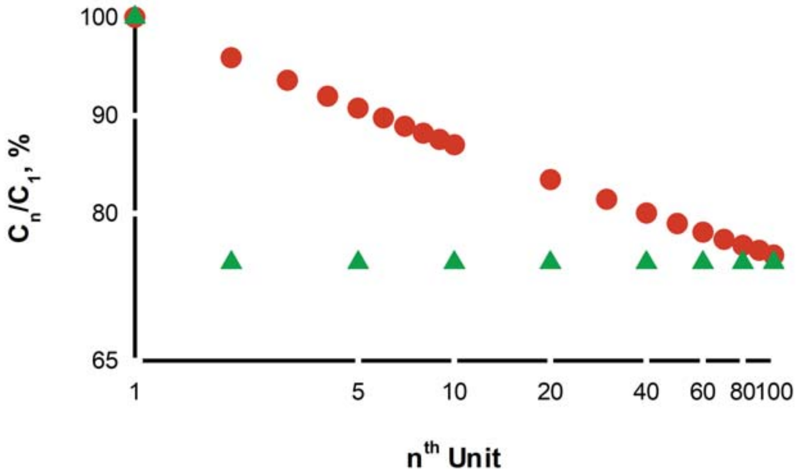

Figure 6.11 Numbering up (high pressure configuration) reduces capital cost for the n^{th} unit. Red circles according to literature (Edward M Merrow, 1989), green triangles following our estimation.

Numbering up the proposed MRU will result in a profit from 2 to 3.5 times higher being the final unit price equal to 400 000 USD. In this case operating an MRU unit becomes attractive even before additional profit coming from the heat integration.

6.6 Conclusions

In this study, we presented a techno-economic analysis to convert flared natural gas to FT liquid hydrocarbons in Canada. A high pressure (2.0 MPa) CPOX reaction step with air is economic compared to a low pressure CPOX step. High selectivity towards CO and H_2 and high methane conversion are favored at low pressure, but at 1000 °C syngas yield approaches 90 % even at high pressure. Low pressure CPOX requires interstage cooling and expensive compressors that operate with H_2. The CPOX reactor run adiabatically at 2.0 MPa with air at a CH_4/O_2 ratio of 1.45 while operating within the flammable limits. Integration of the unit within the existing battery facilities minimizes CAPEX while making possible to the current operators to monitor the process.

The micro-GTL unit generates a profit below 35 000 USD, assuming that oil-battery operators monitor it as part of their regular duties. We neglect the carbon tax in the calculation, which may add more than 7000 USD to the balance sheet. The profit is an order of magnitude higher if the MRU allows companies to bring on-stream wells that have been shut-in due to excess associated gas.

The final carbon efficiency involving SCT-CPOX and single pass FT, considering the carbon molecules entering and the one leaving the MRU as liquid products, is as low as 47 %. While it is possible to reach higher syngas yield increasing the reaction temperature, the final FT CO conversion and selectivities mainly depends on catalyst design. The heat integration could generate energy that reduces compression and energy costs at the expense of increasing the capital investment.

CHAPTER 7 ARTICLE 4 : SHORT CONTACT TIME CH_4 PARTIAL OXIDATION OVER NI BASED CATALYST AT 1.5 MPa

Gianluca Pauletto, Mathilde Mendil, Nicole Libretto, Paolo Mocellin, Jeffrey T. Miller, Gregory S. Patience

Article submitted to Chemical Engineering Journal (I.F. 8.3)

7.1 Abstract

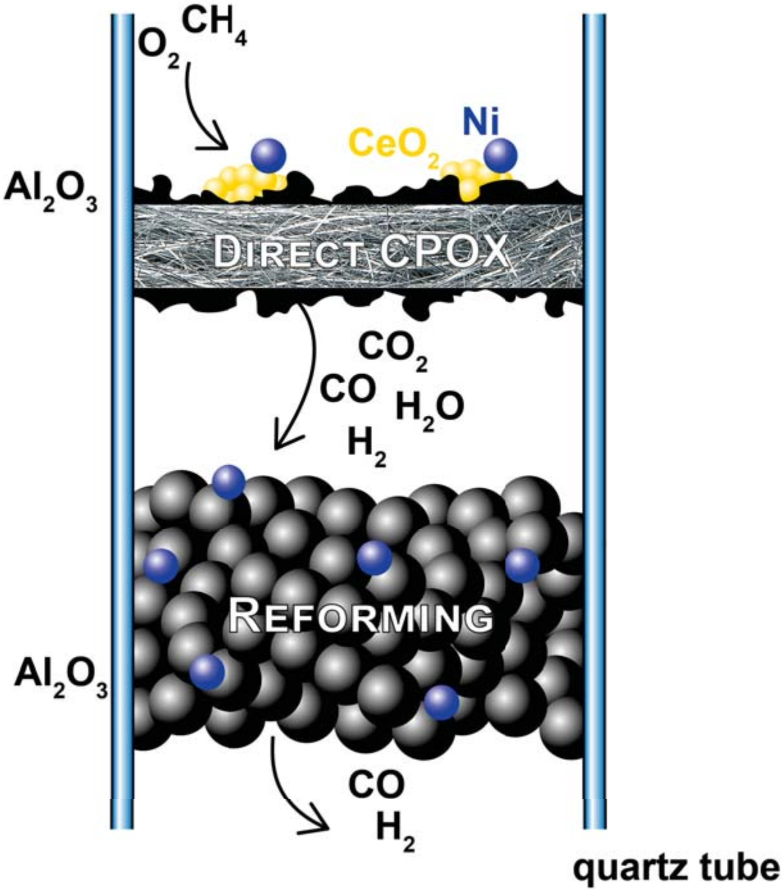

Gas-to-liquid technologies and reforming are economically sustainable only at very large scales—like 30 000 bbl d^{-1} with respect to Fischer-Tropsch fuel, for example. Mass manufacture of reformers reduces CAPEX of syngas units but to achieve an economic process at a capacity of less than 100 bbl d^{-1} also requires a compact design such a short contact time (SCT) reactors. We tested the activity of 2.25 %Ni/0.1 %Ru/CeO_2 supported on FeCrAl gauze (Ni2510) to partially oxide methane in <0.050 s^{-1}. Besides, the very short contact time, an

additional feature of this work is that the catalyst activated on-stream without a hydrogen pretreatment step. The reactor operated at 1.5 MPa, 800 °C to 950 °C, and a CH_4/O_2 ratio varying from 1.6 to 1.8 v/v. Oxygen and methane reacted following the direct mechanism rather than the indirect mechanism in which methane combusts to CO_2 and H_2O and afterwards reforms to syngas. We observed the following phenomena that support the hypothesis of a direct mechanism : i) the selectivity improved when reducing residence time, ii) the mass spectrometer detected both O_2 and CO at the effluent (simultaneously), iii) metallic Ni clusters on the Ni2510 were absent under reaction conditions based on in situ x-ray absorption spectroscopy (XAS). Loading Ni/Al_2O_3 powder downstream of the Ni2510 increased syngas yield, as the catalyst promoted steam and dry. Soot forms upstream of the Ni2510 catalyst via a retro-propagation in which methyl radicals produced on the catalyst surface react with the incoming feed gas.

7.1.1 Keyword

CH_4 partial oxidation, CPOX mechanism, Short contact time reactor, Syngas, Reforming

7.2 Introduction

The design of efficient and low CAPEX small syngas production units (CO and H_2) is a requirement to develop decentralized small scale gas-to-liquid and H_2 supply units T. et al. (2017); Joan (2002); Dincer and Acar (2015). These equipment would convert flared gas (contributing to 1 % of the total CO_2 emission Elvidge et al. (2018); Amaechi and Biose (2016)), as well as bio- and landfill gases into high added-value-products such as hydrogen or methanol and hydrocarbon Weiland (2010); Wood et al. (2012); Ma et al. (2016b). Chemicals rather than power production maximizes exergy Götz et al. (2016); Hosseini and Wahid (2016). Options for the syngas production step include steam methane reforming (SMR), auto-thermal reforming (ATR) and non-catalytic partial oxidation (POX) while catalytic partial oxidation (CPOX) has not been demonstrated at the industrial scale. While SMR, ATR and POX are common and mature solutions, they still include high technological complexity and limitations particularly for treating the above mentioned feedstock Rostrup-Nielsen and Rostrup-Nielsen (2002); Holladay et al. (2009); Dahl et al. (2014); Wismann et al. (2019b). CPOX remains the most promising technology Christian Enger et al. (2008), with less limitations on feedstock compositions and CAPEX. The remaining CPOX issues that prevent industrialization are the possibility of controlling gas phase reactions and the large axial temperature gradients inside the catalytic beds. To overcome these problems it is important to reduce the contribution of subsequent total oxidation and steam-CO_2 reforming reactions.

In many experimental works that use transition or noble metals-beased catalysts and perform reaction in kinetically controlled conditions, the syngas production occurs with subequent total combustion and steam-CO_2 reforming Tavazzi et al. (2007); Donazzi et al. (2008); Maestri et al. (2009); Chin and Iglesia (2011); Chin et al. (2011a,b). Clearly this two-step pathway originates large temperature gradients with extremely hot inlet zones (particularly at high pressure) that ignite rather unselective gas phase chemistry that challenges the possibility of designing industrial applications Hickman and Schmidt (1993); Schmidt et al. (1994). Many other authors have also reported the possibility of performing direct partial oxidation reactions even at high oxygen partial pressure with metals supported on MgO, CeO_2, ZrO_2, FeO_2Gaffney (2000); Li et al. (2010b); Urasaki et al. (2018); Ma et al. (2020); Pauletto et al. (a). If this could be developed inside an adiabatic short contact time (i.e. 0.01 s or lower) industrial reactor operating with a moderate reactant preheating not requiring furnaces, the decrease of the reactor dimensions and complexity would result in mayor advantages compared the other syngas production technologies Seo et al. (2002); Energy.gov; Basini et al. (2001); Basini and Guarinoni (2013). Among these advantages a relevant reduction of the CO_2 emissions oddly, the total emissions from SMR burners represent 1 % of global CO_2 Wismann et al. (2019a). Short contact time reactor concepts can be developed into a technology if direct reaction mechanism would prevail thus reducing the two step mechanism. Indeed, two step models have been developed with experimental data collected below 0.5 MPa, under dilute concentration, and temperature lower than 700 °C, conditions that are far away from those of an industrial reactor Wright et al. (2003); Basini and Guarinoni (2013); Wei and Iglesia (2004); Kondratenko et al. (2014); eni. These mild conditions avoid heat and mass transfer limitations, minimize radial and axial concentration gradients while avoiding coke deposition. In this work we completed a SCT-CPOX experimental study at 1.5 MPa and temperature from 800 °C to 950 °C, co-feeding CH_4 and air at CH_4/O_2 ratio from 1.6 to 1.8 inside the flammable limits Pauletto et al. (b). Noteworthy a Ni based catalyst (Ni2510) allowing lower turnover rate than Rh, Ru, Pt has been used to providing new fundamental understanding on reaction mechanism at very low residence times Christian Enger et al. (2008); Wei and Iglesia (2004).

More in detail in this work we report and discuss :

i) SCT-CPOX reactivity tests performed with catalyst obtained via deposition of Ni-Ru/CeO_2 species on a FeCrAl gauze (Ni2510) ;

ii) SCT-CPOX reactivity tests performed with two subsequent catalytic beds being the first Ni2510 and the second the Ni/Al_2O_3 powder (reforming catalyst) ;

iii) the soot formation in homogeneous gas phase reactions ;

iv) the identification of Ni oxidation states during reaction of Ni2510 and Ni/Al_2O_3

Conversion and selectivity were related to the statistically relevant reaction parameters with *Statistica*®.

7.3 Experimental

7.3.1 Catalyst

Ni2510 was synthesized as described in Pauletto et al. (a) using FeCrAl knitted fibers (Fig. 7.1) 3 mm thick.

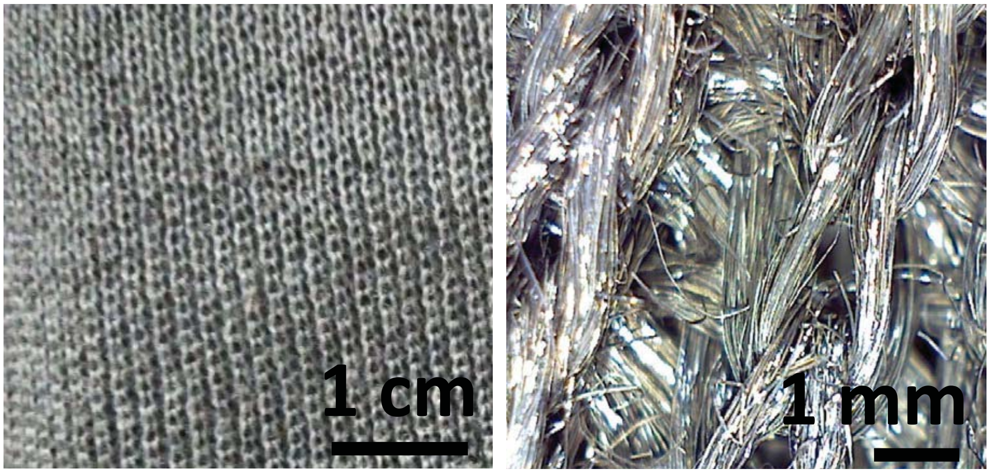

Figure 7.1 FeCrAl knitted fibers, support of Ni2510, at different magnification.

After FeCrAl preoxidation in air at 600 °C followed by impregnation of $Ce(NO_3)_3{\cdot}6H_2O$ on the metallic support after solvent evaporation. Afterward the materiel was calcined at 600 °C before deposition of $Ni(NO_3)_2{\cdot}6H_2O$ and $Cl_3Ru{\cdot}6H_2O$. Finally the catalyst oxidized in air at 800 °C. 25 % Ni/Al_2O_3 powder was bought at Novament, Wyckoff N.J. Silicon carbide (SiC, 200 mesh) (Sigma Aldrich) was used as catalyst dilutant.

7.3.2 Catalyst characterization

The detailed characterization of the Ni2510 catalyst is reported in Pauletto et al. (a). Joel JSM-7600TFE scanning electron microscope produced micrographs of Ni/Al_2O_3. X-ray detector (EDS) identified the elements present on the surface of the powders while Empyrean X-ray diffratometer (XRD) equipped with a CuKα radiation at 45 keV and 10 mA scanned the sample from 5° to 70° in a 20 min analysis. In situ XAS was performed at the 10-BM beamline at the Advanced Photon Source (APS) at Argonne National Laboratory. Measurements were performed in fast scan mode at the Ni K edge (8.333 keV) for both Ni2510 and Ni/Al_2O_3. The samples were pressed into a stainless steel sample holder and placed in a sealed quartz tube cell. The catalysts were treated sequentially by 1) 750 °C in CH_4 and 2) 750 °C in CH_4-air with cooling down to room temperature in He and scanning in between. The data was processed using WinXAS 3.1 and fit using standard fitting procedures.

7.3.3 Reactor setup

Two mass flow controllers (MFC) fed CH_4 and $O_{2/}$Ar while a *Labview*® program monitored temperature and pressure of the reactor equipment. A third MFC controlled the flow rate of Ar, which purged the reactor between experiments and when a process parameter triggers emergency interlock. We used 20 % O_2 in Ar rather than N_2 to avoid overlap of N_2 with CO Perreault et al. (2019). The reactor was made of 316SS with an inner quartz tube 15 mm in diameter. Disposable metal gasket and high temperature polymeric glue bind the metal walls with the quartz tube to seal the reactor at the entrance. A back pressure regulator maintains the pressure from 0.1 MPa to 1.5 MPa, and relieve valves at the top of the reactor and the outlet line ensure safe operation. Two manometers and two movable 1/16” K-type thermocouples (sealed using Teflon Swagelock ferrules) monitored pressure and temperature (Fig. 7.2). One thermocouple measured the temperature on the top of the catalyst and the other one on the bottom. After reaction, the gases pass across a drierite H_2O absorber before entering the mass spectrometer (MS, Hiden QIC-20) while the samples before the dryer enter an online gas chromatographer (GC, Bruker Scion 456) through a heated transfer line.

7.3.4 Reactivity test methodology

Methane reacted to syngas in a fixed bed gauze reactor 15 mm diameter, 3 mm thickness corresponding to 0.64 g (configuration a) Fig. 7.3). In a second experimental layout (configuration b) Fig. 7.3) the Ni2510 gauze was placed above and in contact with a second catalytic bed containing 2 g of Ni/Al_2O_3 catalyst diluted with 9 g of SiC. In a third experimental layout (configuration c) Fig. 7.3) the Ni2510 gauze and the Ni/Al_2O_3 catalytic bed were spaced apart by 25 mm with a 8 mm diameter quartz pipe.

In all these configurations the reactor operated from 800 °C to 950 °C, 1.5 MPa and CH_4/O_2 ratio from 1.6 to 1.8. CH_4 (99.99 % v/v) volumetric flow rate varied from $1\,\mathrm{L\,min^{-1}}$ to $4\,\mathrm{L\,min^{-1}}$ (Table 7.1) determining GHSV between $100\,000\,\mathrm{h^{-1}}$ to $200\,000\,\mathrm{h^{-1}}$ considering only the volume of the Ni2510. A mass spectrometer (MS) and a gas chromatograph monitored the product composition respectively in transient and steady state conditions. After 4 h on stream, we used to repeat a standard test (experiment 1 Table 7.1) to assess catalytic activity. This minimizes confounding factors between reaction conditions and deactivation.

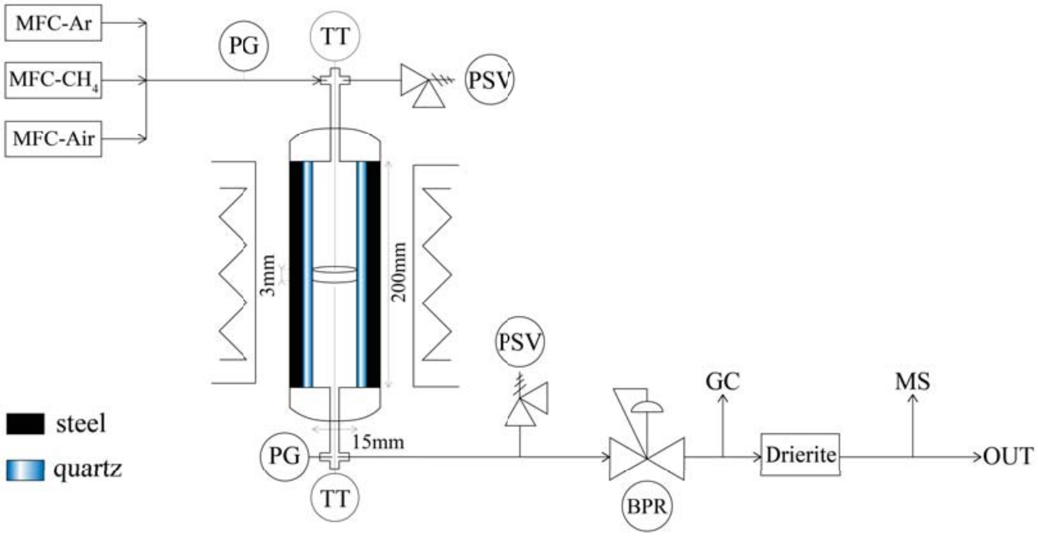

Figure 7.2 Overview of the setup

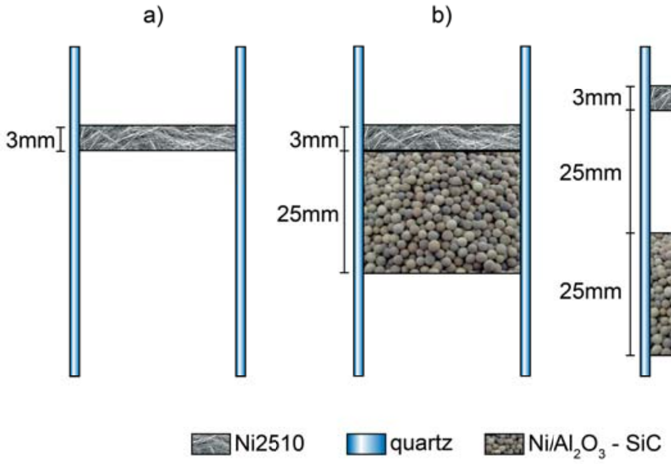

Figure 7.3 Configuration : a) Ni2510, b) Ni2510 in contact with Ni/Al_2O_3, c) Ni2510 and Ni/Al_2O_3 separated by a quartz pipe.

The experimental sequence consisted of the following steps : 1) Ar purge, 2) CH_4 and $O_{2/}$Ar reaction, 3) Ar purge, and 4) $O_{2/}$Ar oxidation of the carbon species, when formed, in order regenerate the catalyst. In step (4) coke formation was confirmed by measuring the amounts of produced CO and CO_2 with MS. The experimental observations taken with configuration a) correlated the reaction parameters with the methane conversion and syngas selectivity. During experiments with configurations b) and c) we measured the extent of steam-CO_2 reforming reactions occurring on the Ni/Al_2O_3 catalyst and provided information on the gas phase reactions. We identified the major factors with *Statistica*® software ; We considered only the 2-way linear-linear interactions, repeated half of the experimental conditions, and ignored higher terms.

CH_4 conversion and CO, CO_2, C, H_2 and H_2O are (Eq. 7.1,7.2,7.4) :

$$X_{\mathrm{CH_4}} = \frac{\text{moles of CH}_4\text{ reacted}}{\text{moles of CH}_4\text{ fed}} \times 100 \tag{7.1}$$

$$S_i = \frac{\text{moles of C or CO or CO}_2\text{ produced}}{\text{moles of CH}_4\text{ reacted}} \times 100 \tag{7.2}$$

$$S_{ii} = \frac{\text{moles of H}_2\text{ or H}_2\text{O produced}}{\text{2 moles of CH}_4\text{ reacted}} \times 100 \tag{7.3}$$

$$\mathrm{H_2:CO} = \frac{\text{moles of H}_2}{\text{moles of CO}} \tag{7.4}$$

We also calculated the equilibrium temperatures of steam reforming T_{SMR} (Eq. 7.5) and of dry reforming T_{DR} (Eq. 7.6). These values helped to quantify the approach to equilibrium compared to the product gas composition and catalyst temperature.

$$T_{\mathrm{SMR}} = -\Delta G_{\mathrm{SMR}}\ \ln \frac{P_{\mathrm{H_2}}^3\ P_{CO}}{P_{\mathrm{CH_4}}\ P_{\mathrm{H_2O}}} \tag{7.5}$$

$$T_{\mathrm{DR}} = -\Delta G_{\mathrm{DR}}\ \ln \frac{P_{\mathrm{H_2}}^2\ P_{CO}^2}{P_{\mathrm{CH_4}}\ P_{\mathrm{CO_2}}} \tag{7.6}$$

7.4 Results and discussion

7.4.1 Experiments with configuration a)

With these tests we investigated the effect of temperature and CH_4 volumetric flow rate on CPOX performance at 1.5 MPa and CH_4/O_2 ratios of 1.6 and 1.8 v/v. The design of experiment (DOE) considered in 12 tests (2 levels for temperature, 3 levels for CH_4 volumetric flow rate and 2 $CH_{4/}O_2$ ratio), 6 tests were repeated to assure their reproducibility and we reported the average. Table 7.1 includes the operating conditions of the DOE while Table 7.2 the results.

Table 7.1 Full factorial DOE of CPOX at 1.5 MPa for each of the three reactor configurations.

Exp't	CH_4/O_2, -	T, °C	$\dot{V}_{CH_4}$, $L\,min^{-1}$
1	1.6	800	1
2	1.6	800	1.5
3	1.6	800	2
4	1.6	900	1
5	1.6	900	1.5
6	1.6	900	2
7	1.8	800	1
8	1.8	800	1.5
9	1.8	800	2
10	1.8	900	1
11	1.8	900	1.5
12	1.8	900	2

Following the reaction protocol we analyzed the product stream with a GC injection after the MS signal showed a stationary state. Temperature values (Fig 7.2) measured on both side of the Ni2510 gauze were the same and slightly exceeded the preheating temperatures as the CPOX reaction generated heat. Temperatures partially increased with flow rates as the percentage of heat exchanged through the reactor walls decreased. The obtained results showed that O_2 was always completely consumed and that the selectivity towards partial oxidation products increased with reactant flow rates that decrease contact times from 0.030 s to 0.015 s. These results suggest a direct partial oxidation reaction mechanism of CH_4 and not reforming reactions that would lead to higher selectivities in the cases of higher conversion Lyubovsky et al. (2005); Kondratenko et al. (2014). Higher selectivities toward CO and H_2 at higher temperature are also consistent with the favored desorption of partially oxidized products at temperatures above 750 °C Richardson and Cale (1986); Hoang-Van et al. (1989). In addition to the experiments listed in Table 7.1, we have further increased CH_4 flow rate to 4 $L\,min^{-1}$ to further decrease contact time. In this case we observed O_2 blow-out and co-existence of partial and total oxidation products (Fig. 7.4). These results obtained at extremely short contact times (0.008 s) are possible only if CPOX follows a direct reaction mechanism. Clearly the observed situation is different from the one discussed by Chin et al. reporting that, under kineticlly controlled regime, CO cannot leave the reactor until O_2 is

Table 7.2 Reaction performance of CPOX at 1.5 MPa with experimental configuration a) Fig. 7.3.

Exp't	T, °C	X_{CH_4}	S_{CO}	S_C	S_{H_2}	$\text{Ratio}_{H_2/CO}$	T_{SMR}, °C	T_{DR}, °C
1	820	56	56	9	46	1.6	632	671
2	825	54	66	3	51	1.5	643	683
3	830	53	69	0	58	1.7	662	694
4	900	59	69	8	51	1.5	659	707
5	900	58	76	1	55	1.4	668	716
6	950	56	82	2	63	1.5	688	737
7	820	51	56	12	42	1.5	615	661
8	820	49	64	6	47	1.5	630	674
9	830	48	69	1	55	1.6	649	685
10	900	55	57	12	43	1.5	626	671
11	900	51	67	3	54	1.5	652	689
12	940	51	71	0	58	1.6	661	696

completely consumed as reaction rate of CO oxidation is higher than for CH_4 Chin et al. (2011a).

7.4.2 Experiments with configuration b) and c)

With experimental configuration b) and c), we forced the kinetically controlled steam and dry reforming reaction using a second catalytic bed of Ni/Al_2O_3 powders diluted with SiC downstream Ni2510. In preliminary experiments with the configuration b), we diluted 2 g of Ni/Al_2O_3 catalyst with 4 g, 9 g, and 14 g of SiC powder (Fig. 7.5) to remove heat and mass transfer limitations in the packed bed and therefore obtaining a full kinetically controlled reaction regime Koros and Nowak (1967); Madon and Boudart (1982). Configuration c) respect to b) prevents temperature artifacts given the distance between the two catalytic beds. This makes easier to operate under isothermal conditions as most of the highly exothermic CH_4-O_2 reactions, that generate heat, take place within Ni2510. Without dilution Ni/Al_2O_3 could work under mass transfer limitations and therefore any oxygen leaving Ni2510 would react on Ni/Al_2O_3 following an apparent direct reaction mechanism Chin et al. (2011a). Even if during experiments at GHSV lower than 200 000 h^{-1} with configuration a) no O_2 was detected in the gas phase, in configuration b) we cannot predict and assume that all O_2 is consumed on the first catalytic bed. This is possible if there is a thermal effect caused by the conductive heat transfer between Ni2510 and Ni/Al_2O_3. In these experiments the catalyst reacted at active space velocities between 0.4 $L\,min^{-1}\,g^{-1}$ to 0.6 $L\,min^{-1}\,g^{-1}$ (from 1 $L\,min^{-1}$

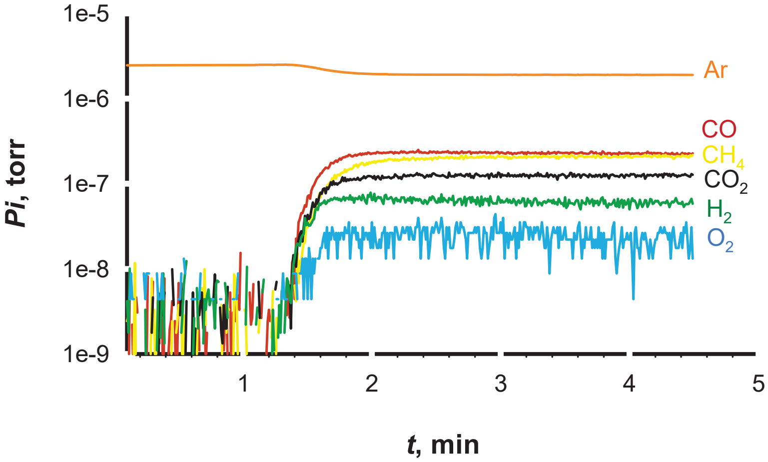

Figure 7.4 MS signal of CPOX products during reaction with 4 L min^{-1} of CH_4 ratio 1.6 at 800 °C

to 2 L min^{-1}) at 800 °C and $CH_{4/}O_2$ 1.6 v/v. This ratio is more challenging with respect to 1.8 as the thermodynamic conversion and selectivity of exothermic reactions are higher. The results in Fig. 7.5 showed that methane conversion was independent from catalyst dilution and not limited by equilibrium when Ni/Al_2O_3 was mixed with 9 g or 14 g of SiC. We fixed the mass diluent at 9 g (ratio 4.5) in all the following experiments since the conversion was only function of the CH_4 active space velocity and not of the dilution ratio.

We then completed 36 experiments, 12 with configuration b) and 12 with configuration c). The results obtained with experimental configuration b) and c) gave the same performance within the limit of the experimental errors. We experimentally obtained the trend of methane conversion and syngas selectivities vs. gas flow rate when an indirect mechanism, in this case induced, partially oxidized methane. With these configurations, both hydrogen selectivity and methane conversion decreases with flow rate, differently from the result of configuration a). This confirmed that Ni2510 partially oxidized methane through a different mechanism because if an indirect mechanism was involved, than the reaction performance vs. gas flow rates would have follow the same trend obtained with configuration b) and c).

We conclude that when we combined the two catalysts while Ni2510 partially oxidized methane through a direct mechanism, the following Ni/Al_2O_3 catalyst promoted reforming reactions.

CH_4 conversions, CO and H_2 (Table 7.3) were higher compared to the results of the experi-

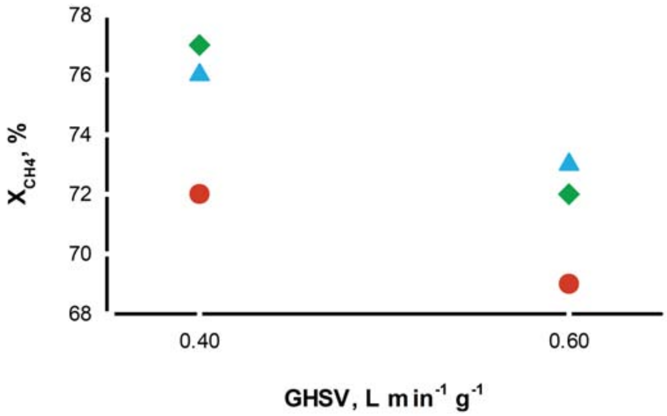

Figure 7.5 CH_4 conversion rate vs function of active space velocity at 800 °C and 1.6 CH_4/O_2 ratio. Red dots 4 g, Blue triangles 9 g, Green diamond 14 g of SiC.

mental configuration a) (Table 7.2). This points out a possible advantage of combining direct partial oxidation with steam-CO_2 reforming in two separate catalytic beds. The approach to the equilibrium values were more than 100 °C higher respect to the same values obtained with only NI2510. CH_4 conversion, CO and H_2 selectivity were also increased (Table 7.4).

Table 7.3 Reaction performance of CPOX at 1.5 MPa with experimental configuration b) and c) Fig. 7.3.

Exp, -	X_{CH_4}	S_{CO}	S_C	S_{H_2}	Ratio$_{H_2/CO}$	T_{SMR}, °C	T_{DR}, °C
1	77	72	7	75	1.9	767	778
2	72	79	1	72	2.2	749	772
3	71	82	0	70	2.3	740	768
4	78	77	4	80	1.9	790	794
5	75	79	1	78	2.0	779	789
6	73	82	1	77	2.1	770	783
7	73	74	8	76	2.0	766	784
8	70	79	3	77	2.1	761	779
9	68	82	1	77	2.1	758	775
10	74	74	9	78	1.9	775	788
11	71	78	4	78	2.0	770	723
12	71	81	0	77	2.1	767	782

The experiments with and without Ni/Al_2O_3 gave similar carbon selectivity this means that while second catalytic bed does not react carbon or affect the gas phase reaction, all the soot is produced upstream the first catalytic bed.

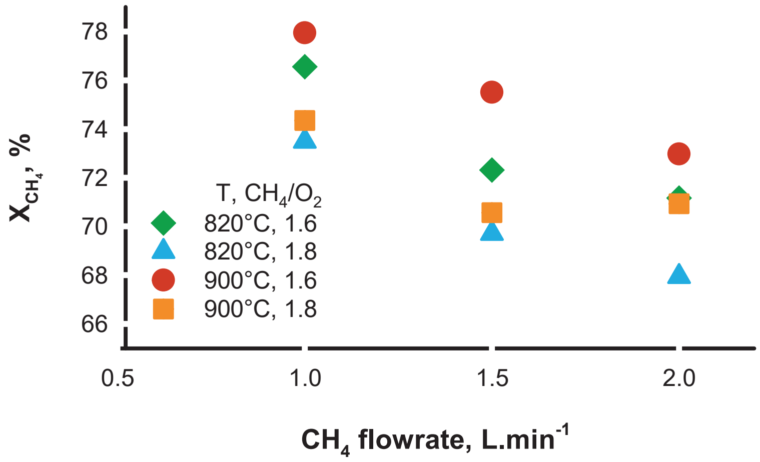

Figure 7.6 CH_4 conversion as function of CH_4 flowrate at different ratio and temperature

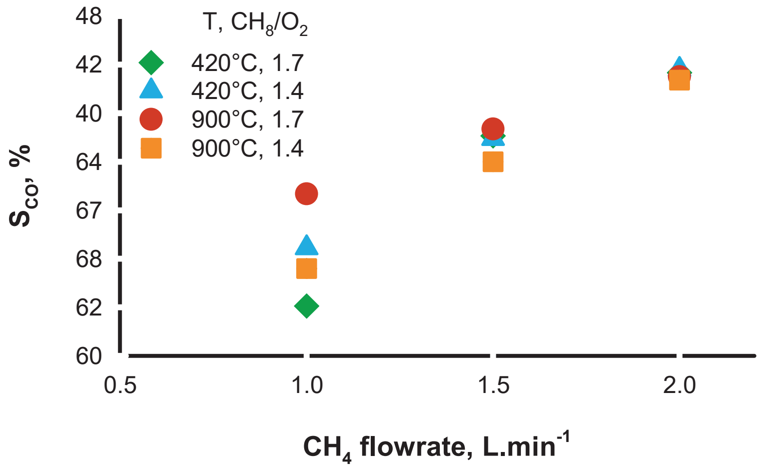

Figure 7.7 CO selectivity as function of CH_4 flowrate at different ratio and temperature

Table 7.4 Enhanced reactor performance of configuration b) and c) with respect to a). The data in the column are the absolute change in performance versus data in Tables 7.2 and 7.3 (at 1.5 MPa).

Exp, -	ΔX_{CH4}	ΔS_{CO}	ΔS_{C}	$\Delta S_{\mathrm{H_2}}$	$\mathrm{Ratio}_{\mathrm{H_2/CO}}$	ΔT_{SMR}, °C	ΔT_{DR}, °C
1	21	16	-2	29	0.3	135	107
2	18	13	-2	21	0.7	106	89
3	18	13	0	12	0.6	78	74
4	19	8	-4	29	0.4	131	87
5	17	3	0	23	0.6	111	73
6	17	0	-1	14	0.6	82	46
7	22	18	-4	34	0.5	151	123
8	21	15	-3	30	0.6	131	105
9	20	13	0	22	0.5	109	90
10	19	17	-3	35	0.4	149	117
11	20	11	1	24	0.5	118	34
12	20	10	0	19	0.5	106	86

7.4.3 Gas phase reaction contributions

Experiments performed with configuration b) and c) gave the same results ; this together with the absence of soot in the inter-phase zone, between the catalytic beds in configuration c), excludes unselective gas phase reaction downstream the first catalytic bed. Instead a relevant amount of carbon forms before the first catalytic. Soot forms without involving a sub-stoichiometric flame as the thermocouple, placed above the first catalytic bed, measured constant values. The negligible amount of coke on the Ni2510 catalyst surface (confirmed by catalyst oxidation/regeneration) suggests that gas phase reactions are ignited at the catalyst surfaces and retro-propagated into the incoming reactants flow. Blank tests, performed with the empty reactor and with a pre-oxidized FeCrAl without supporting Ni and Ru species, excluded thermal gas phase activation of the reactive mixture. Soot was formed only in the presence of the catalyst indicating that the homogeneous reactions are heterogeneously ignited as reported in other short contact time experimental works Goetsch and Schmidt (1996). Radical species form exclusively on the catalyst surface that is much hotter compared to the gaseous phase of the incoming reactants Basini and Guarinoni (2013). Basini et al. has also shown that the surface catalyst temperature, measured with infra-red thermography,is often hundreds of degrees higher compared to the one measure with the thermocouples Basini and Guarinoni (2013). This is consistent with findings reported by Li etal. and Kahle et al. in the case of DR Li et al. (2008); Kahle et al. (2013); Wittich et al. (2020). Traces of

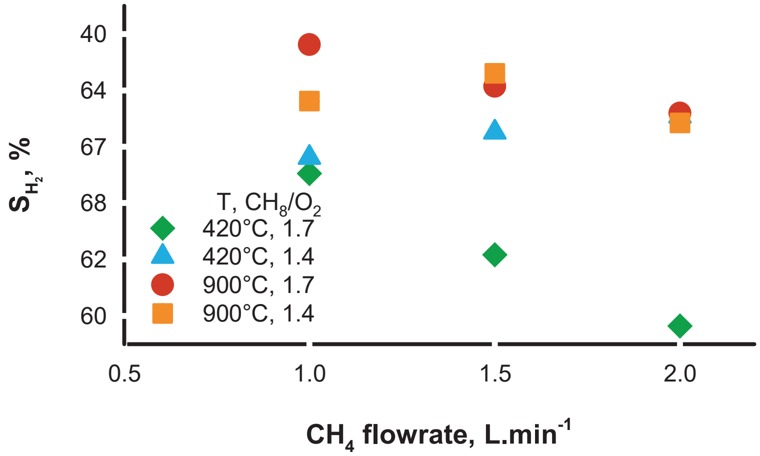

Figure 7.8 H_2 selectivity as function of CH_4 flowrate at different ratio temperature

ethylene (< 1000 ppm), detectable by GC, further substantiates gas phase reaction that produces soot or its precursors Basini et al. (2017). The methyl radicals, formed on the catalyst surfaces, combine exclusively in the gas phase as it has been proved in the oxidative coupling of methane Schwach et al. (2015a,b); Karakaya et al. (2017). These desorb only in the presence of oxygen and therefore, they must react upstream of the catalytic bed rather than downstream, where the oxygen partial pressure is zero for all the experiments at GHSV lower than 200 000 h^{-1} Kwapien et al. (2014). In agreement, higher volumetric flow rates decrease carbon selectivity, because the increasing convection reduces the diffusive retro-propagation of radical species formed at the front-end of the first catalytic bed.

7.4.4 Catalyst characterization

SEM-EDS micrographs of the Ni/Al_2O_3 powder catalyst showed that Ni coats the Al_2O_3 particles (Fig. 7.9). Only the sharp edges are exposed while the metal forms a homogeneous and uniform layer only on the flat surfaces. determining a BET surface area lower then $0.6\,m\,g^{-1}$. Quantification of the surface area, based on geometrical considerations, from the particle size distribution analysis agrees with N_2 physisorption data. The particles have a Gaussian distribution with median size $D_{v,0.5}$ of 253 µm where $D_{v,0.1}$ and $D_{v,0.9}$ are respectively 160 µm and 387 µm ; these dimensions agree with SEM images. Low surface area, compared to Ni2510, reduces the activity of the reforming catalyst allowing operation at high effectiveness factors thus under kinetic regime Pauletto et al. (a); Rostrup-Nielsen and Christiansen (2011). The

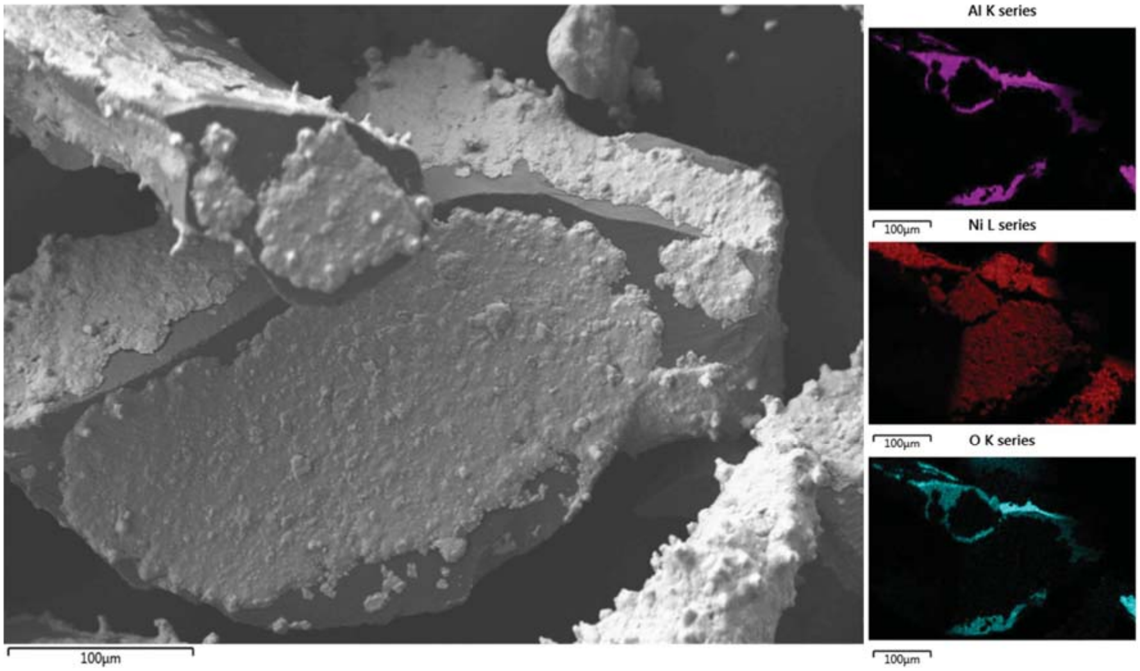

Figure 7.9 SEM micrograph and SEM-EDS mapping of the Ni/Al_2O_3 particles.

structures of Ni/Al_2O_3 was also verified by XRD, although the high crystallinity of the Al_2O_3 support leads to sharp peaks, making it difficult to deconvolve the signal from small NiOx clusters of Ni/Al2O3. Reflections at approximately 40.0, 46.1, 59.6, and 61.1 ° are attributed to NiO_x. The diffractograms show the peaks corresponding to alumina that is exposed and visible with SEM.

To identify the oxidation state of Ni under reaction conditions, *in situ* XAS was performed in : 1) pure CH_4, 2) CH_4/O_2 ratio of 2 to understand the role of each reactant gas. The normalized XANES spectra are shown in Fig. 7.10. When both Ni2510 and Ni/Al_2O_3 were treated in only CH_4, the XANES energy was 8.333 keV, consistent with metallic Ni. Hydrogen formed via CH_4 cracking was therefore present either on the surface or in the gas phase because methane would have not affected the Ni-NiO equilibrium Rostrup-Nielsen and Christiansen (2011). The samples were then treated in a reaction gas mixture CH_4-O_2 ; Ni2510 completely oxidized to NiO, evidenced by a pre-edge feature at about 8.334 keV, consistent with predominantly Ni^{2+}. The XANES energy of the sample (8.345 keV) is consistent with that of NiO. However, the white line intensity of Ni/Al_2O_3 increased to a lesser extent compared to Ni2510, suggesting that it did not completely oxidize.

A linear combination XANES fit between the Ni obtained after CH_4 only treatment and NiO was performed on Ni/Al_2O_3 after the treatment in CH_4/O_2= 2 to determine the ratio of Ni^0

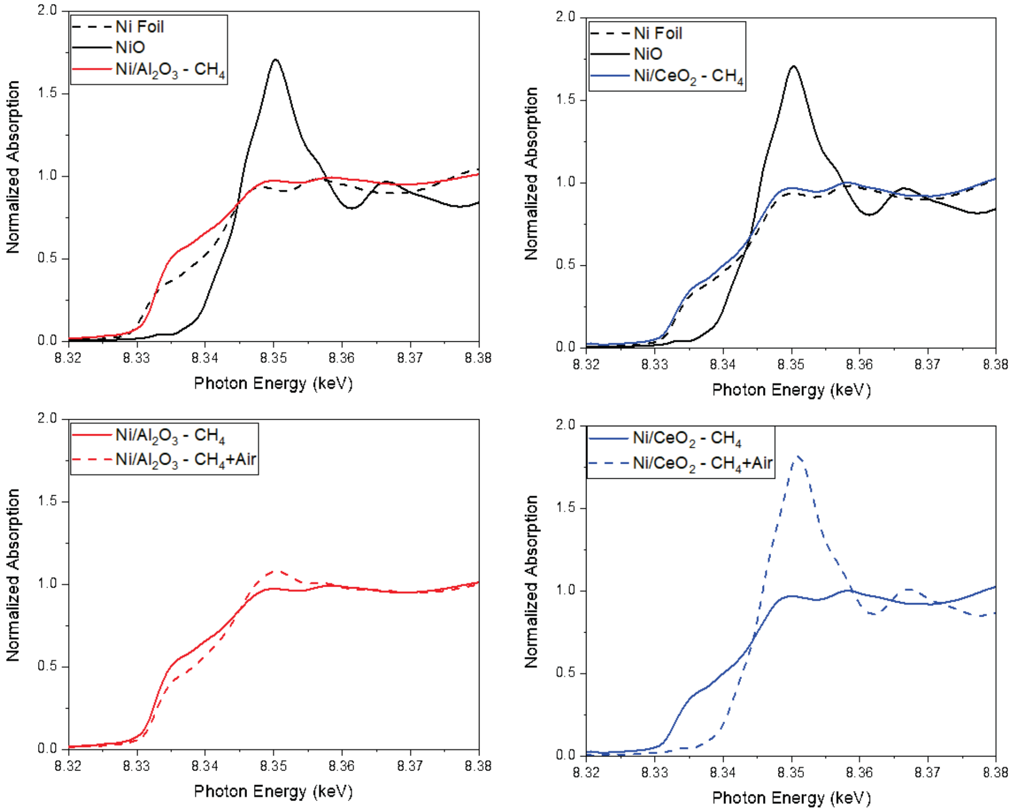

Figure 7.10 Normalized XANES at the Ni K edge of Ni2510 (Ni/CeO$_2$) and Ni/Al$_2$O$_3$ in CH$_4$ and CH$_4$/O$_2$= 2 compared to Ni foil and NiO

and Ni^{2+}. This yielded 83 % Ni^0 and 17 % Ni^{2+}. In both samples, the CH_4 only treatment showed only Ni-Ni scattering (Fig. 7.11). After the CH_4-O_2 reaction gas treatment, the Ni2510 completely oxidized to NiO while only a small fraction of Ni/Al_2O_3 oxidized. Due to the large signal from metallic Ni in Ni/Al_2O_3, Ni-O scattering was verified by performing a difference analysis on the metallic Ni obtained from the CH_4 treatment minus 0.4 Ni foil. This removes the signal from the Ni-Ni scattering pair. With this, a Ni-O fits with a coordination number of 1.1 and bond distance of 2.07 Å was obtained, consistent with only a small fraction of Ni-O observed in the XANES. The fraction of NiO can be estimated from the Ni-O coordination number (CN), e.g., NiO has 6 Ni-O bonds. A Ni-O CN of 1.1 is consistent with 17 % Ni^{2+} oxide and agrees with the fraction of oxidized NiO from the XANES fit.

For Ni2510, the XANES and EXAFS are consistent with metallic Ni after treatment in only CH_4. When $CH_4/O_2 = 2$ was performed, the pre-edge feature in the XANES is consistent with Ni^{2+} and the XANES closely matches that of NiO. In the EXAFS, only Ni-O scattering is observed. If Ni^0 is present, there is only a small fraction, that is not detected by XAS. Under reaction conditions where stoichiometric ratio $CH_4/O_2 < 2$, Ni/CeO_2 has predominantly NiO. For Ni/Al_2O_3, the XANES and EXAFS are consistent with metallic Ni after treatment in only CH_4. When $CH_4 : O_2 = 2 : 1$ was performed, only a slight increase in white line intensity was observed and no pre-edge feature was detected. The EXAFS fit well with only a Ni-Ni and Ni-O scattering pairs.

Table 7.5 EXAFS fitting parameters over a Fourier transform range from 2.7 Å to 11.0 Å at the Ni K edge for Ni2510 and Ni/Al_2O_3 treated at 800 °C in CH_4 and CH_4-air $CH_4/O_2 = 2$.

Sample -	Treatment -	Pre-edge keV	XANES keV	Pair -	CN -	R, Å Å	σ^2 Å	ΔE eV
Ni foil			8.333	Ni-Ni	12.0	2.49		
NiO		8.334	8.345	Ni-O	6.0	2.07	0.005	-5.7
				Ni-O-Ni	12.0	2.94	0.005	
Ni/Al_2O_3	CH_4		8.333	Ni-Ni	5.1	2.48	0.005	5.7
Ni/Al_2O_3	CH_4 - air		8.333	Ni-Ni	5.0	2.48	0.005	6.4
				Ni-O	1.1	2.07	0.005	
Ni/CeO_2	CH_4		8.333	Ni-Ni	9.4	2.48	0.005	-5.0
Ni/CeO_2	CH_4 - air	8.334	8.345	Ni-O	6.0	2.06	0.005	-6.0
				Ni-O-Ni	12.0	2.94	0.005	

Interestingly, CeO_2 and Al_2O_3 supports yield different ratios of Ni^0 and Ni^{2+}. The unique nature of CeO_2 support stabilizing effect of metal nanoparticles Datye and Wang (2018), resistance to deactivation Xu and Wang (2005), O_2 storage Santos et al. (2005); Tada et al. (2012) and mobility Dong et al. (2002) facilitates the complete oxidation of Ni to NiO_x, when

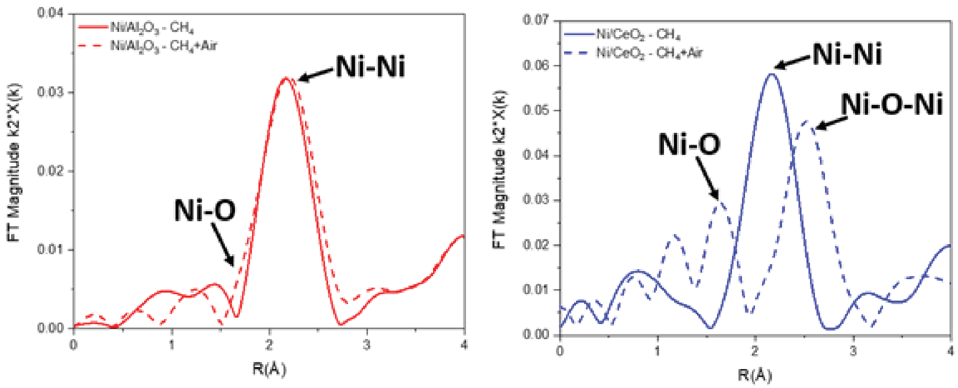

Figure 7.11 Ni-edge magnitude of the Fourier transforms after samples were treated in reaction conditions at 800 °C in CH_4 and CH_4/O_2= 2.

air is present Paier et al. (2013); Montini et al. (2016). However, this is not the case on Al_2O_3, where only about 17 % of the Ni oxidizes to Ni^{2+} at ratio 2.

Under reaction conditions the mixture of oxidation states leads to a completely different reaction activity. Ni2510 is not active in reforming the product as only reduced Ni reforms CH_4 ; NiO, instead, is active in partial oxidation but it cannot reform the products. This is the reasons why at high gas flow rates experiments, necessary to measure reforming intrinsic kinetic, the absence of H_2 back diffusion requires H_2 co-feed to prevent Ni oxidation Rostrup-Nielsen and Christiansen (2011). Therefore, at these reaction parameters, Ni2510 is reacting methane following a direct reaction mechanism as reforming requires Ni^0. Even if Ni2510 is working under mass transfer limitations, that is often the case of SCT-CPOX Bizzi et al. (2002, 2003), reforming is not involved as the catalyst does not contain Ni^0. It appears that CeO_2 is stabilizing NiO either supplying O_2 or favoring oxidation or forming a solid solution Ni-Ce oxides Jalowiecki-Duhamel et al. (2008). Moreover, Al diffuses from the bulk FeCrAl and oxidizes to Al_2O_3 during calcination at 800 °C. This surface enrichment increases coating adhesion, reduces sintering, and stabilizes the active phase while decreasing coke formation Lu et al. (2012). In the case of Ni/Al_2O_3, metallic Ni is reduced proving absence of spinel $NiAl_2O_4$ or other stable compounds. jun Zhang et al. (2015).

7.5 Conclusions

A 2.25 %Ni/0.1 %Ru/CeO_2 catalyst (Ni2510) supported on FeCrAl gauze partially oxidizes methane at very short contact times with a H_2 pre-reduction step. The Ni2510 was active at 1.5 MPa, from 800 °C to 950 °C and 1.6 CH_4/O_2 ratio. In-situ XAS proved the absence of Ni^0 species under reaction conditions thus excluding any reforming and supporting the hypothesis of a direct reaction mechanism Three experimental configurations underlined the possibility to couple direct SCT-CPOX with steam and dry reforming activated by a downstream Ni/Al_2O_3 catalyst. With this tandem configuration, the reaction approaches equilibrium at 1.5 MPa. We detected soot upstream of the Ni2510 catalyst but not in the catalyst bed nor downstream. Carbon/coke/soot formed only in the presence of a catalyst and not during blank tests and it decreased with reactant flow rates. Methyl radicals forming on the catalyst surface retro-propagate towards the incoming reactants inducing chain reactions to produce soot. We foresee the possibility of coupling direct partial oxidation with steam and dry reforming to develop a more fundamental understanding of the limiting process steps.

CHAPTER 8 GENERAL DISCUSSION

Flared gas released in remote locations is a considerable and unexploited energy source. In these applications, syngas generation commonly involves POX or ATR and accounts for more than 60 % of the total CAPEX. We cannot apply the economy of scale to POX and ATR – scale down is difficult. SMR requires expensive fired furnaces, whereas POX and ATR necessitate pure O_2 to reach operating temperatures. SMR and ATR are strict in terms of reactant composition and flow rate – they are not suitable for decentralized applications. The GTL unit, installed at the well head, handles composition and flow rate fluctuations of the flared gas. The SCT-CPOX reaction minimizes reactor volume and can convert diverse associated gases containing CO_2 and C^{2+} while running adiabatically with air as a co- reactant. However, it is not industry-feasible in its current state due to catalyst deactivation via coke depositions and poor syngas selectivities. Compact, inexpensive, and flexible production units are crucial for decentralized production of syngas, synthetic fuels, and methanol. High-pressure reactors suit industrial applications thanks to their decreased reactor volume (CAPEX) and they minimize costs connected to downstream syngas compression (OPEX). This PhD project aimed to develop a new Ni-based catalyst on a structured support for high pressure SCT-CPOX. Furthermore, we designed a SCT-CPOX coupled with a single-pass FT reactor for field tests— a micro GTL unit deployable at the well head.

The first part of the project involved identifying catalysts – with a FeCrAl support – reported in the literature. FeCrAl is an alloy with a higher thermal conductivity compared to the traditional ceramic materials. It decreases temperature gradients in the catalytic bed – apt for tail gas treatment and syngas generation. As opposed to other high temperature alloys, FeCrAl is unique because it forms a protective layer of α-Al_2O_3 ; this layer facilitates catalyst synthesis. FeCrAl knitted fibers are an inexpensive catalyst support compatible with the SCT reactor. This support is easily scalable without additional improvements. Support modification normally involves monolith or foam. Ni promoted by Pt or Ru on CeO_2 are the active phases in the CPOX reaction. Ni, the cheaper alternative, forms more coke than Rh, Pt, Ru, and Ir. However, lattice O_2 in ceria limits this formation. Pt and Ru are promoters and activated methane at higher TOFs compared to Ni.

In the second part of the project, we synthesized 12 catalysts by combining Ni promoted with 0.1 % Pt and/or Ru. The combination of 2.25 % Ni and 0.1 % Ru on 9 % CeO_2 which, in turn, is on FeCrAl (Ni2510) was the most active system and produced the least carbon relative to the other combinations. Pt's presence increases CO_2 selectivity but prevents full catalyst regeneration on stream with air. Ni2510 yielded CO but no CO_2 until the CH_4/O_2

ratio in the reaction mixture reached 3.4 – indicating the absence of consecutive indirect mechanism.The catalyst at a CH_4/O_2 ratio of 2.5 was poorly selective for CO but stable for 50 on stream cycles with full deactivation followed by air regeneration. The adhesion of the active material to the surface of the fiber and the low catalyst surface area that prevented deactivation via pore blocking are responsible for the lasting stability. The supporting metal matrix minimizes temperature gradients and provides superficial Al, which oxidizes during calcination. The Al_2O_3 enhances adhesion of the superficial active components to the support.

Following these two steps, we developed a techno economic analysis comprising SCT-CPOX and a FT fluidized bed. A thermodynamic study optimized syngas yield while minimizing carbon deposition and identified the flammable limit of the air-methane mixture at 2 MPa. We developed two case studies of CPOX at 0.1 MPa and 2 MPa. In both configurations, the syngas polymerization step involved a single pass FT fluidized bed operating at 2 MPa. A plant working at $100\,\mathrm{m^3\,h^{-1}}$ is economic when both reactions run at the same pressure. A high pressure reduces the volume of the SCT-CPOX reactor and sheds the expensive syngas conditioning unit and compressor. Micro GTL integration into the existing oil battery facility overcomes the economic hurtles for units that produce $7\,\mathrm{bbl\,d^{-1}}$. For example, it decreases costs associated with site preparation, e.g. pipelines and connections to water and electricity. In addition, combustion of gas exiting the separator downstream of the FT unit produces the heat to reach the operating temperature in the three-phase separator. Furthermore, heat integration exploits steam generated by the FT reaction and increases process revenue. Number-up decreases CAPEX by more than 25 %as the learning factor avoids engineering, control, and safety costs while also decreasing equipment prices.

The final step focused on bench scale tests to partially oxidize $1\,\mathrm{L\,min^{-1}}$ to $4\,\mathrm{L\,min^{-1}}$ of CH_4 at 1.5 MPa. We investigated the effect of GHSV on the reaction performance. The trend suggests a direct reaction mechanism substantiated by in-situ XAS. The in-situ characterization identified the oxidation state of the active phase and excluded the presence of reduced Ni. Thus, Ni^{2+} avoids any reforming reaction that is exclusively activated by reduced Ni. CPOX combined with the reforming catalyst – an induced indirect mechanism – enhanced syngas yield (50 % higher). This method is more economical and compact with respect to ATR. It does not require pure oxygen nor temperatures above 1100 °C because POX (CH_4 thermal activation) is absent in the first section of the reactor. We combined Ni2510 and Ni/Al_2O_3 catalysts and studied the gas phase reaction that forms soot under CPOX conditions. Carbon formed upstream of the first catalytic bed via retro-diffusion of radical activated on the catalyst surface. This phenomenon decreases with increasing gas velocity as the back diffusion decreases.

CHAPTER 9 CONCLUSION

9.1 Conclusion

Stricter air emission legislation will reduce oil consumption and decrease oil extraction from wells that contain considerable amounts of light fractions. CPOX of flared gas at low contact time is appealing because it permits the design of compact and economical GTL units to be coupled with oil battery facilities. Air blown adiabatic SCT-CPOX operating mode reduces CAPEX, OPEX, and allows syngas production in decentralized locations where natural gas contains considerable amounts of CO_2. The first step screened 12 catalyst samples with different Ni loadings and promoters. After we identified the best Ni promoter, we selected all samples containing Ni promoted with Ru – Pt formed refractory coke. The 2.25% Ni and 0.1% Ru sample was the most active and selective for CH_4 partial oxidation. A low operating pressure limited the screening in the quartz reactors. A techno-economic analysis confirmed that a small-scale CAPEX GTL is feasible – only when syngas generation occurs at pressures that avoid intermediate syngas compressor. As a result, we tested the most performant catalyst in a 15 mm diameter SCT-CPOX reactor operating at 1.5 MPa. A detailed safety analysis identified the flammable limits. We installed multiple safety loops that shut down the reactor when triggered. In high pressure SCT-CPOX, Ni2510 partially oxidized methane following a direct reaction mechanism. Catalyst-support failure caused problems during the bench scale experiments at a CH_4/O_2 ratio lower than 1.6 ; surface temperatures can reach values hundreds of degrees Celsius higher compared to the gas phase. We have also produced syngas by combining CPOX with downstream reforming using air rather than oxygen (ATR) as the oxidizer.

9.2 Limitation of the solution proposed

The main limitation of this work involves the final reactor design operating at a bench scale. Its geometry does not minimize the gas phase reaction and the electrical furnace heats up other areas aside from the reactive zone.

9.3 Recommendations for the future research

Here, we presented – for the first time – high pressure SCT-CPOX of CH_4 activated by Ni/CeO_2 supported on a FeCrAl gauze. FeCrAl's thermal conductivity enhances performance but is not stable during high pressure CPOX. Its high temperature stability was insufficient in the face of the hot spots that climbed to temperatures above 1000 °C. For future research, we suggest switching to a ceramic support with spheres of SiC and a noble metal (e.g. Ru) rather than Ni. SiC provides high-temperature stability and thermal conductivity values superior to that of FeCrAl. Moreover, Ni is not accepted in the chemical industry in oxidizing environments at temperatures above 700 °C. The higher activity of noble metals makes it possible to operate at higher gas space velocities and decreases the possibility of an O_2 blowout. Based on our experience with the bench scale reactor, we advise focusing on reactor design as opposed to the catalyst. At temperatures bridging 1000 °C, the reactor design must minimize the gas phase reaction and homogenize the temperature within the catalytic bed – surface chemistry and carbon formation on the surface are an afterthought. We suggest a conical catalytic section – similar to ENI Spa - with a narrow inlet. This reduces heat transfer via irradiation to the reactive mixture (low view factor) and achieves higher linear rates that minimizes possible flame retro propagation. In addition to the conical feature, we propose a new reactor geometry that further decreases the heat transfert the incoming gas phase. The central inactive conical refractory eliminates hot-spots often located at the center of the catalytic bed and optimizes the temperature profile.

REFERENCES

"Coke Formation and Metal Dusting of Electroplated Ni_3Al-CeO_2-based Coatings in CO-H_2-H_2O", *Corros. Sci.*, vol. 49, pp. 4134–4153, 2007.

"Washcoating of metallic monoliths and microchannel reactors", dans *Scientific Bases for the Preparation of Heterogeneous Catalysts*, série Studies in Surface Science and Catalysis, E. Gaigneaux, M. Devillers, S. Hermans, P. Jacobs, J. Martens, et P. Ruiz, éds., 2010, vol. 175, pp. 25–33.

"Catalytic partial oxidation of natural gas to syngas", *Fuel Process. Technol.*, vol. 42, no. 2, pp. 109–127, 1995, trends in Natural Gas Utilisation.

dans *Chemical Engineering Design (Second Edition)*, second edition éd., G. Towler et R. Sinnott, éds. Boston : Butterworth-Heinemann, 2013.

"Oxidative decomposition of o-dichlorobenzene over V_2O_5/TiO_2 catalyst washcoated onto wire-mesh honeycombs", *Appl. Catal. A*, vol. 237, no. 1, pp. 81–89, 2002.

"Eni and sabic will jointly develop a technology for natural gas conversion into synthesis gas to produce high value fuels and chemicals". En ligne : `https://www.eni.com/docs/en-IT/enicom/media/press-release/2019/02/PR-ing-Eni-SABIC.pdf`

"Characteristics of kyocera fine ceramics", `https://global.kyocera.com/prdct/fc/list/material/alumina/alumina.html`, accessed Apr.25, 2020.

"Christian hulteberg", `https://www.catalysis.se`, accessed Apr.25, 2020.

I. Aartun, T. Gjervan, H. Venvik, O. Görke, P. Pfeifer, M. Fathi, A. Holmen, et K. Schubert, "Catalytic Conversion of Propane to Hydrogen in Microstructured Rreactors", *Chem. Eng. J.*, vol. 101, pp. 93–99, 2004.

I. Aartun, H. J. Venvik, A. Holmen, P. Pfeifer, O. Görke, et K. Schubert, "Temperature Profiles and Residence Time Effects During Catalytic Partial Oxidation and Oxidative Steam Reforming of Propane in Metallic Microchannel Reactors", *Catal. Today*, vol. 110, pp. 98–107, 2005.

AER, "How are wells abandoned ?" 2019, accessed : 2019-06-29. En ligne : `https://www.aer.ca/regulating-development/project-closure/`

`suspension-and-abandonment/how-are-wells-abandoned`

P. Aghaei, C. G. Visconti, G. Groppi, et E. Tronconi, “Development of a heat Transport Model for Open-cell Metal Foams with High Cell Densities”, *Chem. Eng. J.*, vol. 321, pp. 432–446, 2017.

L. Almeida, O. González, O. Sanz, A. Paul, M. Centeno, J. Odriozola, et M. Montes, “Fischer-tropsch catalyst deposition on metallic structured supports”, dans *Natural Gas Conversion VIII*, série Studies in Surface Science and Catalysis, F. B. Noronha, M. Schmal, et E. F. Sousa-Aguiar, éds., 2007, vol. 167, pp. 79–84.

O. Altin et S. Eser, “Analysis of Carboneceous Deposits from Thermal Stressing of a JP-8 Fuel on Superalloy Foils in a Flow Reactor”, *Ind. Eng. Chem. Res.*, vol. 40, no. 2, pp. 589–595, 2001.

C. Amaechi et E. Biose, “Gas flaring : Carbon dioxide contribution to global warming”, *J. Appl. Sci. Environ. Manage.*, vol. 20, pp. 309–317, 2016.

M. Ambrosetti, M. Bracconi, G. Groppi, et E. Tronconi, “Analytical geometrical model of open cell foams with detailed description of strut-node intersection”, *Chem. Ing. Tech.*, vol. 89, pp. 915–925, 2017.

M. Ambrosetti, R. Balzarotti, C. Cristiani, G. Groppi, et E. Tronconi, “The influence of the washcoat deposition process on high pore density open cell foams activation for co catalytic combustion”, *Catalysts*, vol. 8, p. 510, 2018.

A. M. Amin, E. Croiset, et W. Epling, “Review of methane catalytic cracking for hydrogen production”, *Int. J. Hydrog. Energy*, vol. 36, no. 4, pp. 2904–2935, 2011.

C. Analytics, “Web of science core collection, accessed on 10 october 2018, http ://apps.webofknowledge.com”, 2018.

O. Andersen, U. Waag, L. Schneider, G. Stephani, et B. Kieback, “Novel metallic hollow sphere structures”, *Adv. Eng. Mater.*, vol. 2, pp. 192–195, 04 2000.

P. Avila, M. Montes, et E. E. Miró, “Monolithic reactors for environmental applications : a review on preparation technologies”, *Chem. Eng. J.*, vol. 109, pp. 11–36, 2005.

M. Aziz, H. Setiabudi, L. Teh, N. Annuar, et A. Jalil, “A review of heterogeneous catalysts for syngas production via dry reforming”, *J. Taiwan Inst. Chem. Eng.*, vol. 101, pp. 139–158, 2019.

C. Ballhaus, R. F. Berry, et D. H. Green, “High-pressure experimental calibration of the olivine-ortho-pyroxene-spinel oxygen geobarometer—implications for the oxidation-state of the upper mantle”, *Contrib. to Mineral. Petrol.*, vol. 207, no. 1, pp. 27–40, 1991.

B. P. Barbero, L. Costa-Almeida, O. Sanz, M. R. Morales, L. E. Cadus, et M. Montes, “Washcoating of Metallic Monoliths with a MnCu Catalyst for Catalytic Combustion of Volatile Organic Compounds”, *Chem. Eng. J.*, vol. 139, pp. 430–435, 2008.

F. Basile, G. Fornasari, F. Trifirò, et A. Vaccari, “Partial oxidation of methane : Effect of reaction parameters and catalyst composition on the thermal profile and heat distribution”, *Catal. Today*, vol. 64, no. 1, pp. 21–30, 2001.

——, “Rh–Ni synergy in the catalytic partial oxidation of methane : surface phenomena and catalyst stability”, *Catal. Today*, vol. 77, no. 3, pp. 215–223, 2002.

F. Basile, P. Benito, G. Fornasari, M. Monti, E. Scavetta, D. Tonelli, et A. Vaccari, “Novel rh-based structured catalysts for the catalytic partial oxidation of methane”, *Catal. Today*, vol. 157, pp. 183 – 190, 2010.

F. Basile, P. Benito, P. Del Gallo, G. Fornasari, D. Gary, V. Rosetti, E. Scavetta, D. Tonelli, et A. Vaccari, “Highly Conductive Ni Steam Reforming Catalysts Prepared by Electrodeposition”, *ChemComm*, pp. 2917–2919, 2008.

F. Basile, P. Benito, G. Fornasari, V. Rosetti, E. Scavetta, D. Tonelli, et A. Vaccari, “Electrochemical Synthesis of Novel Structured Catalysts for H_2 Production”, *Appl. Catal. B*, vol. 91, pp. 563–572, 2009.

F. Basile, P. Benito, S. Bugani, W. De Nolf, G. Fornasari, K. Janssens, L. Morselli, E. Scavetta, D. Tonelli, et A. Vaccari, “Combined use of Synchrotron-radiation-based Imaging Techniques for the Characterization of Structured Catalysts”, *Adv. Funct. Mater.*, vol. 20, no. 23, pp. 4117–4126, 2010.

F. Basile, P. Benito, G. Fornasari, M. Monti, E. Scavetta, D. Tonelli, et A. Vaccari, *A Novel Electrochemical Route for the Catalytic Coating of Metallic Supports*, 2010, vol. 175.

L. Basini, K. Aasberg-Petersen, A. Guarinoni, et M. Østberg, “Catalytic partial oxidation of natural gas at elevated pressure and low residence time”, *Catal. Today*, vol. 64, pp. 9–20, 2001.

L. Basini, A. Guarinoni, et A. Aragno, “Molecular and temperature aspects in catalytic partial oxidation of methane”, *J. Catal.*, vol. 190, no. 2, pp. 284–295, 2000.

L. Basini, A. Guarinoni, et A. Lainati, “Process for the production of synthesis gas and hydrogen tarting from liquid or gaseous hydrocarbons”, 14 2012, uS Patent 2013/0028815 A1.

L. Basini, A. Guarinoni, et L. Carluccio, “Catalytic system for catalytic partial oxidation processes with a short contact time”, 2017, uS Patent US20170173568.

L. E. Basini et A. Guarinoni, “Short contact time catalytic partial oxidation (sct-cpo) for synthesis gas processes and olefins production”, *Ind. Eng. Chem. Res.*, vol. 52, pp. 17 023–17 037, 2013.

Y. Bauman, A. Vedyagin, et I. Mishakov, “Carbon Erosion of FeCrAl Bulk Alloy by Chlorinated Hydrocarbons”, *Prot. Met. Phys. Chem. Surf.*, vol. 52, pp. 309–315, 2016.

P. Benito, M. Monti, I. Bersani, F. Basile, G. Fornasari, E. Scavetta, D. Tonelli, et A. Vaccari, “Coating of FeCrAlloy Foam with Rh Catalysts : Optimization of Electrosynthesis Parameters and Ccatalyst Composition”, *Catal. Today*, vol. 197, pp. 162–169, 2012.

P. Benito, W. De Nolf, G. Nuyts, M. Monti, G. Fornasari, F. Basile, K. Janssens, F. Ospitali, E. Scavetta, D. Tonelli, et et al., “Role of Coating-metallic Support Interaction in the Properties of Electrosynthesized Rh-based Structured Catalysts”, *ACS Catal.*, vol. 4, pp. 3779–3790, 2014.

P. Benito, M. Monti, W. De Nolf, G. Nuyts, G. Janssen, G. Fornasari, E. Scavetta, F. Basile, K. Janssens, F. Ospitali, et et al., “Improvement in the Coating Homogeneity in Electrosynthesized Rh Structured Catalysts for the Partial Oxidation of Methane”, *Catal. Today*, vol. 246, pp. 154–164, 2015.

P. Benito, G. Nuyts, M. Monti, W. De Nolf, G. Fornasari, K. Janssens, E. Scavetta, et A. Vaccari, “Stable Rh Particles in Hydrotalcite-derived Catalysts Coated on FeCrAlloy Foams by Electrosynthesis”, *Appl. Catal. B*, vol. 179, pp. 321–332, 2015.

M. J. Bennett, J. R. Nicholls, N. J. Simms, D. Naumenko, W. J. Quadakkers, V. Kochubey, R. Fordham, R. Bachorczyk, D. Goossens, H. Hattendorf, A. B. Smith, et D. Britton, “Lifetime Extension of FeCrAl Alloys in Air : Potential Roles of an Enhanced Al-reservoir and Surface Pre-treatment”, *Mater. Corros.*, vol. 56, pp. 854–866, 2005.

A. Bhattacharya, V. Calmidi, et R. Mahajan, “Thermophysical properties of high porosity metal foams”, *Int. J. Heat Mass Transf.*, vol. 45, pp. 1017–1031, 2002.

M. Bhattacharya, M. P. Harold, et V. Balakotaiah, “Mass-transfer coefficients in washcoated monoliths”, *AIChE J.*, vol. 50, pp. 2939–2955, 2004.

A. Białas, W. Osuch, W. Łasocha, et M. Najbar, “The Influence of the Cr-Al Foil Texture on Morphology of Adhesive Al_2O_3 Layers in Monolithic Environmental Catalysts”, *Catal. Today*, vol. 137, pp. 489–492, 2008.

E. Bianchi, T. Heidig, C. G. Visconti, G. Groppi, H. Freund, et E. Tronconi, “An appraisal of the heat transfer properties of metallic open-cell foams for strongly exo-/endo-thermic catalytic processes in tubular reactors”, *Chem. Eng. J.*, vol. 198–199, pp. 512–528, 2012.

——, “Heat Transfer Properties of Metal Foam Supports for Structured Catalysts : Wall Heat Transfer Coefficient”, *Catal. Today*, vol. 216, pp. 121–134, 2013.

H. Bitter et H. Torres, “Fischer tropsch synthesis - an introduction”, 2012.

M. Bizzi et G. Saracco, “Modeling the Partial Oxidation of Methane in a Fixed Bed with Detailed Chemistry”, *AIChE J.*, vol. 50, no. 6, 2004.

M. Bizzi, L. Basini, G. Saracco, et V. Specchia, “Short contact time catalytic partial oxidation of methane : analysis of transport phenomena effects”, *Chem. Eng. J.*, vol. 90, pp. 97–106, 2002.

——, “Modeling a transport phenomena limited reactivity in short contact time catalytic partial oxidation reactors”, *Ind. Eng. Chem. Res.*, vol. 42, pp. 62–71, 2003.

M. Block, N. Clark, S. Wayne, R. Nine, et W. Miller, “An investigation into the emissions reduction performance of an scr system over two years’ in-use heavy-duty vehicle operation”, 04 2005, pp. 1–25.

L. Bobadilla, A. Muñoz-Murillo, O. Laguna, M. Centeno, et J. Odriozola, “Does shaping catalysts modify active phase sites ? a comprehensive in situ ftir sectroscopic study on the performance of a model ru/Al_2O_3 catalyst for the co methanation”, *Chem. Eng. J.*, vol. 357, pp. 248–257, 2019.

V. A. Borisov, S. S. Sigaeva, P. G. Tsyrul’nikov, M. V. Trenikhin, N. N. Leont’eva, A. A. Slepterev, V. E. Kan, et M. Y. Biryukov, “Carbon Deposits on a Resistive FeCrAl Catalyst for the Suboxidative Pyrolysis of Methane”, *Kinet. Catal.*, vol. 55, pp. 319–326, 2014.

M. Bracconi, M. Ambrosetti, M. Maestri, G. Groppi, et E. Tronconi, “A fundamental investigation of gas/solid mass transfer in open-cell foams using a combined experimental and cfd approach", *Chem. Eng. J.*, vol. 352, pp. 558–571, 2018.

——, "A fundamental analysis of the influence of the geometrical properties on the effective thermal conductivity of open-cell foams", *Chem. Eng. Process.*, vol. 129, pp. 181–189, 2018.

R. Brück, R. Diewald, P. Hirth, et F.-W. Kaiser, "Design criteria for metallic substrates for catalytic converters", dans *SAE Technical Paper.* SAE International, 1995.

D. C. Boffito et T. Van Gerven, *Process Intensification and Catalysis*, 01 2018.

S. H. Cai, S. N. Rashkeev, S. T. Pantelides, et K. Sohlberg, "Phase transformation mechanism between γ- and θ-alumina", *Phys. Rev. B Condens. Matter Mater. Phys.*, vol. 67, 2003.

J. A. Cairns, R. S. Nelson, et G. K. Acres, "The Evolution of Fecralloy® Steel-based Catalysts", *Int. J. Mater. Eng. Applicat.*, vol. 1, pp. 162–166, 1979.

V. V. Calmidi et R. L. Mahajan, "Forced convection in high porosity metal foams", *J. Heat Transfer*, vol. 122, pp. 557–565, 2000.

A. Cao, R. Lu, et G. Veser, "Stabilizing metal nanoparticles for heterogeneous catalysis", *Phys. Chem. Chem. Phys.*, vol. 12, pp. 13 499–13 510, 2010.

X. Cao, R. Vassen, et D. Stoever, "Ceramic materials for thermal barrier coatings", *J. Eur. Ceram. Soc.*, vol. 24, pp. 1–10, 2004.

M. Caplovicova, L. Caplovic, D. Buc, P. Vinduska, et J. Janik, "Carbon Nanostructures Grown on Fe-Cr-Al alloy", *J. Electr. Eng.*, vol. 61, pp. 373–377, 2010.

M. A. Centeno, I. Carrizosa, et J. A. Odriozola, "In situ Drifts Study of the SCR Reaction of NO with NH_3 in the Presence of O_2 over Lanthanide Doped V_2O_5/Al_2O_3 Catalysts", *Appl. Catal. B*, vol. 19, pp. 67–73, 1998.

G. Centi, G. E. Arena, et S. Perathoner, "Nanostructured Catalysts for NOx Storage – Reduction and N_2O Decomposition", *J. Catal.*, vol. 216, pp. 443–454, 2003.

I. Cerri, G. Saracco, F. Geobaldo, et V. Specchia, "Development of a Methane Premixed Catalytic Burner for Household Applications", *Ind. Eng. Chem. Res.*, vol. 39, pp. 24–33, 2000.

H. Chadli, M. Retima, et Y. Khenioui, “Kinetics of Oxidation of Fe-Cr-Al Alloy Characterization by Electrochemical Spectroscopy of Impedance in a 3% Medium NaCl”, *Phys. Procedia*, vol. 2, pp. 1015–1020, 2009.

R. Chai, P. Chen, Z. Zhang, G. Zhao, Y. Liu, et Y. Lu, “Thin-felt NiO-Al_2O_3/FeCrAl-fiber Catalyst for High-throughput Catalytic oxy-methane Reforming to Syngas”, *Catal. Commun.*, vol. 101, pp. 48–50, 2017.

R. Chai, S. Fan, Z. Zhang, P. Chen, G. Zhao, Y. Liu, et Y. Lu, “Free-Standing NiO-MgO-Al_2O_3 Nanosheets Derived from Layered Double Hydroxides Grown onto FeCrAl-Fiber as Structured Catalysts for Dry Reforming of Methane”, *ACS Sustain. Chem. Eng.*, vol. 5, pp. 4517–4522, 2017.

R. Chai, G. Zhao, Z. Zhang, P. Chen, Y. Liu, et Y. Lu, “High Sintering-/coke-resistance Ni@SiO_2/Al_2O_3/FeCrAl-fiber Catalyst for Dry Reforming of Methane : One-step, Macro-to-nano Organization via Cross-linking Molecules”, *Catal. Sci. Technol.*, vol. 7, pp. 5500–5504, 2017.

R.-Y. Chein et W.-H. Hsu, “Thermodynamic analysis of syngas production via tri-reforming of methane and carbon gasification using flue gas from coal-fired power plants”, *J. Clean. Prod.*, vol. 200, pp. 242–258, 2018.

D. Chen, L. H. Zhang, H. Z. Li, et Y. Liu, “A Simple Method for Growing Hexaaluminate on the Surface of FeCrAl Alloy”, *Appl. Surf. Sci.*, vol. 301, pp. 280–288, 2014.

D. Chen, L. Zhang, et Y. Liu, “Vertical and in-situ Growth of Hexaaluminate Embedded in Alumina Intermediate Layer with High Stability”, *RSC Adv.*, vol. 3, pp. 2534–2537, 2013.

J. Chen, H. Arandiyan, X. Gao, et J. Li, “Recent advances in catalysts for methane combustion”, *Catal. Surv. from Asia*, vol. 19, pp. 140–171, 08 2015.

X. Chen et S. S. Mao, “Titanium dioxide nanomaterials : Synthesis, properties, modifications, and applications”, *Chem. Rev.*, vol. 107, no. 7, pp. 2891–2959, 2007.

Y. Chen et J. Xu, “The shale gas boom in the us : Productivity shocks and price responsiveness”, *J. Clean. Prod.*, vol. 229, pp. 399–411, 2019.

Y. Cheng, X. Zhai, Y. Cheng, Z. Zhang, et Y. Jin, “Steam Reforming of Methane over Ni Catalyst in Micro-channel Reactor”, *Int. J. Hydrog. Energy*, vol. 36, no. 12, pp. 7105–7113, 2011.

V. V. Chesnokov et R. A. Buyanov, “The formation of carbon filaments upon decomposition of hydrocarbons catalysed by iron subgroup metals and their alloys”, *Russ. Chem. Rev.*, vol. 69, pp. 623–638, 2000.

Y. H. Chin, J. Hu, C. Cao, Y. Gao, et Y. Wang, “Preparation of a Novel Sstructured Catalyst Based on Aligned Carbon Nanotube Arrays for a Microchannel Fischer-Tropsch Synthesis Reactor”, *Catal. Today*, vol. 110, pp. 47–52, 2005.

Y.-H. C. Chin et E. Iglesia, “Elementary steps, the role of chemisorbed oxygen, and the effects of cluster size in catalytic CH_4–O_2 reactions on palladium”, *J. Phys. Chem. C*, vol. 115, pp. 17 845–17 855, 2011.

Y.-H. C. Chin, C. Buda, M. Neurock, et E. Iglesia, “Selectivity of chemisorbed oxygen in C–H bond activation and co oxidation and kinetic consequences for CH_4-O_2 catalysis on Pt and Rh clusters”, *J. Catal.*, vol. 283, no. 1, pp. 10–24, 2011.

Y.-H. Chin, C. Buda, M. Neurock, et E. Iglesia, “Reactivity of chemisorbed oxygen atoms and their catalytic consequences during CH_4–O_2 catalysis on supported pt clusters”, *J. Am. Chem. Soc.*, vol. 133, pp. 15 958–15 978, 2011.

F.-X. Chiron et G. S. Patience, “Steam carbon gasification of a nickel based oxygen carrier”, *Fuel*, vol. 90, pp. 2461–2466, 2011.

T. V. Choudhary, S. Banerjee, et V. R. Choudhary, “Catalysts for Combustion of Methane and Lower Alkanes”, *Appl. Catal. A*, vol. 234, pp. 1–23, 2002.

V. R. Choudhary, P. B, et R. A. M, “Beneficial Effects of Noble Metal Addition to Ni/Al_2O_3 Catalyst for Oxidative Methane-to-Syngas Conversion”, *J. Catal.*, vol. 157, pp. 752–754, 1995.

B. Christian Enger, R. Lødeng, et A. Holmen, “A Review of Catalytic Partial Oxidation of Methane to Synthesis Gas with Emphasis on Reaction Mechanisms over Transition Metal Catalysts”, *Appl. Catal. A*, vol. 346, pp. 1–27, 2008.

S. Cimino, R. Gerbasi, L. Lisi, G. Mancino, M. Musiani, L. Vázquez-Gómez, et E. Verlato, “Oxidation of CO and CH_4 on Pd-Fecralloy Foam Catalysts Prepared by Spontaneous Deposition”, *Chem. Eng. J.*, vol. 230, pp. 422–431, 2013.

S. Cimino, A. Gambirasi, L. Lisi, G. Mancino, M. Musiani, L. Vázquez-Gómez, et E. Verlato, “Catalytic Combustion of Methanol on Pt-Fecralloy Foams Prepared by Electrodeposition”, *Chem. Eng. J.*, vol. 285, pp. 276–285, 2016.

A. Civera, M. Pavese, G. Saracco, et V. Specchia, “Combustion Synthesis of Perovskite-type Catalysts for Natural Gas Combustion”, *Catal. Today*, vol. 83, pp. 199–211, 2003.

Clarivate Analytics, “Web of Science^{TM} Core Collection, accessed on 1 june 2019”, 2019. En ligne : `http://apps.webofknowledge.com`

B. J. Cooper et J. Beecham, “A Study of Platinum Group Metals in Three-Way Autocatalysts”, *Platin. Met. Rev.*, no. 4, pp. 281–288, 2013.

C. Cristiani, C. G. Visconti, S. Latorrata, E. Bianchi, E. Tronconi, G. Groppi, et P. Pollesel, “Coating method for ni/$MgAl_2O_4$ deposition on metallic foams”, dans *Scientific Bases for the Preparation of Heterogeneous Catalysts*, série Studies in Surface Science and Catalysis, E. Gaigneaux, M. Devillers, S. Hermans, P. Jacobs, J. Martens, et P. Ruiz, éds., 2010, vol. 175, pp. 653–656.

C. Cristiani, E. Finocchio, S. Latorrata, C. G. Visconti, E. Bianchi, E. Tronconi, G. Groppi, et P. Pollesel, “Activation of Metallic Open-cell Foams via Washcoat Deposition of Ni/$MgAl_2O_4$ Catalysts for Steam Reforming Reaction”, *Catal. Today*, vol. 197, pp. 256–264, 2012.

A. Cybulski et J. Moulijn, *Structured Catalysts and Reactors*, série Chemical Industries. Boca Raton : CRC Press, 2005.

A. Czyrska-Filemonowicz, D. Clemens, et W. Quadakkers, “The effect of high temperature exposure on the structure and oxidation behaviour of mechanically alloyed ferritic ods alloys”, *J. Mater. Process. Technol.*, vol. 53, pp. 93–100, 1995.

J. Dahl, T. S. Christensen, S. Winter-Madsen, et S. M. King, “Proven autothermal reforming technology for modern large-scale methanol plants”, 2014.

X. P. Dai, R. J. Li, C. C. Yu, et Z. P. Hao, “Unsteady-state direct partial oxidation of methane to synthesis gas in a fixed-bed reactor using $aFeO_3$ (a = LaNdEu) perovskite-type oxides as oxygen storage”, *J. Phys. Chem. B*, vol. 110, no. 45, pp. 22 525–22 531, 2006.

A. Datye et Y. Wang, “Atom trapping : a novel approach to generate thermally stable and regenerable single-atom catalysts”, *Natl. Sci. Rev.*, vol. 5, pp. 630–632, 2018.

M. Davis, “Ordered porous materials for emerging applications”, *Nature*, vol. 417, pp. 813–821, 07 2002.

N. De Miguel, J. Manzanedo, J. Thormann, P. Pfeifer, et P. L. Arias, “Ni Catalyst Coating on Fecralloy Microchanneled Foils and Testing for Methane Steam Reforming”, *Chem. Eng. Technol.*, vol. 33, pp. 155–166, 2010.

M. Denchak, “Paris Climate Agreement : Everything You Need to Know”, 2018.

C. Descorme, P. Gallezot, C. Geantet, et C. George, “Heterogeneous catalysis : a key tool toward sustainability”, *ChemCatChem*, vol. 4, pp. 1897–1906, 2012.

R. Dhar, P. D. Pedrow, K. C. Liddell, Q. Ming, T. M. Moeller, et M. A. Osman, “Synthesis of Pt/ZrO_2 Catalyst on Fecralloy Substrates Using Composite Plasma-polymerized films”, *IEEE Trans. Plasma. Sci.*, vol. 33, pp. 2035–2045, 2005.

Y. Diaz, A. Sevilla, A. Mónaco, F. J. Méndez, P. Rosales, L. Garcí, et J. L. Brito, “Metallic Monoliths of AISI 304 Stainless Steel, Aluminum, FeCrAlloy® and Brass, Coated by Mo and W Oxides for Thiophene Hydrodesulfurization”, *Fuel*, vol. 110, pp. 235–248, 2013.

I. Dincer et C. Acar, “Review and evaluation of hydrogen production methods for better sustainability”, *Int. J. Hydrog. Energy*, vol. 40, no. 34, pp. 11 094–11 111, 2015.

M. Domínguez, A. Pérez, M. Centeno, et J. Odriozola, “Metallic structured catalysts : Influence of the substrate on the catalytic activity”, *Appl. Catal. A*, vol. 478, pp. 45–57, 2014.

A. Donazzi, A. Beretta, G. Groppi, et P. Forzatti, “Catalytic partial oxidation of methane over a 4% rh/α-Al_2O_3 catalyst : Part i : Kinetic study in annular reactor”, *J. Catal.*, vol. 255, pp. 241–258, 2008.

W.-S. Dong, K.-W. Jun, H.-S. Roh, Z.-W. Liu, et S.-E. Park, “Comparative study on partial oxidation of methane over Ni/ZrO_2, ni/CeO_2 and Ni/Ce$-$$ZrO_2$ catalysts”, *Catal. Letters*, vol. 78, pp. 215–222, 2002.

L. Dou, C. Yan, L. Zhong, D. Zhang, J. Zhang, X. Li, et L. Xiao, “Enhancing CO_2 methanation over a metal foam structured catalyst by electric internal heating”, *Chem. Commun.*, vol. 56, pp. 205–208, 2020.

M. Downey, K. Müller-Haas, T. Park, R. Diewald, et R. Radovanovic, “Structured foil catalysts : A road map to highly effective, compact aftertreatment systems”, dans *SAE Technical Paper*. SAE International, 2007.

M. E. Dry, “The fischer–tropsch process : 1950–2000”, *Catal. Today*, vol. 71, pp. 227–241, 2002.

I. Dybkjaer et K. Aasberg-Petersen, “Synthesis gas technology large-scale applications”, *Can. J. Chem. Eng.*, vol. 94, pp. 607–612, 2016.

G. Dyos, *The Handbook of Electrical Resistivity : New Materials and pressure effects*, 01 2012.

F. J. Echave, O. Sanz, I. Velasco, J. A. Odriozola, et M. Montes, “Effect of the Alloy on Micro-structured Reactors for Methanol Steam Reforming”, *Catal. Today*, vol. 213, pp. 145–154, 2013.

F. J. Echave, O. Sanz, et M. Montes, “Washcoating of Microchannel Reactors with PdZnO Catalyst for Cethanol Steam Reforming”, *Appl. Catal. A*, vol. 474, pp. 159–167, 2014.

D. Edouard, T. T. Huu, C. P. Huu, F. Luck, et D. Schweich, “The effective thermal properties of solid foam beds : Experimental and estimated temperature profiles”, *Int. J. Heat Mass Transf.*, vol. 53, pp. 3807–3816, 2010.

Edward M Merrow, “An analysis of cost improvements in chemical process technologies”, 1989, accessed 25 October 2019. En ligne : `https://www.rand.org/content/dam/rand/pubs/reports/2006/R3357.pdf`

A. Eleta, P. Navarro, L. Costa, et M. Montes, “Deposition of Zeolitic Coatings onto Fecralloy Microchannels : Washcoating vs. in situ Growing”, *Microporous and Mesoporous Mater.*, vol. 123, pp. 113–122, 2009.

C. D. Elvidge, M. Zhizhin, K. Baugh, F.-c. Hsu, et T. Ghosh, “Methods for Global Survey of Natural Gas Flaring from Visible Infrared Imaging Radiometer Suite Data”, *Energies*, no. 4, pp. 14–20, 2016.

C. D. Elvidge, M. D. Bazilian, M. Zhizhin, T. Ghosh, K. Baugh, et F.-C. Hsu, “The potential role of natural gas flaring in meeting greenhouse gas mitigation targets”, *Energy Strategy Rev.*, vol. 20, pp. 156–162, 2018.

A. Emam, “Gas Flaring in Industry : an Overview”, *Petroleum Coal*, vol. 57, no. 5, pp. 532–555, 2015.

Energy.gov, *Hydrogen Production : Natural Gas Reforming*, accessed : 2020-03-02. En ligne : `https://www.energy.gov/eere/fuelcells/`

`hydrogen-production-natural-gas-reforming`

B. C. Enger, J. Walmsley, E. Bjørgum, R. Lødeng, P. Pfeifer, K. Schubert, A. Holmen, et H. J. Venvik, “Performance and SEM Characterization of Rh Impregnated Microchannel Reactors in the Catalytic Partial Oxidation of Methane and Propane”, *Chem. Eng. J.*, vol. 144, pp. 489–501, 2008.

P. Engineer, “Intrinsic safety in hazardous locations”, 2019, accessed : 2019-07-11. En ligne : `https://www.plantengineering.com/articles/intrinsic-safety-in-hazardous-locations/`

J. Engkvist, S. Canovic, F. Liu, H. Götlind, J. E. Svensson, L. G. Johansson, M. Olsson, et M. Halvarsson, “Oxidation of FeCrAl Foils at 500 °C to 900 °C in Dry O_2 and O_2 with 40% H_2O”, *Mater. at High Temp.*, vol. 26, pp. 199–210, 2009.

K. Everaert et J. Baeyens, “Catalytic combustion of volatile organic compounds”, *J. Hazard. Mater.*, vol. 109, pp. 113–139, 2004.

X. Fan, F. Wang, T. Zhu, et H. He, “Effects of Ce on Catalytic Combustion of Methane over Pd-Pt/Al_2O_3 Catalyst”, *J. Environ. Sci.*, vol. 24, pp. 507–511, 2012.

W. Fei, S. C. Kuiry, Y. Sohn, et S. Seal, “Sol Gel Alumina Coating On Fe–Cr–Al–Y Fibre Media for Catalytic Converters”, *Surf. Eng.*, vol. 19, pp. 189–194, 2003.

D. Feriyanto, A. M. Leman, I. Baba, F. Rahman, et F. A. Jajuli, “Diffusion and Bonding Mechanism of Protective γ-Al_2O_3 on FeCrAl Foil for Metallic Three-Way Catalytic Converter”, *MATEC Web Conf.*, vol. 02019, 2017.

K. G. Field, M. Snead, Y. Yamamoto, et K. A. Terrani, *Handbook on the Material Properties of FeCrAl Alloys for Nuclear Power Production Applications*, 2015.

P. Fornasiero, T. Montini, M. Graziani, S. Zilio, et M. Succi, “Development of Functionalized Fe-Al-Cr Alloy Fibers as Innovative Catalytic Oxidation Devices”, *Catal. Today*, vol. 137, pp. 475–482, 2008.

P. Forzatti, G. Groppi, et C. Cristiani, *Catalytic Combustion*, 2008, ch. 11.6, pp. 2411–2426.

D. M. Frías, S. Nousir, I. Barrio, M. Montes, L. M. Martínez T, M. A. Centeno, et J. A. Odriozola, “Nucleation and Growth of Manganese Oxides on Metallic Surfaces as a Tool to Prepare Metallic Monoliths”, *Appl. Catal. A*, vol. 325, pp. 205–212, 2007.

G. F. Froment et J. Xu, “Methane Steam Reforming , Methanation and Water-Gas Shift : 1 . Intrinsic Kinetics”, *AIChE J.*, vol. 35, no. 1, pp. 88–96, 1989.

L. Frost, E. Elangovan, et J. Hartvigsen, “Production of synthetic fuels by high-temperature co-electrolysis of carbon dioxide and steam with fischer-tropsch synthesis”, *Can. J. Chem. Eng.*, vol. 94, pp. 636–641, 2016.

K. Fukuda, K. Takao, T. Hoshi, Y. Usui, et O. Furukimi, “Improvement of High Temperature Oxidation Resistance of Rare Earth Metal-added Fe-20%Cr-5%Al Alloys by Pre-annealing Treatment”, *Mater. at High Temp.*, vol. 20, pp. 319–326, 2003.

A. Gaffney, “Catalytic partial oxidation process and promoted nickel based catalysts supported on magnesum oxide”, 2000, uS Patent US6402989 B1.

A. Galadima et O. Muraza, “Revisiting the oxidative coupling of methane to ethylene in the golden period of shale gas : a review”, *J. Ind. Eng. Chem.*, vol. 37, pp. 1–13, 2016.

E. García-Bordejé, Y. Liu, D. S. Su, et C. Pham-Huu, “Hierarchically structured reactors containing nanocarbons for intensification of chemical reactions”, *J. Mater. Chem. A*, vol. 5, pp. 22 408–22 441, 2017.

D. Garnett et G. Patience, “Why do scale-up power laws work ?” *Chem. Eng. Prog.*, vol. 89, pp. 76–78, 1993.

G. I. Garrido, F. C. Patcas, S. Lang, et B. Kraushaar-Czarnetzki, “Mass transfer and pressure drop in ceramic foams : a description for different pore sizes and porosities”, *Chem. Eng. Sci.*, vol. 63, pp. 5202–5217, 2008.

J. Gascon, J. R. van Ommen, J. A. Moulijn, et F. Kapteijn, “Structuring catalyst and reactor – an inviting avenue to process intensification”, *Catal. Sci. Technol.*, vol. 5, pp. 807–817, 2015.

P. Gélin et M. Primet, “Complete Oxidation of Methane at Low Temperature Over Noble Metal Based Catalysts : a Review”, *Appl. Catal. B*, vol. 39, pp. 1–37, 2002.

S. Ghoneim, R. Elsalamony, et S. EL-Temtamy, “Review on innovative catalytic reforming of natural gas to syngas”, *W. J. Eng. Tech.*, vol. 04, pp. 116–139, 2016.

L. Giani, G. Groppi, et E. Tronconi, “Mass-transfer characterization of metallic foams as supports for structured catalysts”, *Ind. Eng. Chem. Res.*, vol. 44, pp. 4993–5002, 2005.

——, “Heat transfer characterization of metallic foams”, *Ind. Eng. Chem. Res.*, vol. 44, pp. 9078–9085, 2005.

L. Giani, C. Cristiani, G. Groppi, et E. Tronconi, “Washcoating method for pd/γ-Al_2O_3 deposition on metallic foams”, *Appl. Catal. B*, vol. 62, pp. 121–131, 01 2006.

L. J. Gibson et M. F. Ashby, *Cellular Solids, Structures and Properties.* Oxford : Pergamon Press, 1988.

M. Gil-calvo, C. Jiménez-gonzález, B. D. Rivas, J. I. Gutiérrez-ortiz, et R. López-fonseca, “Effect of Ni/Al molar ratio on the performance of substoichiometric $NiAl_2O_4$ spinel-based catalysts for partial oxidation of methane”, *Appl. Catal. B*, vol. 209, pp. 128–138, 2017.

D. A. Goetsch et L. D. Schmidt, “Microsecond catalytic partial oxidation of alkanes”, *Science*, vol. 271, pp. 1560–1562, 1996.

S. Govender et H. Friedrich, “Monoliths : A review of the basics, preparation methods and their relevance to oxidation”, *Catalysts*, vol. 7, no. 2, pp. 62–91, 2017.

P. Gregory S. et B. Daria C., “Distributed production : Scale-up versus Experience”, *J. Adv. Manufact. & Proc.*, vol. 2, p. e10039, 2020.

A. A. Greish, L. M. Glukhov, E. D. Finashina, L. M. Kustov, J. S. Sung, K. Y. Choo, et T. H. Kim, “Comparison of Activities of Bulk and Monolith Mn-Na_2WO_4/SiO_2 Catalysts in Oxidative Coupling of Methane”, *Mendeleev Commun.*, vol. 19, pp. 337–339, 2009.

A. M. D. Groote et G. F. Froment, “Simulation of the catalytic partial oxidation of methane to synthesis gas”, *Appl. Catal. A*, vol. 138, no. 2, pp. 245 – 264, 1996.

G. Groppi et E. Tronconi, “Continuous vs. discrete models of nonadiabatic monolith catalysts”, *AIChE J.*, vol. 42, pp. 2382–2387, 1996.

G. Groppi, E. Tronconi, G. Bozzano, et M. Dente, “Experimental and theoretical study of gas/solid mass transfer in metallic filters as supports for micro-structured catalysts”, *Chem. Eng. Sci.*, vol. 65, pp. 392–397, 2010.

G. Groppi et E. Tronconi, “Honeycomb supports with high thermal conductivity for gas/solid chemical processes”, *Catal. Today*, vol. 105, pp. 297–304, 2005.

M. Götz, J. Lefebvre, F. Mörs, A. M. Koch, F. Graf, S. Bajohr, R. Reimert, et T. Kolb, “Renewable power-to-gas : A technological and economic review”, *Renew. Energ.*, vol. 85, pp. 1371–1390, 2016.

Y. Guo, L. Zhou, et H. Kameyama, “Thermal and hydrothermal stability of a metal monolithic anodic alumina support for steam reforming of methane”, *Chem. Eng. J.*, vol. 168, pp. 341–350, 2011.

N. Hargreaves, *Roll out of smaller scale GTL technology at ENVIA Energy's plant in Oklahoma City, USA*, 2017, accessed : 2020-03-02. En ligne : `https://www.velocys.com/press/ppt/Gastech2017_Velocys_FINAL_4.3_web.pdf`

H. Hattendorf, R. Hojda, D. Naumenko, et A. Kolb-Telieps, “A new austenitic alumina forming alloy : an aluminium-coated $FeNi_{32}Cr_{20}$”, *Mater. Corros.*, vol. 59, pp. 449–454, 2008.

R. D. Hawthorn, “After burner catalysts : Effect of heat and mass transfer between gas and catalyst surface”, *AIChE Symp. Ser.*, vol. 70, pp. 428–438, 1974.

R. E. Hayes et S. T. Kolaczkowski, *Introduction to Catalytic Combustion.* Amsterdam : Gordon and Breach Science Publishers, 1997.

R. M. Heck, S. Gulati, et R. J. Farrauto, “The application of monoliths for gas phase catalytic reactions”, *Chem. Eng. J.*, vol. 82, pp. 149–156, 2001.

T. P. Herbell, D. R. Hull, et A. Garg, “Hot hydrogen exposure degradation of the strength of mullite”, *J. Am. Ceram. Soc.*, vol. 81, no. 4, pp. 910–916, 1998.

G. Herz, E. Reichelt, et M. Jahn, “Design and evaluation of a Fischer-Tropsch process for the production of waxes from biogas”, *Energy*, vol. 132, pp. 370–381, 2017.

D. A. Hickman et L. D. Schmidt, “Production of syngas by direct catalytic oxidation of methane”, *Science*, vol. 259, pp. 343–346, 1993.

P. H. Ho, M. Ambrosetti, G. Groppi, E. Tronconi, J. Jaroszewicz, F. Ospitali, E. Rodríguez-Castellón, G. Fornasari, A. Vaccari, et P. Benito, “One-step electrodeposition of pd–CeO_2 on high pore density foams for environmental catalytic processes”, *Catal. Sci. Technol.*, vol. 8, pp. 4678–4689, 2018.

P. H. Ho, M. Monti, E. Scavetta, D. Tonelli, E. Bernardi, L. Nobili, G. Fornasari, A. Vaccari, et P. Benito, “Reactions Involved in the Electrodeposition of Hydrotalcite-type Compounds on FeCrAlloy Foams and Flates”, *Electrochim. Acta*, vol. 222, pp. 1335–1344, 2016.

P. H. Ho, W. de Nolf, F. Ospitali, A. Gondolini, G. Fornasari, E. Scavetta, D. Tonelli, A. Vaccari, et P. Benito, “Coprecipitated-like hydrotalcite-derived coatings on open-cell metallic foams by electrodeposition : Rh nanoparticles on oxide layers stable under harsh reaction conditions”, *Appl. Catal. B*, vol. 560, pp. 12–20, 2018.

P. H. Ho, M. Ambrosetti, G. Groppi, E. Tronconi, G. Fornasari, A. Vaccari, et P. Benito, “Electrodeposition of CeO_2 and pd-CeO_2 on small pore size metallic foams : Selection of deposition parameters”, *Catal. Today*, vol. 334, pp. 37–47, 2019.

P. H. Ho, M. Jabłońska, R. Palkovits, E. Rodríguez-Castellón, F. Ospitali, G. Fornasari, A. Vaccari, et P. Benito, “N_2O catalytic decomposition on electrodeposited rh-based open-cell metallic foams”, *Chem. Eng. J.*, vol. 379, p. 122259, 2020.

C. Hoang-Van, Y. Kachaya, S. Teichner, Y. Arnaud, et J. Dalmon, “Characterization of nickel catalysts by chemisorption techniques, x-ray diffraction and magnetic measurements : Effects of support, precursor and hydrogen pretreatment”, *Appl. Catal.*, vol. 46, pp. 281–296, 1989.

A. Hoek et L. Kersten, *The Shell Middle Distillate Synthesis Process : Technology, Products and Perspective*, 12 2004, vol. 147, pp. 25–30.

K. Hohn et L. Schmidt, “Partial oxidation of methane to syngas at high space velocities over rh-coated spheres”, *Appl. Catal. A*, vol. 211, pp. 53–68, 2001.

J. Holladay, J. Hu, D. King, et Y. Wang, “An overview of hydrogen production technologies”, *Catal. Today*, vol. 139, pp. 244–260, 2009.

M. M. Hossain et H. I. de Lasa, “Chemical-looping combustion (clc) for inherent CO_2 separations—a review”, *Chem. Eng. Sci.*, vol. 63, no. 18, pp. 4433–4451, 2008.

S. E. Hosseini et M. A. Wahid, “Hydrogen production from renewable and sustainable energy resources : Promising green energy carrier for clean development”, *Renew. Sust. Energ. Rev.*, vol. 57, pp. 850–866, 2016.

N. Hotz, M. J. Stutz, S. Loher, W. J. Stark, et D. Poulikakos, “Syngas production from butane using a flame-made $Rh/Ce_0 \cdot 5\,Zr_0 \cdot 5\,O_2$ catalyst”, *Appl. Catal. B*, vol. 73, no. 3, pp. 336–344, 2007.

J. Hu, K. P. Brooks, J. D. Holladay, D. T. Howe, et T. M. Simon, “Catalyst Development for Microchannel Reactors for Martian in situ Propellant Production”, *Catal. Today*, vol. 125, pp. 103–110, 2007.

J. Hu, Y. Wang, C. Cao, D. C. Elliott, D. J. Stevens, et J. F. White, “Conversion of Biomass-derived Syngas to Alcohols and C2 Oxygenates Using Supported Rh Catalysts in a Microchannel Reactor”, *Catal. Today*, vol. 120, pp. 90–95, 2007.

K. W. Hutchenson, C. L. Marca, G. S. Patience, J.-P. Laviolette, et R. E. Bockrath, “Parametric study of n-butane oxidation in a circulating fluidized bed reactor”, *Appl. Catal. A*, vol. 376, pp. 91–103, 2010.

T. T. Huu, M. Lacroix, C. P. Huu, D. Schweich, et D. Edouard, “Towards a more realistic modeling of solid foam : Use of the pentagonal dodecahedron geometry”, *Chem. Eng. Sci.*, vol. 64, p. 5131–5142, 2009.

A. Inayat, H. Freund, T. Zeiser, et W. Schwieger, “Determining the specific surface area of ceramic foams : the tetrakaidecahedra model revisited”, *Chem. Eng. Sci.*, vol. 66, pp. 1179–1188, 2011.

Infra, 2020, accessed : 2020-03-03. En ligne : `file:///C:/Users/gianluca/Downloads/INFRA%20Technology%20Presentation.pdf`

O. S. Ismail, “Global Impact of Gas Flaring”, *Energy and Power Engineering*, vol. 4, pp. 290–302, 2012.

M. Jaber, D. Mahboub, J. Wright, D. C. Bo, J.-l. Dubois, et G. S. Patience, “ Cs , V , Cu Keggin-type Catalysts Partially Oxidize 2-methyl-1, 3-propanediol to Methacrylic Acid”, *Appl. Catal. A*, vol. 554, pp. 105–116, 2018.

L. Jalowiecki-Duhamel, H. Zarrou, et A. D’Huysser, “Hydrogen production at low temperature from methane on cerium and nickel based mixed oxides”, *Int. J. Hydrog. Energy*, vol. 33, pp. 5527–5534, 2008.

Z. Jaworski et P. Pianko-Oprych, “A comparative thermodynamic study of equilibrium conditions for carbon deposition from catalytic c–h–o reformates”, *Energies*, vol. 11, p. 1177, 2018.

J. Jia, J. Zhou, J. Zhang, Z. Yuan, et S. Wang, “The Influence of Preparative Parameters on the Adhesion of Alumina Washcoats Deposited on Metallic Supports”, *Appl. Surf. Sci.*, vol. 253, pp. 9099–9104, 2007.

J. Jia, J. Zhou, C. Zhang, Z. Yuan, S. Wang, L. Cao, et S. Wang, “Preparation and Characterization of Ir-based Catalysts on Metallic Supports for High-temperature Steam Reforming of Methanol”, *Appl. Catal. A*, vol. 341, pp. 1–7, 2008.

L. Jia, M. Shen, et J. Wang, “Preparation and Characterization of Dip-coated γ-alumina Based Ceramic Materials on FeCrAl Foils”, *Surf. Coat. Technol.*, vol. 201, pp. 7159–7165, 2007.

B. Jönsson, R. Berglund, J. Magnusson, P. Henning, et M. Hättestrand, “High temperature properties of a new powder metallurgical fecral alloy”, *Mater. Sci. Forum*, vol. 464, pp. 455–462, 01 2004.

B. Jönsson, Q. Lu, D. Chandrasekaran, R. Berglund, et F. Rave, “Oxidation and creep limited lifetime of kanthal apmt®, a dispersion strengthened fecralmo alloy designed for strength and oxidation resistance at high temperatures”, *Oxid. Met.*, vol. 79, pp. 29–39, 02 2012.

O. Joan, *Review of Small Stationary Reformers for Hydrogen Production*, 2002, accessed : 2020-03-02. En ligne : `https://https://afdc.energy.gov/files/pdfs/31948.pdf`

T. Johnson, “Vehicular emissions in review”, *SAE Int. J. Engines*, vol. 9, no. 2, pp. 1258–1275, 2016.

T. Johnson et A. Joshi, *Chapter 1 : Review of deNOx Technology for Mobile Applications*, 01 2018, pp. 1–35.

R. jun Zhang, G. fu Xia, M. feng Li, Y. Wu, H. Nie, et D. dong Li, “Effect of support on the performance of ni-based catalyst in methane dry reforming”, *J. Fuel Chem. Technol.*, vol. 43, pp. 1359–1365, 2015.

L. C. S. Kahle, T. Roussière, L. Maier, K. Herrera Delgado, G. Wasserschaff, S. A. Schunk, et O. Deutschmann, “Methane dry reforming at high temperature and elevated pressure : Impact of gas-phase reactions”, *Ind. Eng. Chem. Res.*, vol. 52, no. 34, pp. 11 920–11 930, 2013.

W. Kaltner, M. Veprek-Heijman, A. Jentys, et J. A. Lercher, “Effect of Chromium Migration from Metallic Supports on the Activity of Diesel Exhaust Catalysts”, *Appl. Catal. B*, vol. 89, pp. 123–127, 2009.

C. Karakaya, H. Zhu, B. Zohour, S. Senkan, et R. J. Kee, “Detailed reaction mechanisms for the oxidative coupling of methane over La_2O_3/CeO_2 nanofiber fabric catalysts”, *ChemCatChem*, vol. 9, pp. 4538–4551, 2017.

S. Katheria, G. Deo, et D. Kunzru, “Washcoating of $Ni/MgAl_2O_4$ Catalyst on FeCralloy Monoliths for Steam Reforming of Methane”, *Energy Fuels*, vol. 31, pp. 3143–3153, 2017.

R. Kikuchi, S. Maeda, K. Sasaki, S. Wennerström, Y. Ozawa, et K. Eguchi, “Catalytic Activity of Oxide-supported Pd Catalysts on a Honeycomb for Low-temperature Methane Oxidation”, *Appl. Catal. A*, vol. 239, pp. 169–179, 2003.

D. H. Kim, B. Y. Yu, P. R. Cha, W. Y. Yoon, J. Y. Byun, et S. H. Kim, “A Study on FeCrAl Foam as Effective Catalyst Support under Thermal and Mechanical Stresses”, *Surf. Coat. Technol.*, vol. 209, pp. 169–176, 2012.

D. H. Kim, S. H. Kim, et J. Y. Byun, “A Microreactor with Metallic Catalyst Support for Hydrogen Production by Partial Oxidation of Dimethyl Ether”, *Chem. Eng. J.*, vol. 280, pp. 468–474, 2015.

V. A. Kondratenko, C. Berger-Karin, et E. V. Kondratenko, “Partial oxidation of methane to syngas over γ-Al_2O_3-supported rh nanoparticles : Kinetic and mechanistic origins of size effect on selectivity and activity”, *ACS Catal.*, vol. 4, pp. 3136–3144, 2014.

M. V. Konishcheva, D. A. Svintsitskiy, D. I. Potemkin, V. N. Rogozhnikov, V. A. Sobyanin, et P. V. Snytnikov, “Catalytic performance and characterization of highly efficient composite Ni(Clx)/CeO_2/η-Al_2O_3/fecral wire mesh catalysts for preferential co methanation”, *ChemistrySelect*, vol. 5, pp. 1228–1234, 2020.

M. Konishcheva, P. Snytnikov, V. Rogozhnikov, A. Salanov, D. Potemkin, et V. Sobyanin, “Structured NiCl/CeO_2/η-Al_2O_3/fecral wire mesh catalyst for selective co methanation”, *Catal. Commun.*, vol. 118, pp. 25–29, 2019.

B. U. Koo, Y. Yi, M. Lee, et B. K. Kim, “Effects of Particle Size and Forming Pressure on Pore Properties of Fe-Cr-Al Porous Metal by Pressureless Sintering”, *Met. Mater. Int.*, vol. 23, pp. 336–340, 2017.

K. Y. Koo, H. J. Eom, U. H. Jung, et W. L. Yoon, “Ni Nanosheet-coated Monolith Catalyst with High Performance for Hydrogen Production via Natural Gas Steam Reforming”, *Appl. Catal. A*, vol. 525, pp. 103–109, 2016.

K. Y. Koo, H. J. Eom, S. C. Kwon, U. H. Jung, et W. L. Yoon, “Ru-coated Metal Monolith Catalyst Prepared by Novel Coating Method for Hydrogen Production via Natural Gas Steam Reforming”, *Catal. Today*, vol. 293-294, pp. 129–135, 2017.

R. Koros et E. Nowak, “A diagnostic test of the kinetic regime in a packed bed reactor”, *Chem. Eng. Sci.*, vol. 22, p. 470, 1967.

O. Korotkikh et R. Farrauto, “Selective catalytic oxidation of co in H_2 : Fuel cell applications”, *Catal. Today*, vol. 62, pp. 249–254, 2000.

J. Kryca, M. Iwaniszyn, M. Piatek, P. J. Jodlowski, R. Jedrzejczyk, R. Pedrys, A. Wrobel, J. Lojewska, et A. Kolodziej, “Structured Foam Reactor with CuSSZ-13 Catalyst for SCR of NOx with Ammonia”, *Top. Catal.*, vol. 59, pp. 887–894, 2016.

J. Kryca, P. Jodłowski, M. Iwaniszyn, B. Gil, M. Sitarz, A. Kołodziej, T. Łojewska, et J. Łojewska, “Cu ssz-13 zeolite catalyst on metallic foam support for scr of nox with ammonia : Catalyst layering and characterisation of active sites”, *Catal. Today*, vol. 268, pp. 142–149, 2016.

L. M. Kustov et O. P. Tkachenko, “Spectral Study of Catalysts for the Oxidative Condensation of Methane”, *Russ. J. Phys. Chem. A*, vol. 87, pp. 2005–2012, 2013.

K. Kwapien, J. Paier, J. Sauer, M. Geske, U. Zavyalova, R. Horn, P. Schwach, A. Trunschke, et R. Schlögl, “Sites for methane activation on lithium-doped magnesium oxide surfaces”, *Angew. Chem. Int. Ed.*, vol. 53, pp. 8774–8778, 2014.

O. Laguna, M. Domínguez, M. Centeno, et J. Odriozola, “Chapter 4 - catalysts on metallic surfaces : Monoliths and microreactors”, dans *New Materials for Catalytic Applications*, V. I. Parvulescu et E. Kemnitz, éds., Amsterdam, 2016, pp. 81–120.

——, “Forced deactivation and postmortem characterization of a metallic microchannel reactor employed for the preferential oxidation of co (prox)”, *Chem. Eng. J.*, vol. 302, pp. 650–662, 2016.

C. Lahousse, A. Bernier, P. Grange, B. Delmon, P. Papaefthimiou, T. Ioannides, et X. Verykios, “Evaluation of γ -MnO_2 as a VOC Removal Catalyst : Comparison with a Noble Metal Catalyst”, *J. Catal.*, vol. 225, pp. 214–225, 1998.

C. Lambert, J. Theis, et G. Cavataio, *Chapter 16 : LNT Catalysis at Ford Motor Company - A Case History*, 01 2018, pp. 467–489.

N. Laosiripojana et S. Assabumrungrat, “Methane steam reforming over Ni/Ce–ZrO_2 catalyst : Influences of Ce–ZrO_2 support on reactivity, resistance toward carbon formation, and intrinsic reaction kinetics”, *Appl. Catal. A*, vol. 290, no. 1, pp. 200–211, 2005.

J.-P. Laviolette, G. S. Patience, et J. Chaouki, “Non-premixed fluidized bed combustion of c1-c4 n-alkanes”, *Fuel*, vol. 90, pp. 2850–2857, 2011.

C.-J. Lee et C. Han, “Comparative economic analysis of gas-to-liquid processes for optimal product selection”, dans *Proceedings of the 1st Annual Gas Processing Symposium*, série Advances in Gas Processing, H. E. Alfadala, G. R. Reklaitis, et M. M. El-Halwagi, éds. Amsterdam : Elsevier, 2009, vol. 1, pp. 354–361.

J. Lee, J. R. Theis, et E. A. Kyriakidou, “Vehicle Emissions Trapping Materials : Successes, Challenges, and the Path Forward”, *Appl. Catal. B*, vol. 243, pp. 397–414, 2019.

A. Leman, J. Afiqah, F. Rahman, D. Feriyanto, S. Zakaria, et R. Rahmad, “Catalytic converter developed by washcoat of γ-alumina on nickel oxide (nio) catalyst in fecral substrate for exhaust emission control : A review”, *MATEC Web Conf.*, vol. 78, 01 2016.

A. Leman, D. Feriyanto, N. Farhana, R. Rahmat, B. Bakar, et I. Baba, “Oxidation resistance analysis of metallic (fecral foil) catalytic converter developed by ultrasonic approach”, *MATEC Web Conf.*, vol. 78, 2016.

R. Lemlich, “A theory for the limiting conductivity of polyhedral foam at low density”, *J. Colloid Interface Sci.*, vol. 64, pp. 107–110, 1978.

E. A. Leone, A. Rabinkin, et B. Sarna, “Microstructure of Thin-gauge Austenitic and Ferritic Stainless Steel Joints Brazed Using Metglas Amorphous Foil”, *J. Adv. Mater.*, vol. 38, pp. 28–39, 2006.

J. Lercher, J. Bitter, W. Hally, W. Niessen, et K. Seshan, “Design of stable catalysts for methane-carbon dioxide reforming”, dans *11th International Congress On Catalysis - 40th Anniversary*, série Studies in Surface Science and Catalysis, J. W. Hightower, W. N. Delgass, E. Iglesia, et A. T. Bell, éds., 1996, vol. 101, pp. 463–472.

J. J. Lerou, A. L. Tonkovich, L. Silva, S. Perry, et J. McDaniel, “Microchannel reactor architecture enables greener processes”, *Chem. Eng. Sci.*, vol. 65, no. 1, pp. 380–385, 2010.

S. LeViness, S. R. Deshmukh, L. A. Richard, et H. J. Robota, “Velocys fischer–tropsch synthesis technology—new advances on state-of-the-art”, *Top. Catal.*, vol. 57, pp. 518–525, 2014.

A. Li, K. Norinaga, W. Zhang, et O. Deutschmann, “Modeling and simulation of materials synthesis : Chemical vapor deposition and infiltration of pyrolytic carbon”, *Compos. Sci. Technol.*, vol. 68, pp. 1097–1104, 2008, recent Advances in Experimental and Applied Research of Composite Materials.

B. Li, K. Maruyama, M. Nurunnabi, K. Kunimori, et K. Tomishige, “Temperature profiles of alumina-supported noble metal catalysts in autothermal reforming of methane”, *Appl. Catal. A*, vol. 275, no. 1, pp. 157 – 172, 2004.

F. Li, H. R. Kim, D. Sridhar, F. Wang, L. Zeng, J. Chen, et L.-S. Fan, “Syngas chemical looping gasification process : Oxygen carrier particle selection and performance”, *Energy Fuels*, vol. 23, no. 8, pp. 4182–4189, 2009.

H. Li, Y. Wang, X. Chen, S. Liu, Y. Zhou, Q. Zhu, Y. Chen, et H. Lu, “Preparation of Metallic Monolithic Pt/FeCrAl Fiber Catalyst by Suspension Sspraying for VOCs Combustion”, *RSC Adv.*, vol. 8, no. 27, pp. 14 806–14 811, 2018.

J. Li, X. Lu, F. Wu, W. Cheng, W. Zhang, S. Qin, Z. Wang, et Z. You, “Electroplated Palladium Catalysts on FeCrAlloy for Joule-Heat-Ignited Catalytic Elimination of Ethylene in Air”, *Ind. Eng. Chem. Res.*, vol. 56, pp. 12 520–12 528, 2017.

J. Li, X. Lu, F. Wu, S. Qin, et Z. You, “Metallic-substrate-supported Manganese Oxide as Joule-heat-ignition Catalytic Reactor for Removal of Carbon Monoxide and Toluene in Air”, *Chem. Eng. J.*, vol. 328, pp. 1058–1065, 2017.

K. Li, H. Wang, Y. Wei, et D. Yan, “Syngas production from methane and air via a redox process using Ce – Fe mixed oxides as oxygen carriers”, *Appl. Catal. B*, vol. 97, no. 3-4, pp. 361–372, 2010.

——, “Direct conversion of methane to synthesis gas using lattice oxygen of ceo2–fe2o3 complex oxides”, *Chem. Eng. J.*, vol. 156, pp. 512–518, 2010, recent Advances in Chemical Engineering in Sustainable Development.

W. B. Li, J. X. Wang, et H. Gong, “Catalytic Combustion of VOCs on non-noble Metal Catalysts”, *Catal. Today*, vol. 148, pp. 81–87, 2009.

Y. Li, Y. Li, Q. Yu, et L. Yu, “The Catalytic Oxidation of Toluene over Pd-based FeCrAl Wire Mesh Monolithic Catalysts Prepared by Electroless Plating Method”, *Catal. Commun.*, vol. 29, pp. 127–131, 2012.

Y. Li, Y. Fan, J. Jian, L. Yu, G. Cheng, J. Zhou, et M. Sun, “Pt-based Structured Catalysts on Metallic Supports Synthesized by Electroless Plating Deposition for Toluene Complete Oxidation”, *Catal. Today*, vol. 281, pp. 542–548, 2017.

H. Liander, “The utilisation of natural gases for the ammonia process”, *Trans. Faraday Soc.*, vol. 25, pp. 462–472, 1929.

H. Liu et W. Chen, “Carburization Behavior of Electrodeposited Ni_3Al-CeO_2-base Coatings on Fe-Ni-Cr Alloys”, *Oxid. Met.*, vol. 67, pp. 129–152, 2007.

L. Liu et A. Corma, “Metal catalysts for heterogeneous catalysis : From single atoms to nanoclusters and nanoparticles”, *Chem. Rev.*, vol. 118, no. 10, pp. 4981–5079, 2018.

Y. Liu, L. Qin, Z. Cheng, J. W. Goetze, F. Kong, J. A. Fan, et L.-S. Fan, “near 100% co selectivity in nanoscaled iron-based oxygen carriers for chemical looping methane partial oxidation”, *Nat. Commun.*, vol. 10, p. 5503, 2019.

A. Lofberg, A. Essakhi, S. Paul, Y. Swesi, M. L. Zanota, V. Meille, I. Pitault, P. Supiot, B. Mutel, V. Le Courtois, et et al., “Use of Catalytic Oxidation and Dehydrogenation of Hydrocarbons Reactions to Highlight Improvement of Heat Transfer in Catalytic Metallic Foams”, *Chem. Eng. J.*, vol. 176-177, pp. 49–56, 2011.

T. Longson, J. Maddocks, et A. Kashani, “Morphological impact on thermal interface resistance of self catalyzing fecralloy mwnt tims”, 07 2015.

S. Lotfi, D. C. Boffito, et G. S. Patience, “Gas-Phase Partial Oxidation of Lignin to Carboxylic Acids over Vanadium Pyrophosphate and Aluminum – Vanadium – Molybdenum”, *ChemSusChem*, vol. 8, pp. 3424–3432, 2015.

Y. Lou, M. Steib, Q. Zhang, K. Tiefenbacher, A. Horváth, A. Jentys, Y. Liu, et J. A. Lercher, “Design of Stable Ni/ZrO_2 Catalysts for Dry Reforming of Methane”, *J. Catal.*, vol. 356, pp. 147–156, 2017.

J. Lu, B. Fu, M. C. Kung, G. Xiao, J. W. Elam, H. H. Kung, et P. C. Stair, “Coking- and sintering-resistant palladium catalysts achieved through atomic layer deposition”, *Science*, vol. 335, pp. 1205–1208, 2012.

T. J. Lu, J. A. Stone, et M. F. Ashby, “Heat transfer in open-cell metal foams”, *Acta Mater.*, vol. 46, pp. 3619–3635, 1998.

I. V. Lukiyanchuk, V. S. Rudnev, M. M. Serov, B. L. Krit, G. D. Lukiyanchuk, et P. M. Nedozorov, “Effect of Copper Coating on Fibers Made of Aluminum Alloy, Titanium, and FeCrAl Alloy on Surface Morphology and Activity in CO Oxidation”, *Appl. Surf. Sci.*, vol. 436, pp. 1–10, 2018.

J. H. Lunsford, “The catalytic oxidative coupling of methane”, *Angew. Chem. Int. Ed.*, vol. 34, no. 9, pp. 970–980, 1995.

A. E. Lutz, R. W. Bradshaw, J. O. Keller, et D. E. Witmer, “Thermodynamic analysis of hydrogen production by steam reforming”, *Int. J. Hydrog. Energy*, vol. 28, no. 2, pp. 159 – 167, 2003.

M. Lyubovsky, S. Roychoudhury, et R. LaPierre, “Catalytic partial “oxidation of methane to syngas” at elevated pressures”, *Catal. Letters*, vol. 99, pp. 113–117, Feb 2005.

Z. Ma, P. Ouzilleau, C. Trevisanut, C. Neagoe, S. Lotfi, D. C. Boffito, et G. S. Patience, “Partial Oxidation of Methane to Syngas over Pt/Rh/MgO Catalyst Supported on FeCralloy Woven Fiber”, *Can. J. Chem. Eng.*, vol. 94, pp. 642–649, 2016.

Z. Ma, C. Trevisanut, C. Neagoe, D. C. Boffito, S. M. Jazayeri, C. Jagpal, et G. S. Patience, “A micro-refinery to reduce associated natural gas flaring”, *Sustain. Cities Soc.*, vol. 27, pp. 116–121, 2016.

Z. Ma, P. Perreault, D. C. Pelegrin, D. C. Boffito, et G. S. Patience, “Thermodynamically unconstrained forced concentration cycling of methane catalytic partial oxidation over CeO_2 fecralloy catalysts”, *Chem. Eng. J.*, vol. 380, p. 122470, 2020.

T. E. Madey, H. A. Engelhardt, et D. Menzel, “Adsorption of oxygen and oxidation of CO on the ruthenium (001) surface”, *Surf. Sci.*, vol. 48, pp. 304 – 328, 1975.

R. J. Madon et M. Boudart, “Experimental criterion for the absence of artifacts in the measurement of rates of heterogeneous catalytic reactions”, *Ind. Eng. Chem. Fundam.*, vol. 21, pp. 438–447, 1982.

M. Maestri, A. Beretta, G. Groppi, E. Tronconi, et P. Forzatti, “Comparison among structured and packed-bed reactors for the catalytic partial oxidation of CH_4 at short contact times”, *Catal. Today*, vol. 105, pp. 709–717, 2005.

M. Maestri, D. G. Vlachos, A. Beretta, G. Groppi, et E. Tronconi, “A c1 microkinetic model for methane conversion to syngas on rh/al2o3”, *AIChE Journal*, vol. 55, pp. 993–1008, 2009.

A. Maione, F. André, et P. Ruiz, “The Effect of Rh Addition on Pd/γ-Al_2O_3 Catalysts Deposited on FeCrAlloy Fibers for Total Combustion of Methane”, *Appl. Catal. A*, vol. 333, pp. 1–10, 2007.

L. L. Makarshin, V. A. Sadykov, D. V. Andreev, A. G. Gribovskii, V. V. Privezentsev, et V. N. Parmon, “Syngas Production by Partial Oxidation of Methane in a Microchannel Reactor Over a Ni-Pt/$La_{0.2}Zr_{0.4}Ce_{0.4}$Ox Catalyst”, *Fuel Process. Technol.*, vol. 131, pp. 21–28, 2015.

S. Marklund, R. Andersson, M. Tysklind, C. Rappe, K.-E. Egebäck, E. Björkman, et V. Grigoriadis, “Emissions of pcdds and pcdfs in gasoline and diesel fueled cars”, *Chemosphere*, vol. 20, pp. 553–561, 1990.

P. Marsh, F. Acke, R. Konieczny, R. Brück, et P. Hirth, “Application guideline to define a catalyst layout for maximum catalytic efficiency”, dans *SAE Technical Paper*. SAE International, 2001.

L. M. Martínez T, M. I. Domínguez, N. Sanabria, W. Y. Hernández, S. Moreno, R. Molina, J. A. Odriozola, et M. A. Centeno, “Deposition of Al-Fe Pillared Bentonites and Gold Supported Al-Fe Pillared Bentonites on Metallic Monoliths for Catalytic Oxidation Reactions”, *Appl. Catal. A*, vol. 364, pp. 166–173, 2009.

L. M. Martínez Tejada, M. I. Domínguez, O. Sanz, M. A. Centeno, et J. A. Odriozola, “Au/CeO_2 Metallic Monolith Catalysts : Influence of the Metallic Substrate”, *Gold Bulletin*, vol. 46, no. 4, pp. 221–231, 2013.

Y. Matsumura et T. Nakamori, “Steam reforming of methane over nickel catalysts at low reaction temperature”, *Appl. Catal. A*, vol. 258, no. 1, pp. 107–114, 2004.

E. McCafferty et J. P. Wightman, “Determination of the concentration of surface hydroxyl groups on metal oxide films by a quantitative xps method”, *Surf. Interface Anal.*, vol. 26, no. 8, pp. 549–564, 1998.

B. C. McDonald, J. A. de Gouw, J. B. Gilman, S. H. Jathar, A. Akherati, C. D. Cappa, J. L. Jimenez, J. Lee-Taylor, P. L. Hayes, S. A. McKeen, et et al., “Volatile chemical products emerging as largest petrochemical source of urban organic emissions”, *Science*, vol. 359, no. 6377, pp. 760–764, 2018.

S. Mehla, J. Das, D. Jampaiah, S. Periasamy, A. Nafady, et S. K. Bhargava, “Recent advances in preparation methods for catalytic thin films and coatings”, *Catal. Sci. Technol.*, vol. 9, pp. 3582–3602, 2019.

V. Meille, “Review on methods to deposit catalysts on structured surfaces”, *Appl. Catal. A*, vol. 315, pp. 1–17, 2006.

D. Merino, O. Sanz, et M. Montes, “Effect of the Thermal Conductivity and Catalyst Layer Thickness on the Fischer-Tropsch Synthesis Selectivity Using Structured Catalysts”, *Chem. Eng. J.*, vol. 327, pp. 1033–1042, 2017.

N. Mizuno et M. Misono, “Heterogeneous catalysis”, *Chem. Rev.*, vol. 98, no. 1, pp. 199–218, 1998.

S. Mohajerani, A. Kumar, et A. O. Oni, “A techno-economic assessment of gas-to-liquid and coal-to-liquid plants through the development of scale factors”, *Energy*, vol. 150, pp. 681–693, 2018.

A. Montebelli, C. G. Visconti, G. Groppi, E. Tronconi, C. Cristiani, C. Ferreira, et S. Kohler, “Methods for the catalytic activation of metallic structured substrates”, *Catal. Sci. Technol.*, vol. 4, pp. 2846–2870, 2014.

T. Montini, M. Melchionna, M. Monai, et P. Fornasiero, “Fundamentals and catalytic applications of CeO_2-based materials”, *Chem. Rev.*, vol. 116, no. 10, pp. 5987–6041, 2016.

M. R. Morales, B. P. Barbero, et L. E. Cadús, “MnCu Catalyst Deposited on Metallic Monoliths for Total Oxidation of Volatile Organic Compounds”, *Catal. Letters*, vol. 141, pp. 1598–1607, 2011.

R. Morales, B. P. Barbero, et L. E. Cadu, “Combustion of Volatile Organic Compounds on Manganese Iron or Nickel Mixed Oxide Catalysts”, *Appl. Catal. B*, vol. 74, pp. 1–10, 2007.

P. M. Mortensen, R. Klein, et K. Aasberg-Peterse, “Steam reforming heated by resistance heating”, Mai 31 2018, european Patent 3574991 A1.

P. Munnik, P. E. de Jongh, et K. P. de Jong, “Recent developments in the synthesis of supported catalysts”, *Chem. Rev.*, vol. 115, no. 14, pp. 6687–6718, 2015.

M. Musiani, S. Cattarin, S. Cimino, N. Comisso, L. Mattarozzi, L. Vázquez-Gómez, et E. Verlato, “Preparation of 3D Electrocatalysts and Catalysts for Gas-phase Reactions, Through Electrodeposition or Galvanic Displacement”, *J. Appl. Electrochem.*, vol. 45, pp. 715–725, 2015.

J. Namkung, M. C Kim, et W. W Park, “Fabrication of fe–cr–al base alloy strips by melt dragging and their oxidation resistance at elevated temperature”, *J. Mater. Process. Technol.*, vol. 115, pp. 391–395, 09 2001.

C. Neagoe, D. C. Boffito, Z. Ma, C. Trevisanut, et G. S. Patience, “Pt on Fecralloy Catalyses Methane Partial Oxidation to Syngas at High Pressure”, *Catal. Today*, vol. 270, pp. 43–50, 2016.

J. R. Nicholls, M. J. Bennett, et R. Newton, “A Life Prediction Model for the Chemical Failure of FeCrAl Alloys : Preliminary Assessment of Model Extension to Lower Temperatures”, *Mater. at High Temp.*, vol. 20, pp. 429–438, 2003.

T. A. Nijhuis, A. E. W. Beers, T. Vergunst, I. Hoek, F. Kapteijn, et J. A. Moulijn, “Preparation of monolithic catalysts”, *Catal. Rev.*, vol. 43, pp. 345–380, 2001.

A. M. noz Murillo, L. M. T., M. Domínguez, J. Odriozola, et M. Centeno, “Selective co methanation with structured RuO_2/Al_2O_3 catalysts”, *Appl. Catal. B*, vol. 236, pp. 420–427, 2018.

J. Ochonska, A. Rogulska, P. J. Jodowski, M. Iwaniszyn, M. Michalik, W. Lasocha, A. Kolodziej, et J. Lojewska, “Prospective Catalytic Structured Converters for NH_3-SCR of NOx from Biogas Stationary Engines : in situ Template-free Synthesis of ZSM-5 Cu Exchanged Catalysts on Steel Carriers”, *Top. Catal.*, vol. 56, pp. 56–61, 2013.

J. Ochonska-Kryca, M. Iwaniszyn, M. Piatek, P. J. Jodlowski, J. Thomas, A. Kolodziej, et J. Lojewska, “Mass Transport and Kinetics in Structured Steel Foam Reactor with Cu-ZSM-5 Catalyst for SCR of NOx with Ammonia”, *Catal. Today*, vol. 216, pp. 135–141, 2013.

K. Oshima, T. Shinagawa, Y. Nogami, R. Manabe, S. Ogo, et Y. Sekine, “Low temperature catalytic reverse water gas shift reaction assisted by an electric field”, *Catal. Today*, vol. 232, pp. 27–32, 2014.

E. Ostbye Pedersen et E. Blekkan, “Noble metal promoted comn catalysts for fischer–tropsch synthesis”, *Catal. Letters*, vol. 148, pp. 1027–1034, 2018.

K. Otsuka, Y. Wang, E. Sunada, et I. Yamanaka, “Direct partial oxidation of methane to synthesis gas by cerium oxide”, *J. Catal.*, vol. 175, no. 2, pp. 152 – 160, 1998.

M. Ozawa et K.-i. Araki, “Effect of la modification on stability of coating alumina layer on fecral alloy substrate”, *Surf. Coat. Technol.*, vol. 271, pp. 80–86, 01 2015.

C. Padovani et P. Francetti Giorn, “Incomplete oxidation of methane with oxygen and air”, *Giorn. Chim. Ind. Applicata.*, vol. 15, pp. 429–432, 1929.

J. Paier, C. Penschke, et J. Sauer, “Oxygen defects and surface chemistry of ceria : Quantum chemical studies compared to experiment”, *Chem. Rev.*, vol. 113, no. 6, pp. 3949–3985, 2013.

D. R. Palo, R. A. Dagle, et J. D. Holladay, “Methanol steam reforming for hydrogen production”, *Chem. Rev.*, vol. 107, no. 10, pp. 3992–4021, 2007.

G. S. Patience et R. E. Bockrath, “Butane oxidationoxidation process development in a circulating fluidized bed”, *Appl. Catal. A*, vol. 376, pp. 4–12, 2010.

G. Pauletto, N. Libretto, D. C. Boffito, J. Miller, A. Jentys, G. S. Patience, et J. A. Lercher, “Ni/CeO_2 supported fecral gauze for cycling methane catalytic partial oxidation cpox”, *Manuscript in preparation.*

G. Pauletto, P. Mocellin, A. Gaillardet, F. Galli, et G. S. Patience, “Design and economic evaluation of a micro gtl unit for production of hydrocarbons from stranded natural gas”, *Manuscript in preparation.*

M. A. Peluso, L. Costa-Almeida, O. Sanz, J. E. Sambeth, H. J. Thomas, et M. Montes, “Washcoating of MnOx on FeCrAlloy Monoliths”, *Lat. Am. Appl. Res.*, vol. 43, pp. 301–306, 2013.

H. Peng, X. Zhang, L. Zhang, C. Rao, J. Lian, W. Liu, J. Ying, G. Zhang, Z. Wang, N. Zhang, et et al., “One pot facile fabrication of multiple-nickel confined in microporous silica with multiple-core@shell structure as a highly efficient catalyst for methane dry reforming”, *ChemCatChem*, pp. 127–136, 2017.

C. Perego et R. Millini, “Porous materials in catalysis : Challenges for mesoporous materials”, *Chem. Soc. Rev.*, vol. 42, pp. 3956–3976, 2012.

H. Pérez, P. Navarro, et M. Montes, “Deposition of SBA-15 Layers on Fecralloy Monoliths by Washcoating”, *Chem. Eng. J.*, vol. 158, pp. 325–332, 2010.

N. C. Pérez, E. E. Miró, et J. M. Zamaro, “Cu, Ce/mordenite Coatings on FeCrAl-alloy Corrugated Foils Employed as Catalytic Microreactors for CO Oxidation”, *Catal. Today*, vol. 213, pp. 183–191, 2013.

P. Perreault, E. Robert, et G. S. Patience, “Experimental methods in chemical engineering : Mass spectrometry—ms”, *Can. J. Chem. Eng.*, vol. 97, no. 5, pp. 1036–1042, 2019.

M. S. Peters, K. D. Timmerhaus, et R. E. West, *Plant design and economics for economical for chemical engineers*, 5e éd. New York : McGraw Hill, 2003.

B. A. Pint, “Experimental observations in support of the dynamic-segregation theory to explain the reactive-element effect”, *Chem. Rev.*, vol. 45, pp. 1–37, 1996.

D. Potemkin, E. Filatov, A. Zadesenets, V. Rogozhnikov, E. Gerasimov, P. Snytnikov, S. Korenev, et V. Sobyanin, "Bimetallic pt-co/η-Al_2O_3/fecral wire mesh composite catalyst prepared via double complex salt $[Pt(NH_3)_4][Co(C_2O_4)_2(H_2O)_2]$-$2H_2O$ decomposition", *Mater. Lett.*, vol. 236, pp. 109–111, 2019.

R. Prasad, L. A. Kennedy, et E. Ruckenstein, "Catalytic combustion", *Catalysis Rev.*, vol. 26, pp. 1–58, 1984.

M. Prettre, C. Eichner, et M. Perrin, "The catalytic oxidation of methane to carbon monoxide and hydrogen", *Trans. Faraday Soc.*, vol. 42, pp. 335–339, 1946.

H. Pérez, P. Navarro, et M. Montes, "Deposition of sba-15 layers on fecralloy monoliths by washcoating", *Chem. Eng. J.*, vol. 158, pp. 325–332, 04 2010.

G. Qi, Y. Zhang, A. Chen, et Y. Yu, "Potassium-Activated Wire Mesh : A Stable Monolithic Catalyst for Diesel Soot Combustion", *Chem. Eng. Technol.*, vol. 40, pp. 50–55, 2017.

L. Qin, M. Guo, Y. Liu, Z. Cheng, J. A. Fan, et L.-S. Fan, "Enhanced Methane Conversion in Chemical Looping Partial Oxidation Systems Using a Copper Doping Modification", *Appl. Catal. B*, vol. 235, pp. 143–149, 2018.

W. J. Quadakkers, D. Naumenko, E. Wessel, et V. Kochubey, "Growth Rates of Alumina Scales on Fe–Cr–Al Alloys", *Oxid. Met.*, vol. 61, pp. 17–37, 2004.

C. Rallan, R. Al-Rubaye, et A. Garforth, "Generation of Catalytic Films of Alumina and Zeolites on FeCralloy Rods", *Chem. Eng. Trans.*, vol. 43, pp. 907–912, 2015.

C. Rallan et A. Garforth, "Growth of Hierarchically Structured High-surface Area Alumina on FeCralloy® Rods", *Chin. J. Chem. Eng.*, vol. 22, pp. 861–868, 2014.

C. Rallan, R. Alrubaye, et A. Garforth, "Generation of catalytic films of alumina and zeolites on fecralloy rods", *Chem. Eng. Trans.*, vol. 43, 05 2015.

D. J. Ramberg, Y. H. Chen, S. Paltsev, et J. E. Parsons, "The economic viability of gas-to-liquids technology and the crude oil–natural gas price relationship", *Energy Econ.*, vol. 63, pp. 13–21, 2017.

E. Rebrov, M. Mies, M. Croon, de, et J. Schouten, *Hydrothermal Synthesis of Zeolitic Coatings for Applications in Micro-structured Reactors.* Elsevier, 2009, pp. 311–334.

J. Rehr, C. Booth, F. Bridges, et S. Zabinsky, “X-ray absorption fine structure in embedded atoms”, *Phys. Rev. B*, vol. 49, p. 12347, 01 1994.

E. Reichelt, M. P. Heddrich, M. Jahn, et A. Michaelis, “Fiber based structured materials for catalytic applications”, *Appl. Catal. A*, vol. 476, pp. 78–90, 2014.

E. Reichelt et M. Jahn, “Generalized correlations for mass transfer and pressure drop in fiber-based catalyst supports”, *Chem. Eng. J.*, vol. 325, pp. 655 – 664, 2017.

T. Ressler, “*WinXAS* : a Program for X-ray Absorption Spectroscopy Data Analysis under MS-Windows”, *J. Synchrotron Radiat.*, vol. 5, pp. 118–122, 1998.

K. Reszka, J. Rakoczy, Z. Zurek, A. Czyzniewski, A. Gilewicz, et M. Homa, “Catalytic Properties of Al_2O_3 Deposited by Ion Sputtering Using DC and RF Sources”, *Vacuum*, vol. 78, pp. 149–155, 2005.

K. Reszka, J. Morgiel, et J. Reszka, “Structure and properties of an alumina/amorphous-alumina/platinum catalytic system deposited on fecral steel”, *J. Microsc.*, vol. 224, pp. 46–48, 11 2006.

K. Reszka, M. Szczypiński, et M. Pomorska, “Influence of Substrate Local Heating on Morphology of Al and Al_2O_3 Nanofilms”, *Acta Phys. Pol.*, vol. 120, pp. 177–180, 2011.

I. Reyero, I. Velasco, O. Sanz, M. Montes, G. Arzamendi, et L. M. Gandía, “Structured Catalysts Based on Mg-Al Hydrotalcite for the Synthesis of Biodiesel”, *Catal. Today*, vol. 216, pp. 211–219, 2013.

I. Reyero, A. Moral, F. Bimbela, J. Radosevic, O. Sanz, M. Montes, et L. M. Gandía, “Metallic Monolithic Catalysts Based on Calcium and Cerium for the Production of Biodiesel”, *Fuel*, vol. 182, pp. 668–676, 2016.

J. T. Richardson, D. Remue, et J. K. Hung, “Properties of ceramic foam catalyst supports : Mass and heat transfer”, *Appl. Catal. A*, vol. 250, pp. 319–329, 2003.

J. T. Richardson et T. S. Cale, “Interpretation of hydrogen chemisorption on nickel catalysts”, *J. Catal.*, vol. 102, pp. 419–432, 1986.

M. Rieks, R. Bellinghausen, N. Kockmann, et L. Mleczko, “Experimental Study of Methane Dry Reforming in an Electrically Heated Reactor”, *Int. J. Hydrog. Energy*, vol. 40, pp. 15 940–15 951, 2015.

S. Rifflart, F.-X. Chiron, et G. S. Patience, “Method for producing synthesis gas, us patent 8,974,699 b2.” 2018.

V. Rogozhnikov, P. Snytnikov, A. Salanov, A. Kulikov, N. Ruban, D. Potemkin, V. Sobyanin, et V. Kharton, “Rh/θ-Al_2O_3/fecralloy wire mesh composite catalyst for partial oxidation of natural gas”, *Mater. Lett.*, vol. 236, pp. 316–319, 2019.

J. Rostrup-Nielsen et L. J. Christiansen, *Concepts in Syngas Manufacture.* Imperial College Press, 2011.

J. R. Rostrup-Nielsen et T. Rostrup-Nielsen, “Large-scale hydrogen production”, *CATTECH*, vol. 6, pp. 150–159, Aug 2002.

J. R. Rostrup-Nielsen, J. Sehested, et J. K. Nørskov, “Hydrogen and synthesis gas by steam- and CO_2 reforming”, série Advances in Catalysis. Academic Press, 2002, vol. 47, pp. 65–139.

S. K. Ryi, J. S. Park, S. H. Cho, et S. H. Kim, “Fast Start-up of Microchannel Fuel Processor Integrated with an Igniter for Hydrogen Hombustion”, *J. Power Sources*, vol. 161, pp. 1234–1240, 2006.

J. H. Ryu, K. Y. Lee, H. La, H. J. Kim, J. I. Yang, et H. Jung, “Ni Catalyst Wash-coated on Metal Monolith with Enhanced Heat-transfer Capability for Steam Reforming”, *J. Power Sources*, vol. 171, pp. 499–505, 2007.

V. Sadykov, V. Sobyanin, N. Mezentseva, G. Alikina, Z. Vostrikov, Y. Fedorova, V. Pelipenko, V. Usoltsev, S. Tikhov, A. Salanov, et et al., “Transformation of CH_4 and Liquid Fuels into Syngas on Monolithic Catalysts”, *Fuel*, vol. 89, pp. 1230–1240, 2010.

J. E. Samad, J. A. Nychka, et N. V. Semagina, “Structured Catalysts via Multiple Stage Thermal Oxidation Synthesis of FeCrAl Alloy Sintered Microfibers”, *Chem. Eng. J.*, vol. 168, pp. 470–476, 2011.

Sánchez M., J. F., O. J. González Bello, M. Montes, G. M. Tonetto, et D. E. Damiani, “Pd/Al_2O_3-cordierite and Pd/Al_2O_3-Fecralloy Monolithic Catalysts for the Hydrogenation of Sunflower Oil”, *Catal. Commun.*, vol. 10, pp. 1446–1449, 2009.

P. Sandvik, M. Kathe, W. Wang, F. Kong, et L.-s. Fan, “High-Pressure Chemical Looping Reforming Processes : System Analysis for Syngas Generation from Natural Gas and Reducing Tail Gases”, *Energy Fuels*, vol. 32, pp. 10 408–10 420, 2018.

A. Santos, S. Damyanova, G. Teixeira, L. Mattos, F. Noronha, F. Passos, et J. Bueno, “The effect of ceria content on the performance of $Pt/CeO_2/Al_2O_3$ catalysts in the partial oxidation of methane”, *Appl. Catal. A*, vol. 290, pp. 123–132, 2005.

A. Scarpa, P. S. Barbato, G. Landi, R. Pirone, et G. Russo, “Combustion of Methane-hydrogen Mixtures on Catalytic Tablets”, *Chem. Eng. J.*, vol. 154, no. 1-3, pp. 315–324, 2009.

L. Schmidt, M. Huff, et S. Bharadwaj, “Catalytic partial oxidation reactions and reactors”, *Chem. Eng. Sci.*, vol. 49, pp. 3981–3994, 1994.

H. Schulz, “Short history and present trends of fischer–tropsch synthesis”, *Appl. Catal. A*, vol. 186, pp. 3–12, 1999.

L. A. Schulz, L. C. Kahle, K. H. Delgado, S. A. Schunk, A. Jentys, O. Deutschmann, et J. A. Lercher, “On the coke deposition in dry reforming of methane at elevated pressures”, *Appl. Catal. A*, vol. 504, pp. 599–607, 2015.

P. Schwach, W. Frandsen, M.-G. Willinger, R. Schlögl, et A. Trunschke, “Structure sensitivity of the oxidative activation of methane over mgo model catalysts : I. kinetic study”, *J. Catal.*, vol. 329, pp. 560–573, 2015.

P. Schwach, N. Hamilton, M. Eichelbaum, L. Thum, T. Lunkenbein, R. Schlögl, et A. Trunschke, “Structure sensitivity of the oxidative activation of methane over mgo model catalysts : Ii. nature of active sites and reaction mechanism”, *J. Catal.*, vol. 329, pp. 574–587, 2015.

Y.-S. Seo, A. Shirley, et S. Kolaczkowski, “Evaluation of thermodynamically favourable operating conditions for production of hydrogen in three different reforming technologies”, *J. Power Sources*, vol. 108, pp. 213–225, 2002.

T. Serres, L. Dreibine, et Y. Schuurman, “Synthesis of enamel-protected catalysts for microchannel reactors : Application to methane oxidative coupling”, *Chem. Eng. J.*, vol. 213, pp. 31–40, 2012.

A. Setiawan, E. M. Kennedy, et M. Stockenhuber, “Development of Combustion Technology for Methane Emitted from Coal-Mine Ventilation Air Systems”, *Energy Technol.*, pp. 521–538, 2017.

M.-q. Shen, L.-w. Jia, W.-l. Zhou, J. U. N. Wang, et Y. Huang, “Influence of $Ce_{0.68}Zr_{0.32}O_2$

Solid Solution on Depositing γ-alumina Washcoat on FeCrAl Foils", *Bull. Mater. Sci.*, vol. 29, no. 1, pp. 73–76, 2006.

X. Shi, S. Ji, K. Wang, et C. Li, "Oxidative Dehydrogenation of Ethane with CO_2 over Novel Cr / SBA-15 / Al_2O_3 / FeCrAl Monolithic Catalysts", *Energy Fuels*, vol. 22, pp. 3631–3638, 2008.

Y. Shi, J. V. Pelt, J. Cross, D. Pollica, C. O. Brien, et M. Leshchiner, "Catalysis Studies for H_2 Production by Metallic Heat Exchanger-Coated Catalysts", *Sci. World J.*, vol. 12, pp. 511–522, 2008.

T. B. Shoynkhorova, V. N. Rogozhnikov, P. A. Simonov, P. V. Snytnikov, A. N. Salanov, A. V. Kulikov, E. Y. Gerasimov, V. D. Belyaev, D. I. Potemkin, et V. A. Sobyanin, "Highly Dispersed Rh/$Ce_{0.75}Zr_{0.25}O_{2\text{-}\delta}$-$\eta$-$Al_2O_3$ /FeCrAl wire Mesh Catalyst for Autothermal n-Hexadecane Reforming", *Mater. Lett.*, vol. 214, pp. 290–292, 2018.

J. Sichinga et A. Buchanan, *Unlocking the Potential Wealth of Coal Introducing Sasol's Unique Coal-To-Liquids Technology*, 2005.

S. S. Sigaeva, V. A. Likholobov, et P. G. Tsyrul'nikov, "Pyrolysis of Methane on a Heat-treated FeCrAl Coil Heated with Electric Current", *Kinet. Catal.*, vol. 54, pp. 199–206, 2013.

S. Sigaeva, V. Temerev, N. Kuznetsova, et P. Tsyrul'nikov, "Pyrolysis of Methane on Ooxide Catalysts Supported by Resistive Fechral and Carborundum", *Catal. Ind.*, vol. 9, pp. 181–188, 2017.

T. L. Silbaugh et C. T. Campbell, "Energies of formation reactions measured for adsorbates on late transition metal surfaces", *J. Phys. Chem. C*, vol. 120, no. 44, pp. 25 161–25 172, 2016.

R. K. Singha, A. Shukla, A. Yadav, L. N. S. Konathala, et R. Bal, "Effect of Metal-support Interaction on Activity and Stability of Ni-CeO_2 Catalyst for Partial Oxidation of Methane", *Appl. Catal. B*, vol. 202, pp. 473–488, 2017.

A. Sirijaruphan, J. G. Goodwin, R. W. Rice, D. Wei, K. R. Butcher, G. W. Roberts, et J. J. Spivey, "Metal Foam Supported Pt Catalysts for the Selective Oxidation of CO in Hydrogen", *Appl. Catal. A*, vol. 281, pp. 1–9, 2005.

K. I. Slovetskaya et L. M. Kustov, "High-temperature Methane Oxidation over Metallic

Monolith-supported Zeolite Catalysts Containing Mn, Co, and Pd Ions", *Russ. Chem. Bull.*, vol. 52, pp. 1933–1939, 2003.

F. Smeacetto, A. Chrysanthou, M. Salvo, T. Moskalewicz, F. D. Bytner, L. Ajitdoss, et M. Ferraris, "Thermal cycling and ageing of a glass-ceramic sealant for planar sofcs", *Int. J. Hydrog. Energy*, vol. 36, no. 18, pp. 11 895–11 903, 2011.

M. Y. Smirnov, A. V. Kalinkin, D. A. Nazimov, V. I. Bukhtiyarov, E. I. Vovk, et E. Ozensoy, "An XPS Study of the Interaction of Model Ba/TiO_2 and Ba/ZrO_2 NSR Catalysts with NO_2", *Journal of Structural Chemistry*, vol. 55, pp. 757–763, 2014.

M. Y. Smirnov, A. V. Kalinkin, D. A. Nazimov, A. V. Toktarev, et V. I. Bukhtiyarov, "Model Sulfur-resistant NSR Catalysts : an XPS Study of the Interaction of BaO/TiO_2-ZrO_2 and Pt-BaO/TiO_2-ZrO_2 with NO_2", *Kinetics and Catalysis*, vol. 56, pp. 540–548, 2015.

M. W. Smith et D. Shekhawat, "Chapter 5 - catalytic partial oxidation", dans *Fuel Cells : Technologies for Fuel Processing*, D. Shekhawat, J. J. Spivey, et D. A. Berry, éds. Amsterdam : Elsevier, 2011, pp. 73–128.

S. Somacescu, N. Cioatera, P. Osiceanu, et J. M. Calderon-moreno, " Bimodal mesoporous NiO/CeO_2- δ -YSZ with enhanced carbon tolerance in catalytic partial oxidation of methane — Potential IT-SOFCs anode", *Appl. Catal. B*, vol. 241, no. August 2018, pp. 393–406, 2019.

S. Specchia, A. Civera, et G. Saracco, "In situ Combustion Synthesis of Perovskite Catalysts for Efficient and Clean Methane Premixed Metal Burners", *Chem. Eng. Sci.*, vol. 59, pp. 5091–5098, 2004.

S. Specchia, M. A. Ahumada Irribarra, P. Palmisano, G. Saracco, et V. Specchia, "Aging of Premixed Metal Fiber Burners for Natural Gas Combustion Catalyzed with Pa/$LaMnO_3$ $2ZrO_2$", *Ind. Eng. Chem. Res.*, vol. 46, pp. 6666–6673, 2007.

S. Specchia, C. Galletti, et V. Specchia, "Solution combustion synthesis as intriguing technique to quickly produce performing catalysts for specific applications", dans *Scientific Bases for the Preparation of Heterogeneous Catalysts*, série Stud. Surf. Sci. Catal., E. Gaigneaux, M. Devillers, S. Hermans, P. Jacobs, J. Martens, et P. Ruiz, éds., 2010, vol. 175, pp. 59 – 67.

S. Specchia, G. Ercolino, S. Karimi, C. Italiano, et A. Vita, "Solution combustion synthesis for preparation of structured catalysts : a mini-review on process intensification for energy applications and pollution control", *Int. J. self Propag. high Temp. Synth.*, vol. 26, pp. 166–186, 07 2017.

J. G. Speight, "Chapter 5 - the fischer-tropsch process", dans *Gasification of Unconventional Feedstocks*, J. G. Speight, éd. Boston : Gulf Professional Publishing, 2014, pp. 118–134.

C. Stampfl et M. Scheffler, "Theoretical study of o adlayers on ru(0001)", *Phys. Rev. B*, vol. 54, pp. 2868–2872, 1996.

P. Stefanov, S. Todorova, A. Naydenov, B. Tzaneva, H. Kolev, G. Atanasova, D. Stoyanova, Y. Karakirova, et K. Aleksieva, "On the Development of Active and Stable Pd-Co/γ-Al_2O_3 Catalyst for Complete Oxidation of Methane", *Chem. Eng. J.*, vol. 266, pp. 329–338, 2015.

M. Stucchi, F. Galli, C. L. Bianchi, C. Pirola, D. C. Boffito, F. Biasioli, et V. Capucci, "Simultaneous photodegradation of voc mixture by TiO_2 powders", *Chemosphere*, vol. 193, pp. 198–206, 2018.

P. Sudarsanam, R. Zhong, S. Van den Bosch, S. Coman, V. I Parvulescu, et B. Sels, "Functionalised heterogeneous catalysts for sustainable biomass valorisation", *Chem. Soc. Rev.*, vol. 47, pp. 8349–8402, 2018.

B. T., M. T., et T. G., "A Comparative Exergoeconomic Evaluation of the synthesis routes for methanol production from natural gas", *Appl. Sci.*, vol. 7, pp. 1–23, 2017.

L. T. Mika, E. Cséfalvay, et A. Nemeth, "Catalytic conversion of carbohydrates to initial platform chemicals : Chemistry and sustainability", *Chem. Rev.*, vol. 118, pp. 505–613, 11 2017.

S. Tada, T. Shimizu, H. Kameyama, T. Haneda, et R. Kikuchi, "Ni/CeO_2 catalysts with high CO_2 methanation activity and high CH_4 selectivity at low temperatures", *Int. J. Hydrog. Energy*, vol. 37, pp. 5527–5531, 2012.

A. R. Tadd, B. D. Gould, et J. W. Schwank, "Packed Bed Versus Microreactor Performance in Autothermal Reforming of Isooctane", *Catal. Today*, vol. 110, pp. 68–75, 2005.

N. Takahashi, H. Shinjoh, et T. Suzuki, "The New Concept 3-way Catalyst for Automotive Lean-burn Engine : NOx Storage and Reduction Catalyst", *Catal. Today*, vol. 27, pp. 63–69, 1996.

I. Tavazzi, A. Beretta, G. Groppi, A. Donazzi, M. Maestri, E. Tronconi, et P. Forzatti, "Catalytic partial oxidation of CH_4 and C_3H_8 : experimental and modeling study of the dynamic and steady state behavior of a pilot-scale reformer", dans *Natural Gas Conversion VIII*, série Studies in Surface Science and Catalysis, F. B. Noronha, M. Schmal, et E. F. Sousa-Aguiar, éds., 2007, vol. 167, pp. 319–324.

O. Thoda, G. Xanthopoulou, G. Vekinis, et A. Chroneos, "Review of recent studies on solution combustion synthesis of nanostructured catalysts", *Adv. Eng. Mater.*, vol. 20, no. 8, p. 1800047, 2018.

H. Toulhoat, *Heterogeneous Catalysis : Use of Density Functional Theory*, 12 2010, pp. 1–7.

T. P. Tran, Y. Guo, L. Zhou, et H. Kameyama, "Anodic Alumina Catalyst Support with High Heat-resistance for Hydrocarbon Steam Reformers", *J. Chem. Eng. Japan*, vol. 40, pp. 1229–1234, 2007.

C. Trevisanut, S. M. Jazayeri, S. Bonkane, C. Neagoe, A. Mohamadalizadeh, D. C. Boffito, C. Bianchi, C. Pirola, C. G. Visconti, L. Lietti, N. Abatzoglou, L. F. J. Lerou, W. Green, et G. S. Patience, "Micro-syngas technology options for gtl", *Can. J. Chem. Eng.*, vol. 94, pp. 613–622, 2016.

D. Trimm, "Coke formation and minimisation during steam reforming reactions", *Catal. Today*, vol. 37, no. 3, pp. 233–238, 1997.

F. Trippe, M. Fröhling, F. Schultmann, R. Stahl, E. Henrich, et A. Dalai, "Comprehensive techno-economic assessment of dimethyl ether (DME) synthesis and fischer–tropsch synthesis as alternative process steps within biomass-to-liquid production", *Fuel Process. Technol.*, vol. 106, pp. 577–586, 2013.

E. Tronconi et P. Forzatti, "Adequacy of lumped parameter models for scr rreactors with monolith structure", *AIChE J.*, vol. 38, pp. 201–210, 1992.

M. Tsagkari, J.-L. Couturier, A. Kokossis, et J.-L. Dubois, "Early-stage capital cost estimation of biorefinery processes : A comparative study of heuristic techniques", *ChemSusChem*, vol. 9, pp. 2284–2297, 2016.

C. L. Tucker et E. van Steen, "Activity and selectivity of a cobalt-based fischer-tropsch catalyst operating at high conversion for once-through biomass-to-liquid operation", *Catal. Today*, vol. 342, pp. 115–123, 2018.

M. V. Twigg et J. T. Richardson, "Fundamentals and applications of structured ceramic foam catalysts", *Ind. Eng. Chem. Res.*, vol. 46, pp. 4166–4177, 2007.

T. Uda, M. Tanaka, et K. Munakata, “Characteristics of Honeycomb Catalysts for Oxidation of Tritiated Hydrogen and Methane Gases”, *Fusion Eng. Des.*, vol. 83, pp. 1715–1720, 2008.

T. Uda, T. Sugiyama, Y. Asakura, K. Munakata, et M. Tanaka, “Development of High Performance Catalyst for Oxidation of Tritiated Hydrogen and Methane Gases”, *Fusion Sci. Technol.*, vol. 48, no. 1, pp. 480–483, 2005.

D. Ugues, S. Specchia, et G. Saracco, “Optimal Microstructural Design of a Catalytic Premixed FeCrAlloy Fiber Burner for Methane Combustion”, *Ind. Eng. Chem. Res.*, vol. 43, pp. 1990–1998, 2004.

K. Urasaki, S. Kado, A. Kiryu, K.-i. Imagawa, K. Tomishige, R. Horn, O. Korup, et Y. Suehiro, “Synthesis gas Production by Catalytic Partial Oxidation of Natural Gas Using Ceramic Foam Catalyst”, *Appl. Catal. A*, vol. 299, pp. 219–228, 2018.

M. Valentini, G. Groppi, C. Cristiani, M. Levi, E. Tronconi, et P. Forzatti, “The Deposition of γ-Al_2O_3 Layers on Ceramic and Metallic Supports for the Preparation of Structured Catalysts”, *Catal. Today*, vol. 69, pp. 307–314, 2001.

C. R. Valle, A. V. Perales, F. Vidal-Barrero, et A. Gómez-Barea, “Techno-economic assessment of biomass-to-ethanol by indirect fluidized bed gasification : Impact of reforming technologies and comparison with entrained flow gasification”, *Appl. Energy*, vol. 109, pp. 254–266, 2013.

N. J. van Eck et L. Waltman, “Software survey : Vosviewer, a computer program for bibliometric mapping”, *Scientometrics*, vol. 84, pp. 523–538, 2010.

K. M. Van Geem, V. V. Galvita, et G. B. Marin, “Making chemicals with electricity”, *Science*, vol. 364, pp. 734–735, 2019.

T. Van Gerven et A. Stankiewicz, “Structure, energy, synergy, time-the fundamentals of process intensification”, *Ind. Eng. Chem. Res.*, vol. 48, pp. 2465–2474, 02 2009.

L. Vázquez-Gómez, S. Cattarin, N. Comisso, P. Guerriero, M. Musiani, et E. Verlato, “Spontaneous Deposition of Pd onto Fe-Cr-Al Alloys”, *Electrochim. Acta*, vol. 68, pp. 114–122, 2012.

J. A. Velasco, C. Fernandez, L. G. Lopez Nina, S. Cabrera, M. Boutonnet, et S. G. Jars, “Catalytic partial oxidation of methane over nickel and ruthenium based catalysts under low O_2/CH_4 ratios and with addition of steam”, *Fuel*, vol. 153, pp. 192–201, 2015.

E. Verlato, S. Barison, S. Cimino, F. Dergal, L. Lisi, G. Mancino, M. Musiani, et L. Vázquez-Gómez, “Catalytic Partial Ooxidation of Methane over Nanosized Rh Supported on Fecralloy Foams”, *Int. J. Hydrog. Energy*, vol. 39, pp. 11 473–11 485, 2014.

E. Verlato, S. Barison, S. Cimino, L. Lisi, G. Mancino, M. Musiani, et F. Paolucci, “Electrochemical Preparation of Nanostructured CeO_2-Pt Catalysts on Fe-Cr-Al Alloy Foams for the Low-temperature Combustion of Methanol”, *Chem. Eng. J.*, vol. 317, pp. 551–560, 2017.

G. Veser, J. Frauhammer, et U. Friedle, “Syngas formation by direct oxidation of methane : Reaction mechanisms and new reactor concepts”, *Catal. Today*, vol. 61, no. 1, pp. 55 – 64, 2000.

C. G. Visconti, G. Groppi, et E. Tronconi, “Accurate prediction of the effective radial conductivity of highly conductive honeycomb monoliths with square channels”, *Chem. Eng. J.*, vol. 223, pp. 224–230, 2013.

L. Vázquez-Gómez, S. Cattarin, N. Comisso, P. Guerriero, M. Musiani, et E. Verlato, “Spontaneous deposition of pd onto fe–cr–al alloys”, *Electrochim. Acta*, vol. 68, pp. 114–122, 2012.

M. Wallenstein, M. Kind, et B. Dietrich, “Radial two-phase thermal conductivity and wall heat transfer coefficient of ceramic sponges–experimental results and correlation”, *Int. J. Heat Mass Transf.*, vol. 79, pp. 486–495, 2014.

F. Wang, W.-z. Li, J.-d. Lin, Z.-q. Chen, et Y. Wang, “Crucial Support Effect on the Durability of Pt/$MgAl_2O_4$ for Partial Oxidation of Methane to Syngas”, *Appl. Catal. B*, vol. 231, no. December 2017, pp. 292–298, 2018.

J. Wang, H. Chen, Z. Hu, M. Yao, et Y. Li, “A review on the pd-based three-way catalyst”, *Catal. Rev.*, vol. 57, no. 1, pp. 79–144, 2015.

K. Wang, X. Li, S. Ji, S. Sun, D. Ding, et C. Li, “CO_2 reforming of methane to syngas over ni/sba-15/fecral”, dans *Natural Gas Conversion VIII*, série Studies in Surface Science and Catalysis, F. B. Noronha, M. Schmal, et E. F. Sousa-Aguiar, éds., 2007, vol. 167, pp. 367–372.

K. Wang, X. Li, S. Ji, B. Huang, et C. Li, “Preparation of Ni-based Metal Monolithic Catalysts and a Study of their Performance in Methane Reforming with CO_2”, *ChemSusChem*, vol. 1, no. 6, pp. 527–533, 2008.

W. Wang, Z. Zhang, et S. Ji, “Particle/metal-based Monolithic Catalysts Dual-bed Reactor with Beds-interspace Ssupplementary Oxygen : Construction and Performance for Oxidative Coupling of Methane”, *J. Nat. Gas Chem.*, vol. 21, pp. 400–406, 2012.

X. Wang, J. Jia, X. Mu, L. Pan, et S. Wang, “Methanol Steam Reforming over Metal Wall-Coated PdZn/Al_2O_3/FeCrAl Catalyst for Hydrogen Production”, *Chinese J. Catal.*, vol. 29, pp. 99–101, 2008.

R. S. Weber et L. J. Snowden-Swan, “The economics of numbering up a chemical process enterprise”, *J. Adv. Manufact. & Proc.*, vol. 1, 2019.

J. Wei et E. Iglesia, “Isotopic and kinetic assessment of the mechanism of reactions of ch4 with co2 or h2o to form synthesis gas and carbon on nickel catalysts”, *J. Catal.*, vol. 224, pp. 370–383, 2004.

P. Weiland, “Biogas production : current state and perspectives”, *Appl. Microbiol. Biotechnol.*, vol. 85, pp. 849–860, 2010.

F. Weinberg, “Combustion temperatures : The future ?” *Nature*, vol. 233, pp. 239–241, 1971.

S. Weinberger, E. Scher, et R. Iyer, “Natural gas to ethylene in one step siluria technologies ocm (oxidative coupling of methane)”, *12AIChE - 2012 AIChE Spring Meeting and 8th Global Congress on Process Safety, Conference Proceedings*, 01 2012.

J. Wellendorff, T. L. Silbaugh, D. Garcia-Pintos, J. K. Nørskov, T. Bligaard, F. Studt, et C. T. Campbell, “A benchmark database for adsorption bond energies to transition metal surfaces and comparison to selected dft functionals”, *Surf. Sci.*, vol. 640, pp. 36–44, 2015.

J. Weng, X. Lu, et P.-X. Gao, “Nano-array integrated structured catalysts : A new paradigm upon conventional wash-coated monolithic catalysts ?” *Catalysts*, vol. 7, pp. 253–280, 2017.

I. Wierzba et Q. Wang, “The flammability limits of H_2–co–CH_4 mixtures in air at elevated temperatures”, *Int. J. Hydrog. Energy*, vol. 31, pp. 485–489, 2006.

S. T. Wismann, J. S. Engbæk, S. B. Vendelbo, F. B. Bendixen, W. L. Eriksen, K. Aasberg-Petersen, C. Frandsen, I. Chorkendorff, et P. M. Mortensen, “Electrified methane reforming : a compact approach to greener industrial hydrogen production”, *Science*, vol. 364, pp. 756–759, 2019.

S. T. Wismann, J. S. Engbæk, S. B. Vendelbo, W. L. Eriksen, C. Frandsen, P. M. Mortensen, et I. Chorkendorff, “Electrified methane reforming : Understanding the dynamic interplay”, *Ind. Eng. Chem. Res.*, vol. 58, no. 51, pp. 23 380–23 388, 2019.

K. Wittich, M. Krämer, N. Bottke, et S. A. Schunk, “Catalytic dry reforming of methane : Insights from model systems”, *ChemCatChem*, vol. 12, pp. 2130–2147, 2020.

E. Włoch, A. Łukaszczyk, Z. Zurek, et B. Sulikowski, “Synthesis of Ferrierite Coatings on the FeCrAl Substrate”, *Catal. Today*, vol. 114, pp. 231–236, 2006.

D. A. Wood, C. Nwaoha, et B. F. Towler, “Gas-to-liquids (gtl) : A review of an industry offering several routes for monetizing natural gas”, *J. Nat. Gas Sci. Eng.*, vol. 9, pp. 196–208, 2012.

H. A. Wright, J. D. Allison, D. S. Jack, G. H. Lewis, et S. R. Landis, “ConocoPhillips GTL Technology : The COPox^{TM} Process as the SynGas Generator”, *ACS Division of Fuel Chemistry, Preprints*, vol. 48, no. 2, pp. 791–792, 2003.

R. E. Wright et H. I. Wolff, “Refractory problems in production of hydrogen by pyrolisis of natural gas”, *J. Am. Ceram. Soc.*, vol. 31, no. 2, pp. 31–38, 1948.

D. Wu, Y. Zhang, et Y. Li, “Mechanical Stability of Monolithic Catalysts : Improving Washcoat Adhesion by FeCrAl Alloy Substrate Treatment”, *J. Ind. Eng. Chem.*, vol. 56, pp. 175–184, 2017.

P. Wu, X. Li, S. Ji, B. Lang, F. Habimana, et C. Li, “Steam Reforming of Methane to Hydrogen over Ni-based Metal Monolith Catalysts”, *Catal. Today*, vol. 146, pp. 82–86, 2009.

X. Wu, D. Weng, L. Xu, et H. Li, “Structure and Performance of α-alumina Washcoat Deposited by Plasma Spraying”, *Surf. Coat. Technol.*, vol. 145, pp. 226–232, 2001.

X. Wu, D. Weng, S. Zhao, et W. Chen, “Influence of an Aluminized Intermediate Layer on the Adhesion of a γ-Al_2O_3 Washcoat on FeCrAl”, *Surf. Coat. Technol.*, vol. 190, pp. 434–439, 2005.

S. Xu et X. Wang, “Highly active and coking resistant Ni/CeO_2-ZrO_2 catalyst for partial oxidation of methane”, *Fuel*, vol. 84, pp. 563–567, 2005.

Q. Yan, T. Wu, W. Weng, H. Toghiani, R. Toghiani, H. Wan, et C. Pittman, “Partial oxidation of methane to h2 and co over rh/sio2 and ru/sio2 catalysts”, *J. Catal.*, vol. 226, pp. 247–259, 09 2004.

C. Yang, X. Yu, S. Heißler, P. G. Weidler, A. Nefedov, Y. Wang, C. Wçll, T. Kropp, J. Paier, et J. Sauer, “O_2 Activation on Ceria Catalysts — The Importance of Substrate Crystallographic Orientation Angewandte”, *Angewandte Chemie International Edition*, vol. 56, pp. 16 399–16 404, 2017.

H. S. Yang, D. H. Jang, et K. J. Lee, “Aluminum Oxide Formation on Fecral atalyst Support by Electro-chemical Coating”, *Arch. Metall. Mater.*, vol. 60, pp. 1503–1506, 2015.

J. Yang et Y. Guo, “Nanostructured perovskite oxides as promising substitutes of noble metals catalysts for catalytic combustion of methane”, *Chin. Chem. Lett.*, vol. 29, pp. 252–260, 2018.

Q. Yang, Q. Yang, Y. Man, D. Zhang, et H. Zhou, “Technoeconomic and environmental evaluation of oil shale to liquid fuels process in comparison with conventional oil refining process”, *J. Clean. Prod.*, vol. 255, p. 120198, 2020.

Z. Yang, P. Yang, L. Zhang, J. Ran, M. Guo, et Y. Yan, “Research progress in fluidized combustion technology for low-concentration coalbed methane”, *Nat. Gas Ind.*, vol. 35, pp. 98–104, 12 2015.

F. Yin, S. Ji, N. Chen, M. Zhang, L. Zhao, C. Li, et H. Liu, “$Ce_{1-x}Cu_xO_{2-x}/Al_2O_3$/FeCrAl Catalysts for Catalytic Combustion of Methane”, *Catal. Today*, vol. 105, no. 3-4, pp. 372–377, 2005.

F. Yin, S. Ji, B. Chen, L. Zhao, H. Liu, et C. Li, “Preparation and Characterization of $LaFe_{1-x}Mg_xO_3/Al_2O_3$/FeCrAl : Catalytic properties in Methane Combustion”, *Appl. Catal. B*, vol. 66, pp. 265–273, 2006.

F. Yin, S. Ji, B. Chen, Z. Zhou, H. Liu, et C. Li, “Catalytic Combustion of Methane over $Ce_{1-x}La_xO_{2-x/2}/Al_2O_3$/FeCrAl Catalysts”, *Appl. Catal. A*, vol. 310, pp. 164–173, 2006.

F. Yin, S. Ji, P. Wu, F. Zhao, H. Liu, et C. Li, “Preparation of Pd-based metal monolithic catalysts and a study of their performance in the catalytic combustion of methane”, *ChemSusChem*, vol. 1, pp. 311–319, 2008.

F. Yin, S. Ji, H. Mei, Z. Zhou, et C. Li, “Coupling of Highly Exothermic and Endothermic Reactions in a Metallic Monolith Catalyst Reactor : a Preliminary Experimental Study”, *Chem. Eng. J.*, vol. 155, no. 1-2, pp. 285–291, 2009.

H. Yu, H. Chen, M. Pan, Y. Tang, K. Zeng, F. Peng, et H. Wang, “Effect of the Metal Foam

Materials on the Performance of Pethanol Steam Micro-reformer for Fuel Cells", *Appl. Catal. A*, vol. 327, pp. 106–113, 2007.

Y. H. Yuan, X. G. Zhou, W. Wu, Y. R. Zhang, W. K. Yuan, et L. Luo, "Propylene Epoxidation in a Microreactor with Electric Heating", *Catal. Today*, vol. 105, pp. 544–550, 2005.

J. M. Zamaro, M. A. Ulla, et E. E. Miró, "Growth of Mordenite on Monoliths by Secondary Synthesis. Effects of the Substrate on the Coating Structure and Catalytic Activity", *Appl. Catal. A*, vol. 314, pp. 101–113, 2006.

——, "ZSM5 Growth on a FeCrAl Steel Support. Coating Characteristics upon the Catalytic Behavior in the NOx SCR", *Microporous Mesoporous Mater.*, vol. 115, pp. 113–122, 2008.

S. H. Zeng et Y. Liu, "Nd- or Zr-modified CuO-CeO_2/Al_2O_3/FeCrAl Monolithic Catalysts for Preferential Oxidation of Carbon Monoxide in Hydrogen-rich Gases", *Appl. Surf. Sci.*, vol. 254, pp. 4879–4885, 2008.

S. H. Zeng, Y. Liu, et Y. Q. Wang, "CuO-CeO_2/Al_2O_3/FeCrAl Monolithic Catalysts Prepared by Sol-pyrolysis Mmethod for Preferential Oxidation of Carbon Monoxide", *Catal. Letters*, vol. 117, pp. 119–125, 2007.

S. Zeng, H. Su, Y. Liu, Y. Wang, et D. Wang, "CuO-CeO_2/Al_2O_3/FeCrAl Monolithic Catalysts Prepared by in situ Combustion Synthesis Method for Preferential Oxidation of Carbon Monoxide", *J. Rare Earths*, vol. 29, pp. 69–73, 2011.

D. Zhang, "The Ductility Below the Ductile-to-brittle Transition Temperature of the FeCrAlloy", *J. Alloys Compd.*, vol. 479, pp. 47–49, 2009.

D. Zhang, L. Zhang, B. Liang, et Y. Li, "Effect of Acid Treatment on the High-temperature Surface Oxidation Behavior of FeCrAlloy Foil Used for Methane Combustion Catalyst Support", *Ind. Eng. Chem. Res.*, vol. 48, pp. 5117–5122, 2009.

J. Zhang et F. Li, "Coke-resistant ni@SiO_2 catalyst for dry reforming of methane", *Appl. Catal. B*, vol. 176-177, pp. 513–521, 2015.

L. Zhang, T. Li, M. Zhang, et Y. Li, "Effect of Intermediate Layer on the Activity and Adhesion Stability of Metal Monolith Supported LaMn-hexaaluminate Catalyst for Methane Combustion", *J. Rare Earths*, vol. 29, pp. 758–762, 2011.

F. Zhao, S. Ji, P. Wu, Z. Li, et C. Li, "Catalytic Oxidation of CO over $Cu_xCe_{1-x}O_{2-x}$/SBA-15/FeCrAl Monolithic Catalysts", *Catal. Today*, vol. 147, pp. 215–219, 2009.

G. Zhao, R. Chai, Z. Zhang, W. Sun, Y. Liu, et Y. Lu, “High-performance ni-$CeAlO_3$-Al_2O_3/fecral-fiber catalyst for catalytic oxy-methane reforming to syngas”, *Fuel*, vol. 258, p. 116102, 2019.

S. Zhao, J. Zhang, D. Weng, et X. Wu, “A Method to Form Well-adhered γ-Al_2O_3 Layers on FeCrAl Metallic Supports”, *Surf. Coat. Technol.*, vol. 167, pp. 97–105, 2003.

I. A. Zlochower, “Experimental flammability limits and associated theoretical flame temperatures as a tool for predicting the temperature dependence of these limits”, *J. Loss Prev. Process Ind.*, vol. 25, pp. 555–560, 2012.

M. F. M. Zwinkels, S. G. Järås, P. G. Menon, T. A. Griffin, M. F. M. Zwinkels, S. G. Järås, P. G. Menon, et T. A. Griffin, “Catalytic Materials for High-Temperature Combustion”, *Catalysis Rev.*, vol. 4940, pp. 319–358, 2006.

ANNEXE A REACTOR OPERATING PROCEDURE

REACTORS OPERATION PROCEDURE
CPOX REACTOR

Gianluca Pauletto
Alice Gaillardet

May 20, 2019

1 Setup

The setup consists of the reactor identified with ID: CPOXHood1 located in the lab A-675 under the walking hood identified with the number UBUWB-96-FRP, certified for working with explosive gases.The volume of the reactor is smaller then 80 l so it is considered as fitting and require no certification. The reactor is made from:

1. metal pipe 4815T142 (McMasterCarr identification) 316/316L Stainless Steel, 1 3/64" OD, schedule 80 that meet the specifications ASTM A312
2. Swagelock fittings (SS-16-VCR-1, SS-16-VCR-3-16MTW, SS-16-VCR-1-16, SS-16-VCR-2) all peaces in 316SS 1" OD that can operate at max 3000 psi

VCR fittings and pipe were welded together at Universite de Montreal workshop by certified welders. Inside this reactor a quartz pipe prevents the contact between reactive gases and metal reactors walls. The size of the inside quartz reactor is 12.5 mm. All the additional parts needed for the installation of the reactor were bought from McMasterCar and Swagelock and are certified to be used at pressure higher than 2000 psi. They are used as bought without any mechanical modification that could compromise the certification. Connected to the reactor there are the following instruments:

1. 3 Mass Flow Controllers Bronkhorst: M11202337A, M11202337B, M11202337C (MFC 1, MFC 2, MFC 3)
2. 2 Thermocouples Omega 0 °C to 1000 °C (TT01, TT02)
3. 2 Pressure gauges range 0-500 psi (PG01. PG02)
4. Swagelock back pressure regulator range 0-500 psi: KBP1JOD4A5A20000 (VA01)
5. 2 Swagelock safety valves calibrated at 320 psi: MZ1866001 AND 923124001 (PSV01, PSV02).

2 Methane partial oxidation

The methane partial oxidation takes place at 280 psi inside the reactor with diameter of 12.5 mm and total height of 76 cm. The cross section of the reactor is shown in Figure 1.
The reactor contains a fixed catalytic bed that activates methane. Mass flow controllers feed air and methane during reaction and only air during regeneration. The gasses are fed and premixed in a 1/4" tube with internal diameter of 0.18" before being fed to the reactor. The outlet of the reactor has a back pressure regulator and after decreasing the pressure until atmosphere conditions it is vented in the hood. From this stream the Hiden mass spectrometer probe analyses the products. The main goal is to avoid any storage of gas in the lab to prevent hazardous gas accumulating outside the hood. Two Honeywell gas sensor to detect CO and H_2 are located in the room. They monitor the atmosphere of the lab and they give an alarm when the measured composition of H_2 and CO is higher then 25 ppm.

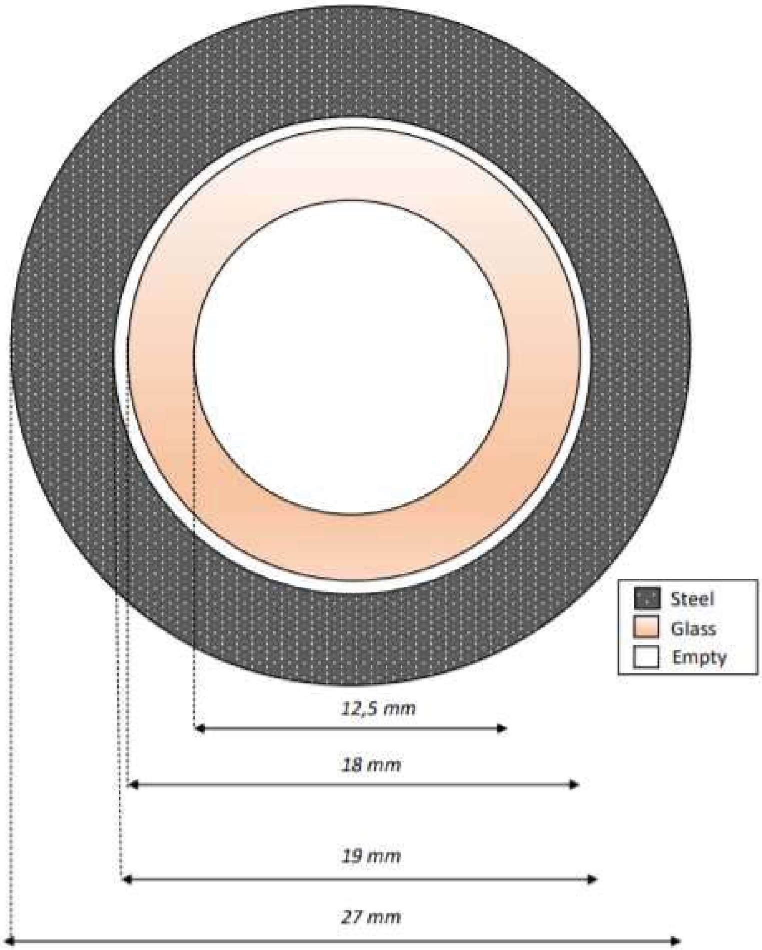

Figure 1: Internal cross section of the reactor

2.1 Control and safety loops

The setup is controlled by a Labview program that has being designed by Neosoft Technologies Inc, certified by National Instrument. All the parameters coming from the instruments connected with the setup (3 MFC flows, 2 thermocouples and 2 gas sensors) are shown at the control panel and they are recorded every 2 s.
Being aware of the explosion limit of CH_4 in air all the experiments are carried out outside the explosion limits in the meaning that the reactant mixtures will always contain CH_4, O_2 and Ar in proportion that are outside the dark region (Fig. 3). Ar will always used to purge the lines and the reactor before starting and changing the experiment. Preliminary cold tests were done to monitor the formation of explosive mixture that could appear from remixing phenomena occurring in the reactor. When this conditions are detected initially only methane will be fed and afterward air.
To assure safe operation the implemented safety procedures are:

1. Safety 1: there will be an emergency button on the panel next to the setup. In case of

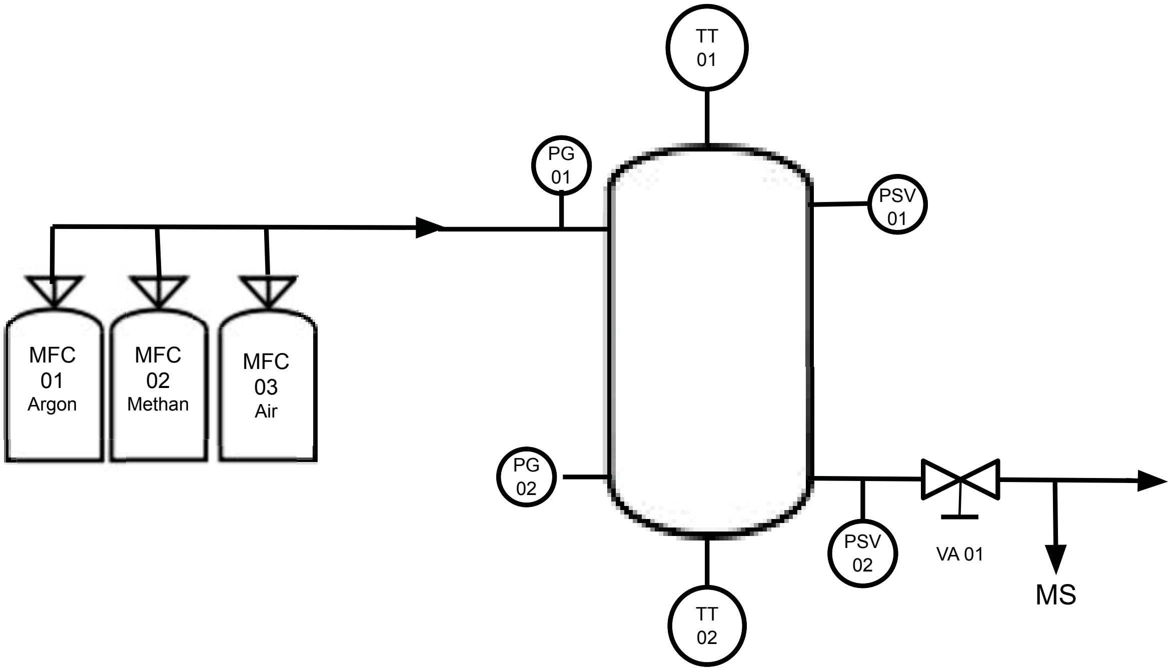

Figure 2: P&ID Internal cross section of the reactor

emergency the heaters will turn off, all the flow will be stopped and only Ar will enter in the system.

2. Safety 2: CO and H_2 safety sensors. If the measured concentration of the CO or H_2 inside the lab will be higher then 25 ppm all the flow will be stopped and only Ar will enter in the system. Moreover a visual and acoustic alarm will turn on until an action will be taken and the measure values will be lower then the set limits.

2.2 Gas storage

During all the experiments in the room, only one 50 L bottle will be always present and connected to the setup for the following gases: CH_4, Air, Ar. All the other gas bottles needed for the experiments will be stored in the lab A-674 following the procedure reported in document “Chemical Engineering Diligent Management of HW and SST Date : 5-April-04” of Polytechnique Montreal.
The maximum CH_4 flow rate that will be $6\,\mathrm{L\,min^{-1}}$. This value is lover then the maximum value that can be fed to the reactor, equal to 2% of the volumetric flow rate of the hood equal to $1700\,\mathrm{L\,min^{-1}}$.
H_2 and CO will never be stored but immediately vented after leaving the reactor via the exhaust hood.

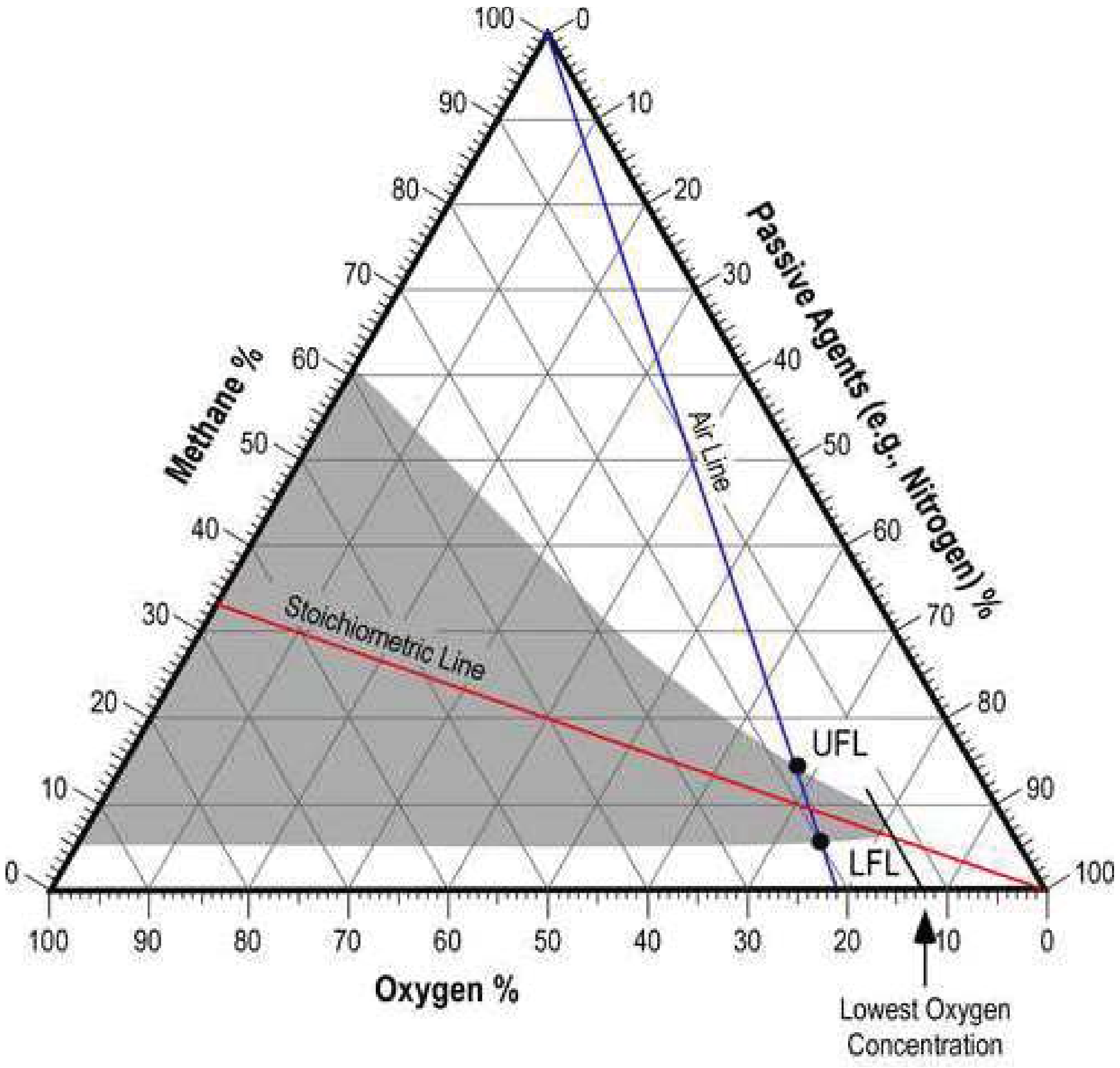

Figure 3: Internal cross section of the reactor

2.3 Operating procedure

All the experiments will be reported into a sequence that can last a maximum of 48 h. The different setpoint here reported will be checked and controlled by two people to prevent any possible mistakes in the calculation that could create a safety hazard. All the sequence with the initial time and date will be printed, signed and stored in a proper lab notebook that will be always present next to the control station.
This operating procedure has to be done every time and a report will be attached to the lab notebook after any mechanical modification to the setup has been done and before starting any new sequence.

1. Step 1: Open the flow of Ar MFC1 on the Labview program with a flow of $2\,\mathrm{l\,min^{-1}}$
2. Step 2: Adjust the back pressure regulator until setpoint (280 psi) is reached and

monitor the pressure from PG01 and PG02

3. Step 3 : Close the flow of Ar and check if teh pressure drop exceeds 1 psi every 10 minute
4. Step 4: Inspect all the connection with Snoop
5. Step 5: After making sure that there is no leakage at low temperature turn on the furnace until setpoint max 950 °C from the power supply station next to the reactor. $2\,\mathrm{l\,min^{-1}}$ of Ar will constantly flow during heating up steps.
6. Step 6: Close the flow of Ar and check if after 1 h the pressure is constant or has changed within a range of 10%
7. Step 7: After making sure that there is no leakage at the set point temperature the leakage test is completed and this will be reported in the lab notebook

Table 1: Example Sequence

Ar, $\mathrm{L\,min^{-1}}$	CH_4, $\mathrm{L\,min^{-1}}$	O_2, Ar, $\mathrm{L\,min^{-1}}$	Time, min
1	1	1	10
...	...	...	...
...	...	...	
...	...		

An example of sequence is reported in the table above. The sequence has to be written in excel before being transferred into the Labview program. MFC1, MFC2 and MFC3 are the only parameters that can be modified and set. Corresponding time can also be fixed for every set of flow (fixed by the first 3 columns). For example with the sequence in Tab. 1 the following flows will be set for 10 minutes: CH_4 $1\,\mathrm{l\,min^{-1}}$, Ar $1\,\mathrm{l\,min^{-1}}$ and air $1\,\mathrm{l\,min^{-1}}$.
While the sequence is running in case of emergency it is always possible to immediately stop and start a safety loop. The safety loop will stop all the flow of gases and will only feed Ar with volumetric flow rate of $20\,\mathrm{l\,min^{-1}}$.

2.4 Setup inspection

Prof Gregory Patience and Prof Daria Boffito on Friday 17th May 2019 inspected the lab setup including control station, piping disposition, reactor setup and analytical instrumentation connected to the unit. The committee suggested a modification that had to be done before the reactor could be started. The modification consisted of moving the analytical instrumentation (Hiden Mass Spectrometer) that was located 4 m away from the outlet line of the reactor and that was connected via a 1/8” SS316 pipe to the reactor outlet. The decision was taken to keep all the reaction products within the hood even for the analysis of the products that could lead to a leakage in the laboratory.
It was decided that after this disposition was put in place another inspection would have taken place to grant the starting up permission.

2.5 Explosion scenario

For the TNT calculation we have used the “Estimating pressure increase and explosive energy release associated with explosions” form the “United States Nuclear Regulatory Commission”. The calculation in attach to this documents reports the increase of pressure from a confined explosion and the TNT mass equivalent. The amount of CH_4 that could potentially explodes was considered equal to the reactor volume (diameter 1.9 cm, height 76 cm) filled with gas at 25 °C and 280 psi and volumetric percentage of 30% CH_4, 15% O_2 and 55% Ar. The total mass of methane that could take part in the explosion is equal to 1 g.

2.6 Start up approval

Date and Location:

Name and Signature:

Name and Signature:

Prescription:

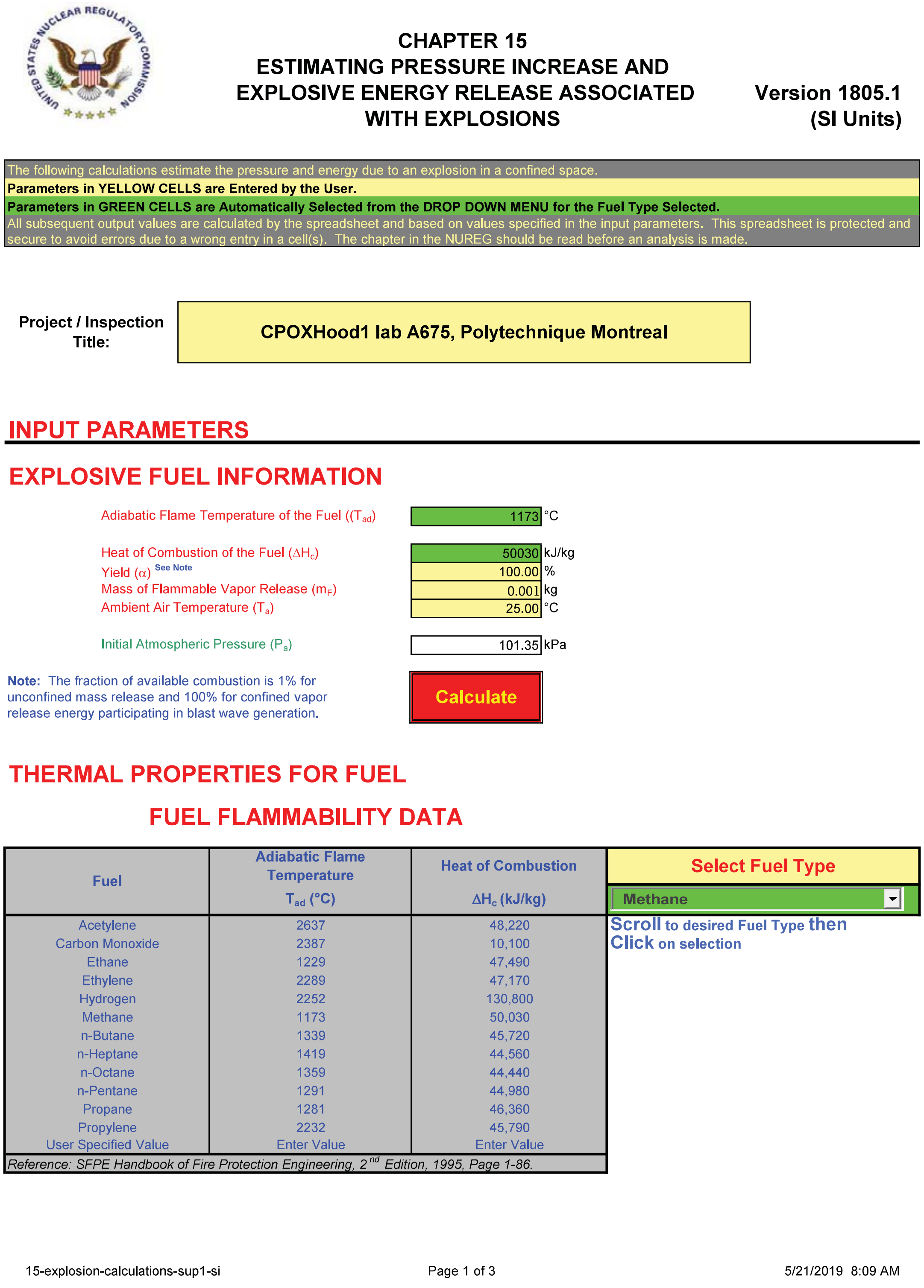

CHAPTER 15
ESTIMATING PRESSURE INCREASE AND EXPLOSIVE ENERGY RELEASE ASSOCIATED WITH EXPLOSIONS

Version 1805.1
(SI Units)

The following calculations estimate the pressure and energy due to an explosion in a confined space.
Parameters in YELLOW CELLS are Entered by the User.
Parameters in GREEN CELLS are Automatically Selected from the DROP DOWN MENU for the Fuel Type Selected.
All subsequent output values are calculated by the spreadsheet and based on values specified in the input parameters. This spreadsheet is protected and secure to avoid errors due to a wrong entry in a cell(s). The chapter in the NUREG should be read before an analysis is made.

Project / Inspection Title: **CPOXHood1 lab A675, Polytechnique Montreal**

INPUT PARAMETERS

EXPLOSIVE FUEL INFORMATION

Adiabatic Flame Temperature of the Fuel ((T_{ad})	1173	°C
Heat of Combustion of the Fuel (ΔH_c)	50030	kJ/kg
Yield (α) See Note	100.00	%
Mass of Flammable Vapor Release (m_F)	0.001	kg
Ambient Air Temperature (T_a)	25.00	°C
Initial Atmospheric Pressure (P_a)	101.35	kPa

Note: The fraction of available combustion is 1% for unconfined mass release and 100% for confined vapor release energy participating in blast wave generation.

THERMAL PROPERTIES FOR FUEL

FUEL FLAMMABILITY DATA

Fuel	Adiabatic Flame Temperature T_{ad} (°C)	Heat of Combustion ΔH_c (kJ/kg)
Acetylene	2637	48,220
Carbon Monoxide	2387	10,100
Ethane	1229	47,490
Ethylene	2289	47,170
Hydrogen	2252	130,800
Methane	1173	50,030
n-Butane	1339	45,720
n-Heptane	1419	44,560
n-Octane	1359	44,440
n-Pentane	1291	44,980
Propane	1281	46,360
Propylene	2232	45,790
User Specified Value	Enter Value	Enter Value

Reference: SFPE Handbook of Fire Protection Engineering, 2nd Edition, 1995, Page 1-86.

Select Fuel Type

Methane

Scroll to desired Fuel Type then Click on selection

CHAPTER 15
ESTIMATING PRESSURE INCREASE AND EXPLOSIVE ENERGY RELEASE ASSOCIATED WITH EXPLOSIONS

Version 1805.1
(SI Units)

METHOD OF ZALOSH

Reference: SFPE Handbook of Fire Protection Engineering, 2nd Edition, 1995, Page 3-312.

Pressure Rise from a Confined Explosion

$$(P_{max})/P_a = (T_{ad}/T_a)$$
$$P_{max} = (T_{ad}/T_a)\ P_a$$

Where,
P_{max} = maximum pressure developed at completion of combustion (kPa)
P_a = initial atmospheric pressure (kPa)
T_{ad} = adiabatic flame temperature (K)
T_a = ambient temperature (K)

P_{max} = 491.79 kPa 71.33 psi

Blast Wave Energy Calculation

$$E = \alpha\ \Delta H_c\ m_F$$

Where,
E = blast wave energy (kJ) [E is the Trinitrotoluene (TNT) equivalent energy]
α = yield (a is the fraction of available combustion energy participating in blast wave generation)
ΔH_c = heat of combustion (kJ/kg)
m_F = mass of flammable vapor release (kg)

E = 50.03 kJ 47.38 Btu

TNT Mass Equivalent Calculation

$$W_{TNT} = E/4500$$

Where,
W_{TNT} = weight of TNT (kg)
E = explosive energy release (kJ)

W_{TNT} = 0.01 kg 0.02 lb

CHAPTER 15
ESTIMATING PRESSURE INCREASE AND EXPLOSIVE ENERGY RELEASE ASSOCIATED WITH EXPLOSIONS

Version 1805.1
(SI Units)

Results Summary

Pressure Rise from a Confined Explosion

$$P_{max} = (T_{ad}/T_a)\ P_a$$

Answer	P_{max} =	**491.79 kPa**	**71.33 psi**

Blast Wave Energy

$$E = \alpha\ \Delta H_c\ m_F$$

Answer	E =	**50.03 kJ**	**47.38 Btu**

TNT Mass Equivalent

$$W_{TNT} = E/4500$$

Answer	W_{TNT} =	**0.01 kg**	**0.02 lb**

NOTE:
The above calculations are based on principles developed in the SFPE Handbook of Fire Protection Engineering, 2nd Edition, 1995. Calculations are based on certain assumptions and have inherent limitations. The results of such calculations may or may not have reasonable predictive capabilities for a given situation and should only be interpreted by an informed user. Although each calculation in the spreadsheet has been verified with the results of hand calculation, there is no absolute guarantee of the accuracy of these calculations. Any questions, comments, concerns and suggestions or to report an error(s) in the spreadsheet, please send an email to David.Stroup@nrc.gov or Naeem.Iqbal@nrc.gov.

Prepared by: Gianluca Pauletto Date: 20.05.2019 Organization: Polytechnique Montreal

Checked by: Date: Organization:

Additional Information: